ARO 30068.7-MS

NOVEL ACTUATOR MATERIALS: MONOMORPHS AND PHOTOSTRICTIVE ACTUATORS

FINAL PROGRESS REPORT

(Period June 1, 1992 to November 30, 1995)

KENJI UCHINO

FEBRUARY 9, 1996

U.S.ARMY RESEARCH OFFICE

GRANT NUMBER: DAAL03-92-G-0244

THE PENNSYLVANIA STATE UNIVERSITY

PENNSTATE

International Center for Actuators and Transducers

Intercollege Materials Research Laboratory

University Park, PA

DISCLAIMER NOTICE

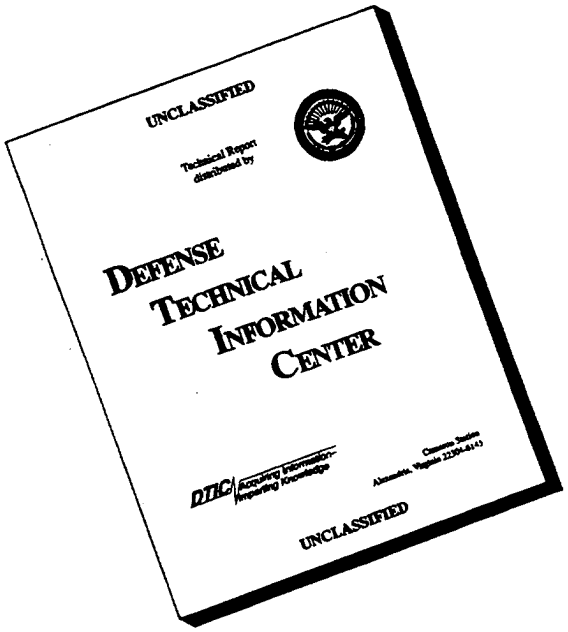

THIS DOCUMENT IS BEST QUALITY AVAILABLE. THE COPY FURNISHED TO DTIC CONTAINED A SIGNIFICANT NUMBER OF PAGES WHICH DO NOT REPRODUCE LEGIBLY.

SF 298 MASTER COPY KEEP THIS COPY FOR REPRODUCTION PURPOSES

REPORT DOCUMENTATION PAGE

Form Approved
OMB NO. 0704-0188

1. AGENCY USE ONLY *(Leave blank)*	2. REPORT DATE	3. REPORT TYPE AND DATES COVERED
	February 9, 1996	Final 1 Jun 92 - 30 Nov 95

4. TITLE AND SUBTITLE

Novel Actuator Materials: Monomorphs and Photostrictive Actuators

5. FUNDING NUMBERS

DAAL03-92-G-0244

6. AUTHOR(S)

Kenji Uchino

7. PERFORMING ORGANIZATION NAMES(S) AND ADDRESS(ES)

The Pennsylvania State University
Sponsored Programs and Contracts Office
]]0 Technology Center Building
University Park, PA]6802

8. PERFORMING ORGANIZATION REPORT NUMBER

9. SPONSORING / MONITORING AGENCY NAME(S) AND ADDRESS(ES)

U.S. Army Research Office
P.O. Box 12211
Research Triangle Park, NC 27709-2211

10. SPONSORING / MONITORING AGENCY REPORT NUMBER

ARO 30068.7-MS

11. SUPPLEMENTARY NOTES

The views, opinions and/or findings contained in this report are those of the author(s) and should not be construed as an official Department of the Army position, policy or decision, unless so designated by other documentation.

12a. DISTRIBUTION / AVAILABILITY STATEMENT

Approved for public release; distribution unlimited.

12 b. DISTRIBUTION CODE

13. ABSTRACT *(Maximum 200 words)*

Photostriction is the superposition of photovoltaic and piezoelectric effects. Perovskite (Pb,La)(Zr,Ti)O_3 ceramics doped with WO_3 exhibit large photostriction under irradiation of near-ultraviolett light, and are applicable to remote control actuators. Highlights of the 3.5 years' activity include: impurity doping study, polarized light effect and photo-induced mechanical resonance. The photostrictive effects in the PLZT were investigated as a function of B-site impurity doping. Donor doping was found to reduce both the grain size and room-temperature dielectric constant, influencing the photovoltatic effect. WO_3 and Ta_2O_5 doping increase the photovoltaic response, but do not significantly affect the piezoelectric effect. Using linearly polarized light, angular dependence of the photovoltaic voltage and current on the light-polarization orientation with respect to the spontaneous polarization was observed in the PLZT. This angular dependence was consistent with the symmetry of the poled ceramic. Photo-mechanical resonance of a PLZT bimorph has been successfully induced using chopped UV irradiation, having neither electric lead wires nor electric circuit. The remarkable response speed improvement by 5 orders of magnitude during these 3.5 years could verify the feasibility of these PLZT photostrictive materials for practical actuator applications which are relevant to Army needs.

14. SUBJECT TERMS

Actuator, Photostriction, Photovoltaic Effect, Piezoelectricity
Photoacoustic Device

15. NUMBER IF PAGES

182

16. PRICE CODE

17. SECURITY CLASSIFICATION OR REPORT	18. SECURITY CLASSIFICATION OF THIS PAGE	19. SECURITY CLASSIFICATION OF ABSTRACT	20. LIMITATION OF ABSTRACT
UNCLASSIFIED	UNCLASSIFIED	UNCLASSIFIED	UL

GENERAL INSTRUCTIONS FOR COMPLETING SF 298

The Report Documentation Page (RDP) is used in announcing and cataloging reports. It is important that this information be consistent with the rest of the report, particularly the cover and title page. instructions for filling in each block of the form follow. It is important to ***stay within the lines*** to meet ***optical scanning requirements.***

Block 1. Agency Use Only *(Leave blank)*

Block 2. Report Date. Full publication date including day, month, and year, if available (e.g. 1 Jan 88). Must cite at least year.

Block 3. Type of Report and Dates Covered. State whether report is interim, final, etc. If applicable, enter inclusive report dates (e.g. 10 Jun 87 - 30 Jun 88).

Block 4. Title and Subtitle. A title is taken from the part of the report that provides the most meaningful and complete information. When a report is prepared in more than one volume, repeat the primary title, add volume number, and include subtitle for the specific volume. On classified documents enter the title classification in parentheses.

Block 5. Funding Numbers. To include contract and grant numbers; may include program element number(s), project number(s), task number(s), and work unit number(s). Use the following labels:

C	- Contract	**PR**	- Project
G	- Grant	**TA**	- Task
PE	- Program Element	**WU**	- Work Unit Accession No.

Block 6. Author(s). Name(s) of person(s) responsible for writing the report, performing the research, or credited with the content of the report. If editor or compiler, this should follow the name(s).

Block 7. Performing Organization Name(s) and Address(es). Self-explanatory.

Block 8. Performing Organization Report Number. Enter the unique alphanumeric report number(s) assigned by the organization performing the report.

Block 9. Sponsoring/Monitoring Agency Name(s) and Address(es). Self-explanatory.

Block 10. Sponsoring/Monitoring Agency Report Number. *(If known)*

Block 11. Supplementary Notes. Enter information not included elsewhere such as; prepared in cooperation with...; Trans. of...; To be published in.... When a report is revised, include a statement whether the new report supersedes or supplements the older report.

Block 12a. Distribution/Availability Statement. Denotes public availability or limitations. Cite any availability to the public. Enter additional limitations or special markings in all capitals (e.g. NORFORN, REL, ITAR).

DOD	- See DoDD 4230.25, "Distribution Statements on Technical Documents."
DOE	- See authorities.
NASA	- See Handbook NHB 2200.2.
NTIS	- Leave blank.

Block 12b. Distribution Code.

DOD	- Leave blank
DOE	- Enter DOE distribution categories from the Standard Distribution for Unclassified Scientific and Technical Reports
NASA	- Leave blank.
NTIS	- Leave blank.

Block 13. Abstract. Include a brief *(Maximum 200 words)* factual summary of the most significant information contained in the report.

Block 14. Subject Terms. Keywords or phrases identifying major subjects in the report.

Block 15. Number of Pages. Enter the total number of pages.

Block 16. Price Code. Enter appropriate price code *(NTIS only).*

Block 17. - 19. Security Classifications. Self-explanatory. Enter U.S. Security Classification in accordance with U.S. Security Regulations (i.e., UNCLASSIFIED). If form contains classified information, stamp classification on the top and bottom of the page.

Block 20. Limitation of Abstract. This block must be completed to assign a limitation to the abstract. Enter either UL (unlimited) or SAR (same as report). An entry in this block is necessary if the abstract is to be limited. If blank, the abstract is assumed to be unlimited.

NOVEL ACTUATOR MATERIALS: MONOMORPHS AND PHOTOSTRICTIVE ACTUATORS

FINAL PROGRESS REPORT

KENJI UCHINO

FEBRUARY 9, 1996

U.S.ARMY RESEARCH OFFICE

GRANT NUMBER: DAAL03-92-G-0244

THE PENNSYLVANIA STATE UNIVERSITY

1. FOREWORD

Novel functions of materials are sometimes realized by superimposing two different effects. Newly discovered materials, monomorphs and photostrictors, are using sophisticatedly coupled effects of piezoelectricity with another different phenomenon. The monomorph is coupled with a semiconductor contact effect, while the photostriction is associated with a bulk photovoltaic effect. These "very smart" multifunctional actuator materials will be utilized as promising devices relevant to Army needs. This final report reviews the recent studies particularly on the photostriction of PLZT.

2. TABLE OF CONTENTS

Abstract	1
Problem Studied	2
Summary of the Most Important Results	3
List of All Publications and Technical Reports	5
List of All Participating Scientific Personnel	6
Report of Inventions	6
Bibliography	7

3. LIST OF APPENDIXES

PAPERS ON PHOTOSTRICTION

1. Chu, S. Y., Z. Ye and K. Uchino, "Effect of Impurity Doping on Photostrictive Effect in PLZT Ceramics," J. Advanced Performance Mater. Vol.1, 129-143 (1994).

2. Chu, S. Y., J. Ye and K. Uchino, "Photovoltaic Effect for the Linearly Polarized Light in (Pb,La)(Zr,Ti)O_3 Ceramics," Smart Mater. & Structures 3, 114-117 (1994).

3. Uchino, K. and S. Y. Chu, "Photostriction and Its Applications," Proc. PacRim Amer. Ceram. Soc., Ferroic Materials, 287-293 (1994).

4. Chu, S. Y., M. L. Mulvihill, Z. Ye and K. Uchino, "Bulk Photovoltaic Effect for the Linearly Polarized Light in $Pb(Zn_{1/3}Nb_{2/3})O_3$ Single Crystals," Jpn. J. Appl. Phys. Vol.34, 527-529 (1995).

5. Uchino, K., "Electrooptic Ceramics and Their Display Applications," Ceramics International Vol.21, 309-315 (1995).

6. Chu, S. Y. and K. Uchino, "Photo-Acoustic Devices Using (Pb,La)(Zr,Ti)O_3 Ceramics," Proc. 9th Int'l Symp. Appl. Ferroelectrics p.743-745 (1995).

7. Uchino, K., "Photostrictive Actuators and "Photophones"," Proc. Int'l Symp. Microsystems, Intelligent Mater. and Robots, p.193-196 (1995).

8. Chu, S. Y., Z. Ye and K. Uchino, "Photo-Acoustic Devices Using (Pb,La)(Zr,Ti)O_3-Based Ceramics," J. Jpn. Ceram. Soc. (1995) (submitted).

9. Chu, S. Y. and K. Uchino, "Photostrictive Effect in PLZT-Based Ceramics and Its Applications," Ferroelectrics (in press).

10. Uchino, K., "Review: Photostriction and Its Applications," J. Innovations in Mater. Res. (in press).

REVIEW PAPERS ON SMART MATERIALS

11. Uchino, K., "Ceramic Actuators: Principles and Applications," Mater. Res. Soc. Bull. **18**, 42 - 48 (1993).

12. Uchino, K., "New Piezoelectric Devices for Smart Actuator/Sonsor Systems," Proc. 4th Int'l Conf. Electronic Ceramics & Appl., p.179-191 (1994).

13. Uchino, K., "Worldwide Research and Development of Ceramic Actuators," New Ceramics (TCI, Tokyo) Vol.7(11), 5-13 (1994).

14. Uchino, K., "Advances in Ceramic Actuator Materials," Mater. Let., Vol.22, 1-4 (1995).

15. Uchino, K., "Novel Ceramic Actuator Materials," Proc. US/Japan Workshop on Smart Mater. and Structures (in press).

4. FINAL REPORT

ABSTRACT

Photostriction is the superposition of photovoltaic and piezoelectric effects. Perovskite (Pb,La)(Zr,Ti)O_3 ceramics doped with WO_3 exhibit large photostriction under irradiation of near-ultraviolett light, and are applicable to remote control actuators.

Highlights of the 3.5 years' activity include: impurity doping study, polarized light effect and photo-induced mechanical resonance. The photostrictive effects in the PLZT were investigated as a function of B-site impurity doping. Donor doping was found to reduce both the grain size and room-temperature dielectric constant, influencing the photovoltaic effect. WO_3 and Ta_2O_5 doping increase the photovoltaic response, but do not significantly affect the piezoelectric effect.

Using linearly polarized light, angular dependence of the photovoltaic voltage and current on the light-polarization orientation with respect to the spontaneous polarization was observed in the PLZT. This angular dependence was consistent with the symmetry of the poled ceramic. The difference between the peak-peak deviations in the current (2%) and voltage (14%) suggests a relatively large dependence of photoconductivity on light-polarization orientation.

Photo-mechanical resonance of a PLZT bimorph has been successfully induced using chopped UV irradiation, having neither electric lead wires nor electric circuit. The resonance frequency was 75 Hz with a mechanical quality factor Q of about 30 under dual beam operation.

The remarkable response speed improvement by 5 orders of magnitude during these 3.5 years could verify the feasibility of these PLZT photostrictive materials for practical actuator applications which are relevant to Army needs.

A. PROBLEM STUDIED

Photostrictive effect is a phenomenon in which strain is induced in the sample when it is illuminated. This effect is focused especially in the fields of micromechanism and optical communication.

With decreasing the size of miniature robots/actuators, the weight of the electric lead wire connecting the power supply becomes significant, and remote control will definitely be required for sub-millimeter devices. A photo-driven actuator is a very promising candidate for micro-robots. On the other hand, the key components in the optical communication are a solid state laser as a light source, an optical fiber as a transfer line, and a display/ telephone as a visual/audible interface with the human. The former two components have been developed fairly successfully, and the photo-acoustic device (i. e. an optical telephone or a "photophone") will be eagerly anticipated in the next century.

Photostrictive devices which are actuated when they receive the energy of light will be particularly suitable for use in the above-mentioned fields. In principle, the photostrictive effect arises from a superposition of a photovoltaic effect, where a large voltage is generated in a ferroelectric through the irradiation of light, and a piezoelectric effect, where the material expands or contracts under the voltage applied. Ii is noteworthy that this photostriction is neither the thermal dilatation nor the pyroelectrically-produced strain associated with a temperature rise due to the light illumination. Also the photovoltaic effect mentioned here generates a greater-than-band-gap voltage (several kV/cm), and is quite different from that based on the p-n junction of semiconductors (i. e. solar battery).

We put a particular focus on improving the response of photostrction: impurity doping study, polarized light effect and photo-induced mechanical resonance. The photostrictive effects in the PLZT are strongly affected by the B-site impurity doping. We determined the optimum concentration of the donor doping such as WO_3 and Ta_2O_5. When the photostrictive actuator is controlled by the intensity modulation of the irradiation light, polarized light will occasionally be used. Angular dependence of the photovoltaic voltage and current on the light-polarization orientation with respect to the spontaneous polarization should be observed in the PLZT; this is also important to clarify the photovoltaic mechanism. Finally, the possibilty of the photo-induced mechanical resonance in the photostrictive actuator must be tested so as to verify the feasibity of these materials to ultrasonic devices and "photophones."

B. SUMMARY OF THE MOST IMPORTANT RESULTS

Highlights of the 3.5 years' activity include: impurity doping study, polarized light effect and photo-induced mechanical resonance.

Our focus was put on the photostrictive effect primarily in (Pb,La)(Zr,Ti)O_3 ceramics, in particular, impurity doping effect to enhance the effect. The elements were 20 x4x0.15 mm^3: the 4x0.15 mm^2 surface was electroded with silver paste before electrical poling. The bimorph actuator consisted of two bonded oppositely-poled ceramic plates. Impurity doping on PLZT affects the photovoltaic response significantly. Regarding the photostriction effect, it is known that as the photovoltaic voltage increases, the strain value increases, and with increasing photo-current, there is an increase in the overall response. The photovoltaic response was enhanced by donor doping onto the B-site (Nb^{5+}, Ti^{5+}, W^{6+}). Figure 1 shows the photovoltaic current, photovoltaic voltage, photo-induced tip displacement and stored energy ($P=(1/2)\ I_{max} \times V_{max}$) in PLZT 3/52/48 bimorph samples plotted as a function of atm% of WO_3 doping concentration. The photo-voltaic voltage reaches 1 kV/mm, and the current is on the order of nA. The maximum of the saturated tip displacement was about 120 μm for 0.4 atm% WO_3 doped samples. On the contrary, the maximum photostriction in Ta_2O_5 doped samples was obtained at 1 at% doping.

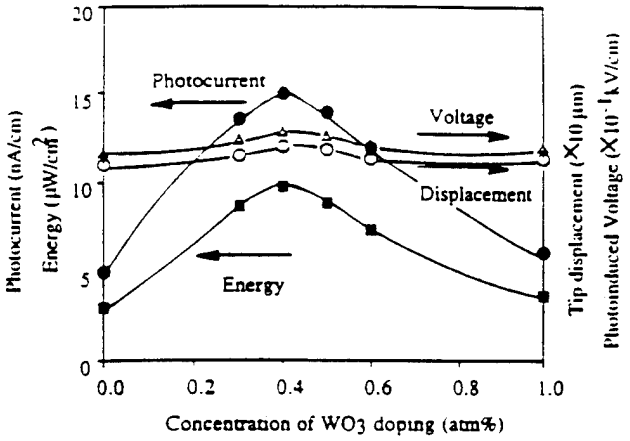

Fig.1. Photovoltaic response as a function of impurity doping.

Using linearly polarized light, angular dependence of the photovoltaic voltage and current on the light-polarization orientation with respect to the spontaneous polarization was observed in the PLZT. This angular dependence was consistent with the symmetry of the

poled ceramic. The difference between the peak-peak deviations in the current (2%) and voltage (14%) suggests a relatively large dependence of photoconductivity on light-polarization orientation.

Photo-induced mechanical resonance was measured using the bimorph sample. Radiation from a high-pressure mercury lamp was passed through an IR blocking filter, an optical focusing lens and an optical chopper to provide intermittent sample irradiation. A wavelength peak of 370 nm, where the maximum photovoltaic effect of PLZT is obtained, was used. A dual beam method was used to irradiate the two sides of the bimorph alternately. Two beams, generated through a beam splitter, were chopped so as to cause a 180 degree phase difference; this overcomes the slow recovery because of the low dark conductivity. The mechanical resonance was then determined by changing the chopper frequency. Photo-induced mechanical resonance was successfully observed at an audible frequency, as in Fig.2. The resonance frequency was 75 Hz with the mechanical quality factor Q of 30. The maximum tip displacement of this photostrictive sample was 5 μm at the resonance.

The remarkable response speed improvement by 5 orders of magnitude during these 3.5 years could verify the feasibility of these PLZT photostrictive materials for practical actuator applications which are relevant to Army needs.

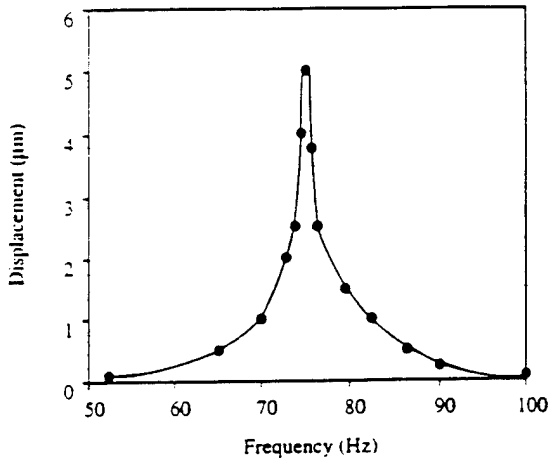

Fig.2. Photo-induced mechanical resonance behavior of the PLZT bimorph.

C. LIST OF ALL PUBLICATIONS AND TECHNICAL REPORTS

PEER REVIEWED JOURNALS

1. Uchino, K., "Applications of Piezoelectric Ceramics in Smart Actuators and Systems," J. Industrial Education Soc. Jpn. 40 (2), 28-32 (1992).

2. Uchino, K., "Photostrictive Actuators," Optronics 129, 86-90 (1992).

3. Uchino, K., "Photostrictive Actuators," J. Precision Engr. Jpn. 58, 419-421 (1992).

4. Uchino, K. and S. Suzuki, "Speakers Utilizing Semiconductive Piezoelectric Monomorph Devices," J. Ceram. Soc. Jpn. 100 (10), 1221-1224 (1992).

5. Uchino, K., "Applications of Piezoelectrics in Smart Actuator," Bull. Ceram. Soc. Jpn. 28 (6), 559-563 (1993).

6. Uchino, K., "Smart Actuators," Ultrasonic Technology 5 (8), 19-23 (1993).

7. Chu, S. Y., J. Ye and K. Uchino, "Photovoltaic Effect for the Linearly Polarized Light in (Pb,La)(Zr,Ti)O_3 Ceramics," Smart Mater. & Structures 3, 114-117 (1994).

8. Chu, S. Y., Z. Ye and K. Uchino, "Effect of Impurity Doping on Photostrictive Effect in PLZT Ceramics," J. Advanced Performance Mater. Vol.1, 129-143 (1994).

9. Uchino, K., "Worldwide Research and Development of Ceramic Actuators," New Ceramics (TCI, Tokyo) Vol.7(11), 5-13 (1994).

10. Chu, S. Y., M. L. Mulvihill, Z. Ye and K. Uchino, "Bulk Photovoltaic Effect for the Linearly Polarized Light in $Pb(Zn_{1/3}Nb_{2/3})O_3$ Single Crystals," Jpn. J. Appl. Phys. Vol.34, 527-529 (1995).

11. Uchino, K., "Electrooptic Ceramics and Their Display Applications," Ceramics International Vol.21, 309-315 (1995).

12. Chu, S. Y. and K. Uchino, "Photostrictive Effect in PLZT-Based Ceramics and Its Applications," Ferroelectrics (in press).

13. Chu, S. Y., Z. Ye and K. Uchino, "Photo-Acoustic Devices Using (Pb,La)(Zr,Ti)O_3-Based Ceramics," J. Jpn. Ceram. Soc. (1995) (submitted).

PROCEEDINGS ETC.

1. Uchino, K., "Piezoelectric Ceramics in Smart Actuators and Systems," Proc. 1st European Conf. on Smart Structures and Materals, 177-180 (1992).

2. Uchino, K., "Applications of Piezoelectric Ceramics in Smart Actuators and Systems," Proc. Conf. on Active Materials and Adaptive Structure, IOP Pub. 229-230 (1992).

3. Uchino, K., "Recent Development of Piezoelectric Actuators for Adaptive Structures," Proc. 3rd Int'l Conf. Adaptive Structures, p.245-257, Technomic Pub., PA (1993).

4. Uchino, K. and S. Y. Chu, "Photostriction and Its Applications," Proc. PacRim Amer. Ceram. Soc., Ferroic Materials, 287-293 (1994).

5. Uchino, K., "Piezoelectric Actuators/Ultrasonic Motors -- Their Developments and Markets," Proc. 9th Int'l Symp. Appl. Ferroelectrics p.319-324 (1995).

6. Chu, S. Y. and K. Uchino, "Photo-Acoustic Devices Using (Pb,La)(Zr,Ti)O_3 Ceramics," Proc. 9th Int'l Symp. Appl. Ferroelectrics p.743-745 (1995).

7. Uchino, K., "New Piezoelectric Devices for Smart Actuator/Sonsor Systems," Proc. 4th Int'l Conf. Electronic Ceramics & Appl., p.179-191 (1994).

8. Takahashi, S., Y. Sasaki, S. Hirose and K. Uchino, "Electro-Mechanical Properties of $PbZrO_3$-$PbTiO_3$-$Pb(Mn_{1/3}Sb_{2/3})O_3$ Ceramics Under Vibration-Level Change," Proc. MRS '94 Fall Mtg., Vol.360, p.305-310 (1995).

9. Uchino, K., "Piezoelectric Actuators/Ultrasonic Motors: Their Developments and Markets," Ferroelectricity Newsletter, Vol.3, No.2, p.2-5 (1995).

10. Uchino, K., "Advances in Ceramic Actuator Materials," Mater. Let., Vol.22, 1-4 (1995).

11. Uchino, K., "Photostrictive Actuators and "Photophones"," Proc. Int'l Symp. Microsystems, Intelligent Mater. and Robots, p.193-196 (1995).

D. LIST OF ALL PARTICIPATING SCIENTIFIC PERSONNEL

Russel P. Brodeur	---	Post Doc. (June 1992-May 1994)
Aydin Dogan	---	Post Doc. (Oct. 1994-March 1995)
Hardial Dewan	---	Post Doc. (Sep. 1995-Nov. 1995)
Sheng-Yuan Chu	---	Graduate Student (June 1992-Aug. 1994) **Ph.D. awarded in August, 1994**
Seung-Ryong Song	---	Graduate Student (Sep. 1994-June 1995)
Yun-Han Chen	---	Graduate Student (July 1995-Nov. 1995)
Patcharin Poosanaas	--	Graduate Student (Sep. 1995-Nov. 1995)

5. REPORT OF INVENTIONS

None

6. BIBLIOGRAPHY (June 1,1992 - November 30, 1995)

PEER REVIEWED JOURNALS

1. Uchino, K., "Applications of Piezoelectric Ceramics in Smart Actuators and Systems," J. Industrial Education Soc. Jpn. 40 (2), 28-32 (1992).

2. Uchino, K., "Photostrictive Actuators," Optronics 129, 86-90 (1992).

3. Uchino, K., "Photostrictive Actuators," J. Precision Engr. Jpn. 58, 419-421 (1992).

4. Oh, K. Y., Y. Saito, A. Furuta and K. Uchino, "Piezoelectricity in the Field-Induced Ferroelectric Phase of Lead Zirconate-Based Antiferroelectrics," J. Amer. Ceram. Soc. 75 (4), 795-799 (1992).

5. Furuta, A., K. Y. Oh and K. Uchino, "Shape Memory Ceramics and Their Application to Latching Relays," Sensors and Mater. 3 (4), 205-215 (1992).

6. Goto, H., K. Imanaka and K. Uchino, "Piezoelectric Actuators for Light Beam Scanners,: Ultrasonic Techno 5, 48-51 (1992).

7. Sugawara, Y., K. Onitsuka, S. Yoshikawa, Q. C. Xu, R. E. Newnham and K. Uchino, "Metal-Ceramic Composite Actuators," J. Amer. Ceram. Soc. 75 (4), 996-998 (1992).

8. Uchino, K. and S. Suzuki, "Speakers Utilizing Semiconductive Piezoelectric Monomorph Devices," J. Ceram. Soc. Jpn. 100 (10), 1221-1224 (1992).

9. Uchino, K., N. Y. Lee, T. Toba, N. Usuki, H. Aburatani and Y. Ito, "Changes in the Crystal Structure of RF-Magnetron Sputtered $BaTiO_3$ Thin Films," J. Ceram. Soc. Jpn. 100 (9), 1091-1093 (1992).

10. Uchino, K., "Ceramic Actuators: Principles and Applications," MRS Bull., XVIII (4), 42-48 (1993).

11. Uchino, K., "Applications of Piezoelectrics in Smart Actuator," Bull. Ceram. Soc. Jpn. 28 (6), 559-563 (1993).

12. Uchino, K., "Smart Actuators," Ultrasonic Technology 5 (8), 19-23 (1993).

13. Furuta, A. and K. Uchino, "Dynamic Observation of Crack Propagation in Piezoelectric Multilayer Actuators," J. Amer. Ceram. Soc. 76 (6), 1615-1617 (1993).

14. Aburatani, H., S. Harada, K. Uchino, A. Furuta and Y. Fuda, "Destruction Mechanisms in Ceramic Multilayer Actuators," Jpn. J. Appl. Phys. 33, 3091-3094 (1994).

15. Lee, N. Y., T. Sekine, Y. Ito and K. Uchino, "Deposition Profile of RF-Magnetron Sputtered $BaTiO_3$ Thin Films," Jpn. J. Appl. Phys. Vol.33, 1484-88 (1994).

16. Lee, D., J. Yuk, N. Lee and K. Uchino, "Humidity-Sensitive Properties of Nb_2O_5-Doped $Pb(Zr,Ti)O_3$," Sensor and Mater. 5 (4), 231-240 (1994).

17. Oh, K. Y., K. Uchino and L. E. Cross, "Optical Study of $Ba(Ti,Sn)O_3$ Ceramics," J. Amer. Ceram. Soc. Vol.77(11), 2809-16 (1994).

18. Chu, S. Y., J. Ye and K. Uchino, "Photovoltaic Effect for the Linearly Polarized Light in $(Pb,La)(Zr,Ti)O_3$ Ceramics," Smart Mater. & Structures 3, 114-117 (1994).

19. Chu, S. Y., Z. Ye and K. Uchino, "Effect of Impurity Doping on Photostrictive Effect in PLZT Ceramics," J. Advanced Performance Mater. Vol.1, 129-143 (1994).

20. Takahashi, S., S. Hirose and K. Uchino, "Stability of PZT Piezoelectric Ceramics Under Vibration Level Change," J. Amer. Ceram. Soc. Vol.77(9), 2429-32 (1994).

21. Uchino, K., "Worldwide Research and Development of Ceramic Actuators," New Ceramics (TCI, Tokyo) Vol.7(11), 5-13 (1994).

22. Furuta, A. and K. Uchino, "Destruction Mechanism of Multilayer Ceramic Actuators: Case of Antiferroelectrics," Ferroelectrics Vol.160, 277-285 (1994).

23. Chu, S. Y., M. L. Mulvihill, Z. Ye and K. Uchino, "Bulk Photovoltaic Effect for the Linearly Polarized Light in $Pb(Zn_{1/3}Nb_{2/3})O_3$ Single Crystals," Jpn. J. Appl. Phys. Vol.34, 527-529 (1995).

24. Uchino, K., "Electrooptic Ceramics and Their Display Applications," Ceramics International Vol.21, 309-315 (1995).

25. Uchino, K., "Manufacturing Technology of Multilayered Transducers," Proc. Amer. Ceram. Soc., Manufacture of Ceramic Components, p.81-93 (1995).

26. Mulvihill, M. L., L. E. Cross and K. Uchino, "Low Temperature Dynamic Observation of Relaxor Ferroelectric Domains in Lead Zinc Niobate," J. Amer. Ceram. Soc. Vol.78, 3345-3351 (1996).

27. Lee, N. Y., N. Usuki, T. Sekine, Y. Ito, H. Aburatani and K. Uchino, "Pb/Ti Ratio of RF-Magnetron Sputtered $PbTiO_3$ Thin Films," Jpn. J. Appl. Phys. (1994) (in press).

28. Chu, S. Y. and K. Uchino, "Photostrictive Effect in PLZT-Based Ceramics and Its Applications," Ferroelectrics (in press).

29. Chu, S. Y., Z. Ye and K. Uchino, "Photo-Acoustic Devices Using $(Pb,La)(Zr,Ti)O_3$-Based Ceramics," J. Jpn. Ceram. Soc. (1995) (submitted).

30. Mulvihill, M. L., K. Uchino, Z. Li and W. Cao, "In-situ Observation of the Domain Configurations During the Phase Transitions in Barium Titanate," Phil. Mag. (1995) (submitted).

31. Thakahashi, S., S. Hirose, K. Uchino and K.-Y. Oh, "Electro-Mechanical Characteristics of Lead-Zirconate-Titanate Ceramics Under Vibration-Level Change," Ferroelectrics (1994) (submitted).

32. Mulvihill, M. L., S. E. Park, G. Risch, Z. Li, K. Uchino and T. R. Shrout, " The Role of Processing Variables in the Flux Growth of PZN-PT Relaxor Ferroelectric Single Crystals," Jpn. J. Appl. Phys. (1995) (submitted).

33. Zheng, J., S. Takahashi, S. Yoshikawa, K. Uchino and J. W. C. de Vries, "Heat Generation in Multilayer Piezoelectric Actuators," J. Amer. Ceram. Soc. (1995) (submitted).

34. Koc B., A. Dogan, J. F. Fernandez, R. E. Newnham and K. Uchino, "Accelerometer Application of the Modified Moonie (Cymbal) Transduer," Jpn. J. Appl. Phys. (1995) (submitted).

PROCEEDINGS ETC.

1. Uchino, K., "Piezoelectric Ceramics in Smart Actuators and Systems," Proc. 1st European Conf. on Smart Structures and Materals, 177-180 (1992).

2. Uchino, K., "Applications of Piezoelectric Ceramics in Smart Actuators and Systems," Proc. Conf. on Active Materials and Adaptive Structure, IOP Pub. 229-230 (1992).

3. Uchino, K. and A. Furuta, "Destruction Mechanism of Multilayer Ceramic Actuators," Proc. 8th International Symp. on Appl. Ferroelectrics, 195-198 (1992).

4. Sugawara, Y., K. Onitsuka, S. Yoshikawa, Q. C. Xu, R. E. Newnham and K. Uchino, "Metal-Ceramic Composite Actuators," Proc. ADPA/AIAA/SPIE Conf. on Active Materials and Adaptive Structures, IOP Pub., 143-148 (1992).

5. Uchino, K., "Recent Development of Piezoelectric Actuators for Adaptive Structures," Proc. 3rd Int'l Conf. Adaptive Structures, p.245-257, Technomic Pub., PA (1993).

6. Uchino, K., "Relaxor Ferroelectric Devices," Ferroelectrics, 151 (Proc. 8th Int'l Mtg. Ferroelectricity), p.321-330 (1994).

7. Tressler, J. F., Q. C. Xu, S. Yoshikawa, K. Uchino and R. E. Newnham, "Composite Flextensional Transducers for Sensing and Actuating," Ferroelectrics, Vol 156 (Proc. 8th Int'l Mtg. Ferroelectricity), 67-72 (1994).

8. Uchino, K. and S. Y. Chu, "Photostriction and Its Applications," Proc. PacRim Amer. Ceram. Soc., Ferroic Materials, 287-293 (1994).

9. Uchino, K. and H. Aburatani, "Destruction Detection Techniques for Safety Piezoelectric Actuator Systems," Proc. 2nd Int'l Conf. Intelligent Materials p.1248-56 (1994).

10. Uchino, K., "New Piezoelectric Devices for Smart Actuator/Sonsor Systems," Proc. 4th Int'l Conf. Electronic Ceramics & Appl., p.179-191 (1994).

11. Oh, K. Y., K.Uchino and L.E.Cross, "Electrical Properties and Domain Structures in Ba(Ti,Sn)O_3 Ceramics," Proc. 9th Int'l Symp. Appl. Ferroelectrics p.218-220 (1995).

12. Takahashi, S., S.Hirose, K.Uchino and K.Y.Oh, "Electro-Mechanical Characteristics of Lead-Sirconate-Titanate Ceramics under Vibration-Level Change," Proc. 9th Int'l Symp. Appl. Ferroelectrics p.377-382 (1995).

13. Uchino, K., "Piezoelectric Actuators/Ultrasonic Motors -- Their Developments and Markets," Proc. 9th Int'l Symp. Appl. Ferroelectrics p.319-324 (1995).

14. Aburatani, H., K. Uchino, A. Furuta and Y. Fuda,"Destruction Mechanism and Destruction Detection Technique for Multilayer Ceramic Actuators," Proc. 9th Int'l Symp. Appl. Ferroelectrics p.750-752 (1995).

15. Chu, S. Y. and K. Uchino, "Photo-Acoustic Devices Using (Pb,La)(Zr,Ti)O_3 Ceramics," Proc. 9th Int'l Symp. Appl. Ferroelectrics p.743-745 (1995).

16. Hirose, S., S. Takahashi, K. Uchino, M. Aoyagi and Y. Tomikawa,"Measuring Methods for High-Power Characteristics of Piezoelectric Materials," Prof. MRS, '94 Fall Mtg., Vol.360, p.15-20 (1995).

17. Takahashi, S., Y. Sasaki, S. Hirose and K. Uchino, "Electro-Mechanical Properties of $PbZrO_3$-$PbTiO_3$-$Pb(Mn_{1/3}Sb_{2/3})O_3$ Ceramics Under Vibration-Level Change," Proc. MRS '94 Fall Mtg., Vol.360, p.305-310 (1995).

18. Uchino, K., "Piezoelectric Actuators/Ultrasonic Motors: Their Developments and Markets," Ferroelectricity Newsletter, Vol.3, No.2, p.2-5 (1995).

19. Uchino, K., "Advances in Ceramic Actuator Materials," Mater. Let., Vol.22, 1-4 (1995).

20. Hirose, S., M. Aoyagi, Y. Tomikawa, S. Takahashi and K. Uchino, "High-Power Characteristics at Antiresonance Frequency of Piezoelectric Transducers," Proc. Ultrasonic Int'l, p.1-4 (1995).

21. Uchino, K., "Photostrictive Actuators and "Photophones"," Proc. Int'l Symp. Microsystems, Intelligent Mater. and Robots, p.193-196 (1995).

22. Mulvihill, M. L., L. E. Cross and K. Uchino, "Dynamic Motion of the Domain Configuration in Relaxor Ferroelectric Single Crystals as a function of Temperature and Electric Field," Proc. 8th European Mtg. Ferroelectrics, Ferroelectrics (1995) (in press).

23. Tressler, J. F., J. F. Fernandez, K. Uchino and R. E. Newnham, "Capped Ceramic Hydrophones," Proc. Ultrasonic Symp. (1995) (in press).

BOOKS

1. Advanced Technologies 3; Remarkable Bio Science. Edit. K. Uchino, Morikita Pub. Co., Tokyo (1992).

2. Electronic Ceramics (Partial Charge: Applied Aspects of Piezoelectricity). Trans. Tech. Pub. (1992).

3. Ceramic Data Book '92 (Partial Charge: Recent Development of Ceramic Actuators). Inst. Industrial Manufacturing Technology, Tokyo (1992).

4. Materials Science and Technology (Partial Charge: Vol. II, Chapter 12 - Ferroelectric Ceramics). VCH, Germany (1994).

5. Handbook on New Actuators for Precision Position Control (Partial Charge: Part I, Introduction, Shape Memory Ceramics, Photostrictive Actuators; Part II, Piezoelectric/Electrostrictive Effects), Edit. in Chief K. Uchino. Fuji Technosystem, Tokyo (1994).

6. Applied Solid State Chemistry (Partial Charge: Section 3.3 Pyroelectric and Piezoelectric Materials), Asakura Pub. Co., Tokyo (1994).

7. Encyclopedia of Advanced Materials, Edit. D.Bloor et al. (Partial Charge: Ceramic Actuators), Pergamon, UK (1994).

8. Encyclopedia of Science & Technology (Partial Charge: Inchworm), Maruzen, Tokyo (1995).

CONFERENCE PRESENTATIONS

INVITED

1. Uchino, K., "Novel Actuator Materials: Monomorphs & Photostrictors," ARO Workshop, Materials by Design at Small Dimension, Georgia, May 20-22 (1992).

2. Yoshikawa, S. and K. Uchino, "Recent Development of Multilayer Actuators - Review of Materials and Structures," Amer. Ceram. Soc. 95th Annual Mtg. (SXVII-9-93), Cincinnati, April 18-22 (1993).

3. Uchino, K., "Relaxor Ferroelectric Devices," 8th Int'l Mtg. Ferroelectricity, (Inv:26), Gaithersburg, August 8-13 (1993).

4. Uchino, K., "Photostriction and Its Applications," Amer. Ceram. Soc. Pac Rim Conf., Hawaii, November 7-10 (1993).

5. Uchino, K., "Manufacturing Technology of Multilayered Transducers," Amer. Ceram. Soc., Symp. Design for Manufacturability and Manufacture of Ceramic Components, Indianapolis, April 24-28 (1994).

6. S.Takahashi, S.Hirose, K.Uchino and K.Y.Oh, "Electro-Mechanical Characteristics of PZT under High Vibration Level," 9th Int'l Symp. Appl. Ferroelectrics, State College, August 7-10 (1994).

7. K. Uchino, "Piezoelectric Actuators/Ultrasonic Motors -- Their Developments and Markets," 9th Int'l Symp. Appl. Ferroelectrics, State College, August 7-10 (1994).

8. K.Uchino, "New Piezoelectric Devices for Smart Actuator/Sonsor Systems," 4th Int'l Conf. Electronic Ceram. & Appl., Aachen, Germany, Sept.5-7 (1994).

9. Takahashi, S., S. Hirose and K. Uchino,"Piezoelectric Characteristics in PZT Under High Vibration Level," Amer. Ceram. Soc., Los Angels, Fall (1994).

10. Uchino, K., "New Piezoelectric Devices for Smart Actuator/Sensor Systems," The 4th ASEAN Sci. & Tech. Week, Bangkok, Thailand, Aug.21-Sep.1 (1995).

11. Uchino, K., "Piezoelectric Sensors and Actuators: Overview," Sensors Expo '95, Chicago, Il., Sep. 12-14 (1995).

12. Takahashi, S., S. Hirose and K. Uchino, "Materials for Piezoelectric Actuators," Mtg. Ferroelectric Mater. and Appl. (1995).

13. Uchino, K., "Ceramic Actuators in Smart Systems," 4th Japan Int'l SAMPE Symp. & Exhibition, Tokyo, Japan, Sept. 25-28 (1995).

14. Uchino, K., "Photostrictive Actuators and "Photophones"," Int'l Symp. on Microsystems, Intelligent Mater. and Robots, IM1-1, Sendai, Japan, Sept. 27-28 (1995).

15. Uchino, K., "Photostrictive Actuators and "Photophones", " 7th US-Japan Seminar on Dielectric and Piezoelectric Ceramics, V-2, Tsukuba, Japan, Nov.14-17 (1995).

16. Uchino, K., "Novel Actuator Materials," 1st US-Japan Workshop on Smart Mater. and Structures, Seattle, Washington, Dec. 4-5 (1995).

CONTRIBUTED

1. Uchino, K., M. L. Mulvihill and R. P. Brodeur, "Dynamical Observation of the Domain Movement in Relaxor Ferroelectrics," Amer. Ceram. Soc., (II-S VIII-92), Minnesota, April 13-15 (1992).

2. Uchino, K., "Piezoelectric Ceramics in Smart Actuators and Systems," First European Conf. Smart Structures and Materials, Glasgow, May 12-14 (1992).

3. Uchino, K. and A. Furuta, "Destruction Mechanism of Multilayer Ceramic Actuators," Int'l. Symp. Appl. Ferroelectrics '92, South Carolina, August 31-September 2 (1992).

4. Uchino, K., "Piezoelectric/Electrostrictive Actuators - Tutorial Lecture," 3rd Smart Actuator Symp., State College, October 22-23 (1992).

5. Uchino, K., "Fabrication Processes and Actuator Characteristics: Introduction," 4th Smart Actuator Symp., State College, January 21-22 (1993).

6. Uchino, K., "Electrodes for Ceramic Actuators," 4th Smart Actuator Symp., State College, January 21-22 (1993).

7. Uchino, K., "Fabrication of Multilayer Piezoelectric Actuators," 4th Smart Actuator Symp., State College, January 21-22 (1993).

8. Uchino, K., "Optical Domain Studies," ONR Transduer Materials Review, State College, April 6-8 (1993).

9. Tressler, J. F., Q. C. Xu, S. Yoshikawa, K. Uchino and R. E. Newnham, "Composite Flextensional Transducers for Sensing and Actuating," Amer. Ceram. Soc. 95th Annual Mtg. (SXVII-3-93), Cincinnati, April 18-22 (1993).

10. Dogan, A., Q. C. Xu, S. Yoshikawa, K. Uchino and R. E. Newnham, "High-Displacement Ceramic Composite Actuators (Moonies)," Amer. Ceram. Soc. 95th Annual Mtg. (SXVII-4-93), Cincinnati, April 18-22 (1993).

11. Onitsuka, K., A. Dogan, J. F. Tressler, Q. C. Xu, S. Yoshikawa, K. Uchino and R. E. Newnham, "Design Optimization for Metal-Ceramic Composite Actuator," Amer. Ceram. Soc. 95th Annual Mtg. (SXVII-6-93), Cincinnati, April 18-22 (1993).

12. Dogan, A., S. Sentz, S. Yoshikawa, Q. C. Xu, B. R. Tittmann, K. Uchino and R. E. Newnham, "Bonding in Metal-Ceramic Composite Actuators (Moonies)," Amer. Ceram. Soc. 95th Annual Mtg. (SXVII-7-93), Cincinnati, April 18-22 (1993).

13. Uchino, K., "Novel Ceramic Actuator Materials," Amer. Ceram. Soc. 95th Annual Mtg. (SXVII-12-93), Cincinnati, April 18-22 (1993).

14. Chu, S. Y., K. Uchino and Z. Ye, "Photostrictive Effect in Doped PLZT Ceramics," Amer. Ceram. Soc. 95th Annual Mtg. (SXVII-21-93), Cincinnati, April 18-22 (1993).

15. Brodeur, R. P., C. O. Ruud and K. Uchino, "Non-Uniform Electrical Field-Induced Strain in Semiconducting Lead Zirconate-Based Ceramics," Amer. Ceram. Soc. 95th Annual Mtg. (SXVIIP-13-93), Cincinnati, April 18-22 (1993).

16. Aburatani, H., K. Uchino and S. Harada, "Destruction Mechanism of Multilayer Ceramic Actuators," Amer. Ceram. Soc. 95th Annual Mtg. (SXVIIP-17-93), Cincinnati, April 18-22 (1993).

17. Mulvihill, M. L., L. E. Cross and K. Uchino, "Low Temperature Dynamic Observation of Felaxor Ferroelectric Domains," Amer. Ceram. Soc. 95th Annual Mtg. (SXVIIP-19-93), Cincinnati, April 18-22 (1993).

18. Oh, K. Y., K. Uchino, L. E. Cross, B. M. Kulwicki and A. Amin, "Dynamic Observation of Domain Motion in Ferroelectric Polycrystalline Ceramics," Amer. Ceram. Soc. 95th Annual Mtg. (SXVIIP-21-93), Cincinnati, April 18-22 (1993).

19. Ye, Z., S. Y. Chu, C. Gu and K. Uchino, "Spatial Light Modulator Using Photostrictive Ceramics," Amer. Ceram. Soc. 95th Annual Mtg. (EP-13-93), Cincinnati, April 18-22 (1993).

20. Lee, N. Y., N. Usuki, K. Uchino and Y. Ito, "Pb/Ti Ratio of the RF-Magnetron Sputtered $PbTiO_3$ Thin Films," Amer. Ceram. Soc. 95th Annual Mtg. (E-76-93), Cincinnati, April 18-22 (1993).

21. Dogan, A., Q. C. Xu, K. Onitsuka, S. Yoshikawa, K. Uchino and R. E. Newnham, "High-Displacement Ceramic Composite Actuators (Moonies)," 8th Int'l. Mtg. Ferroelectricity (P2:203), Gaithersburg, Ausust 8-13 (1993).

22. Tressler, J. F., Q. C. Xu, S. Yoshikawa, K. Uchino and R. E. Newnham, "Composite Flextensional Transducers for Sensing and Actuating," 8th Int'l. Mtg. Ferroelectricity (P2:218), Gaithersburg, Ausust 8-13, 1993.

23. Uchino, K., "Introduction to Piezoelectric Actuators/ Ultrasonic Motors," 7th Smart Actuator Symp., State College, October 21-22 (1993).

24. Uchino, K., M. L. Mulvihill, K. Y. Oh, R. Brodeur and L. E. Cross, "Optical Studies of Domains in Ferroelectric Actuators," US-JPN Ceram. Seminar, Hawaii, November 11-12 (1993).

25. Aburatani, H., K. Uchino, S. Harada, A. Furuta and Y. Fuda, "Destruction Mechanisms of Multilayer Piezoelectric Acturators," Symp. Ultrasonic and Electronics, Yokohama, December 7-9 (1993).

26. Uchino, K., "Drive/Control Techniques of Ceramic Actuators: General Review," 8th Smart Actuator Symp., State College, January 20-21 (1994).

27. Uchino, K., "Control Techniques of Ultrasonic Motors," 8th Smart Actuator Symp., State College, January 20-21 (1994).

28. Uchino, K., "Active/Passive Vibration Damping," 8th Smart Actuator Symp., State College, January 20-21 (1994).

29. Oh, K. Y. and K. Uchino, "Shape Memory Ceramic Actuators," 8th Smart Actuator Symp., State College, January 20-21 (1994).

30. Oh, K. Y., L. E. Cross and K. Uchino, "Observation of Domain Structures in Ba(Ti,Sn)O3 Ceramics," Amer. Ceram. Soc. 96th Annual Mtg. (SVI-35-94), Indianapolis, April 24-28 (1994).

31. Mulvihill, M. L., L. E. Cross and K. Uchino, "Dynamic Observation of the Domain Configuration in Lead Mangesium Niobate and Lead Zinc Niobate Single Crystals," Amer. Ceram. Soc. 96th Annual Mtg. (SVI-45-94), Indianapolis, April 24- 28 (1994).

32. Ye, Z., S. Y. Chu and K. Uchino, "Ring-Disc-Type Ultrasonic Motors," Amer. Ceram. Soc. 96th Annual Mtg. (SVI-41-94), Indianapolis, April 24- 28 (1994).

33. Mulvihill, M. L., L.E.Cross and K.Uchino, "Dynamic Domain Observation in Relaxor Ferroelectrics," '94 ONR Transducer Materials and Transducers Workshop, State College, April 11-13 (1994).

34. Uchino, K., S.Takahashi and Z.Ye, "Compact Piezoelectric Ultrasonic Motors," '94 ONR Transducer Materials and Transducers Workshop, State College, April 11-13 (1994).

35. Dogan, A., S.Yoshikawa, K.Uchino and R.E.Newnham,"Flextensional "Moonie" Actuator: New Endcap Design and Reliability," '94 ONR Transducer Materials and Transducers Workshop, State College, April 11-13 (1994).

36. Oh, K.Y., K.Uchino and L.E.Cross, "Optical Study of Ba(Ti,Sn)O3 Ceramics," 9th Smart Actuator Symp., State College, April 20-21 (1994).

37. Mulvihill, M. L., L.E.Cross and K.Uchino, "Domain Reversal Mechanisms in Rhombohedral Relaxor Ferroelectrics," 9th Smart Actuator Symp., State College, April 20-21 (1994).

38. Aburatani, H. and K. Uchino "Destruction Mechanisms of Multilayer Actuators," 9th Smart Actuator Symp., State College, April 20-21 (1994).

39. Uchino, K. and H.Aburatani, "Destruction Detection Techniques for Safety Piezoelectric Actuator Systems," 2nd Int'l Conf. Intelligent Mater., Williamsburg, June 6-8 (1994).

40. Oh, K. Y., K.Uchino and L.E.Cross, "Electrical Properties and Domain Structures in Ba(Ti,Sn)O3 Ceramics," 9th Int'l Symp. Appl. Ferroelectrics, State College, August 7-10 (1994).

41. Mulvihill, M. L., L.E.Cross and K.Uchino, "Dynamic Observation of the Domain Configuration in Lead Magnesium Niobate and Lead Zinc Niobate Relaxor Ferroelectric Single Crystals," 9th Int'l Symp. Appl. Ferroelectrics, State College, August 7-10 (1994).

42. Aburatani, H. and K.Uchino,"Destruction Mechanism and Destruction Detection Technique for Multilayer Ceramic Actuators," 9th Int'l Symp. Appl. Ferroelectrics, P4-9, State College, August 7-10 (1994).

43. Chu, S.Y., Z.Ye and K.Uchino,"Photo-Acoustic Devices Using PLZT-Doped Ceramics," 9th Int'l Symp. Appl. Ferroelectrics, P4-7, State College, August 7-10 (1994).

44. Tressler, J.F., Q.C.Xu, S.Yoshikawa, K.Uchino and R.E.Newnham,"Composite Flextensional Transducers for Sensing and Actuating," 9th Int'l Symp. Appl. Ferroelectrics, P4-11, State College, August 7-10 (1994).

45. Dogan, A., S.Yoshikawa, K.Uchino and R.E.Newnham, "Reliability of Flextensional Moonie Actuator," 9th Int'l Symp. Appl. Ferroelectrics, P4-12, State College, August 7-10 (1994).

46. Dogan, A., K.Uchino and R.E.Newnham, "Reliability of Ceramic-Metal Composite Actuator "Moonie"," 4th Int'l Conf. Electronic Ceram. & Appl., Aachen, Germany, Sept.5-7 (1994).

47. Uchino, K., "Introduction to Ceramic Actuators," 11th Smart Actuator Symp., State College, October 24-25 (1994).

48. Uchino, K., "Ultrasonic Motors-Overview," 12th Smart Actuator Symp., State College, October 26-27 (1994).

49. Uchino, K., "How to Design Ultrasonic Motors," 12th Smart Actuator Symp., State College, October 26-27 (1994).

50. Uchino, K., S. Takahashi, S. Hirose and J. Zheng, "Drive Voltage Dependence of Electro-mechanical Coupling in Piezoelectric Ceramics," Mat. Res. Soc., I1-1.5, Boston, November 28-December 2 (1994).

51. Hirose, S., S. Takahashi and K. Uchino, "Measuring Methods for High-Power Characteristics of Piezoelectric Materials," Mat. Res. Soc., I1-1.6, Boston, November 28-December 2 (1994).

52. Oh, K. Y., H. Yamamoto, K. Uchino and L. E. Cross, "Optical Study of Domains in Antiferroelectric Ceramics," Mat. Res. Soc., I1-1.8, Boston, November 28-December 2 (1994).

53. Chu, S. Y. and K. Uchino, "Photostrictive Effect in PLZT-Based Ceramics and Its Applications," Mat. Res. Soc., I1-2.9, Boston, November 28-December 2 (1994).

54. Zheng, J., H. Yamamoto, P. Moses, S. Takahashi and K. Uchino, "Uniaxial Stress Dependence of Piezostriction," Mat. Res. Soc., I1-7.11, Boston, November 28-December 2 (1994).

55. Takahashi, S., S. Hirose and K. Uchino, "Electro-Mechanical Properties of $PbZrO_3$-$PbTiO_3$-$Pb(Mn_{1/3}Sb_{2/3})O_3$ Under Vibration-Level Change," Mat. Res. Soc., I1-7.12, Boston, November 28-December 2 (1994).

56. Uchino, K., "Remaining Theoretical Problems in Ceramic Actuators," ONR Workshop on Fundamental Ferroelectrics, Williamsburg, February 5-8 (1995).

57. Fielding, J. T. Jr., J. F. Fernandez, A. Dogan, K. Uchino and R. E. Newnham, "Characterization of Ceramic-Metal Composite Transducer with Multilayer Piezoceramic Element," Amer. Ceram. Soc. 97th Annual Mtg., E-8, Cincinnati, Ohio, Apr.30-May 3 (1995).

58. Fernandez, J. F., A. Dogan, J. Tressler, J. T. Fielding, K. Uchino and R. E. Newnham, "Temperature Dependence of High Displacement Ceramic-Metal Composite Actuators," Amer. Ceram. Soc. 97th Annual Mtg., E-10, Cincinnati, Ohio, Apr.30-May 3 (1995).

59. Zheng, J., S. Takahashi, S. Yoshikawa, K. Uchino and J.W.C. de Vries, "Heat Generation in Multilayer Piezoelectric Actuators ," Amer. Ceram. Soc. 97th Annual Mtg., E-14, Cincinnati, Ohio, Apr.30-May 3 (1995).

60. Aburatani, H. and K. Uchino, "New Internal Electrode Designs for Multilayer Ceramic Actuators," Amer. Ceram. Soc. 97th Annual Mtg., EP-46, Cincinnati, Ohio, Apr.30-May 3 (1995).

61. Joshi, A., S. Hirose, S. Takahashi and K. Uchino, "High Power Characteristics of Piezoelectric Materials," Amer. Ceram. Soc. 97th Annual Mtg., EP-47, Cincinnati, Ohio, Apr.30-May 3 (1995).

62. Tressler, J. F., K. Uchino and R. E. Newnham, "Ceramic-Metal Composite Transducers for Hydrophone Applications," Amer. Ceram. Soc. 97th Annual Mtg., EP-49, Cincinnati, Ohio, Apr.30-May 3 (1995).

63. Song, S. R. and K. Uchino, "Semiconductive Behavior in the (1-x)Pb $(Zr_{0.9}Ti_{0.1})O_3$-x$(K_{0.5}Bi_{0.5})ZrO_3$ Monomorph Materials," Amer. Ceram. Soc. 97th Annual Mtg., E-65, Cincinnati, Ohio, Apr.30-May 3 (1995).

64. Mulvihill, M. L., L. E. Cross and K. Uchino, "Dynamic Motion of the Domain Configuration in Relaxor Ferroelectric Single Crystals as a Function of Temperature and Electric Field," The 8th European Mtg. Ferroelectricity, P16-08, Nijmegen, July (1995).

65. Hirose, S., M. Aoyagi, Y. Tomikawa, S. Takahashi and K. Uchino, "High-Power Characteristics at Antiresonance Frequency of Piezoelectric Transducers," Ultrasonic Int'l, Edinburgh, July 4-7 (1995).

66. Uchino, K., "Photostrictive Actuators and Their Applications," 4th Japan Int'l SAMPE Symp. & Exhibition, Tokyo, Japan, Sept. 25-28 (1995).

67. Mulvihill, M. L., L. E. Cross and K. Uchino, "Dynamic Motion of the Domain Configuration in Relaxor Ferroelectric Single Crystals as a Function of Temperature and Electric Field," 7th US-Japan Seminar on Dielectric and Piezoelectric Ceramics, IV-18, Tsukuba, Japan, Nov. 14-17 (1995).

68. Dogan, A., K. Uchino and R. E. Newnham, "Unique Flextensional Composite Transducer Designs for Both Sensor and Actuator Applications," 1st US-Japan Workshop on Smart Materials and Structures, Seattle, Washington, Dec. 4-5 (1995).

7. APPENDIXES

PAPERS ON PHOTOSTRICTION

1. Chu, S. Y., Z. Ye and K. Uchino, "Effect of Impurity Doping on Photostrictive Effect in PLZT Ceramics," J. Advanced Performance Mater. Vol.1, 129-143 (1994).

2. Chu, S. Y., J. Ye and K. Uchino, "Photovoltaic Effect for the Linearly Polarized Light in (Pb,La)(Zr,Ti)O_3 Ceramics," Smart Mater. & Structures 3, 114-117 (1994).

3. Uchino, K. and S. Y. Chu, "Photostriction and Its Applications," Proc. PacRim Amer. Ceram. Soc., Ferroic Materials, 287-293 (1994).

4. Chu, S. Y., M. L. Mulvihill, Z. Ye and K. Uchino, "Bulk Photovoltaic Effect for the Linearly Polarized Light in $Pb(Zn_{1/3}Nb_{2/3})O_3$ Single Crystals," Jpn. J. Appl. Phys. Vol.34, 527-529 (1995).

5. Uchino, K., "Electrooptic Ceramics and Their Display Applications," Ceramics International Vol.21, 309-315 (1995).

6. Chu, S. Y. and K. Uchino, "Photo-Acoustic Devices Using (Pb,La)(Zr,Ti)O_3 Ceramics," Proc. 9th Int'l Symp. Appl. Ferroelectrics p.743-745 (1995).

7. Uchino, K., "Photostrictive Actuators and "Photophones"," Proc. Int'l Symp. Microsystems, Intelligent Mater. and Robots, p.193-196 (1995).

8. Chu, S. Y., Z. Ye and K. Uchino, "Photo-Acoustic Devices Using (Pb,La)(Zr,Ti)O_3-Based Ceramics," J. Jpn. Ceram. Soc. (1995) (submitted).

9. Chu, S. Y. and K. Uchino, "Photostrictive Effect in PLZT-Based Ceramics and Its Applications," Ferroelectrics (in press).

10. Uchino, K., "Review: Photostriction and Its Applications," J. Innovations in Mater. Res. (in press).

REVIEW PAPERS ON SMART MATERIALS

11. Uchino, K., "Ceramic Actuators: Principles and Applications," Mater. Res. Soc. Bull. **18**, 42 - 48 (1993).

12. Uchino, K., "New Piezoelectric Devices for Smart Actuator/Sonsor Systems," Proc. 4th Int'l Conf. Electronic Ceramics & Appl., p.179-191 (1994).

13. Uchino, K., "Worldwide Research and Development of Ceramic Actuators," New Ceramics (TCI, Tokyo) Vol.7(11), 5-13 (1994).

14. Uchino, K., "Advances in Ceramic Actuator Materials," Mater. Let., Vol.22, 1-4 (1995).

15. Uchino, K., "Novel Ceramic Actuator Materials," Proc. US/Japan Workshop on Smart Mater. and Structures (in press).

APPENDIXES

PAPERS ON PHOTOSTRICTION

1. Chu, S. Y., Z. Ye and K. Uchino, "Effect of Impurity Doping on Photostrictive Effect in PLZT Ceramics," J. Advanced Performance Mater. Vol.1, 129-143 (1994).

Advanced Performance Materials, 1, 129–143 (1994)

Impurity Doping Effect on Photostriction in PLZT Ceramics

SHENG-YUAN CHU, ZHOU YE AND KENJI UCHINO
International Center for Actuators and Transducers, Materials Research Laboratory, The Pennsylvania State University, University Park, PA 16802

Abstract. Photostriction is the superposition of a photovoltaic and piezoelectric effects. In this study, photostrictive effects in the perovskite (Pb, La) (Zr, Ti)O_3 were investigated as a function of B-site impurity doping. Donor doping was found to reduce both the grain size and room-temperature dielectric constant, influencing photovoltaic response. WO_3 and Ta_2O_5 doping increase the photovoltaic response, but do not significantly affect the piezoelectric effect in this material. Maximum photostriction is obtained for samples with 0.4 at% WO_3 doped or 1 at% Ta_2O_5 doped PLZT

Keywords: doping effect, photostriction effect, photovoltaic effect, PLZT

Introduction

The photovoltaic effect is observed in certain ferroelectrics, wherein a constant electromotive force is induced with application of near-ultraviolet radiation [1]–[3]. This effect was explained by Fridkin et al. in 1974 [4], by Glass et al. [2] and by Brody et al. [5], and probably originated from an excitation of electrons from asymmetric impurity potentials. The main features of the bulk photovoltaic effect are summarized as follows:

1) This effect appears in poled uniform single crystals or ceramics with noncentrosymmetry and is entirely different in nature from the P-N junction effect observed in semiconductors.
2) Constant photo-current and -voltage are generated in the spontaneous polarization direction under uniform illumination in the ferroelectric phase and disappears in the paraelectric phase.
3) The magnitude of the induced voltage is proportional to crystal length in the polarization direction and is much greater than the band gap energy of the crystal.

The expected photostriction effects as a superimposed phenomenon of photovoltaic and piezoelectric effects have been reported in our previous papers [6, 7], and potential applications in photo-driven remote control devices have been proposed [8, 9]. For practical applications, larger strain and quicker response are desired, and materials development and device design are focused on these objectives. One of the authors has firstly pointed out that the PLZT exhibits superior photostrictive effect, and effects of impurity doping in PLZT has also been investigated preliminarily [7].

In this paper, the photostriction effect in PLZT (3/52/48) ceramics is investigated in detail as a function of impurity doping. The effect of doping on grain size and room-temperature dielectric constant are also examined, because the grain size affects the photovoltaic effect [6], and the photovoltage may change with the dielectric constant for the constant photo-induced charge.

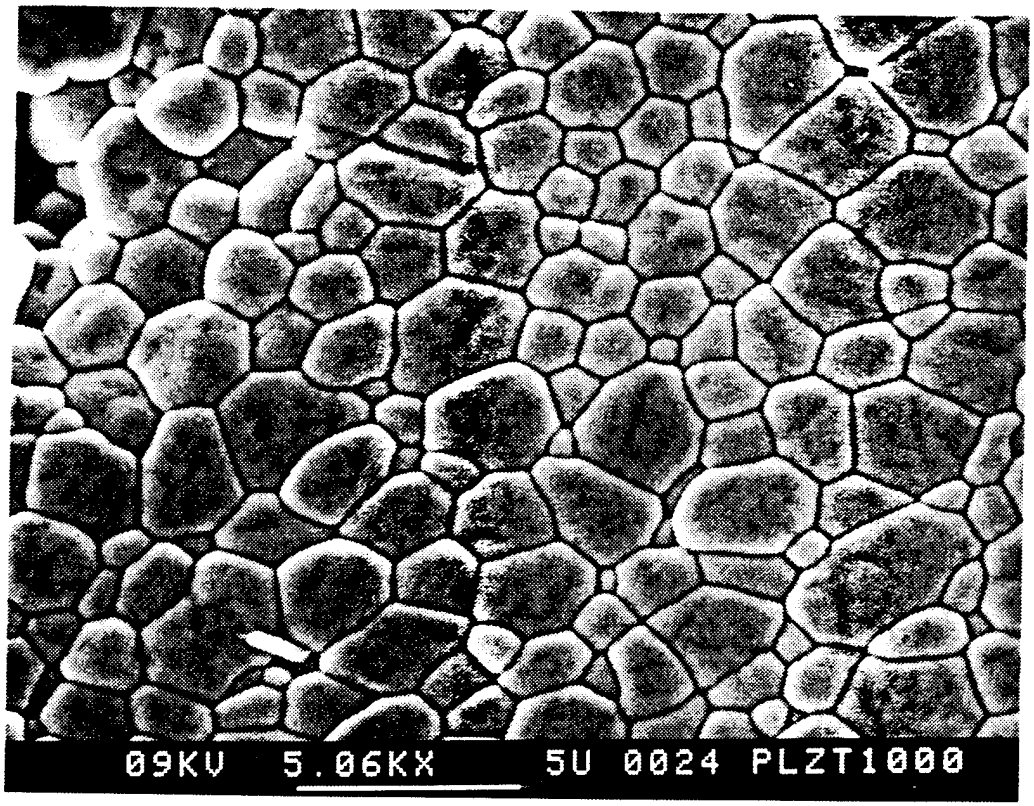

(a)

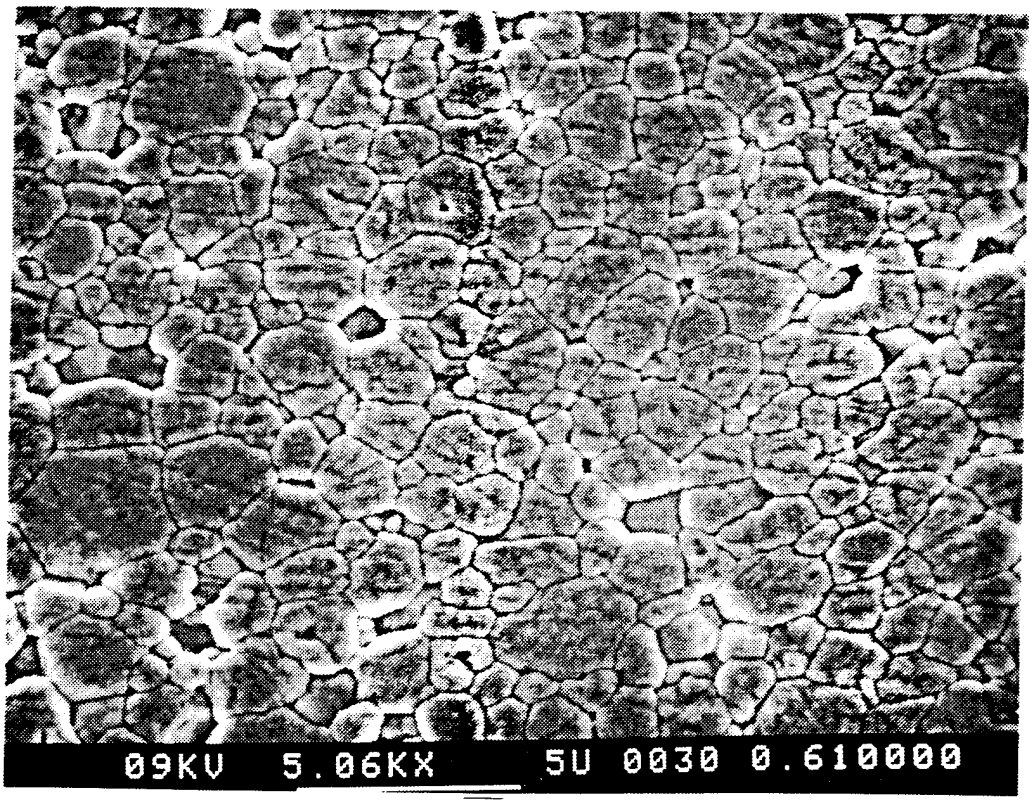

(b)

Figure 1. SEM photomicrographs of thermally-etched samples of (a) PLZT, (b) PLZT-WO_3 and (c) PLZT-Ta_2O_5.

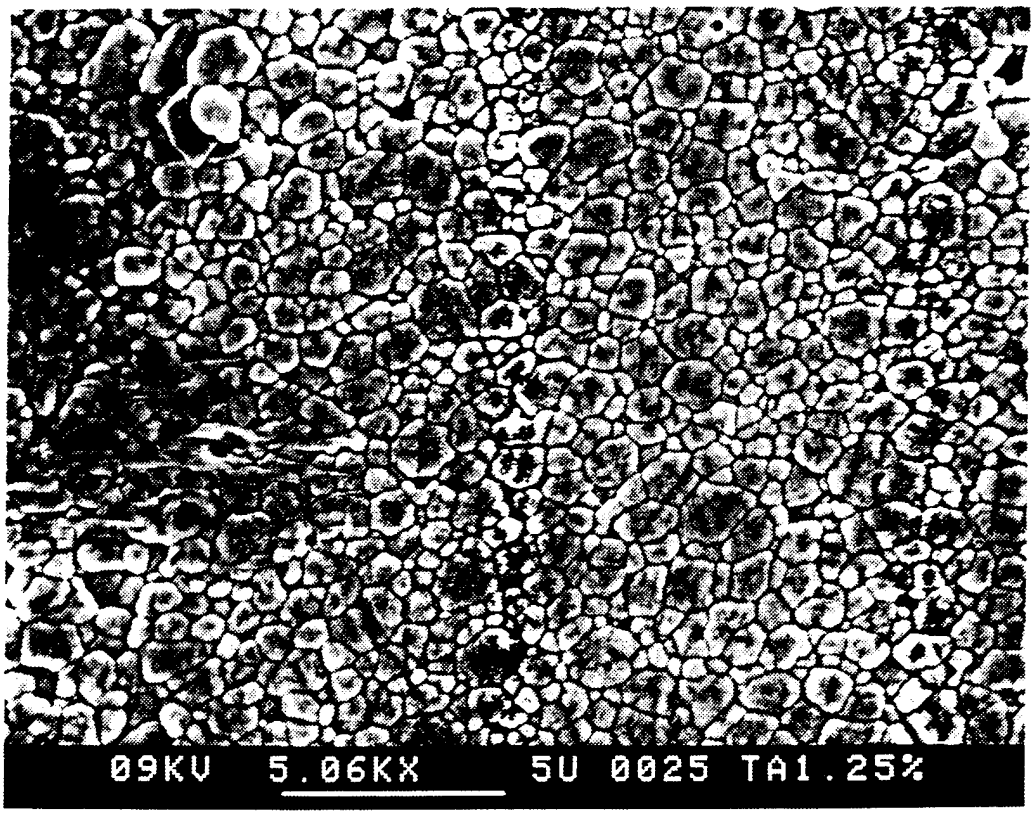

(c)

Sample preparation

PLZT $(x/y/z)$ samples were prepared in accordance with the following composition formula:

$$Pb_{1-y}La_y(Zr_{1-x}Ti_x)_{1-\frac{y}{4}}O_3.$$

PLZT (3/52/48) was selected due to its optimum photostriction ($x_{ph} = d_{33}E_{ph}$) within the PLZT system [6].

The ceramic powder was prepared by a conventional mixed oxide technique. $PbCO_3$, La_2O_3, ZrO_2, TiO_2 and dopant were weighed in the appropriate proportions and mixed in a ball mill for 2 days using ethanol and zirconia grinding media. 0.5 wt% excess $PbCO_3$ was added to compensate for weight loss during calcination and sintering. The slurry was dried, then calcined in a closed crucible at 950°C for 10 hrs. The calcined powder was ball-milled again for 48 hrs. The samples were sintered in sealed alumina crucibles at 1270°C/ 2 hrs. A PbO rich atmosphere was maintained with lead zirconate powder to minimize lead loss during sintering. An x-ray diffractometer did not monitor any secondary phases other than the perovskite structure. Sintered samples were electroded with silver paste. Finally, each sample was cut and poled in silicone oil at 120°C under a 15 kV/cm electric field.

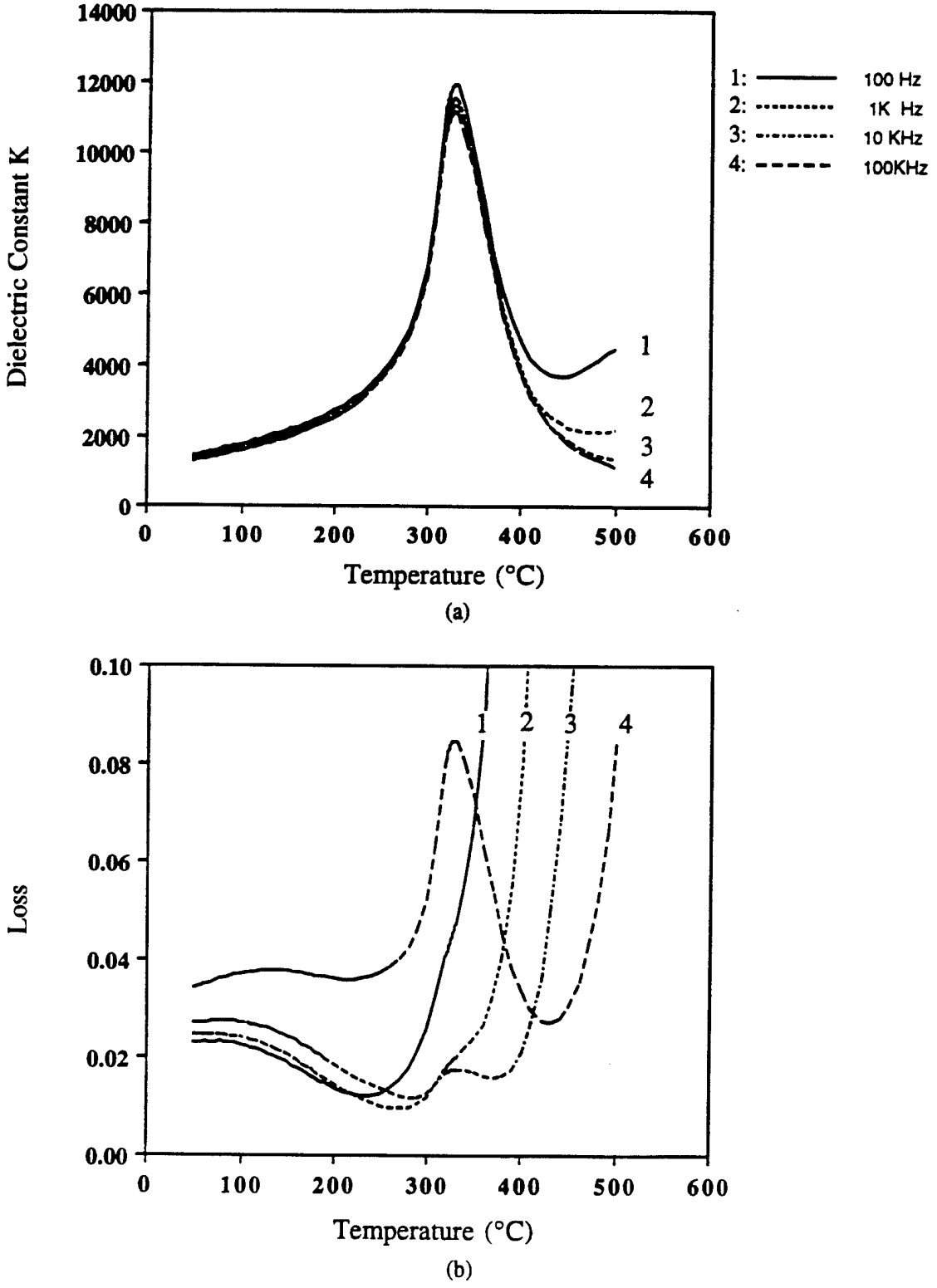

Figure 2. Dielectric constant and loss vs. temperature for PLZT-WO_3 (0.4 at%).

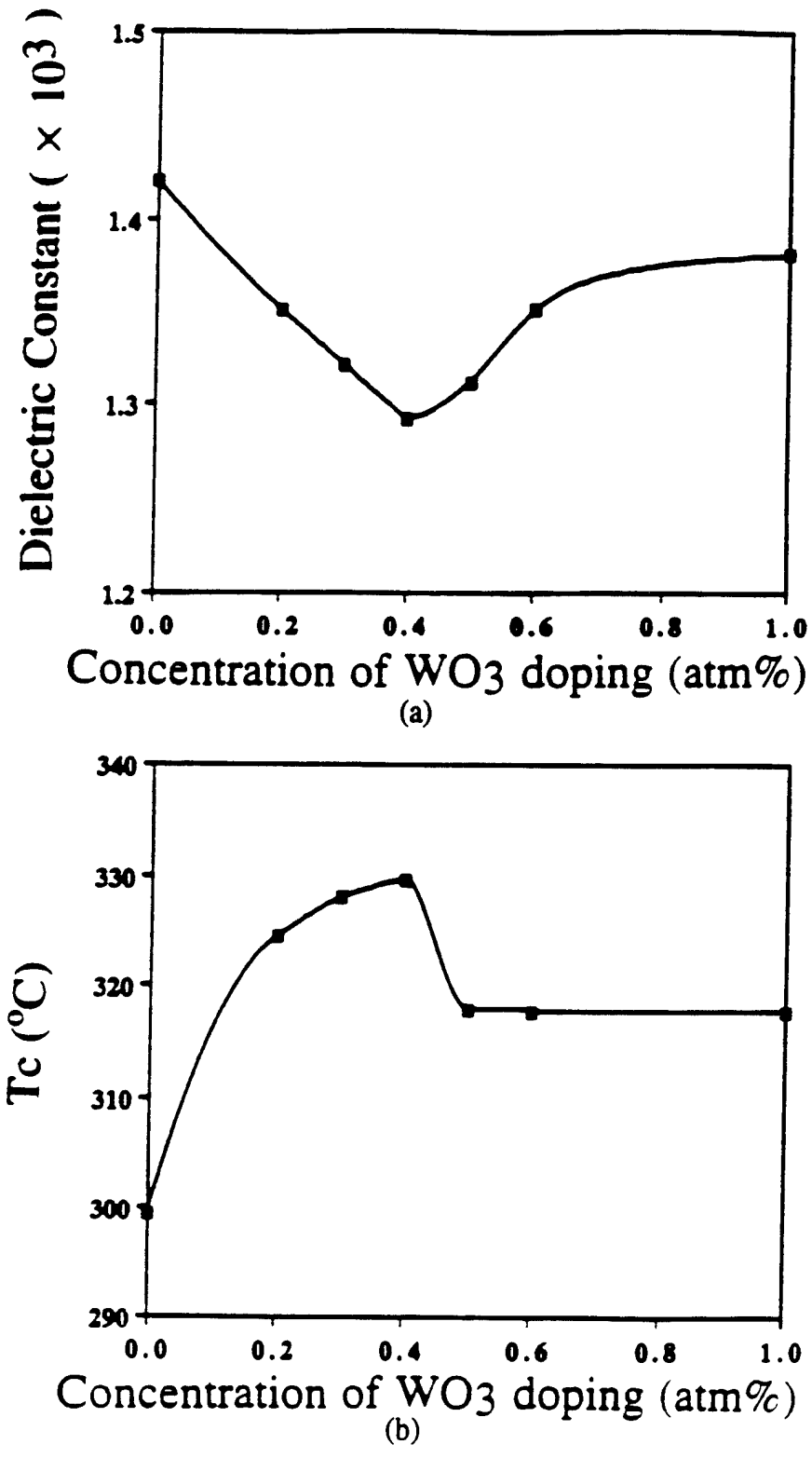

Figure 3. Room-temperature dielectric constant (a) and Curie temperature (b) vs. WO_3 doping level.

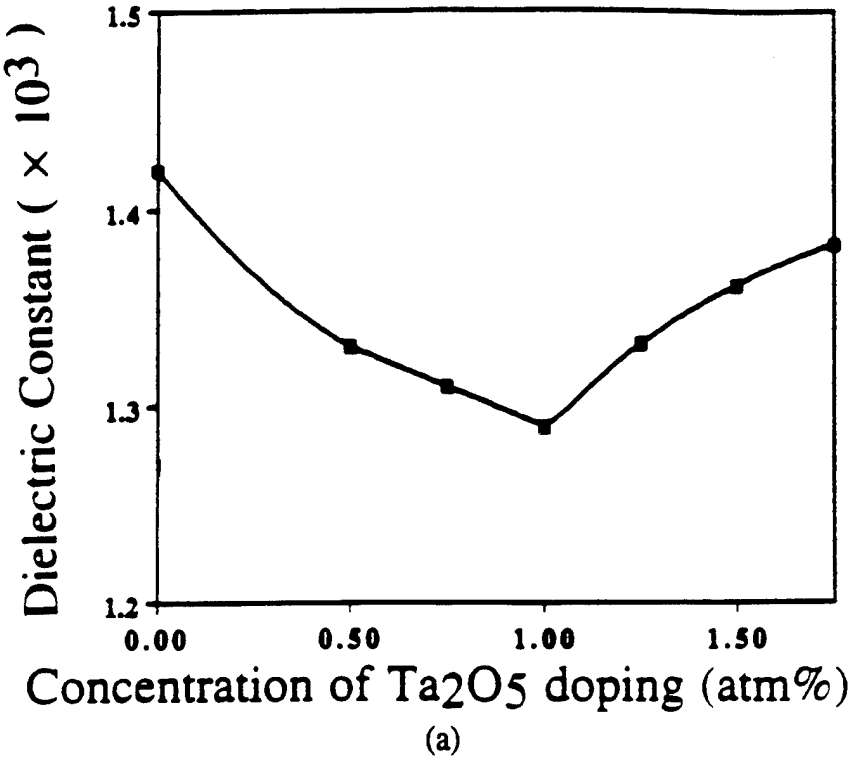

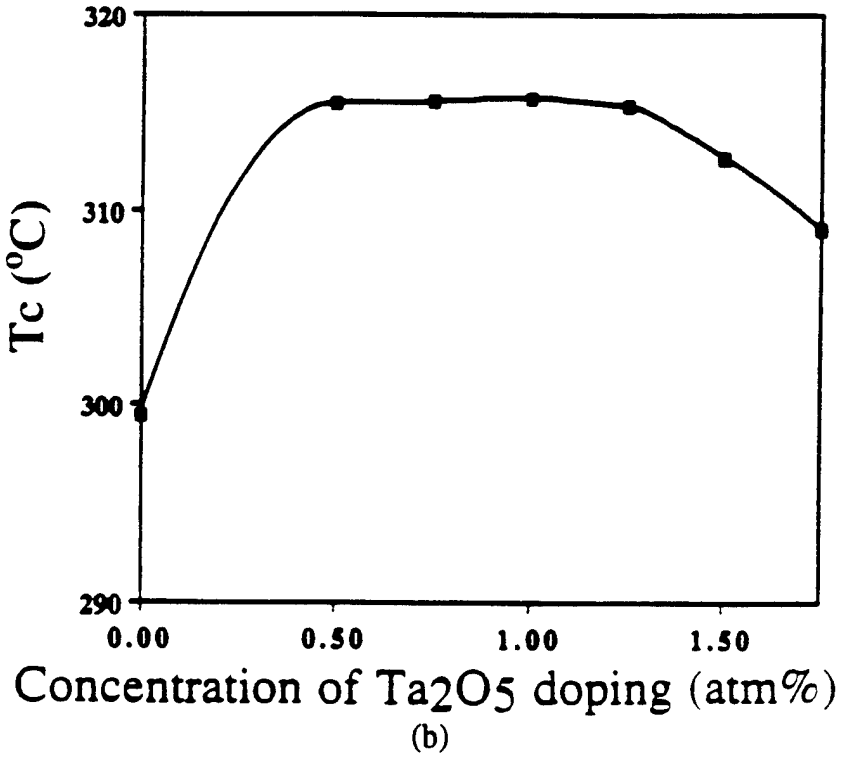

Figure 4. Room-temperature dielectric constant (a) and Curie temperature (b) vs. Ta_2O_5 doping level.

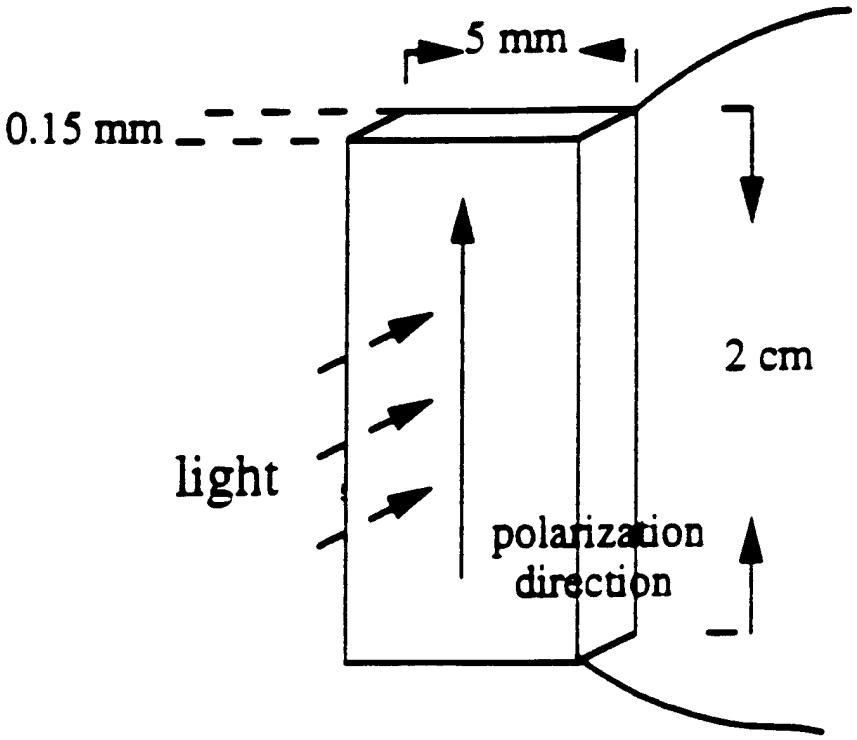

Figure 5. Sample configuration for photovoltaic effect measurements.

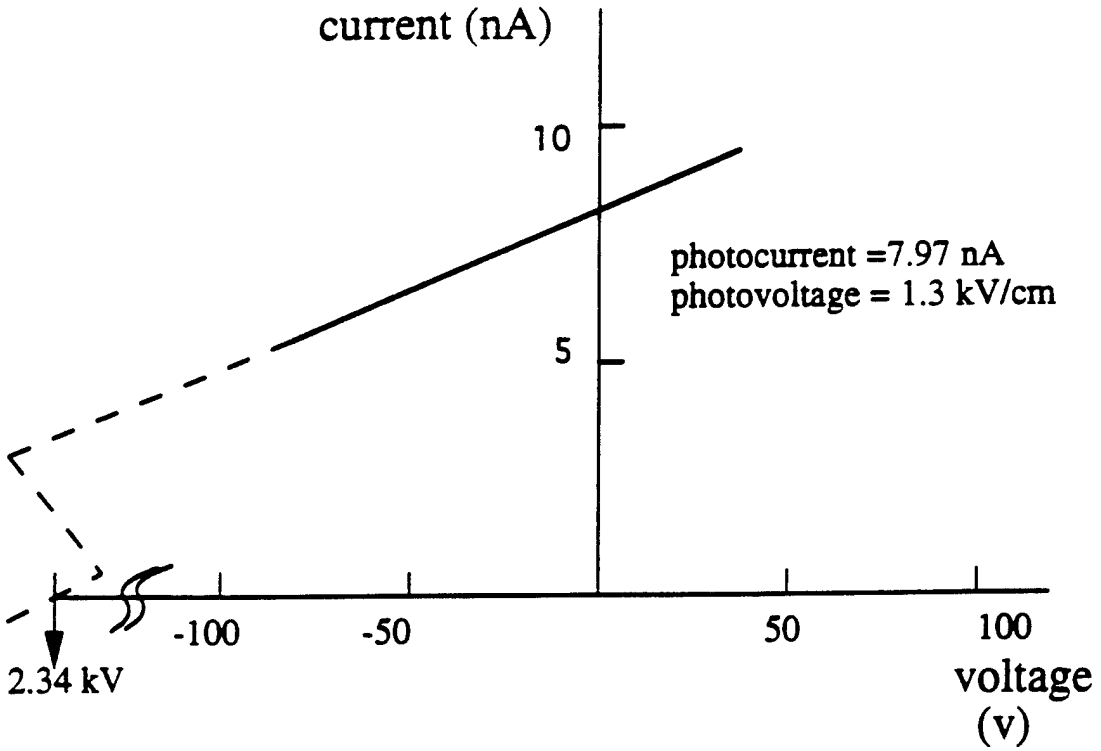

Figure 6. Photocurrent measured as a function of applied voltage for a 0.4% WO_3 doped PLZT sample. Light intensity is 4 mW/cm^2.

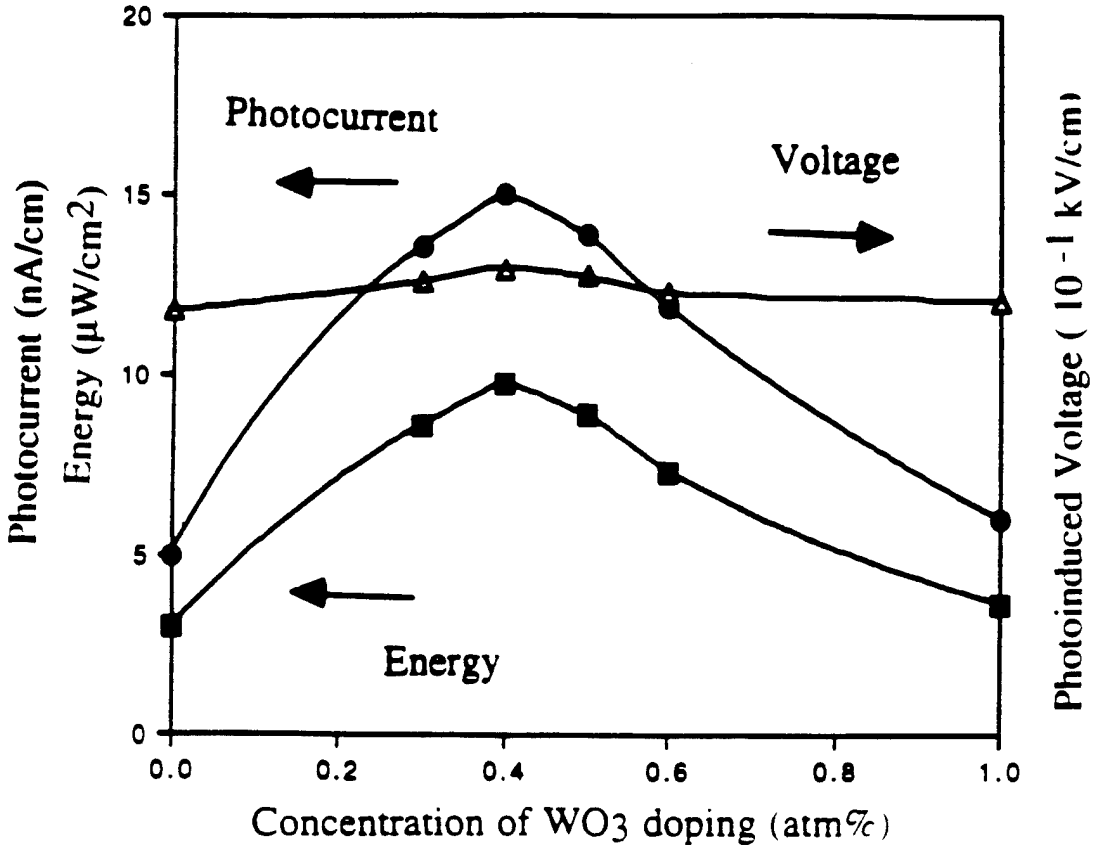

Figure 7. Photovoltaic current, voltage and potential power as a function of dopant concentration in WO_3 doped PLZT.

SEM observation

Figures 1(a), 1(b) and 1(c) show the thermally etched PLZT, PLZT-WO_3 and PLZT-Ta_2O_5 scanning electron microscope (SEM) photomicrographs, respectively. Pure PLZT has the largest grain size; however, it is difficult to determine grain size differences between WO_3 doped and Ta_2O_5 doped samples with different concentration. No additional phase was observed around the grain boundaries.

Dielectric measurements

Samples for dielectric measurements were polished using SiC powders to about 10 mm in diameter and 1 mm in thickness and electroded with sputtered platinum (Pt). Figure 2 shows dielectric constant and loss tan δ behavior as functions of temperature and frequency for 0.4 at% WO_3 doped PLZT. Figure 3(a) shows the change in room-temperature dielectric constant (at 10 kHz) with dopant concentration for WO_3 (0–1.0 at%), and Figure 3(b) shows the dielectric constant maximum temperature, which almost coincides with the Curie temperature (T_c), as a function of WO_3 doping. Consequently, the dielectric constant is

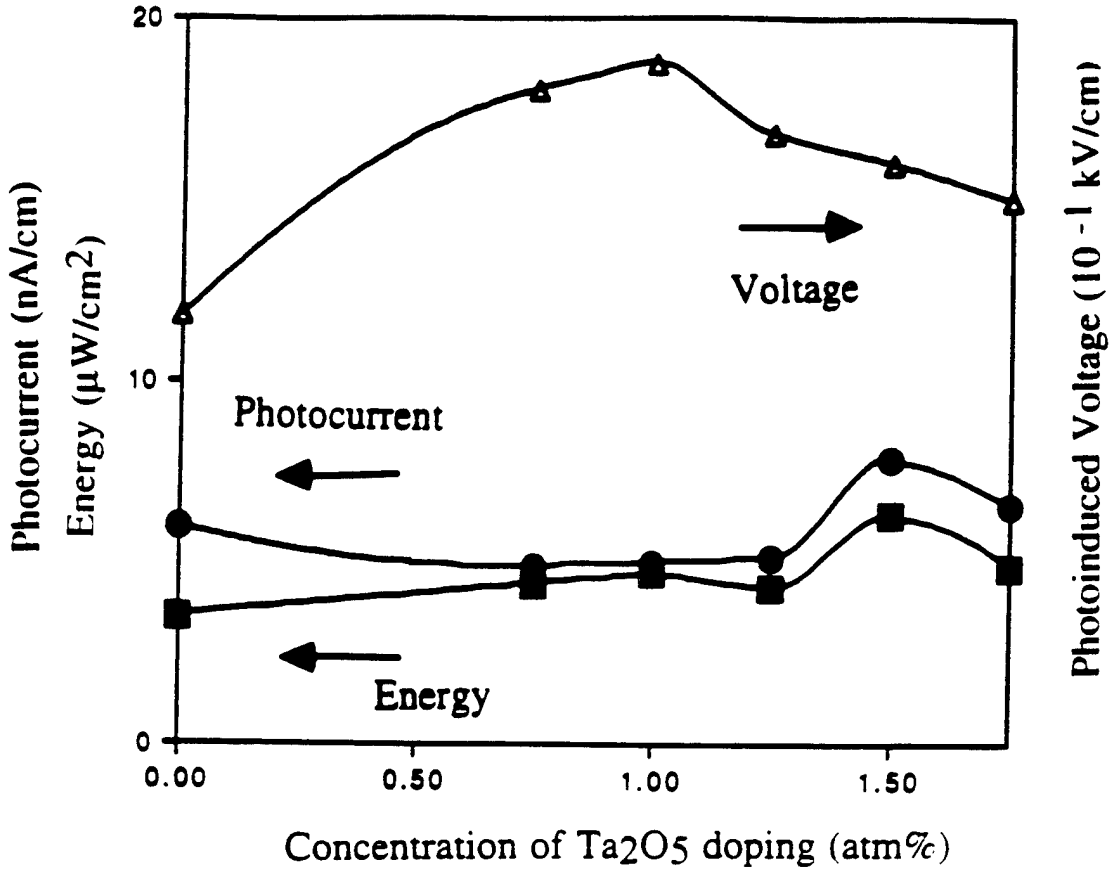

Figure 8. Photovoltaic current, voltage and potential power as a function of dopant concentration of Ta_2O_5 doped PLZT.

minimum at 0.4 atm% WO_3 doping. From Figure 3, it is evident that WO_3 increases T_c and 0.4 at% WO_3 doping shows the maximum Curie temperature.

Figures 4(a) and 4(b) show the changes in the room-temperature dielectric constant (10 kHz) and Curie temperature with Ta_2O_5 doping, respectively. In the case of Ta_2O_5 doping, the maximum Curie temperature and the minimum dielectric constant are obtained at 1.0 at% Ta_2O_5.

We can conclude that a slight donor doping reduces the grain size and shifts the Curie temperature to the higher temperature, as reported by T. Yamamoto et al. [10]. The correlation of these data with the photostriction will be discussed later.

Photovoltaic effect measurements

PLZT (3/52/48) doped with various concentrations of WO_3 and Ta_2O_5 were used for this study. Sample size for this measurement was $20 \times 4 \times 0.15$ mm^3: the 4×0.15 mm^2 surface was electroded with silver paste and silver wires were attached. The configuration of the sample is shown in Figure 5. Radiation from a high-pressure mercury lamp (Ushio

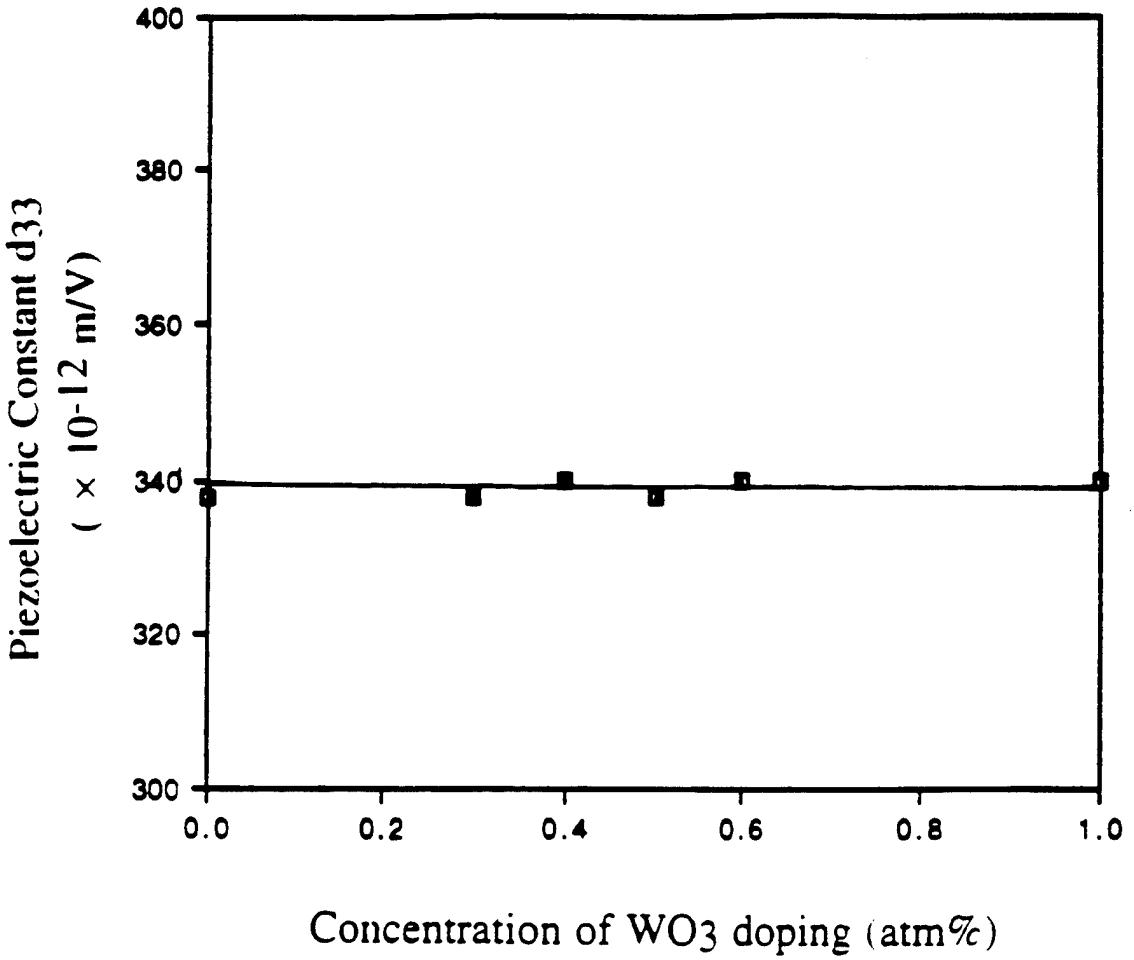

Figure 9. Piezoelectric coefficient (d_{33}) as a function of WO_3 doping.

Electric USH-500D) was passed through a UV bandpass filter (Oriel Co., No. 59811), an IR blocking filter (Oriel Co., No. 59060), and a fused quartz optical focusing lens. The light was almost monochromated to 370 mm, and the intensity was 4 mW/cm^2. Slight temperature increase about 10°C was observed on the sample.

The photovoltaic voltage reaches 1 kV/mm, and the current is on the order of nA. The induced current was measured with a high-input-impedance (200 TΩ) electrometer (Keithley 617) as a function of the external voltage over a range −100 V to + 100 V. The photovoltaic voltage and the current are defined as the maximum open-circuit voltage and short-circuit current, respectively [7]. Upon exposure to UV radiation, a weak pyroelectric current was initially observed, even with the IR blocking filter, and a steady-state photovoltaic current was achieved after several seconds. Measurements were made after the crystals had thermally equilibrated with the radiation to avoid contribution from the pyroelectric effect. The photovoltaic voltage and the current were determined from the intercepts of the horizontal and the vertical axes, respectively. A typical curve is shown in Figure 6 for PLZT doped with 0.4 at% WO_3.

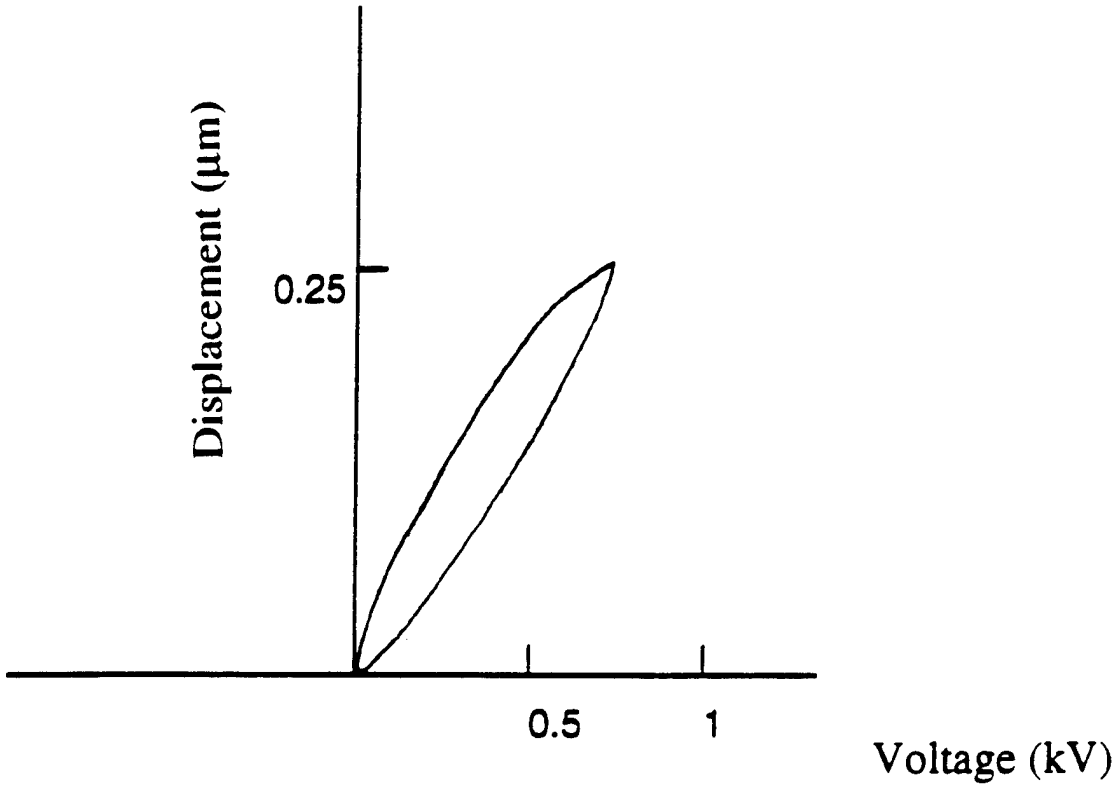

Figure 10. Induced displacement as a function of applied electric field for 0.4% WO_3 doped PLZT. ($t = 0.45$ mm).

Figures 7 and 8 show the photovoltaic current, photovoltaic voltage and stored energy ($P = (1/2)I\max \times V\max$) in PLZT doped with WO_3 and with Ta_2O_5, respectively. Photovoltaic current and voltage show a peak at 0.4 at% for the WO_3 samples, while photovoltaic current and photovoltage show a peak at 1.5 at% and 1 at% for the Ta_2O_5 samples, respectively. It was found that higher photovoltaic current and potential power can be obtained in WO_3 doped samples, while the higher photovoltage can be obtained in Ta_2O_5 doped samples. Notice that the strain magnitude increases as the photovoltaic voltage increases; and with increasing photo-current, there is an increase in the overall response.

Field-induced strain measurements

Since photostriction x_{ph} is defined in terms of the photovoltaic voltage E_{ph} and the piezoelectric coefficient d_{33} as

$$x_{\text{ph}} = d_{33}E_{\text{ph}}, \tag{1}$$

it is increased by increasing the photovoltaic voltage and/or the piezoelectric coefficient.

Samples for induced strain measurements were of the same configurations as for dielectric measurements, except they are electroded with sputtered silver (Ag) and poled in silicone oil at 120°C under a 20 kV/cm electric field. After poling, d_{33} measurements were made using a Berlincourt d_{33} meter (Channel Products, Inc.) at 100 Hz. The measured d_{33}

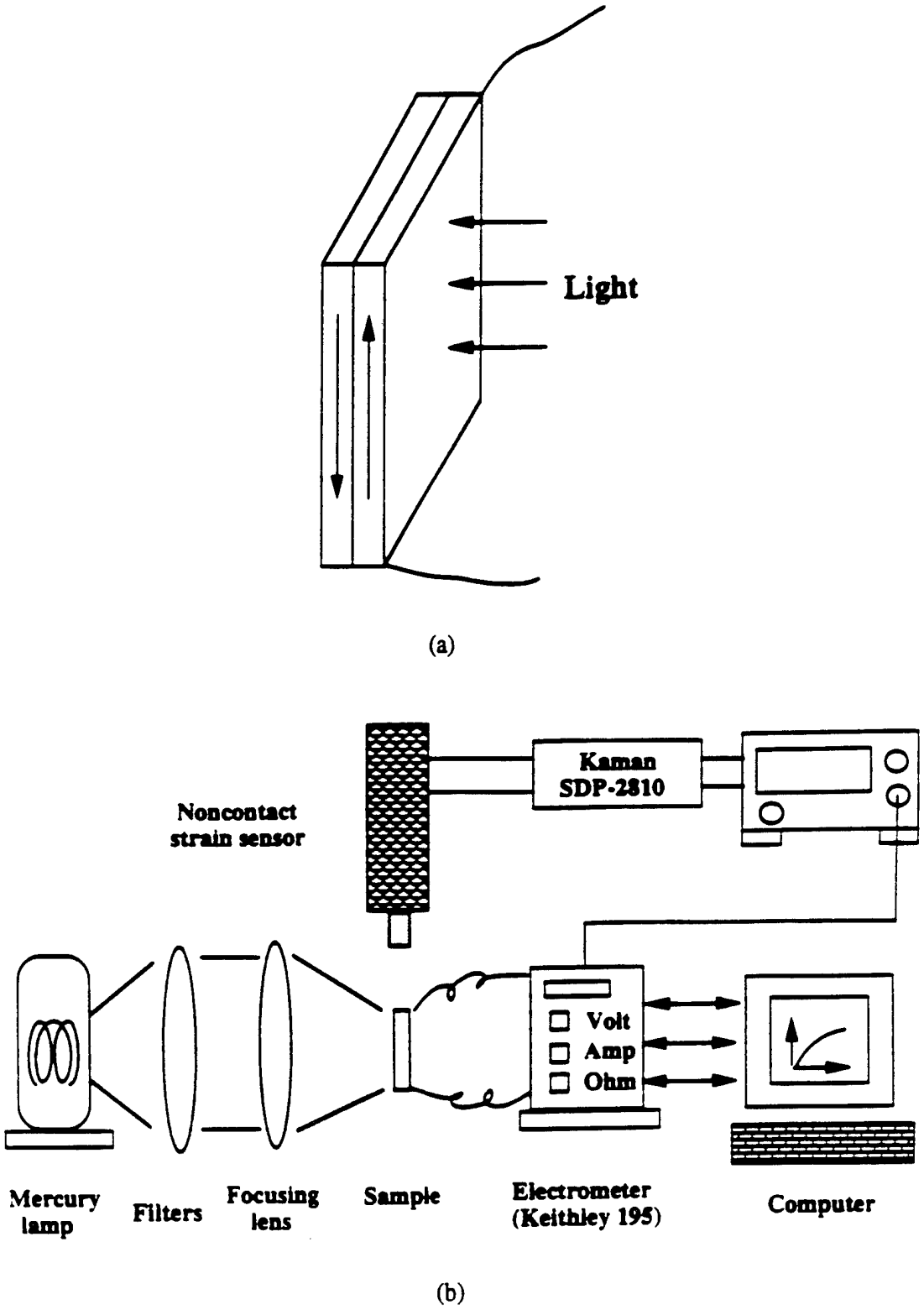

Figure 11. Configuration of bimorph sample (a), and experimental setup (b) for photostrictive-effect measurement.

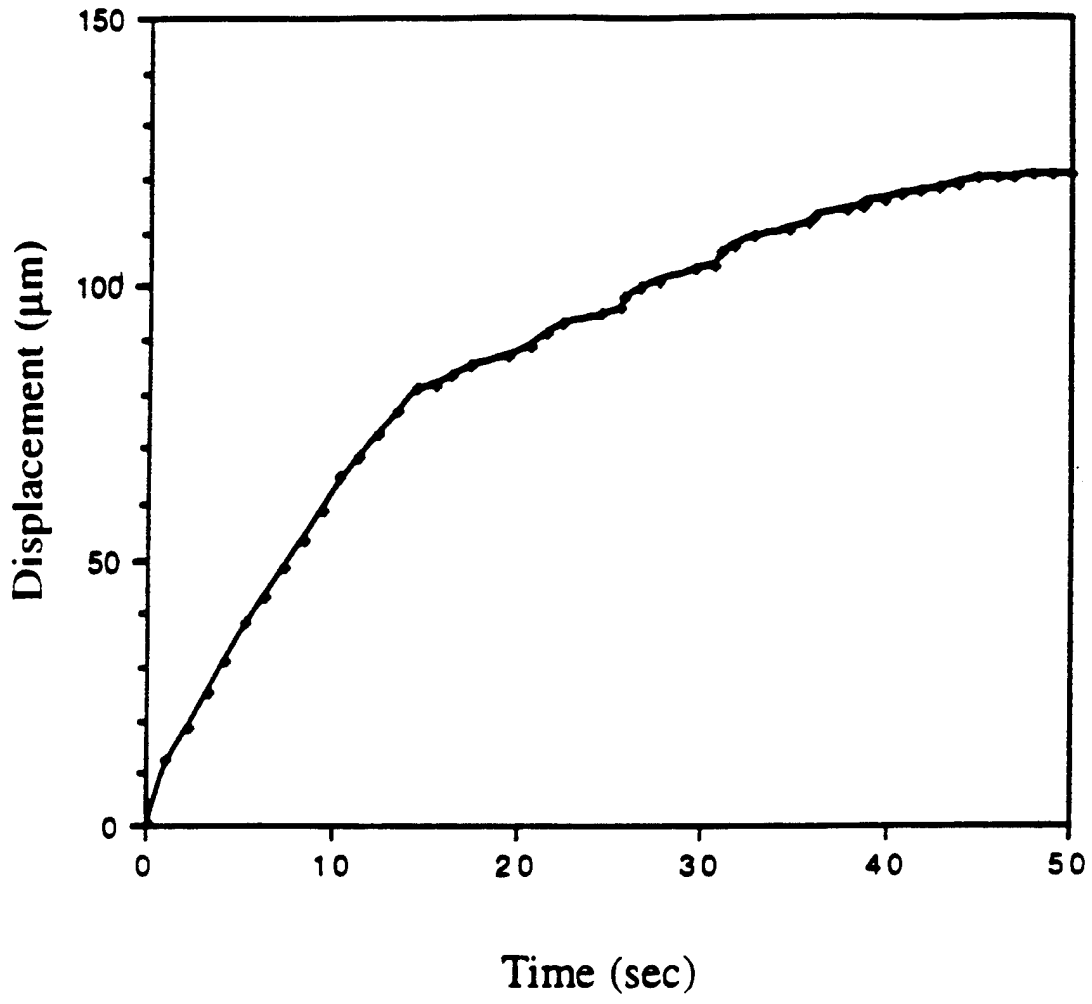

Figure 12. Bimorph deflection of device for 0.4% WO_3 doped PLZT device.

values were about the same for all samples (330×10^{-12} m/V) as seen in Figure 9 for WO_3-doped samples.

The field-induced displacement was also measured (see Figure 10). The average d_{33} constant obtained from the slope is 350×10^{-12} m/V, in good agreement with the Berlincourt meter data.

In spite of impurity doping, the value of the piezoelectric coefficient remains constant, indicating that photostriction is proportional to the photovoltaic voltage for these compositions.

Photostrictive effect measurements

A bimorph design consisting of two oppositely-poled ceramic plates (5 mm × 20 mm × 0.15 mm in size) was used for photostrictive-effect measurements. The configuration of the samples is shown in Figure 11(a). The displacement at the tip of this photostrictive bi-

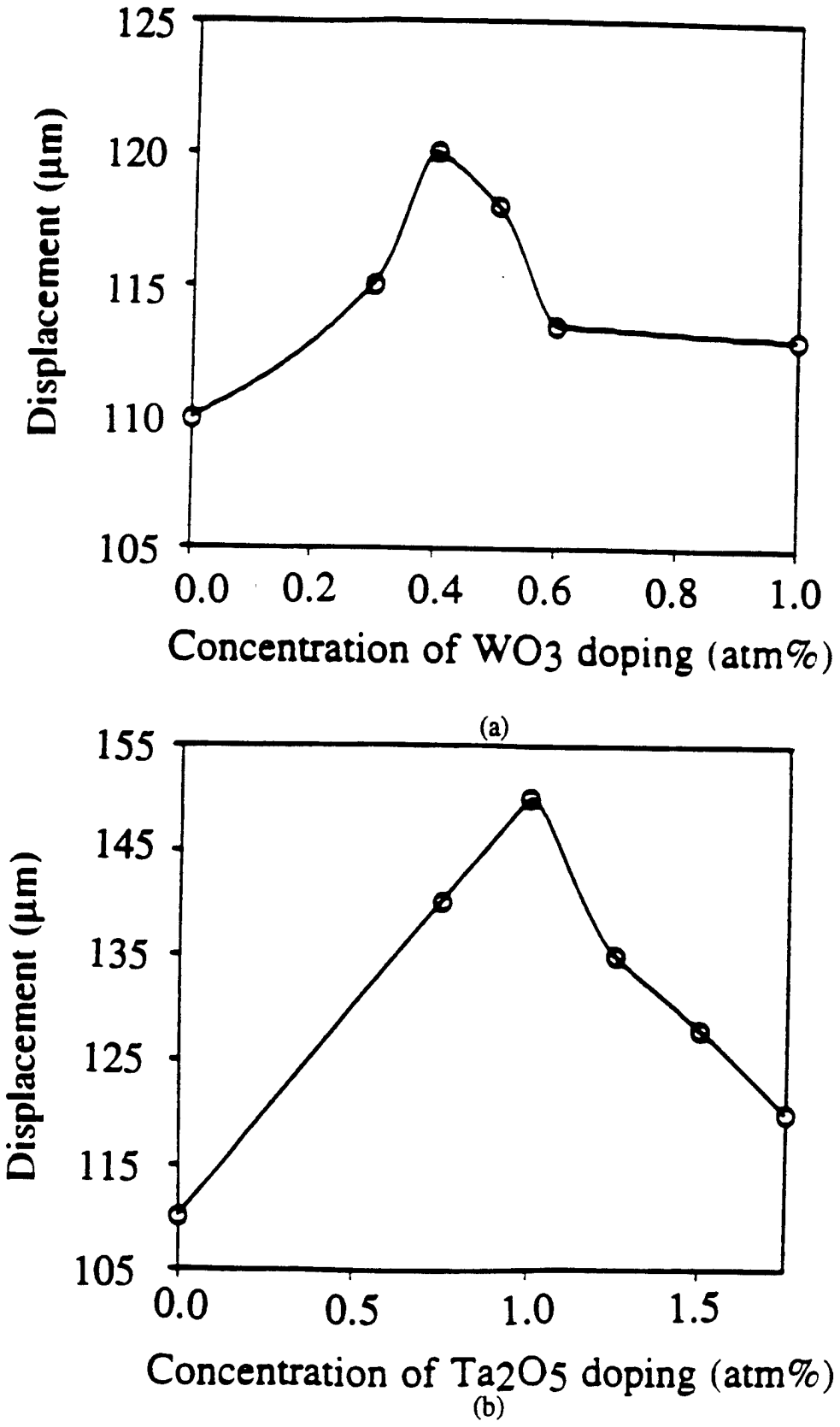

Figure 13. Light-induced displacement as functions of WO_3 and Ta_2O_5 doping.

morph was measured with a noncontact position sensor (Kaman Instrumentation Systems, SDP-2810.). The setup for photostrictive effect measurements is shown in Figure 11(b). The photostrictive effect in 0.4% WO_3 doped PLZT is shown in Figure 12. The displacement reached 50 μm in several seconds and saturated at 120 μm under a light intensity of 4 mW/cm^2. Figures 13(a) and 13(b) show the light-induced tip displacement as functions of WO_3 or Ta_2O_5 doping, respectively.

Conclusion

Donor doping was found to reduce the grain size and increase the Curie temperature, leading to the larger crystal distortion and the larger photo-current. The dielectric constant decrease enhances the larger photo-voltage. On the other hand, slight doping with WO_3 or Ta_2O_5 does not contribute to the piezoelectric effect, consequently, photostriction is mainly governed by the photovoltaic effect. The maximum photocurrent is obtained for 0.4 at% WO_3 doping and the maximum photovoltage is obtained for 1 at% Ta_2O_5 doping.

The tip displacement of a 20 mm long photostrictive bimorph can reach more than 100 μm in a couple of seconds, a great improvement over pure PLZT, and will be applicable to photo-acoustic devices.

Acknowledgment

This work is supported by Army Research Laboratory (ARL), No. DAALO3-92-G-0244. The authors would also thank Dr. Russell Brodeur for his critical review.

References

1. Fridkin, V.M. 1979. Photoferroelectrics: *Solid State Sciences*, Vol. 9.
2. Glass, A.M., von der Linde, D., Austin, D.H., and Negran, T.H. 1975. *J. Elec. Mat.*, Vol. 4, No. 5, 915–943.
3. Fridkin, V.M. and Povov, B.N. 1978. *Sov. Phys. Usp.* 21(12), 981–991.
4. Fridkin, V.M., Grekov, A.A., Ionov, P.V., Rodin, A.I., Savchenko, E.A., and Mikhailina, K.A. 1974. *Ferroelectrics*, Vol. 8. 433–435.
5. Brody, P.S. and Growne, F. 1975. *J. Elec. Mat.*, Vol. 4, No. 5, 955–971.
6. Sada, T., Inoue, M., and Uchino. K. 1987. *J. Ceram. Soc. Jpn.*, Vol. 5, 545.
7. Tanimura, M. and Uchino, K. 1988. Sensors and Materials, 1, 47–56.
8. Tanimura, M., Uchino, K., and Hikita, K. 1989. *Jpn. J. Appl. Phys.*, 28 (Suppl. 28-2), 170–172.
9. Uchino. K. 1989. *J. Rob. Mech.*, 1(2), 124–127.
10. Yamamoto, T. and Okazaki. K. 1990. Seventh International Symposium on the Application of Ferroelectrics.

2. Chu, S. Y., J. Ye and K. Uchino, "Photovoltaic Effect for the Linearly Polarized Light in (Pb,La)(Zr,Ti)O_3 Ceramics," Smart Mater. & Structures 3, 114-117 (1994).

Smart Mater. Struct. 3 (1994) 114–117. Printed in the UK

Photovoltaic effect for the linearly polarized light in (Pb,La)(Zr,Ti)O_3 ceramics

Sheng-Yuan Chu, Zhou Ye and Kengi Uchino

International Center for Actuators and Transducers, Materials Research Laboratory, The Pennsylvania State University, University Park, PA 16802, USA

Received 10 February 1994, accepted for publication 2 May 1994

Abstract. The bulk photovoltaic effect in non-centrosymmetric crystals is caused by asymmetric generation, recombination or scattering of excited non-equilibrium electronic carriers. In this paper, photovoltaic effects in (Pb,La)(Zr,Ti)O_3-based ceramics have been investigated using linearly polarized light. Angular dependence of the photovoltaic voltage and current on the polarization direction of the light was observed in doped (Pb,La)(Zr,Ti)O_3 ceramics. A phenomenological model was proposed to fit the experimental results from which the photovoltaic coefficients were calculated.

1. Introduction

The photovoltaic effect is observed in certain ferroelectrics, wherein a constant electromotive force is induced with application of near-ultraviolet radiation [1–3]. This effect was explained by Fridkin *et al* in 1974 [4], by Glass *et al* [2] and by Brody and Browne [5], and probably originated from an excitation of electrons from asymmetric impurity potentials. The main features of the bulk photovoltaic effect are summarized as follows:

(1) This effect appears in poled uniform single crystals or ceramics with non-centrosymmetry and is entirely different in nature from the P–N junction effect observed in semiconductors.

(2) Constant photocurrent and photovoltage are generated in the spontaneous polarization direction under uniform illumination in the ferroelectric phase and disappear in the para-electric phase.

(3) The magnitude of the induced voltage is proportional to the crystal length in the polarization direction and is much greater than the band-gap energy of the crystal.

So far, most studies have been made on single crystals to clarify the origin of the effect. However, our research group has been focusing on polycrystalline samples such as $PbTiO_3$-based [6, 7] and Pb(Zr,Ti)O_3-based ceramics [8, 9] from a practical application point of view. We have developed a high photovoltage ($\approx$ 1 kV mm^{-1}) generator with relatively quick response ($\approx$ 1 s) in the (Pb,La)(Zr,Ti)O_3 (PLZT) system. Moreover, by superimposing the photovoltaic effect on the inherent piezoelectricity of these compounds, practical photostrictive materials have been realized [10, 11]. A bimorph-type photostrictive element can exhibit a several-hundreds-μm tip deflection under violet light illumination. This actuator is applicable to remote-control devices such as photo-driven relays [10] and micro walking robots [12].

In this paper, the bulk photovoltaic effect in bulk PLZT (3/52/48) ceramics has been investigated by illuminating with linearly polarized light, and the angular dependence of the photovoltaic voltage and current on the polarized-light direction has been determined. This measurement is important particularly when the photostrictor is utilized as a photoacoustic device in conjunction with optical polarizers.

2. Sample preparation

PLZT ($x/y/z$) samples were prepared in accordance with the following composition formula:

$$Pb_{1-y}La_y(Zr_{1-x}Ti_x)_{1-y/4}O_3.$$

Since the photostriction figure of merit is evaluated by the product of the photovoltaic voltage and the piezoelectric coefficient ($x_{ph} = d_{33} \times E_{ph}$) PLZT (3/52/48) was selected due to its optimum photostrictive response within the PLZT system [9].

The ceramic powder was prepared by a conventional mixed-oxide technique. $PbCO_3$, La_2O_3, ZrO_2, TiO_2 and dopant were weighed in the appropriate proportions and mixed in a ball mill for 2 days using ethanol and zirconia grinding media. 0.5 wt.% excess $PbCO_3$ was added to compensate for weight loss during calcination and sintering. The slurry was dried, then calcined in a closed

0964-1726/94/020114+04$19.50

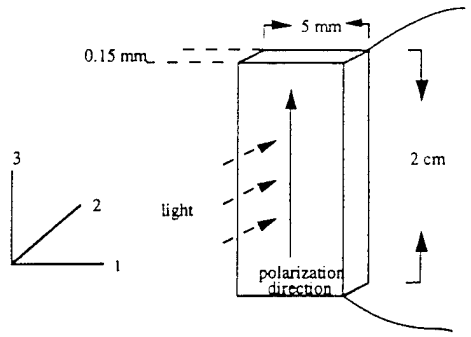

Figure 1. Sample configuration for photovoltaic-effect measurements.

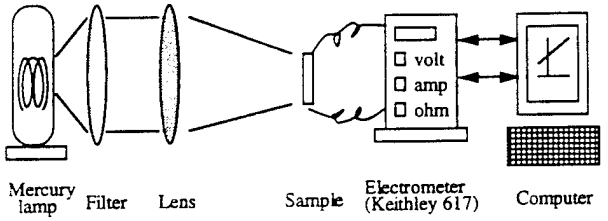

Figure 2. Experimental set-up for photovoltaic-effect measurements.

crucible at 950 °C for 10 h. The calcined powder was ball-milled again for 48 h. The samples were sintered in sealed alumina crucibles at 1270 °C/2 h. A PbO-rich atmosphere was maintained with lead zirconate powder to minimize lead loss during sintering. Sintered samples were electroded with silver paste. Finally, each sample was cut and poled in silicone oil at 120 °C under a 15 kV cm^{-1} electric field.

3. Photovoltaic effect measurements

PLZT (3/52/48) doped with various concentrations of WO_3 and Ta_2O_5 was used for this study. The sample size was $20 \times 4 \times 0.15$ mm^3: the 4×0.15 mm^2 surface was electroded with silver paste and silver wires were attached. The configuration of the sample is shown in figure 1. Radiation from a high-pressure mercury lamp (Ushio Electric USH-500D) was passed through a UV bandpass filter (Oriel Co., No.59811), an IR blocking filter (Oriel Co., No.59060), and an optical focusing lens. The experimental set-up is shown in figure 2. A wavelength peak around 370 nm, where the maximum photovoltaic effect of PLZT is obtained, was applied to the sample.

The photovoltaic voltage reaches 1 kV mm^{-1}, and the current is of the order of nA. The induced current was measured with a high-input-impedance (200 TΩ) electrometer (Keithley 617) as a function of the external voltage over a range −100 V to +100 V. The photovoltaic voltage and the current are defined as the maximum open-circuit voltage and short-circuit current respectively [10]. Upon exposure to UV radiation, a weak pyroelectric current was initially observed even with the IR blocking filter, and a steady-state photoelectric current was achieved after several

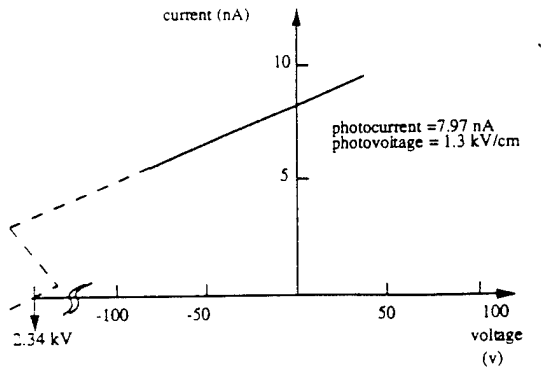

Figure 3. Photocurrent measured as a function of applied voltage for a 0.4% WO_3-doped PLZT sample.

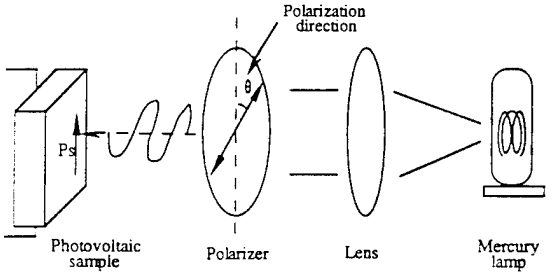

Figure 4. Experimental set-up for light-polarization-dependence measurements.

seconds. Measurements were made after the crystals had thermally equilibrated with the radiation to avoid any contribution from the pyroelectric effect. The photovoltaic voltage and the current were determined from the intercepts of the horizontal and the vertical axes, respectively. A typical curve is shown in figure 3 for PLZT doped with 0.4 at.% WO_3.

4. Angular dependence of the photovoltaic voltage and current

A polarizer was put between the focusing lens and the sample to monitor the angular dependence of the photovoltaic effect under linearly polarized light, as shown in figure 4. The angle θ was measured with respect to the origin of the remnant polarization direction. Figure 5 shows the experimental dependence of the photovoltaic current J and the corresponding voltage V on the light-polarization direction. Both the photovoltage and photocurrent provide the maximum values at $\theta = 0$, 180°, and the minimum at $\theta = 90°$. It was observed that the photocurrent and photovoltage deviations with respect to the change of light-polarization direction are 2% and 14%, respectively, for the WO_3-doped samples, regardless of the absolute values of current and voltage. This is the first observation of angular dependence of the photovoltaic effect in ceramic samples, although this dependence was reported for single-crystal samples [13, 14].

The photovoltaic current density J_i can be described by the third-rank tensor α_{ijk} [15] as

$$J_i = \alpha_{ijk} E_j E_k^*. \qquad (1)$$

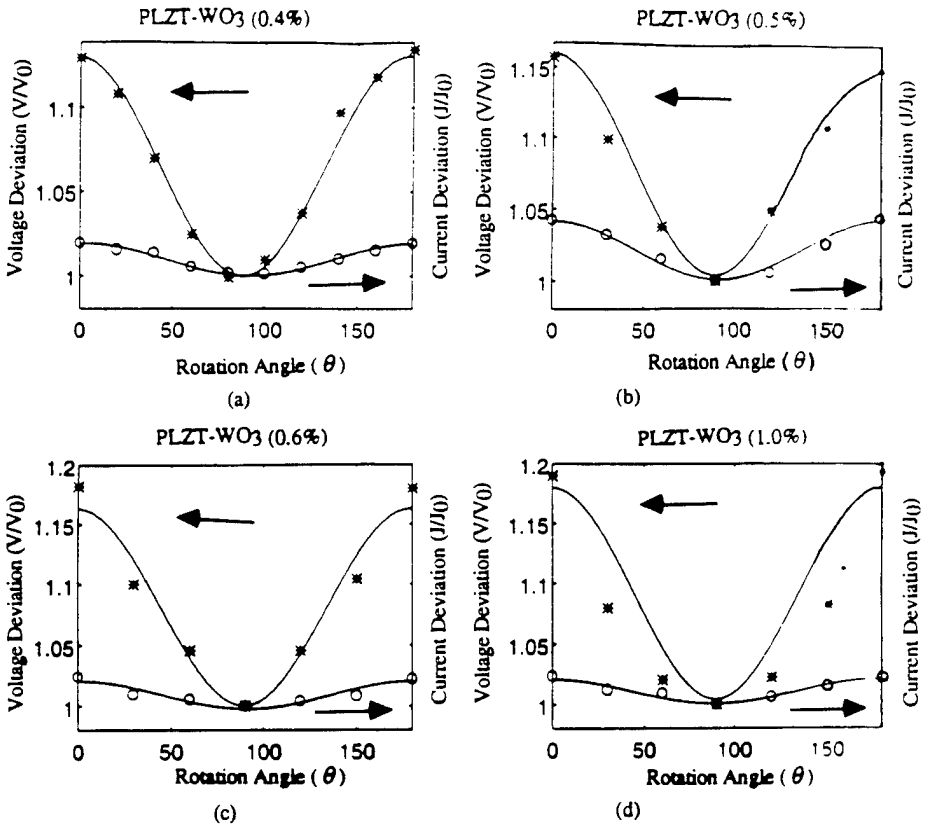

Figure 5. Dependence of the normalized photovoltaic current and photovoltage on the direction of the light-polarization plane and the light for various WO_3-doped PLZT samples. (*a*) 0.4%, (*b*) 0.5%, (*c*) 0.6%, and (*d*) 1%. Solid curves are the theoretically fitted curves.

Table 1. α_{31} and α_{33} coefficients of WO_3 and Ta_2O_5 doped PLZT.

	WO_3 at.%				Ta_2O_5 at.%			
	0.4	0.5	0.6	1	1	1.25	1.5	1.75
α_{31} (10^{-6}) (A W^{-1})	12.487	6.844	6.31	4.49	4.2	4.23	6.57	5.83
α_{33} (10^{-6}) (A W^{-1})	12.787	7.13	6.46	4.55	4.46	4.46	6.955	6.05
α_{33}/α_{31}	1.024	1.042	1.024	1.013	1.062	1.054	1.059	1.038

When a homogeneous ferro- or piezoelectric crystal is illuminated uniformly with linearly polarized light, a photovoltaic current J_i arises in it. The sign and the magnitude of the current depend on the orientation of the light-polarization vector with projections E_j and E_k, E_k^* is the conjugate vector of E_k.

Having the electrodes opened, the photovoltaic current J_i gives rise to the photovoltage

$$V_i = J_i l/(\sigma_d + \sigma_{ph}) \tag{2}$$

where σ_d and σ_{ph} are the dark conductivity and photoconductivity, respectively, and l is the distance between the electrodes. The value of V_i exceeds the energy gap of the ferro- or piezoelectric crystal by several orders of magnitude, (i.e. $V \gg E_g$) [1].

From the non-zero α_{ijk} for poled ceramics (Curie Group ∞m) the expression for J_z (the direction of linearly polarized light propagation is shown in figure 5) is obtained from equation (1):

$$J_z = \alpha_{31} I + (\alpha_{33} - \alpha_{31}) I \cos^2\theta \tag{3}$$

where I is the incident light intensity and $E_2 E_2^*/\sin^2\theta = E_3 E_3^*/\cos^2\theta = I$ (refer to figure 1). The experimental dependence $J_z(\theta)$ is in good agreement with equation (3). The solid curves in figure 5 are calculated from equation (3). The values of α_{31} and α_{33} are tabulated in table 1. Values of α_{31} and α_{33} are of the order of 10^{-6}, and α_{33} is larger than α_{31}. It is also noteworthy that systematic changes of α_{31} and α_{33} values are found with changes in dopant concentration. However, α_{33}/α_{31} remains essentially constant, and α_{33}/α_{31} is somewhat smaller in WO_3-doped than in Ta_2O_5-doped samples.

In order to determine the photovoltaic coefficient values ($k_{ijk} = (1/\alpha^*)\alpha_{ijk}$), the absorption coefficient (α^*) measurements are required.

5. Summary

The angular dependence of the photovoltaic current and the corresponding voltage on the light-polarization orientation with respect to the spontaneous polarization has been successfully observed in ceramic samples of PLZT. This angular dependence of the photovoltaic current is consistent with the symmetry of the poled ceramic. The difference between the peak–peak deviations in the current (2%) and voltage (14%) suggests a relatively large dependence of photoconductivity on light-polarization orientation.

References

[1] Fridkin V M 1979 *Photoferroelectrics (Springer Series on Solid State Sciences 9)* ed M Cardona, P Fulde and H-J Queisser (New York: Springer)

[2] Glass A M, von der Linde D, Austin D H and Negran T J 1975 *J. Electron. Mater.* **4** 915–43

[3] Fridkin V M and Povov B N 1978 *Sov. Phys. Usp.* **21** 981–91

[4] Fridkin V M, Grekov A A, Ionov P V, Rodin A I, Savchenko E A and Mikhailina K A 1974 *Ferroelectrics* **8** 433–5

[5] Brody P S and Growne F 1975 *J. Electron. Mater.* **4** 955–71

[6] Uchino K, Miyazawa Y and Nomura S 1982 *Japan. J. Appl. Phys.* **21** 1671–4

[7] Uchino K, Miyazawa Y and Nomura S 1983 *Japan. J. Appl. Phys.* Suppl. **22–2** 102–5

[8] Uchino K and Aizawa M 1985 *Japan. J. Appl. Phys.* Suppl. **24–3** 139–41

[9] Uchino K, Aizawa M and Nomura S 1985 *Ferroelectrics* **64** 199–208

[10] Tanimura M and Uchino K 1988 *Sensors Mater.* **1** 47–56

[11] Tanimura M, Uchino K and Hikita K 1989 *Japan. J. Appl. Phys.* **28** Suppl. 28–2 170–2

[12] Uchino K 1989 *J. Robot. Mech.* **1** 124–7

[13] Koch W T H, Munser R, Ruppel W and Wurfel P 1976 *Ferroelectrics* **13** 305–7

[14] Fridkin V M and Sturman B I 1992 *The Photovoltaic and Photorefractive Effects in Noncentrosymmetric Materials* ed G W Taylor (Philadelphia, PA: Gordon and Breach)

[15] Fridkin V M, Grekov A A and Rodin A I 1982 *Ferroelectrics* **43** 99–108

3. Uchino, K. and S. Y. Chu, "Photostriction and Its Applications," Proc. PacRim Amer. Ceram. Soc., Ferroic Materials, 287-293 (1994).

PHOTOSTRICTION AND ITS APPLICATIONS

Kenji Uchino and Sheng-Yuan Chu
International Center for Actuators and Transducers
Materials Research Laboratory, The Pennsylvania State University
University Park, PA 16802

Abstract

The photostrictive effect is the superimposing of photovoltaic and piezoelectric effects. (Pb,La)(Zr,Ti)O_3 ceramics doped with WO_3 exhibit large photostriction under irradiation of purple-color light, and are applicable as remote control actuators. Photo-driven relays and micro walking devices which have been developed, are designed to start moving as a result from the irradiation, having neither electric lead wires nor electric circuit.

INTRODUCTION

Photostrictive effect is a phenomenon in which strain is induced in the sample when it is illuminated. This effect is focused especially in the fields of micromechanism and optical communication.

With decreasing the size of miniature robots/actuators, the weight of the electric lead wire connecting the power supply becomes significant, and remote control will definitely be required for sub-millimeter devices. A photo-driven actuator is a very promising candidate for micro-robots. On the other hand, the key components in optical communication are solid state lasers as a light source, optical fibers as a transfer line, and displays/ telephones as a visual/audible interface with the human. The former two components have been developed fairly successfully, and the photo-acoustic device (i. e. optical telephone or "photophone") will be eagerly anticipated in the next century.

Photostrictive devices which function when they receive the energy of light will be particularly suitable for use in the above-mentioned fields. In principle, the photostrictive effect is the superimposing of a photovoltaic effect, where a large voltage is generated in ferroelectrics through the irradiation of light,[1)] and a piezoelectric effect, where the material expands or contracts from the voltage applied. The photovoltaic effect mentioned here generates a greater-than-band-gap voltage, and is quite different from that based on the p-n junction of semiconductors (i. e. solar battery). It is generated when electrons excited by light move in a certain direction of the ferroelectric crystal due to the spontaneous polarization (i. e. crystallographic anisotropy).

This paper describes the details of the fundamental photostrictive effect in $(Pb,La)(Zr,Ti)O_3$ ceramics first, then introduces its applications to a photo-driven relay and a micro walking machine, which are designed to move as a result of irradiation, having neither lead wires nor electric circuit.

PHOTOSTRICTIVE PROPERTIES

Materials Research

PLZT (x/y/z) samples were prepared in accordance with the following composition formula: $Pb_{1-x}La_x(Zr_yTi_z)_{1-x/4}O_3$. The interrelation of photo-voltaic current with remanent polarization is plotted for the PLZT family in Fig. 1. The average remanent polarization exhibiting the same magnitude of photo-current differs by 1.7 times between the tetragonal and rhombohedral phases; this suggests the photo-induced electron excitation is related to the (0 0 1) axis-oriented orbit, i. e. the hybridized orbit of p-orbit of oxygen and d-orbit of Ti/Zr. The photostrictive figure of merit is evaluated by the product of the photovoltaic voltage and the piezoelectric coefficient. Therefore, PLZT (3/52/48) was selected because the largest figure of merit is obtained with this composition.[2,3]

Impurity doping on PLZT also affects the photovoltaic response significantly.[4] Figure 2 shows the photovoltaic response for various dopants with the same concentration of 1 atomic % under an illumination intensity of 4 mW/cm^2 at 366 nm. The dashed line in Fig. 2 represents the constant power curve corresponding to the non-doped PLZT. Regarding the photostriction effect, it is known that as the photovoltaic voltage increases, the strain value increases, and with increasing photo-current, there is an increase in the overall response. The photovoltaic response is enhanced by donor doping onto the B-site (Nb^{5+}, Ti^{5+}, W^{6+}). On the other hand, impurity ions substituting at the A-site and/or acceptor ions substituting at the B-site, whose ionic valences are small (1 to 4), have no effect on the response. Figure 3 shows the photovoltaic response plotted as a function of atm % of WO_3 doping concentration. Note that the maximum power is obtained at 0.4 % of the dopant.

Even when the composition is fixed, the photostriction still depends on the sintering condition or the grain size.[5] Figure 4 shows the dependence of the photostrictive characteristics on the grain size. The smaller grain sample is preferrable, if it is sintered to a high density.

Effect of Light Polarization Direction

Effect of the light polarization direction on the photovoltaic phenomenon was investigated on the polycrystalline PLZT, using an experimental setup shown in Fig. 5 (a). This experiment is important when the photostriction is employed to "photophones", where the sample is illuminated with the polarized light traveling through an optical fiber. The rotation angle θ was taken from the vertical spontaneous polarization direction, as shown in Fig. 5 (b). Both the photovoltaic voltage and current provided the maximum at θ = 0 and 180 deg and the minimum at θ = 90 deg; this also indicates that the contributing electron orbit may be the p-d hybridized orbit mentioned above.

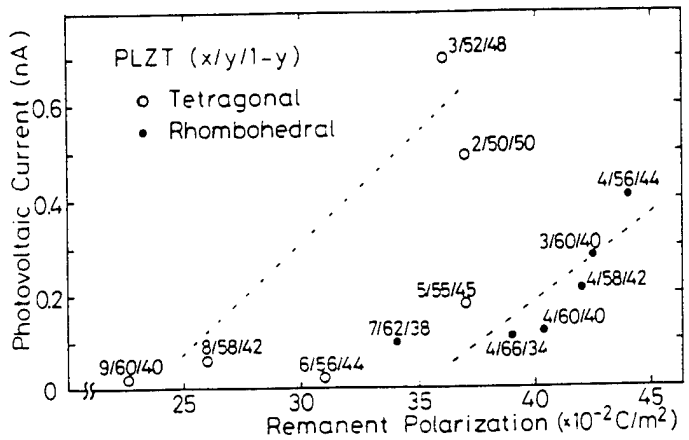

Fig.1. Interrelation of photovoltaic current with remanent polarization in PLZT family.

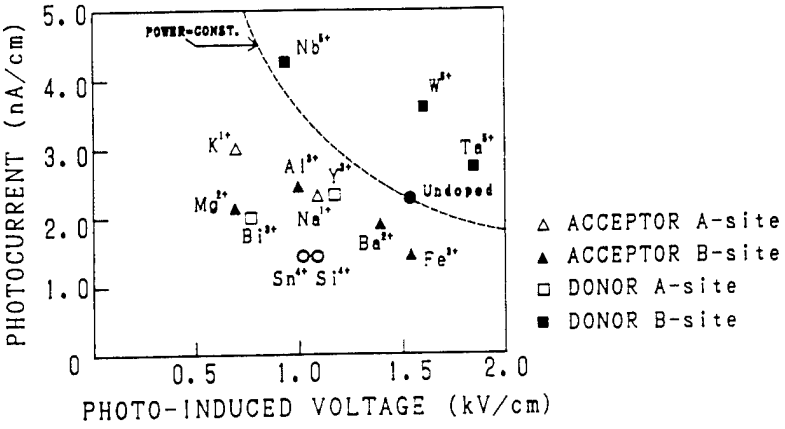

Fig.2. Photovoltaic response as a function of impurity doping.

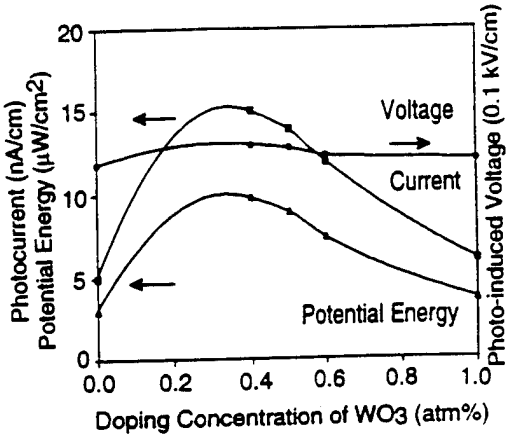

Fig.3. Photovoltaic current and voltage as a function of dopant concentration in WO_3 doped PLZT.

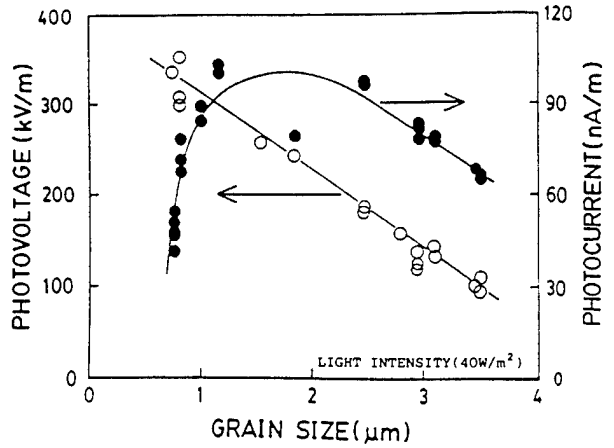

Fig.4. Grain size dependence of photostrictive characteristics in PLZT(3/52/48).

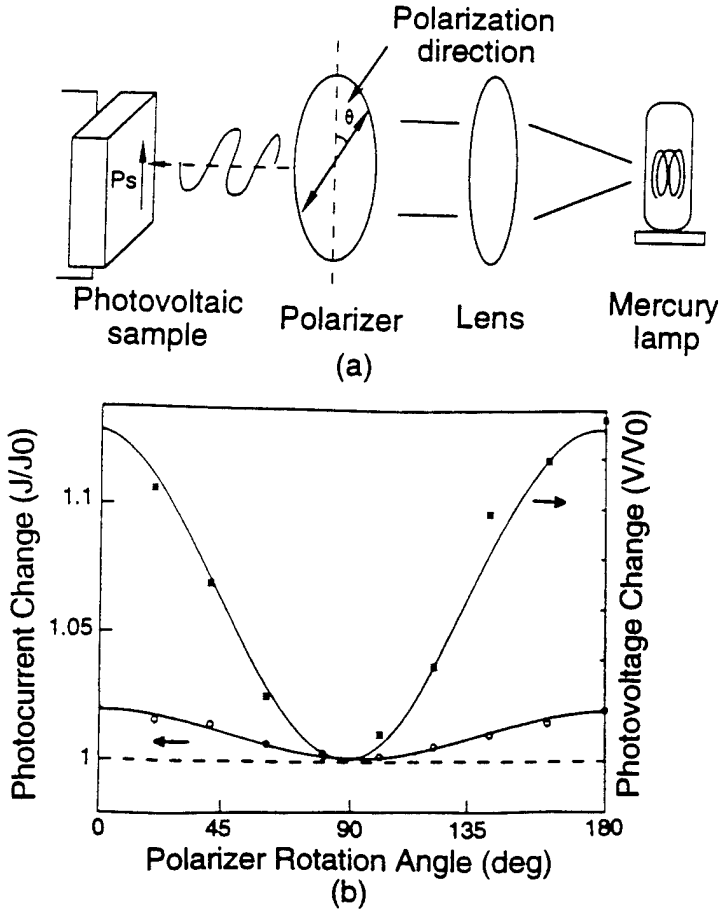

Fig.5. (a) Measuring system of the dependence of photovoltaic effect on light polarization direction, and (b) photovotaic voltage and current as a function of the rotation angle.

PHOTOSTRICTIVE ACTUATORS

Photo-Driven Relay

A photo-driven relay was constructed using a photostrictor as the driver (Fig. 6).[4] The driving part was a bimorph which consisted of two ceramic plates (5mmx20mmx0.16mm in size) joined so that their polarization directions were opposing. A dummy plate was positioned adjacent to the bimorph to cancel the photovoltaic voltage generated on the bimorph. Utilizing a dual beam method, switching was controlled by alternately irradiating the bimorph and the dummy. The time delay of the bimorph that ordinarily occurs in the off process due to a low dark conductivity could be avoided, making use of this dual beam method. Figure 7 shows the response of a photostrictive bimorph made from PLZT doped with 0.5 at% WO_3 under an illumination intensity of 10 mW/cm^2. The amount of displacement observed at a tip of the bimorph (2 cm long and 0.32 mm thick) was 150 μm. A snap action switch was used for the relay. Switching by a displacement of several tens of micron was possible with this device.[6] The On/Off response of the photo-driven relay showed a typical delay time of 1 - 2 sec.

Micro Walking Device

A photo-driven micro walking machine has also been developed using the photostrictive bimorphs.[7] It was simple in structure, having only two ceramic legs (5mmx20mmx0.35mm) fixed to a plastic board (Fig.8). When the two legs were irradiated with purple light alternately, the device moved like an inchworm. The photostrictive bimorph as a whole was caused to bend by 150 μm as if it averted the radiation of light. The inchworm built on a trial basis exhibited rather slow walking speed (several μm/min) as shown in Fig. 9, since slip occurred between the contacting surface of its leg and the floor.

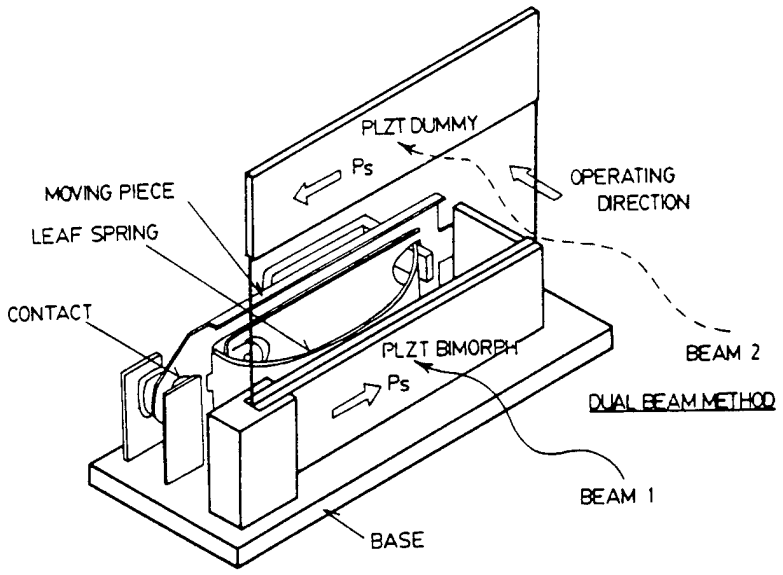

Fig.6. Structure of the photo-driven relay.

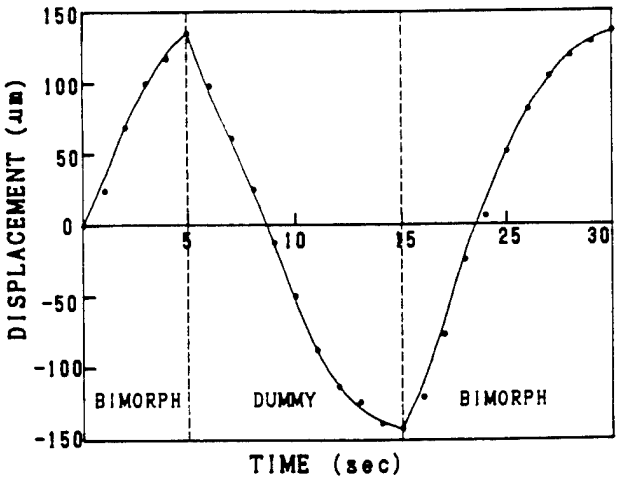

Fig.7. Bimorph deflection of the device made from WO_3 0.5 atm% doped PLZT.

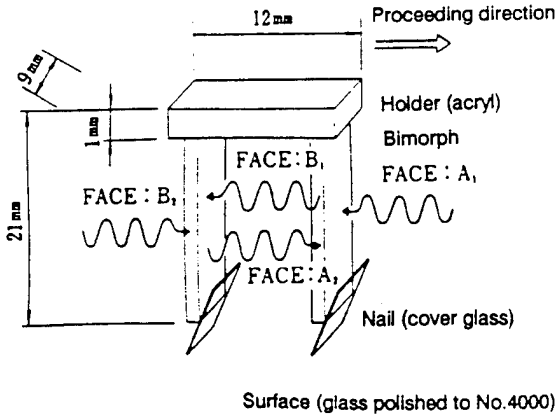

Fig.8. Structure of the photo-driven micro walking machine, and the direction of irradiation.

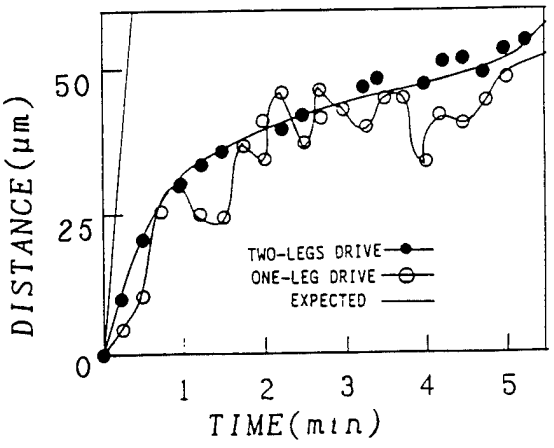

Fig.9. Position change of the photo-driven micro walking machine with time.

CONCLUSION

The photostrictive actuators can be driven by the irradiation of light alone, so that they will be suitable for use in actuators, to which lead wires can hardly be connected because of their ultra-small size or of their employed conditions such as ultra-high vacuum. New actuators of this type have considerable effects upon the future micro-mechatronics.

This work was supported by US Army Research Office through Contract No. DAAL 03-92-G-0244.

References

1) V. M. Fridkin, Photo-ferroelectrics, Solid-State Sciences 9, Springer-Verlag (1979).
2) K. Uchino, Y.Miyazawa and Late S. Nomura, "Photovoltaic Effect in Ferroelectric Ceramics and Its Applications," Jpn. J. Appl. Phys. 22, Suppl. 22-2, 102 (1983).
3) K. Uchino, M. Aizawa and Late S. Nomura, "Photostrictive Effect in (Pb,La)(Zr,Ti)O_3," Ferroelectrics 64,199 (1985).
4) M. Tanimura and K. Uchino, "Effect of Impurity Doping on Photostriction in Ferroelectric Ceramics," Sensors & Mater. 1, 47 (1988).
5) T. Sada, M. Inoue and K. Uchino, "Photostrictive Effect in PLZT Ceramics," J. Ceram. Soc. Jpn. 5, 545 (1987).
6) R. Sato, T. Taniguchi and M. Oba, "Piezoelectric Relays," OMRON Technics, No. 70, 52 (1983).
7) K. Uchino, "Micro Walking Machines Using Piezoelectric Actuators," J. Rob. Mech. 1, 124 (1989).

4. Chu, S. Y., M. L. Mulvihill, Z. Ye and K. Uchino, "Bulk Photovoltaic Effect for the Linearly Polarized Light in $Pb(Zn_{1/3}Nb_{2/3})O_3$ Single Crystals," Jpn. J. Appl. Phys. Vol.34, 527-529 (1995).

Jpn. J. Appl. Phys. Vol. 34 (1995) pp. 527-529
Part 1, No. 2A, February 1995

Bulk Photovoltaic Effect for the Linearly Polarized Light in $Pb(Zn_{1/3}Nb_{2/3})O_3$ Single Crystals

Sheng-Yuan CHU, Maureen L. MULVIHILL, Zhou YE and Kenji UCHINO
International Center for Actuators and Transducers, Materials Research Laboratory, The Pennsylvania State University, University Park, PA 16802, U.S.A.

(Received May 30, 1994; accepted for publication August 20, 1994)

The bulk photovoltaic effect in non-centrosymmetric crystals is caused by asymmetric generation, recombination or scattering of excited nonequilibrium electronic carriers. In this paper, the photovoltaic effect has been investigated in relaxor ferroelectric $Pb(Zn_{1/3}Nb_{2/3})O_3$ single crystals using linearly polarized light. Angular dependence of photovoltaic voltage and current on the polarization direction of light was observed in the crystal. A phenomenological model was proposed to fit the experimental results from which the photovoltaic coefficients were calculated.

KEYWORDS: bulk photovoltaic effect, $Pb(Zn_{1/3}Nb_{2/3})O_3$, relaxor, microdomain, photovoltaic coefficient

1. Introduction

The photovoltaic effect is observed in certain ferroelectrics, wherein a constant electromotive force is induced with application of near-ultraviolet radiation.[1-3] This effect was explained by Fridkin *et al.* in 1974.[4] Glass *et al.*[2] and Brody and Growne,[5] and probably originated from an excitation of electrons from asymmetric impurity potentials. The main features of the bulk photovoltaic effect are summarized below.

1) This effect appears in poled uniform single crystals or ceramics with noncentro-symmetry and is entirely different in nature from the P-N junction effect observed in semiconductors.
2) Constant photocurrent and -voltage are generated in the spontaneous polarization direction under uniform illumination in the ferroelectric phase and disappear in the paraelectric phase.
3) The magnitude of the induced voltage is proportional to the crystal length in the polarization direction and is much greater than the bandgap energy of the crystal.

Most of the studies have been made so far on normal ferroelectric single crystals with linearly polarized light, and significant angular dependence of the photovoltaic voltage and current on the polarization direction of the light with respect to the spontaneous polarization direction of the sample crystal has been reported.[1]

In this paper, the photovoltaic effect has been investigated in relaxor ferroelectric $Pb(Zn_{1/3}Nb_{2/3})O_3$ single crystals, where microdomains may have an effect on the photovoltaic phenomenon. $Pb(Zn_{1/3}Nb_{2/3})O_3$ is a well-known relaxor ferroelectric with a Curie temperature around 140°C, and a peculiar domain reversal mechanism which was also reported by us.[6]

2. Sample Preparation

The raw oxide powders PbO, ZnO and Nb_2O_5 were mixed in stoichiometric proportions. The ratio of flux, PbO, to composition used was 2:1. The powder was heated in a sealed platinum crucible to 1200°C, and cooled to 800°C at a rate of 2°C/h. Then they were cooled to room temperature. The crystals were removed from the flux by soaking in hot 25 vol% nitric acid.

Then, the $Pb(Zn_{1/3}Nb_{2/3})O_3$ single crystal was cut into a (111) plate. Sample size for this measurement was $1.55 \times 0.72 \times 0.56$ mm^3: the 1.55×0.72 mm^2 surface was electroded with silver paste. The crystal orientation of perovskite ⟨111⟩ was taken for the applied electrical field direction. Before photovoltaic-effect measurements, the sample was poled in silicone oil at 110°C under an electric field of 15 kV/cm for 10 min. The configuration of the sample is shown in Fig. 1.

3. Photovoltaic Effect Measurements

The experimental setup is shown in Fig. 2. Light from a high-pressure mercury lamp (Ushio Electric USH-500D) was passed through a UV band-pass filter (Oriel Co., No. 59811), an IR blocking filter (Oriel Co., No. 59060), and an optical focusing lens. A wavelength peak around 370 nm was then applied to the sample on the 1.55×0.56 mm^2 face.

For the unpoled $Pb(Zn_{1/3}Nb_{2/3})O_3$ crystal, the current was on the order of 10^{-12} A and the photovoltaic voltage was about 100 V/cm. However, after poling, the photocurrent and voltage increased to the order of 10^{-10} A and 1 kV/cm. Upon exposure to UV radiation, a weak pyroelectric current was initially observed even with the IR blocking filter, and a steady-state photoelectric current was achieved after 10 s. Figure 3 shows the transient response of current. The induced current was measured with a high-input-impedance (200 TΩ)

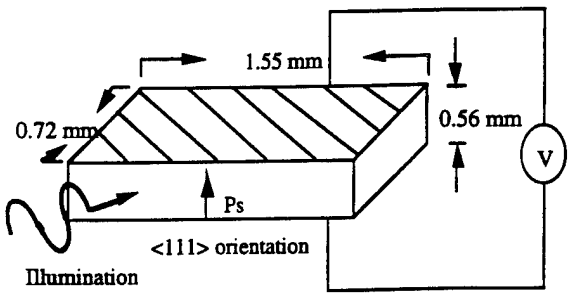

Fig. 1. Sample configuration for the photovoltaic-effect measurement.

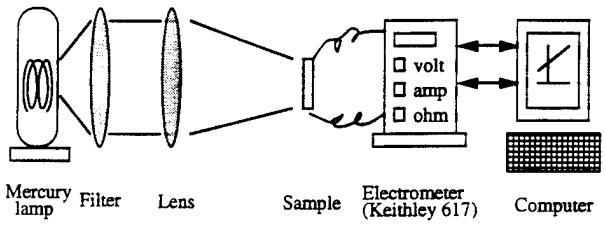

Fig. 2. Experimental setup for the photovoltaic-effect measurement.

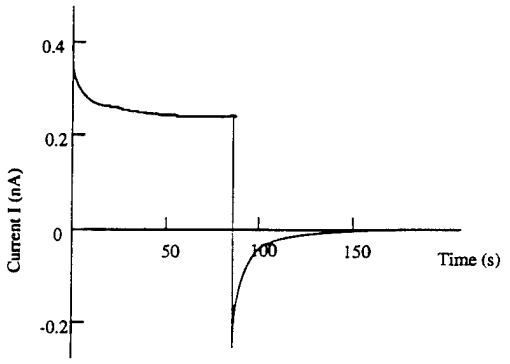

Fig. 3. Transient response of the current in a $Pb(Zn_{1/3}Nb_{2/3})O_3$ single-crystal sample.

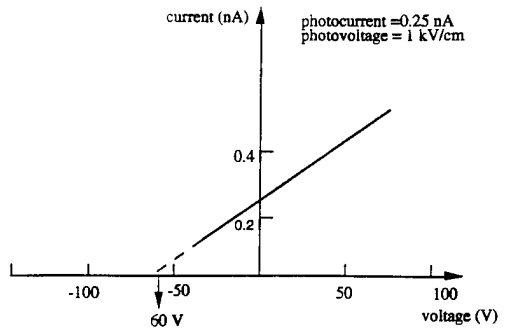

Fig. 4. Photocurrent measured as a function of applied voltage for a $Pb(Zn_{1/3}Nb_{2/3})O_3$ single crystal.

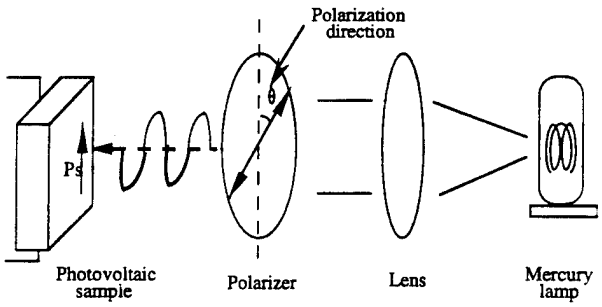

Fig. 5. Experimental setup for light-polarization-dependence measurements.

electrometer (Keithley 617) as a function of the external voltage over the range -100 V to $+100$ V. Measurements were made after the crystals reached thermal equilibrium with the radiation to avoid contribution from the pyroelectric effect. The photovoltaic voltage and the current are defined as the maximum open-circuit voltage and short-circuit current, respectively,[7] and were determined from the intercepts of the horizontal and vertical axes, respectively. A typical curve is shown in Fig. 4.

4. Angular Dependence of Photovoltaic Voltage and Current

A polarizer was placed between the focusing lens and the sample to monitor the angular dependence of the photovoltaic effect under linearly polarized light, as shown in Fig. 5. The angle θ was measured with respect to the origin of the remanent polarization direction. Figure 6 shows the experimental dependence of the photovoltaic current J and the corresponding voltage V on the light polarization direction under the illumination intensity of 1 mW/cm^2 for $\lambda=366$ nm. Both the photovoltage and photocurrent provide the maximum values at $\theta=0$ and 180°, and the minimum at $\theta=90°$. It was observed that the photocurrent and photovoltage deviations with respect to the change of light polarization direction are 16% and 11%, respectively, for the $Pb(Zn_{1/3}Nb_{2/3})O_3$ single-crystal samples, regardless of the absolute values of current and voltage.

To our knowledge, this is the first observation of an

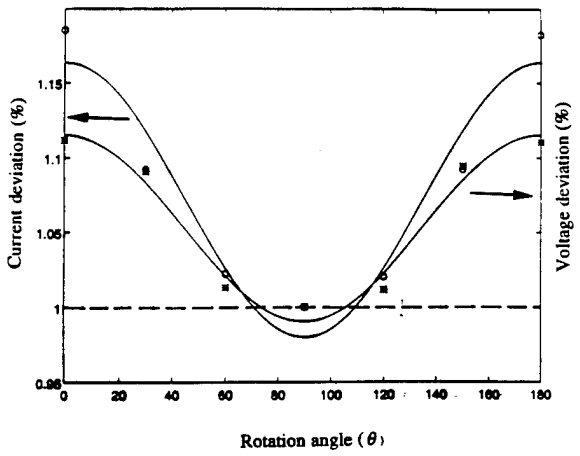

Fig. 6. Dependence of the normalized photovoltaic current and photovoltage on the direction of the light polarization plane with respect to the spontaneous polarization direction for a $Pb(Zn_{1/3}Nb_{2/3})O_3$ single crystal. Solid lines are the theoretically fitted curves. (○: photocurrent, *: photovoltage) Light power= 0.152 ± 0.001 mW.

angular dependence of the photovoltaic effect in a relaxor ferroelectric single crystal, although this dependence was reported for other normal ferroelectric single crystals.[8,9] Compared with normal ferroelectrics such as $LiNbO_3$[10] and SbSI,[11] the deviations in the photocurrent and voltage are relatively small, in a comparable magnitude of the polycrystalline samples

reported in our previous paper.[12] This may be attributed to the microdomain configuration in the relaxor $Pb(Zn_{1/3}Nb_{2/3})O_3$.

When a homogeneous ferro- or piezoelectric crystal is illuminated uniformly with linearly polarized light, a photovoltaic current J_i arises from it. The photovoltaic current density J_i can be described by the third-rank tensor α_{ijk}[13] as

$$J_i=\alpha_{ijk}E_jE_k^*. \tag{1}$$

The sign and the magnitude of the current depend on the orientation of the light polarization vector with projections E_j and E_k.

With the electrodes open, the photovoltaic current J_i gives rise to the photovoltage

$$V_i=J_il/(\sigma_d+\sigma_{ph}), \tag{2}$$

where σ_d and σ_{ph} are the dark and photoconductivity, respectively, and l is the distance between the electrodes. The value of V_i exceeds the energy gap of the ferro- or piezoelectric crystal by several orders of magnitude (i.e., $V\gg E_g$).[1]

From nonzero α_{ijk}'s for $Pb(Zn_{1/3}Nb_{2/3})O_3$ single crystals (Point Group 3m), the expression for J_z (the direction of linearly polarized light propagation is shown in Fig. 5) is obtained from eq. (1):

$$J_z=\alpha_{31}I+(\alpha_{33}-\alpha_{31})I\cos^2\theta \tag{3}$$

where I is the incident light intensity. The experimental dependence $J_z(\theta)$ is in good agreement with eq. (3). The solid lines in Fig. 6 are calculated from eq. (3). Values of α_{31} and α_{33} are then calculated as 2.1×10^{-7} A/W and 3.2×10^{-7} A/W, respectively.

In order to determine the photovoltaic coefficient values ($k_{ijk}=(1/\alpha^*)\alpha_{ijk}$), the absorption coefficient (α^*) measurements are required.

5. Conclusions

The angular dependence of the photovoltaic current and the corresponding voltage on the light polarization orientation with respect to the spontaneous polarization has been successfully observed in relaxor ferroelectric $Pb(Zn_{1/3}Nb_{2/3})O_3$ single crystals. This angular dependence of the photovoltaic current is consistent with the symmetry of the poled single crystal. The difference between the peak-to-peak deviations in the current (16%) and voltage (11%) is relatively small in comparison with the case of normal ferroelectrics. This may be attributed to the microdomain configuration in the relaxor $Pb(Zn_{1/3}Nb_{2/3})O_3$.

Acknowledgement

This work is supported by Army Research Office (ARO), No. DAALO3-92-G-0244.

1) V. M. Fridkin: *Photoferroelectrics*, eds. M. Cardona, P. Fulde and H.-J. Queisser (Solid State Sciences, New York, 1979) Vol. 9, Chap. 6, p. 85.
2) A. M. Glass, D. von der Linde, D. H. Austin and T. J. Negran: J. Electron. Mater. **4** (1975) L915.
3) V. M. Fridkin and B. N. Popov: Sov. Phys. Usp. **21** (1978) L981.
4) V. M. Fridkin, A. A. Grekov, P. V. Ionov, A. I. Rodin, E. A. Savchenko and K. A. Mikhailina: Ferroelectrics **8** (1974) L433.
5) P. S. Brody and F. Growne: J. Electron. Mater. **4** (1975) L955.
6) M. L. Mulvihill, L. E. Cross and K. Uchino: to be published in J. Am. Ceram. Soc.
7) M. Tanimura and K. Uchino: Sens. & Mater. **1** (1988) L47.
8) W. T. H. Koch, R. Munser, W. Ruppel and P. Wurfel: Ferroelectrics **13** (1976) L305.
9) V. M. Fridkin and B. I. Sturman: *The Photovoltaic and Photorefractive Effects in Noncentrosymmetric Materials*, ed. G. W. Taylor (Gordon and Breach Science Publishers, Philadelphia, 1992) Vol. 8, Chap. 3, p. 120.
10) V. M. Fridkin and R. M. Magomadov: Zh. Eksp. Teor. Fiz. Lett. **30** (1979).
11) V. M. Fridkin and A. I. Rodin: Phys. Status Solidi a **61** (1980) 123.
12) S.-Y. Chu, Z. Ye and K. Uchino: J. Smart Mater. & Struct. **3** (1994) 114.
13) V. M. Fridkin, A. A. Grekov and A. I. Rodin: Ferroelectrics **43** (1982) L99.

5. Uchino, K., "Electrooptic Ceramics and Their Display Applications," Ceramics International Vol.21, 309-315 (1995).

Ceramics International 21 (1995) 309–315

Electro-optic Ceramics and their Display Applications

Kenji Uchino

International Center for Actuators and Transducers, Materials Research Laboratory, The Pennsylvania State University, University Park, PA 16802, USA

(Received 3 October 1994; accepted 7 November 1994)

Abstract: Relaxor ferroelectrics are remarked in non-linear optic applications because an extraordinarily large apparent 'electro-optic Kerr effect' can be observed, even in the so-called paraelectric state. This paper describes the fundamental electro-optic properties of perovskite-type polycrystalline and single crystals, $Pb(Zn_{1/3}Nb_{2/3})O_3$, (Pb, La)(Zr, Ti)O_3 and $Pb(Mg_{1/3}Nb_{2/3})O_3$–$PbTiO_3$, firstly. Then, a new type of two-dimensional light valve array for an image projector is introduced. A light shutter array with 10 × 10 pixels was fabricated by a sophisticated tape casting technique. Plate-through and separate electrodes are stacked alternately so as to make vertical addressing by an external electrode connecting separate electrodes and horizontal addressing by a plate-through electrode. The applicative feasibility to a high definition image projector was verified.

1 INTRODUCTION

The electro-optic effect, which is the refractive indices change with an external applied electric field, will provide very promising useful devices such as light valves, deflectors, displays, etc., in the next optical communication age, in conjunction with solid state laser chips and optical fibers. Compared with liquid crystal devices, the ceramic electro-optic components, in general, possess advantages in response speed (μsec), particularly in falling time, durability for strong light illumination and contrast ratio (10^2)/gray scale (16 scales). On the other hand, the present ceramic components require relatively high drive voltage (1 kV) and production cost ($ 100). Therefore, the development of a simple mass-production process and designing of electrode configurations with a narrow gap, as well as the improvement of material properties, will be the key factors to the actual commercialization of the ceramic optical components.

Let us review the principle of a light shutter utilizing the second-order electro-optic effect (Kerr effect), initially. The birefringence Δn is induced in a crystal when an electric field E is applied:

$$\Delta n = -(1/2)Rn^3 E^2 \quad (1)$$

where R ($= R_{11}-R_{12}$) is the quadratic electro-optic coefficient and n is the original refractive index of the crystal. When this sample is placed between crossed polarizers arranged at the 45° direction with respect to the E direction, and light is transmitted transversely to the E field (Fig. 1), the output light intensity is represented by

$$I = I_0 A \sin^2[(\pi Rn^3 L/2\lambda)E^2] \quad (2)$$

where I_0 is the incident light intensity, A an equipment constant, L the optical path length (i.e. the sample thickness), and λ is the wavelength of the light. The voltage required for the first intensity maximum is an essential device parameter and called the half-wavelength voltage.

This paper describes the fundamental electro-optic properties of relaxor ferroelectrics, firstly, searching the possibility of new electro-optic materials. Then, the experimental data are given in detail on the $Pb(Mg_{1/3}Nb_{2/3})O_3$–$PbTiO_3$ system. Finally, a new type of two-dimensional light valve array for an image projector is introduced, which

Ceramics International Printed in Great Britain 0272-8842/95/$9.50

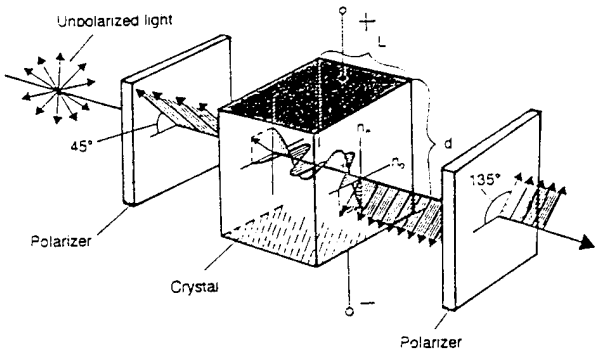

Fig. 1. Fundamental construction of an electro-optic light shutter.

can be mass-produced by a sophisticated tape casting technique. The drive voltage has been remarkably reduced, and FETs can be used directly for operation. This device will be a good candidate for the future high definition image projector.

2 CERAMIC ELECTRO-OPTIC MATERIALS

2.1 $Pb(Zn_{1/3}Nb_{2/3})O_3$

Relaxor ferroelectrics are remarked in non-linear optic applications because an extraordinarily large apparent 'electro-optic Kerr effect' can be observed, even in the so-called paraelectric state. Figure 2 shows the birefringence Δn vs electric field E relation of a $Pb(Zn_{1/3}Nb_{2/3})O_3$ single crystal in the paraelectric phase.[1] The single crystal sample was made by a flux method using excess PbO. The parabolic curve in the low field region tends to approach a straight line in the high field region.

A possible phenomenological analysis of this peculiar phenomenon is based on the model that the crystal is composed of the ferroelectric and paraelectric phases mixed together.[1] Suppose that the volume fraction of the paraelectric phase $x(T)$ is given by the accumulated Gaussian distribution with respect to temperature, the birefringence Δn is estimated by the summation of linear and quadratic electro-optic effects:[2]

$$\Delta n = [1 - x(T)]\, n^3(r_{33} - r_{13})\, E/2 + x(T)\, n^3 R_{11} E^2/2 \quad (3)$$

where n is the refractive index, and r and R represent electro-optic Pockels and Kerr coefficients, respectively. Even if the experimental data can be explained phenomenologically, the actual situation may not be so simple as this model: $x(T)$ should also be a function of electric field E.

Another more realistic explanation is found in a microscopic domain reversal mechanism. $Pb(Zn_{1/3}Nb_{2/3})O_3$ exhibits very small spindle-like domains (5 μm) with ambiguous boundaries arranged perpendicularly to the external electric field. When a field above 0·5 kV/mm is applied, the ambiguous curve domain walls move simultaneously in a certain size region, so that each micro-domain should change synchronously like co-operative phenomena (see Fig. 3).[3] It is noteworthy that the stripe period of the dark and bright domains (corresponding to up and down polarizations) will not be changed by the domain reversal, and that each domain area changes under an AC external field with zero net polarization at zero field. The relaxor crystal can be electrically-poled easily when an electric field is

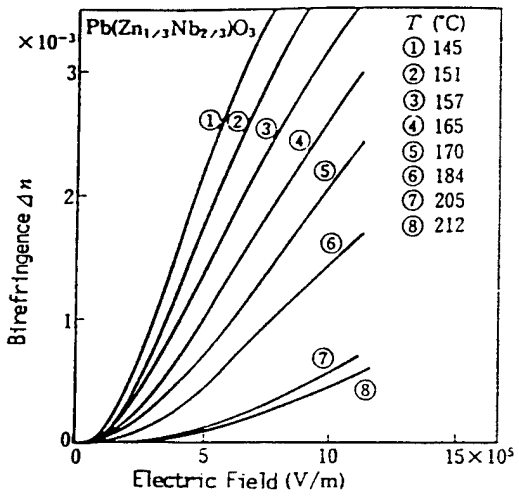

Fig. 2. Birefringence vs field in the paraelectric $Pb(Zn_{1/3}Nb_{2/3})O_3$.

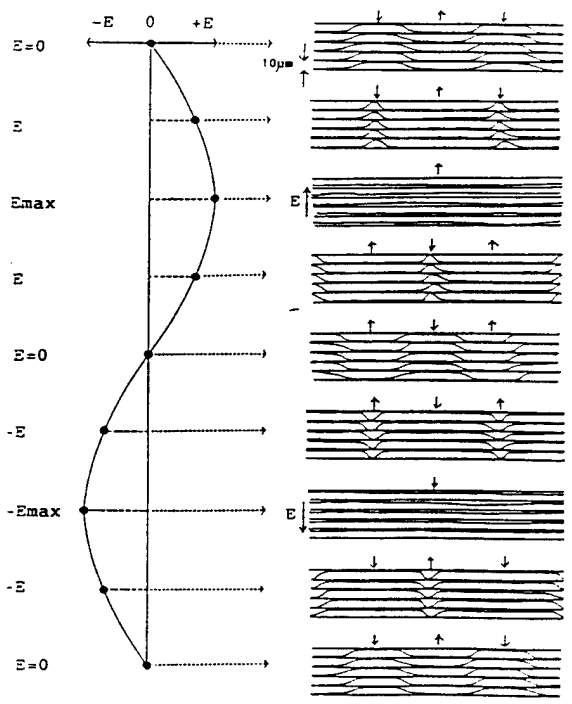

Fig. 3. Domain reversal mechanism in $Pb(Zn_{1/3}Nb_{2/3})O_3$.

applied around the transition temperature, and depoled completely without any remanent polarization. This can explain large 'apparent' secondary non-linear effects in physical properties such as electrostrictive and electro-optic Kerr phenomena, without exhibiting any hysteresis.

2.2 $(Pb,La)(Zr,Ti)O_3$

Famous transparent ceramics PLZT, i.e. $(Pb_{1-x}La_x)(Zr_yTi_z)_{1-x/4}O_3$, are also an example of relaxor ferroelectrics, which exhibit large electro-optic effect ($R = 9{\cdot}1 \times 10^{-16}$ m^{2}V^{-2}) near the composition 9/65/35 and are applicable to practical light shutters, displays, etc.

However, care must be taken for grain size control. Figure 4 shows the grain size dependence of the electro-optic coefficients, R and g (defined as $\Delta n = -(1/2)g\,n^3P^2$), in PLZT 9/65/35.[4] The samples were prepared by hot-press sintering starting from coprecipitated PLZT powders. The electro-optic response is drastically decreased below 2 μm, which corresponds approximately to the critical grain size below which the sample exhibits paraelectric properties.[5] Therefore, relatively large grain size is necessary to reveal the reasonable electro-optic effect.

On the other hand, a serious problem arises in fracture toughness or durability for particularly large grain size samples, probably due to the deficient (B-site vacancy) crystal structure. A normally sintered transparent PLZT ceramic with an average grain size more than 6 μm has fracture toughness of $K_{IC} = 0{\cdot}9$ MNm$^{-3/2}$,[5] which corresponds roughly to 10^8 cycles durability under repeating operation. This means only 2 months durability when the PLZT is used for an image display (TV) driven at 30Hz.

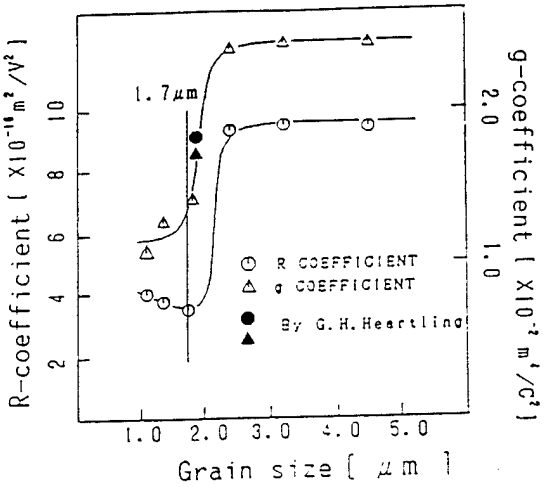

Fig. 4. Grain size dependence on the electro-optic coefficients. R and g, in PLZT 9/65/35.

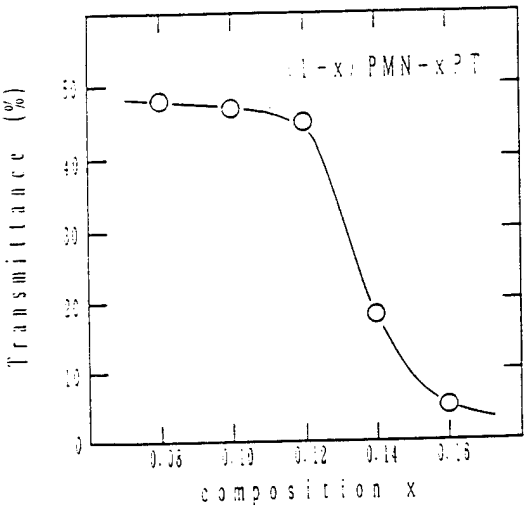

Fig. 5. Transmittance of a 0·5 mm thick sample for $\lambda = 633$ nm in $(1\text{-}x)Pb(Mg_{1/3}Nb_{2/3})O_3$–$xPbTiO_3$.

2.3 $Pb(Mg_{1/3}Nb_{2/3})O_3$–$PbTiO_3$

Discovery of a new ceramic electro-optic material with higher fracture toughness, as well as larger electro-optic coefficients, will be an urgent necessity for image display applications. The following conditions should be satisfied for the ceramic: (1) ceramic transparency requires almost zero birefringence in the original state (i.e. a pseudo-cubic structure) to suppress light scattering, (2) large fracture toughness may be obtained in a sufficiently packed structure, (3) large electro-optic effect is realized in relaxor ferroelectrics.

The $Pb(Mg_{1/3}Nb_{2/3})O_3$–$PbTiO_3$ system, which is known as a superior electrostrictive (secondary effect) material with very high fracture toughness ($K_{IC} = 1{\cdot}7$ MNm$^{-3/2}$), may be a good candidate to investigate from an electro-optic viewpoint. Samples

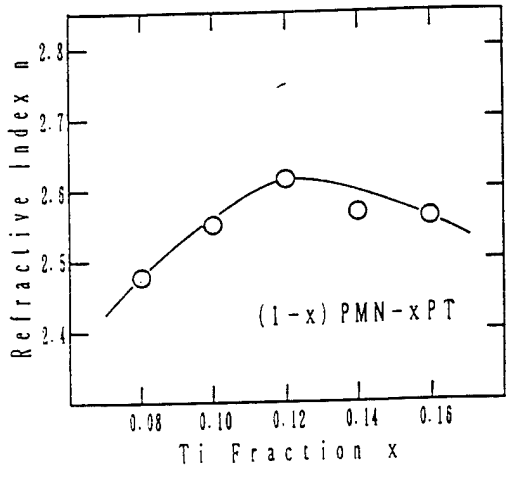

Fig. 6. Refractive index change in $(1\text{-}x)Pb(Mg_{1/3}Nb_{2/3})O_3$ –$xPbTiO_3$.

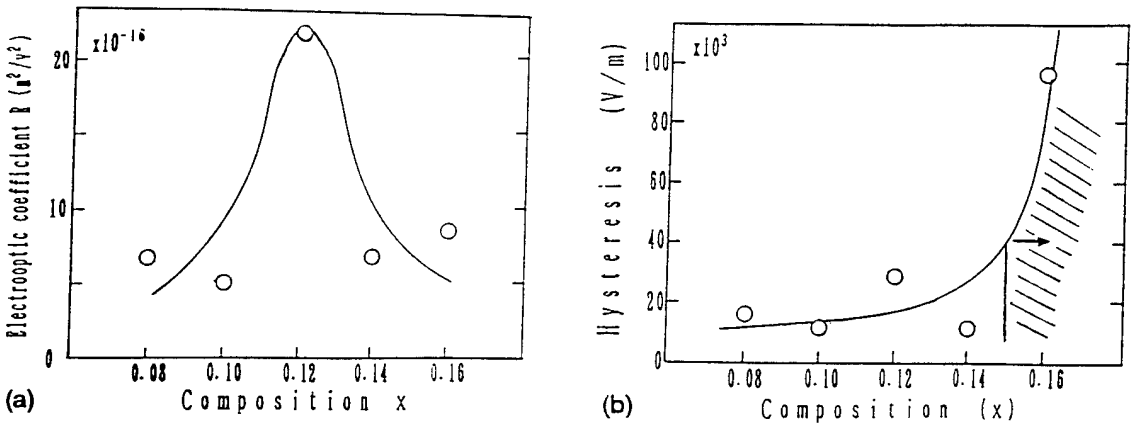

Fig. 7. Changes in (a) the electro-optic coefficient R and (b) the corresponding hysteresis in $(1\text{-}x)Pb(Mg_{1/3}Nb_{2/3})O_3\text{–}xPbTiO_3$.

of the $(1\text{-}x)Pb(Mg_{1/3}Nb_{2/3})O_3\text{–}xPbTiO_3$ system were prepared by hot-press sintering starting from the oxide mixtures. Note that the Curie temperature increases gradually with the $PbTiO_3$ content, passing room temperature around $x = 0{\cdot}12$, and the crystal structure is pseudo-cubic in the region below $x = 0{\cdot}4$. Figure 5 shows the composition x dependence of light transmittance ($\lambda = 633$ nm) of a 0·5 mm thick sample in the $(1\text{-}x)Pb(Mg_{1/3}Nb_{2/3})O_3\text{–}xPbTiO_3$ system. The transmittance is reduced drastically above $x = 0{\cdot}14$, probably due to the scattering caused by the spontaneous birefringence. The best transmittance (49%) is still smaller than 62% in the conventional PLZT; this suggests that more sophisticated powder preparation techniques will be required for the PMN–PT. The refractive index n ($\lambda = 633$ nm) change with x is plotted in Fig. 6, which shows a small maximum around $x = 0{\cdot}12$. The values are slightly larger than $n = 2{\cdot}49$ in PLZT 10/65/35. The most intriguing data can be found in electro-optic measurements. Figures 7(a) and 7(b) show the electro-optic R coefficient and its corresponding hysteresis for $\lambda = 633$ nm, respectively, plotted as a function of composition x. The maximum electro-optic R coefficient of 22×10^{-16} m^2V^{-2} for $x = 0{\cdot}12$ is more than twice as large as $9{\cdot}1 \times 10^{-16}$ m^2V^{-2} in the famous PLZT 9/65/35. The hysteresis, defined as an equivalent bias electric field to fit the experimental Δn curve by the quadratic relation of E, increases drastically above $x = 0{\cdot}16$, the samples in which region can not be used practically.

In conclusion, $0{\cdot}88\ Pb(Mg_{1/3}Nb_{2/3})O_3\text{–}0{\cdot}12\ PbTiO_3$ will be the better electro-optic ceramic with high mechanical toughness, if better light transmission is obtained by improving the preparation technology.

3 TWO-DIMENSIONAL DISPLAYS

This section deals with a concept of a projection type TV utilizing two-dimensional PLZT displays. The development of a simple mass-production

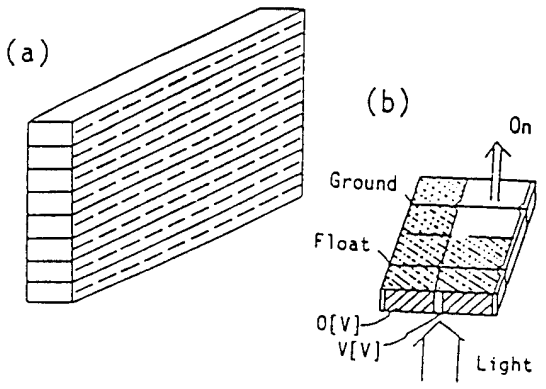

Fig. 8. Newly developed design of a two-dimensional display.

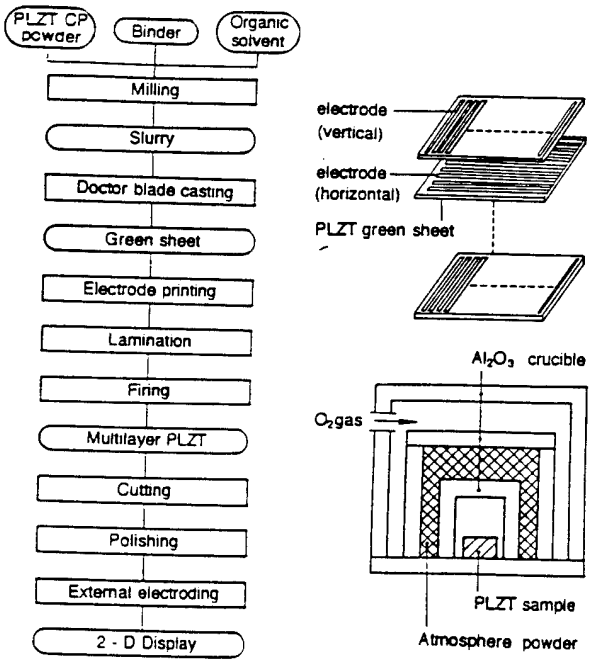

Fig. 9. Fabrication process of the new 2-D display.

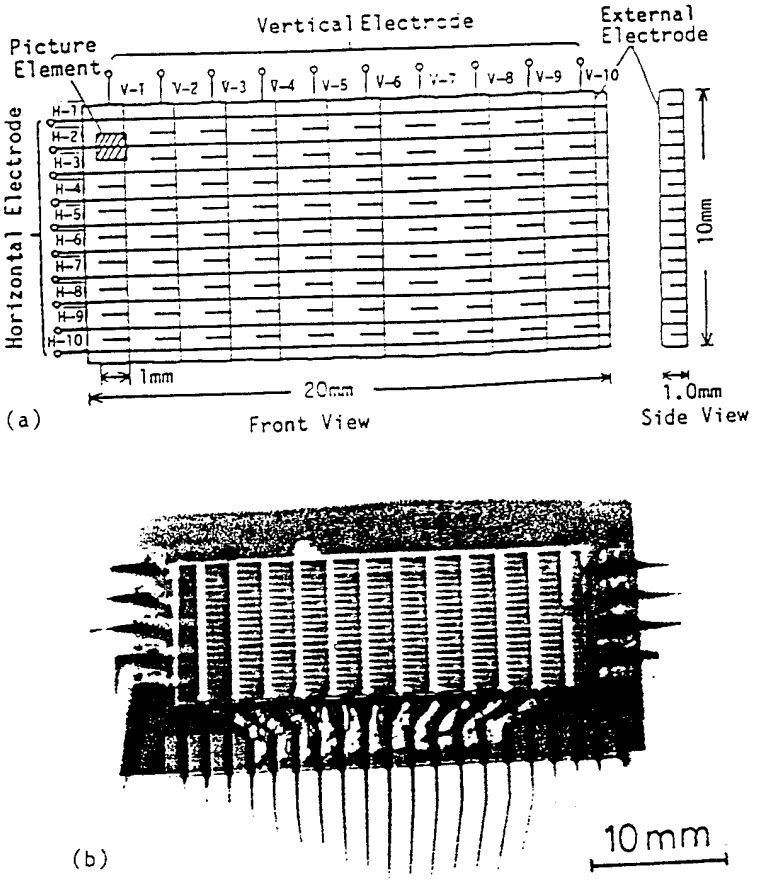

Fig. 10 (a) Schematic electrode configuration of a (10 × 10) matrix PLZT light valve. (b) Top view photograph of a PLZT light valve with external electrodes.

process and the designing of electrode configurations with a narrow gap are the key factors for the PLZT displays. A newly developed design, as shown in Fig. 8, presents a very bright image with a slight crosstalk-related problem and is easy to produce.

3.1 Fabrication process of the 2-D display

The fabrication process of the two-dimensional PLZT light valve array is outlined in Fig. 9.[6] Coprecipitated PLZT 9/65/35 powders were mixed with organic solvent and binder and formed into a green sheet. Platinum internal electrodes were printed on the green sheets. The electroded sheets were then laminated alternately in 90° different orientations under a pressure of 3000 psi, so as to make plate-through and separate electrodes. The laminated body was sintered in an oxygen-controlled atmosphere, and the bulk was cut and polished. Finally the external connecting electrodes were applied to make vertical and horizontal addressing.

Figure 10(a) shows the electrode configuration of a (10 × 10) matrix light valve. The shaded portion of the device in the figure represents one image unit (pixel). The vertical separate internal electrodes were connected by external electrodes printed on the surface of the device. The horizontal plate-through electrodes were embedded 100 μm deeper from the optical surface to avoid shorting with the vertical electrode connectors. Figure 10(b) shows a picture of the newly fabricated display. Note that the layer thickness is about 0·35 mm.

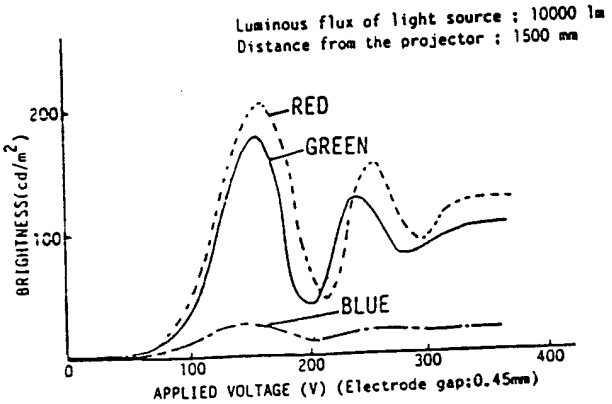

Fig. 11. Brightness on the screen vs applied voltage for red, green or blue light. Note that the half wavelength voltage differs for these three lights.

3.2 Characteristics of the light valve array

The optical transmittance of the PLZT device fabricated by the tape casting technique was 62% at λ = 633 nm, which is in good comparison with 63% for the ideal sample prepared by hot-pressing. The brightness for red, green and blue light was measured as a function of applied voltage (Fig.11), where the electrode gap was 0·45 mm.[6] The contrast ratio, defined by a ratio of brightness on the screen under the application of half-wavelength voltage over brightness under zero volt (220 cd/m^2/2·8 cd/m^2), was about 80, rather superior to the values for the conventional cathode ray tubes or liquid crystal displays. The response time associated with a single pixel of the display was less than 10 μsec for both rising and falling processes, which is rapid enough to drive this shutter array at a raster frequency of the conventional CRTs.

3.3 Construction of the image projector

The driving circuit of the display is represented schematically in Fig. 12(a). When the terminals of the device are addressed as shown in Fig. 12(b), the image appearing in Fig. 12(c) (alphabet 'F') is generated on the screen.[6]

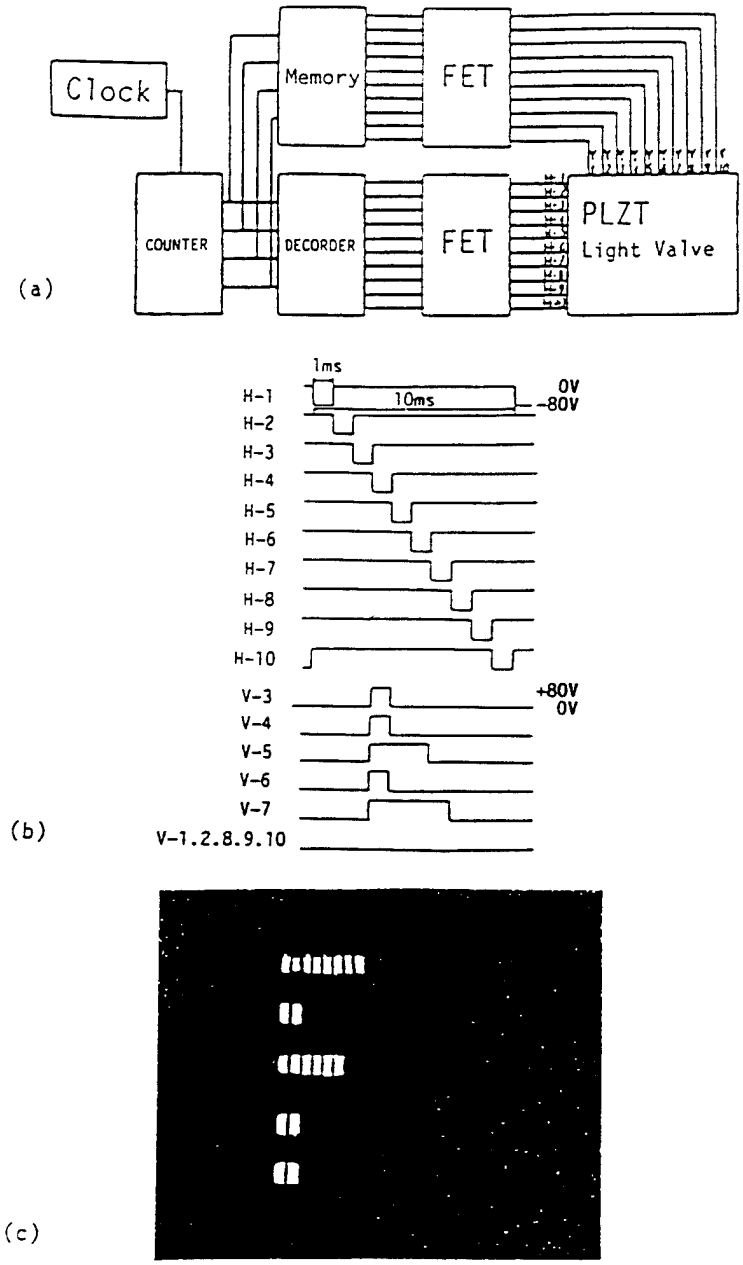

Fig. 12. (a) Driving circuit of the 2-D display. (b) Example wave forms of the driving signal. (c) An example image 'F' on the screen illuminated from the PLZT projector.

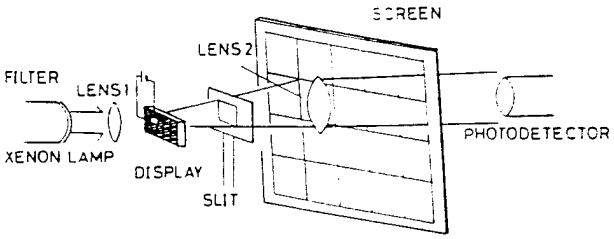

Fig. 13. Crosstalk test system. The light through a slit focused on the screen is measured.

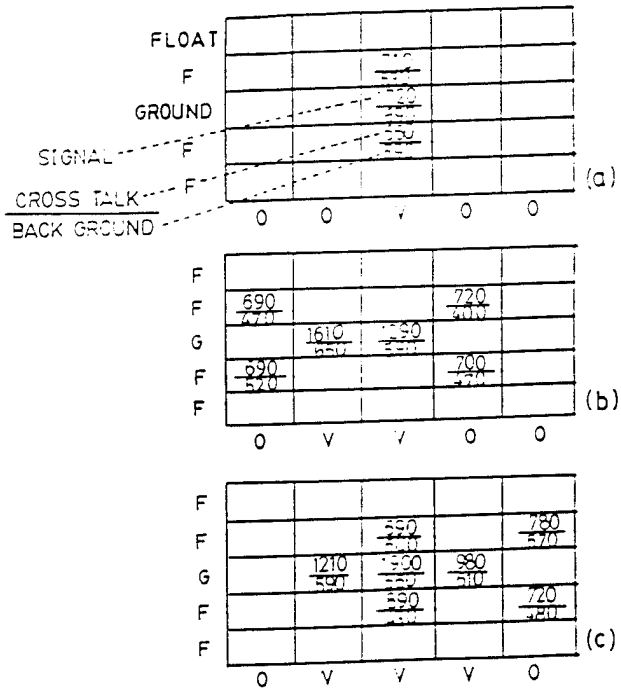

Fig. 14. Crosstalk patterns for different signal addressing: (a) Vertical type, (b) oblique type and (c) complex type.

Crosstalk phenomenon was checked on the 2-D display using a setup as illustrated in Fig. 13 with monochromatic light. The test was made with keeping one vertical terminal on (Ground) and applying high voltage on multiple horizontal terminals. There are three different crosstalk patterns: vertical, horizontal and oblique types. The results are shown in Fig. 14(a)–(c) for the different input number of horizontal terminals, where the top and bottom of a pair of figures indicate the light intensity in μW unit on the screen in ON state and OFF state, respectively. The leakage light intensity associated with the vertical or horizontal crosstalk is 20–30% or 10–20% of the main peak intensity, which does not affect the image contrast significantly. On the contrary, the oblique type crosstalk causes not negligible leakage up to 50% depending on the applied voltage and the number of horizontal addressing input signal (combination type crosstalk). Modification of the internal electrode configurations will be necessary to avoid the crosstalk problem completely.

4 CONCLUSIONS

1. Relaxor ferroelectrics are widely applicable to electro-optic light valves/displays, etc. Superior characteristics of these materials are mainly attributed to the easy poling of the ferroelectric micro-domains.

2. A new electro-optic ceramic, 0·88 $Pb(Mg_{1/3}Nb_{2/3})O_3$–0·12$PbTiO_3$, with high mechanical toughness may provide a breakthrough for long-term display applications.

3. A new type of PLZT two-dimensional light valve fabricated by a tape casting technique has been developed, and a prototype image projector was investigated. It is easy to mass-produce, leading to a low manufacturing cost. This light valve exhibits bright image with a negligible crosstalk-related problem. It can be driven in quick response (10 μsec) by a relatively low drive voltage (100 V/0·35 mm gap) in comparison with the conventional PLZT devices. The applicative feasibility to a high definition image projector was verified.

REFERENCES

1. KOJIMA, F., KUWATA, J. & NOMURA, S., *Proc. 1st Meeting on Ferroelectric Materials and Applications*. Kyoto, 1977, pp. 155–58.
2. KUWATA, J., UCHINO, K. & NOMURA, S., *Ferroelectrics*, **22** (1979) 863–67.
3. UJIIE, R. & UCHINO, K., *Proc. IEEE Ultrasonic Symp.*, pp. 725–28. Hawaii, 1990.
4. TOKIWA, K. & UCHINO, K., *Ferroelectrics*, **94** (1989) 87–92.
5. UCHINO, K. & TAKASU, T., *Inspec.*, **10** (1986) 29–33.
6. UCHINO, K., TOKIWA, K., GINIEWICZ, J., MURAI, Y. & OHMURA, K., *Ceram. Trans.*, **14** (1990) 297–310.

6. Chu, S. Y. and K. Uchino, "Photo-Acoustic Devices Using (Pb,La)(Zr,Ti)O_3 Ceramics," Proc. 9th Int'l Symp. Appl. Ferroelectrics p.743-745 (1995).

PHOTO-ACOUSTIC DEVICES USING (Pb,La)(Zr,Ti)O3 CERAMICS

Sheng-Yuan Chu and Kenji Uchino
International Center for Actuators and Transducers
Intercollege Materials Research Laboratory
The Pennsylvania State University, University Park, PA 16802

Abstract -- Photostriction in ferroelectrics arises from a superposition of photovoltaic and inverse piezoelectric effects. This phenomenon provides promise for photo-acoustic devices, when the response has been sufficiently improved. In this paper, B-site donor doping was investigated in (Pb, La)(Zr, Ti)O3 based ceramics with the aim of improving the response speed. Using a PLZT bimorph configuration, a photoacoustic device was trially fabricated, and the fundamental mechanical resonance was observed under intermittent illumination of purple-color light, having neither electric lead wires nor electric circuit.

INTRODUCTION

Photostrictive effect is a phenomenon in which strain is induced in the sample when it is illuminated. This effect is focused especially in the field of optical communication, where the key components are solid state lasers as a light source, optical fibers as a transfer line, and displays/telephones as a visual/audible interface with the human. The former two components have been developed fairly successfully, and the photo-acoustic device (i. e. optical telephone or "photophone") will be eagerly anticipated in the next century. Photostrictive devices which function when they receive the energy of light will be particularly suitable for use in the above-mentioned fields.

In principle, the photostrictive effect is the superimposing of a photovoltaic effect, where a large voltage is generated in ferroelectrics through the irradiation of light, and a piezoelectric effect, where the material expands or contracts from the voltage applied. The photovoltaic effect mentioned here generates a greater-than-band-gap voltage, and is quite different from that based on the p-n junction of semiconductors (i. e. solar battery).[1-3] It is generated when electrons excited by light move in a certain direction of the ferroelectric crystal due to the spontaneous polarization (i. e. crystallo-graphic anisotropy).

So far, most of the studies on the photovoltaic effect have been made on single crystals to clarify the origin of the effect.[1-3] However, our research group has been focusing on polycrystalline samples such as PbTiO3-based[4,5] and Pb(Zr, Ti)O3-based ceramics[6,7] from a practical application point of view. High photovoltage (≈ 1 kV/cm) generators with relatively quick response (≈ 10 sec) have been developed in the (Pb, La)(Zr, Ti)O3 (PLZT) system. Moreover, bimorph-type photostrictive elements could exhibit large tip deflections under UV light illumination.[6,7].

In this paper, the photovoltaic effect in PLZT(3/52/48) based ceramics has been investigated as a function of B-site donor dopants. Then, using the PLZT bimorph, a photoacoustic device was trially fabricated, and the fundamental mechanical resonance was observed under intermittent illumination.

SAMPLE PREPARATION

PLZT (x/y/z) samples were prepared in accordance with the following composition formula:

$$Pb_{1-y}La_y(Zr_{1-x}Ti_x)_{1-\frac{y}{4}}O_3.$$

Since the photostriction figure of merit is defined as the product o the photovoltaic voltage and piezoelectric coefficien ($x_{ph} = d_{33} \times E_{ph}$), PLZT(3/52/48) was selected due to its optimun photostrictive response within the PLZT system.[6] According t our preliminary study on impurity doping,[7] WO3 doped PLZ ceramics were prepared.

Ceramic powders were prepared by a conventional mixed oxid technique. PbCO3, La2O3, ZrO2, TiO2 and WO3 were weighed i the appropriate proportions and mixed in a ball mill for 2 days usin ethanol and zirconia grinding media. 0.5 wt% excess PbCO3 wa added to compensate for weight loss during calcination an sintering. The slurry was dried, then calcined in a closed alumin crucible at 950 °C for 10 hours. The calcined powder was ball milled again for 48 hours. The samples were sintered in seale alumina crucibles at 1270 °C for 2hrs. A PbO rich atmosphere wa maintained with lead zirconate powder to minimize lead loss durin sintering. Sintered samples were cut, polished and electroded wit silver paste. Finally, each sample was poled at 15 kV/cm in silicon oil at 120°C.

The poled PLZT ceramics were used to make bimorph actuator The elements were 20 x 4 x 0.15 mm^3: the 4 x 0.15 mm^2 surfac was electroded with silver paste and silver wires were attached. Th bimorph actuator consisted of two bonded oppositely-poled cerami plates (refer to Fig. 2).

IMPURITY DOPING EFFECT

Impurity doping on PLZT affects the photovoltaic respons significantly.[7] Regarding the photostriction effect, it is known th as the photovoltaic voltage increases, the strain value increases, an

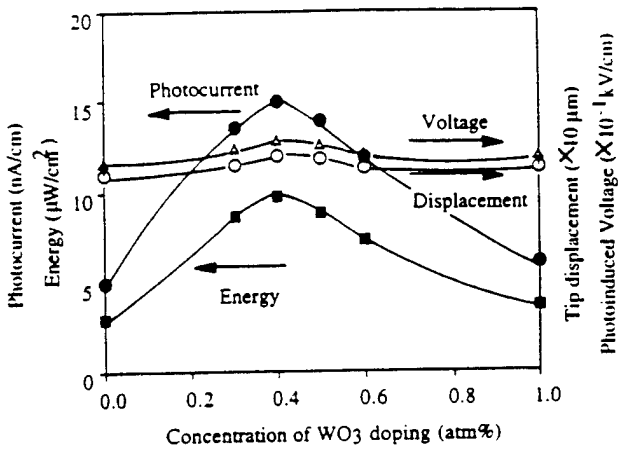

Fig. 1 Changes in photovoltaic current, voltage, power and tip displacement as a function of dopant WO3 concentration ir PLZT (3/52/48).

CH3416-5 0-7803-1847-1/95/$4.00©1995IEEE

with increasing photo-current, there is an increase in the overall response. The photovoltaic response is enhanced by donor doping onto the B-site (Nb^{5+}, Ti^{5+}, W^{6+}). On the other hand, impurity ions substituting at the A-site and/or acceptor ions substituting at the B-site, whose ionic valences are small (1 to 4), have no effect on the response.

Figure 1 shows the photovoltaic current, photovoltaic voltage, photo-induced tip displacement and stored energy (P=(1/2) Imax × Vmax) in PLZT 3/52/48 samples ploted as a function of atm % of WO_3 doping concentration. It was found that higher photovoltaic response can be obtained in WO_3 doped samples. The photovoltaic voltage reaches 1 kV/mm, and the current is on the order of nA. The maximum of the saturated tip displacement was about 120 μm for 0.4 atm% WO_3 doped samples. The displacement of 30 μm could be obtained in one second under a light intensity of 4 mW/cm^2 (λ = 370 nm).

PHOTO-ACOUSTIC MEASUREMENT

The mechanical resonance frequency of this bimorph sample can be estimated according to the equation:

$$f_r = 0.158 \times \frac{t}{l^2}\sqrt{\frac{1}{\rho s_{11}^E}}, \qquad (1)$$

where t and l are the thickness and length of the bimorph sample, respectively, ρ is the density and s_{11}^E is the elastic compliance of the ceramic. The calculated resonance frequency of the PLZT based bimorph, (ρ = 7.9 g/cm^3 and s_{11}^E = 16 × 10^{-12} m^2/N), was about 3 kHz: too high for photo-induced resonance measurements. Therefore, a thin cover glass was attached to the bimorph sample to reduce the resonance frequency, as shown in Fig. 2. Initially, to determine the electromechanical resonance behavior, an ac. voltage was applied to the bimorph, and the tip displacement was monitored by changing the drive frequency, using the experimental setup shown in Fig. 3. Figure 4 shows the mechanical resonance characteristics obtained from this experiment. The resonance frequency was ~ 79 Hz with a mechanical quality factor Q of ~ 30. The maximum displacement of this thin-plate attached sample was about 14 μm at 80 $V_{p\text{-}p}$.

Then, the photo-induced mechanical resonance was measured using the system shown in Fig. 5. Radiation from a high-pressure mercury lamp (Ushio Electric USH-500D) was passed through a UV bandpass filter (Oriel Co., No.59811), an IR blocking filter (Oriel Co., No.59060), an optical focusing lens and an optical chopper to provide intermittent sample irradiation. A wavelength peak of 370 nm, where the maximum photovoltaic effect of PLZT is obtained, was used. A dual beam method was used to irradiate the two sides of the bimorph alternately.[7] Two beams, A and B, were chopped so as to cause a 180 degree phase difference as illustrated

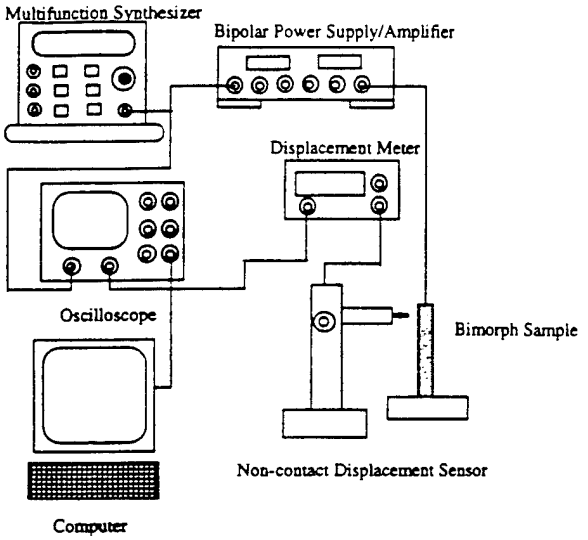

Fig.3 Experimental setup for the electro-mechanical resonance measurement.

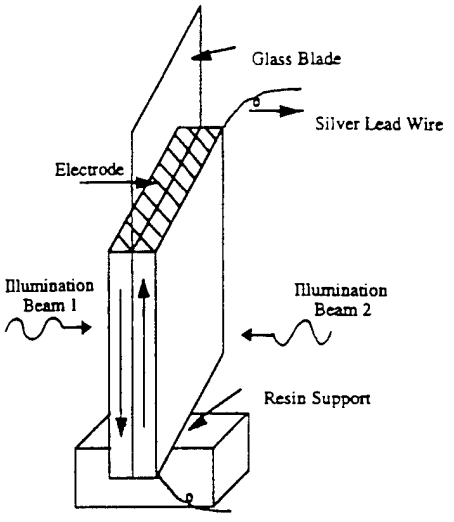

Fig.2 Configuration of a thin-plate attached photo-acoustic bimorph.

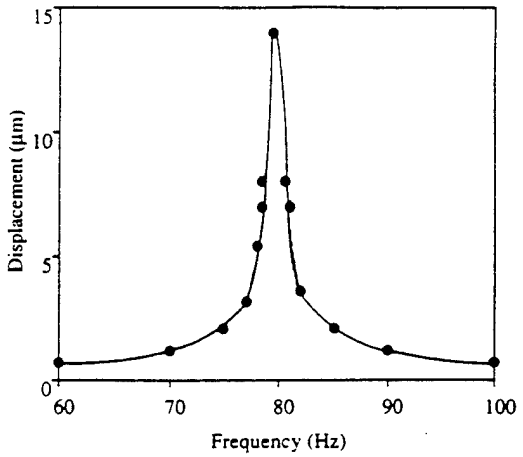

Fig.4 Electromechanical resonance behavior of the PLZT bimorph.

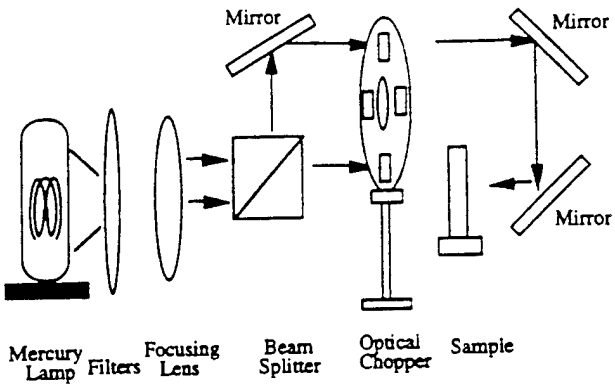

Fig.5 Experimental setup for the photo-induced mechanical resonance measurement.

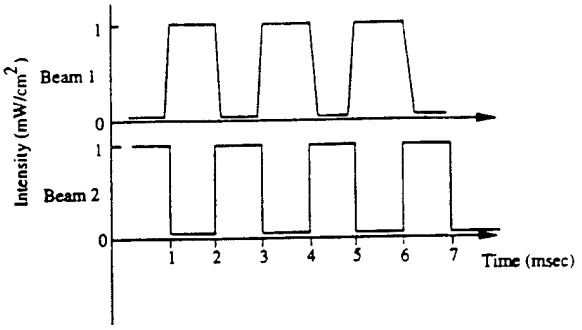

Fig.6 Wave forms for the two beams for illuminating the bimorph sample.

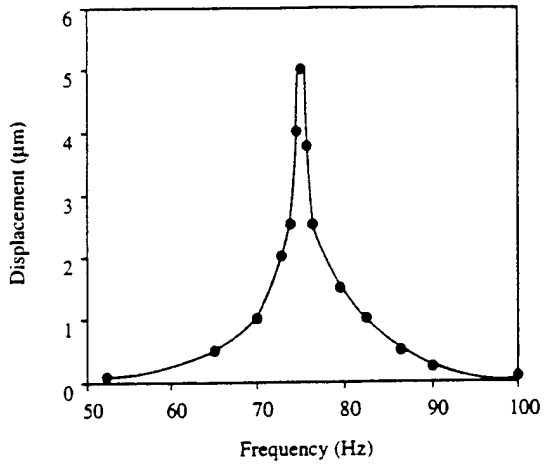

Fig.7 Photo-induced mechanical resonance behavior of the PLZT bimorph.

in Fig. 6. The slow recovery because of the low dark conductivity was overcome using this dual beam method. The mechanical resonance was then determined by changing the chopper frequency.

The tip displacement of the thin-plate-attached sample as a function of chopper frequency is presented in Fig. 7. Photo-induced mechanical resonance was successfully observed. The resonance frequency was about 75 Hz with the mechanical quality factor Q of about 30; in good agreement with the previous electromechanical data. The maximum tip displacement of this photostrictive sample was about 5 μm of resonance.

CONCLUSION

Photo-mechanical resonance of a PLZT ceramic bimorph actuator has been successfully induced using chopped UV irradiation, having neither electric lead wires nor electric circuit. A thin cover glass was attached on the bimorph structure to decrease the resonance frequency so as to easily observe the photo-induced resonance. The resonance frequency was 75 Hz with a mechanical quality factor Q of about 30 under dual beam operation. The maximum tip displacement of this sample was about 5 μm, smaller than the level required for audible sound. However, the achievement of photo-induced mechanical resonance in the audible frequency range suggests the promise of photostrictive PLZT bimorph-type devices as photo-acoustic components, or "photophones", for the next optical communication age.

ACKNOWLEDGEMENT

This work is supported by Army Research Laboratory (ARL), No. DAALO3-92-G-0244.

REFERENCES

[1] V. M. Fridkin, "Photoferroelectrics", Ed. by M. Cardona, P. Fulde, H. -J. Queisser, Solid State Sciences, New York, (1979), pp. 85.
[2] A. M. Glass, D. von der Linde, D. H. Austin and T. J. Negran, *J. Elec. Mat.* **4** [5], 915-943 (1975).
[3] V. M. Fridkin and B. N. Povov, *Sov. Phys. Usp.*, **21**(12), 981-991 (1978).
[4] K. Uchino, Y. Miyazawa and S. Nomura, *Jpn. J. Appl. Phys.*, **21**, [12], 1671-1674 (1982).
[5] K. Uchino, Y. Miyazawa and S. Nomura, *Jpn. J. Appl. Phys.* Suppl. **22-2**, 102-105 (1983).
[6] T. Sada, M. Inoue and K. Uchino, *J. Ceram. Soc. Jpn.*, **5**, 545 (1987).
[7] M. Tanimura and K. Uchino, *Sensors and Materials*, **1**, 47-56 (1988).

7. Uchino, K., "Photostrictive Actuators and "Photophones"," Proc. Int'l Symp. Microsystems, Intelligent Mater. and Robots, p.193-196 (1995).

Proceedings of the International Symposium on
Microsystems, Intelligent Materials and Robots
September 27-29, 1995, Sendai, Japan

PHOTOSTRICTIVE ACTUATORS AND "PHOTOPHONES"

Kenji Uchino
International Center for Actuators and Transducers
Materials Research Laboratory, The Pennsylvania State University
University Park, PA 16802, USA

Photostriction in ferroelectrics arises from a superposition of photovoltaic and inverse piezoelectric effects. (Pb,La)(Zr,Ti)O_3 ceramics doped with WO_3 exhibit large photostriction under irradiation of near-ultraviolet light, and are applicable to remote control actuators and photoacoustic devices. Using a bimorph configuration, a photo-driven relay and a micro walking device have been developed, which are designed to start moving as a result from the irradiation. The mechanical resonance of the bimorph was also induced by an intermittent illumination, verifying the feasibility of the photostriction to "photophone" applications.

INTRODUCTION

Photostrictive effect is a phenomenon in which strain is induced in the sample when it is illuminated. This effect is focused especially in the fields of micromechanism and optical communication.

With decreasing the size of miniature robots/actuators, the weight of the electric lead wire connecting the power supply becomes significant, and remote control will definitely be required for sub-millimeter devices. A photo-driven actuator is a promising candidate for micro-robots. On the other hand, the key components in the optical communication are a solid state laser as a light source, an optical fiber as a transfer line, and a display/ a telephone as a visual/audible interface with the human. The former two components have been developed fairly successfully, and the photo-acoustic device (i. e. a "photophone") will be eagerly anticipated in the next century.

Photostrictive devices which are actuated when they receive the energy of light will be particularly suitable for use in the above-mentioned fields. In principle, the photostrictive effect arises from a superposition of a photovoltaic effect, where a large voltage is generated in a ferroelectric through the irradiation of light,[1] and a piezoelectric effect, where the material expands or contracts under the voltage applied. Ii is noteworthy that this photostriction is neither the thermal dilatation nor the pyroelectrically-produced strain associated with a temperature rise due to the light illumination. Also the photovoltaic effect mentioned here generates a greater-than-band-gap voltage (several kV/cm), and is quite different from that based on the p-n junction of semiconductors (i. e. solar battery).

This paper reviews the fundamental photostrictive effect in (Pb,La)(Zr,Ti)O_3 ceramics first, then describes its applications to a photo-driven relay, a micro walking machine and a photophone, which are designed to function as a result of irradiation, having neither lead wires nor electric circuits.

PHOTOSTRICTIVE PROPERTIES

PRINCIPLE

Although the origin of the bulk photovoltaic effect has not been clarified yet, the key point to understand it is the necessity of both *impurity doping* and *crystal asymmetry*. Figure 1 illustrates one of the proposed models, the electron energy band model proposed for (Pb,La)(Zr,Ti)O_3.[2,3] The energy band is basically generated by the hybridized orbit of p-orbit of oxygen and d-orbit of Ti/Zr. The donor impurity levels induced in accordance with La doping (or other dopants) are present slightly above the valence band. The transition from these levels with an asymmetric potential due to the crystallographic anisotropy may provide the "preferred" momentum to the electron. Electromotive force is generated when electrons excited by light move in a certain direction of the ferroelectric crystal, which may arise along the spontaneous polarization direction.

The asymmetric crystal exhibiting a photovoltaic response is also piezoelectric in principle, and therefore, a photostriction effect is expected as a coupling of the bulk photovoltaic voltage with the piezoelectric d constant.

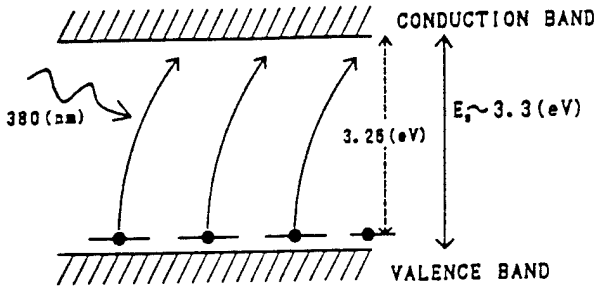

Figure 1 Energy band gap model of excited electron transition from impurity level in PLZT.

The figure of merit of the photostriction is evaluated by the product of the photovoltaic voltage (E^{ph}) and the piezoelectric coefficient (d). PZT based ceramics are currently focused because of their excellent piezoelectric properties, i. e. high d values. PLZT is one of such materials, which is also famous as a transparent (good sintered without pores) ceramic applicable to electrooptic devices.

PLZT (x/y/z) samples were prepared in accordance with the following composition formula:

$$Pb_{1-x}La_x(Zr_yTi_z)_{1-x/4}O_3.$$

Figures 2(a) and 2(b) illustrate the contour maps of the photovoltaic response and the piezoelectric strain constant d_{33} on the PLZT phase diagram.[4,5] The d_{33} shows the maximum around the morphotropic phase boundary (MPB) between the tetragonal and rhombohedral phases, and increases gradually with increasing the La concentration up to 9 mol %. On the contrary, the photovoltage exhibits the maximum also around the MPB, but in the tetragonal region with 3 mol % of La. The largest pruduct $d_{33}\cdot E^{ph}$ was obtained with the composition (3/52/48).

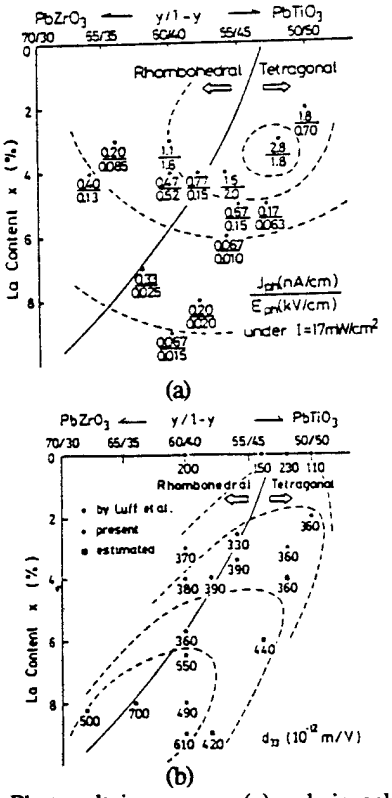

Figure 2 Photovoltaic response (a) and piezoelectric constant d_{33} (b) of PLZT plotted on the phase diagram near the morphotropic phase boundary between the tetragonal and rhombohedral phases.

Impurity doping on PLZT also affects the photovoltaic response significantly.[3] Figure 3 shows the photovoltaic response for various dopants with the same concentration of 1 atomic % into the base PLZT (3/52/48) under an illumination intensity of 4 mW/cm^2 at 366 nm. The dashed line in Fig. 3 represents the constant power curve corresponding to the non-doped PLZT (3/52/48). Regarding the photostriction effect, it is known that as the photovoltaic voltage increases, the strain value increases, and with increasing photocurrent, there is an increase in the overall response. The photovoltaic response is enhanced by donor doping onto the B-site (Nb^{5+}, Ti^{5+}, W^{6+}). On the other hand, impurity ions substituting at the A-site and/or acceptor ions substituting at the B-site, whose ionic valences are small (1 to 4), have no significant effect on the response.

Even when the composition is fixed, the photostriction still depends on the sintering condition or the grain size.[5] Figure 4 shows the dependence of the photostrictive characteristics on the grain size. The smaller grain sample is preferrable, if it is sintered to a high density.

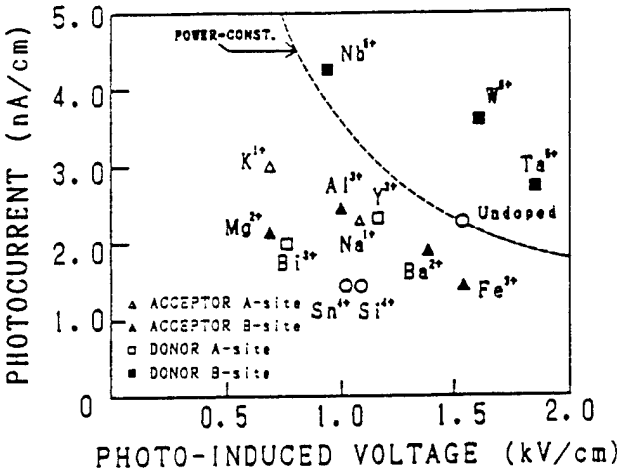

Figure 3 Photovoltaic response of PLZT for various impurity dopants (illumination intensity:4mW/cm^2).

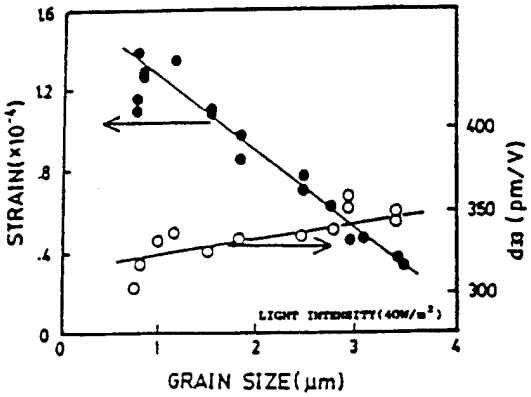

Figure 4 Grain size dependence of photostrictive characteristics in PLZT (3/52/48).

DISPLACEMENT MAGNIFICATION MECHANISM

Since the maximum strain level of the photostriction is only 0.01 % (this corresponds to 1 μm displacement from a 10 mm sample), we need to consider a sophisticated magnification mechanism of the displacement. We employed a bimorph structure, which is anologous to a bimetal consisting of two metalic plates with different thermal expansion coefficients bonded together to generate a bending deformation according to a temperature change. Two PLZT plates were pasted back to back, but were placed in opposite polarization, then connected on the edges electrically, as shown in Fig. 5.[3] A purple light (366 nm) was shined to one side, which generated a photovoltaic voltage of 7 kV across the length. This caused the PLZT plate on that side to expand by nearly 0.01 % of its length, while the plate on the other (unlit) side contracted due to the piezoelectric effect through the photovoltage. Since the two plates were bonded together, the whole device bent away from the light. For this 20 mm long and 0.35 mm thick bi-plate, the displacement at the edge was 150 μm, and the response speed was a couple of seconds.

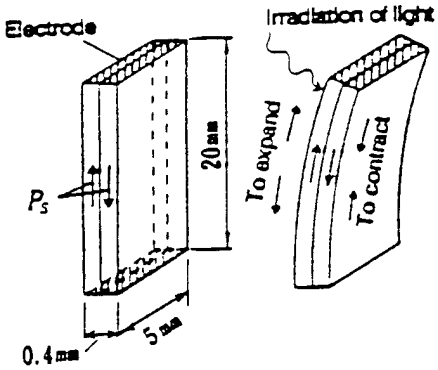

Figure 5 Structure of the photo-driven bimorph and its driving principle.

DEVICE APPLICATIONS

In this section we will introduce the applications of photostriction to a photo-driven relay, a micro walking machine and a photophone, which are designed to function as a result of irradiation, having neither lead wires nor electric circuits.

PHOTO-DRIVEN RELAY

A photo-driven relay was constructed using a PLZT photostrictive bimorph as a driver which consists of two ceramic plates bonded together with their polarization directions opposing each other (Fig. 6).[3] A dummy PLZT plate was positioned adjacent to the bimorph to cancel the photovoltaic voltage generated on the bimorph. Utilizing a dual beam method, switching was controlled by alternately irradiating the bimorph and the dummy. The time delay of the bimorph that ordinarily occurs in the off process due to a low dark conductivity could be avoided, making use of this dual beam method. Figure 7 shows the response of a photostrictive bimorph made from PLZT doped with 0.5 at% WO_3 under an illumination intensity of 10 mW/cm^2. The amount of displacement observed at a tip of the bimorph (20 mm long and 0.35 mm thick) was ±150 μm. A snap action switch was used for the relay. Switching by a displacement of several tens of micron was possible with this device. The on/off response of the photo-driven relay showed a typical delay time of 1 - 2 seconds.

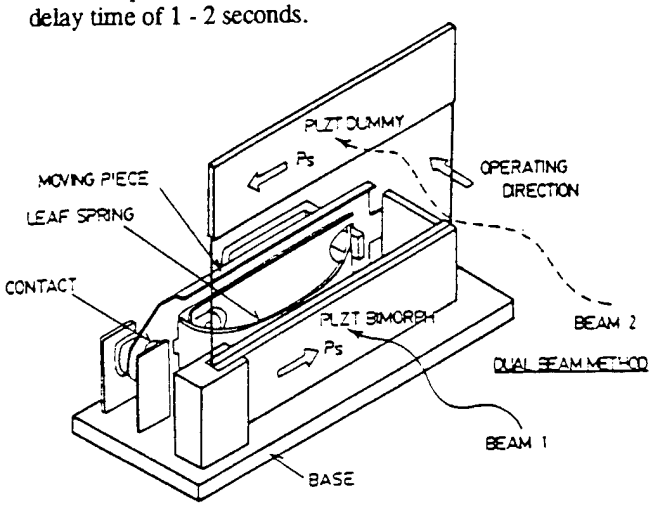

Figure 6 Structure of the photo-driven relay.

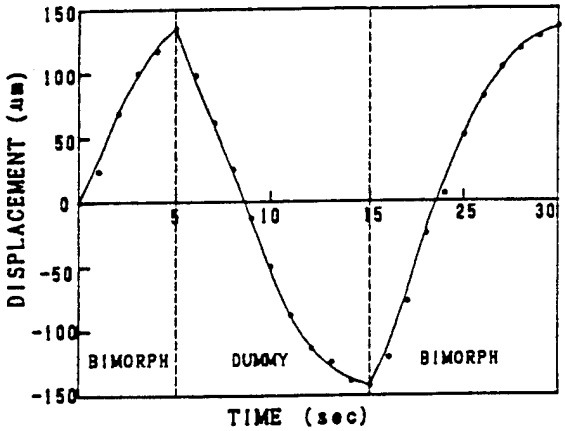

Figure 7 Tip deflection of the bimorph device made from WO_3 0.5 at.% doped PLZT under a dual beam control (illumination intensity: 10 mW/cm^2).

MICRO WALKING DEVICE

A photo-driven micro walking machine has also been developed using the photostrictive bimorphs.[6] It was simple in structure, having only two ceramic legs (5mmx 20mmx 0.35mm) fixed to a plastic board (Fig. 8). When the

two legs were irradiated with purple light alternately, the device moved like an inchworm. The photostrictive bimorph as a whole was caused to bend by ±150 μm as if it averted the radiation of light. The inchworm built on a trial basis exhibited rather slow walking speed (several tens μm/min), since slip occurred between the contacting surface of its leg and the floor. The walking speed can be increased to approximately 1 mm/min by providing some contrivances such as the use of a foothold having microgrooves fitted to the steps of the legs.

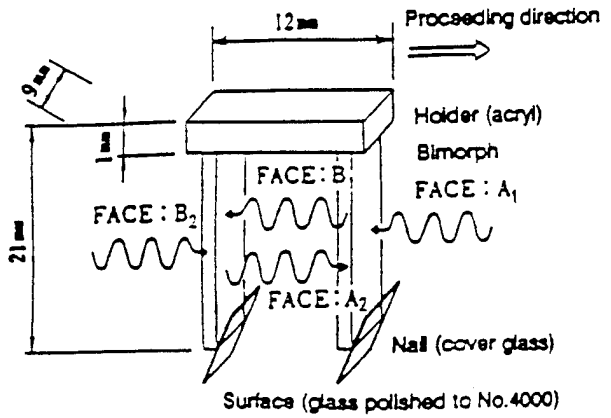

Figure 8 Structure of the photo-driven micro walking machine, and the irradiation directions.

PHOTOPHONE

The technology to transmit voice data (i. e. a phone call) at the speed of light through lasers and fiber optics has been advancing rapidly. However, the end of the line -- interface speaker -- limits the technology, since optical phone signals must be converted from light energy to mechanical sound via electrical energy at present. The photostriction may provide new photoacoustic devices.

Photo-mechanical resonance of a PLZT ceramic bimorph has been successfully induced using chopped near-ultraviolet irradiation, having neither electric lead wires nor electric circuits.[7] A thin cover glass was attached on the photostrictive bimorph structure to decrease the resonance frequency so as to easily observe the photo-induced resonance. A dual beam method was used to irradiate the two sides of the bimorph alternately; intermittently with a 180 deg phase difference. The mechanical resonance was then determined by changing the chopper frequency.

The tip displacement of the thin-plate-attached sample as a function of chopper frequency is presented in Fig. 9. Photo-induced mechanical resonance was successfully observed. The resonance frequency was about 75 Hz with the mechanical quality factor Q of about 30. The maximum tip displacement of this photostrictive sample was about 5 μm at the resonance point, smaller than the level required for audible sound. However, the achievement of photo-induced mechanical resonance in the audible frequency range suggests the promise of photostrictive PLZT bimorph-type devices as photo-acoustic components, or "photophones", for the next optical communication age.

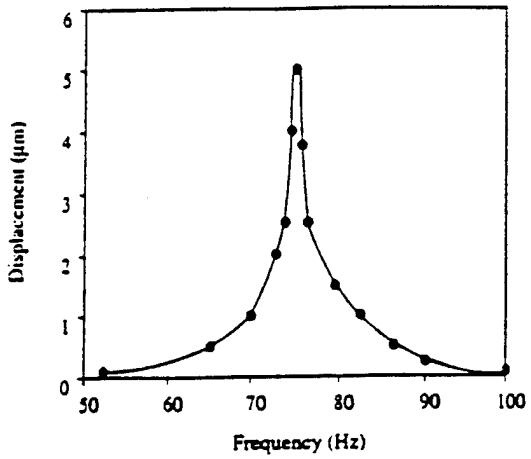

Figure 9 Photo-induced mechanical resonance behavior of the PLZT bimorph.

CONCLUSION

Photostrictive actuators can be driven only by the irradiation of light, so that they will be suitable for use in actuators, to which lead wires can hardly be connected because of their ultra-small size or of their employed conditions such as ultra-high vacuum or outer space. The photostrictive bimorphs will also be applicable to "photophones." The new principle actuators have considerable effects upon the future micro-mechatronics.

This work was partly supported by US Army Research Office through Contract No. DAAL 03-92-G-0244.

REFERENCES

[1] V. M. Fridkin, *Photoferroelectrics*, Ed. by M. Cardona, P. Fulde, H. -J. , Queisser, Solid State Sciences 9, Springer-Verlag, New York (1979).
[2] A. M. Glass, D. von der Linde, D. H. Austin and T. J. Negran, *J. Elec. Mater.*, **4** [5], 915 (1975).
[3] M. Tanimura and K. Uchino, *Sensors and Materials*, **1**, 47 (1988).
[4] K. Uchino, M. Aizawa and Late S. Nomura, *Ferroelectrics*, 64,199 (1985).
[5] T. Sada, M. Inoue and K. Uchino, *J. Ceram. Soc. Jpn.*, **5**, 545 (1987).
[6] K. Uchino, *J. Rob. Mech.*, **1**, 124 (1989).
[7] S. Y. Chu and K. Uchino, *Proc. 9th Int'l Symp. Appl. Ferroelectrics*, State College (1994)[in press].

8. Chu, S. Y., Z. Ye and K. Uchino, "Photo-Acoustic Devices Using (Pb,La) (Zr,Ti)O_3-Based Ceramics," J. Jpn. Ceram. Soc. (1995) (submitted).

J. Ceram. Soc. Jpn. (Submitted)

PHOTO-ACOUSTIC DEVICES USING (Pb, La)(Zr, Ti)O_3-BASED CERAMICS

Sheng-Yuan Chu, Zhou Ye, and Kenji Uchino

International Center for Actuators and Transducers,

Materials Research Laboratory

The Pennsylvania State University

University Park, PA 16802

(Pb, La)(Zr, Ti)O_3系セラミックスを用いた光音響素子の作製

強誘電体における光歪みは光起電力効果と逆圧電効果の重畳現象として引起こされる。この現象は、応答性が改善されれば光音響素子としての応用が有望である。本研究では、まず応答速度の改善を目的として、(Pb, La)(Zr, Ti)O_3系セラミックスの添加物効果を調べた。そして、PLZTバイモルフを用いて、光音響素子を試作し、間断的な光照射によって、基本機械振動が励起されることを観察した。

ABSTRACT

Photostriction in ferroelectrics arises from a superposition of photovoltaic and inverse piezoelectric effects. This phenomenon provides promise for photo-acoustic devices, when the response has been sufficiently improved. In this paper, B-site donor doping was investigated in (Pb, La)(Zr, Ti)O_3 based ceramics with the aim of improving the response speed. Using a PLZT bimorph configuration, a photoacoustic device was trially fabricated and the fundamental mechanical resonance was observed under intermittent illumination.

KEYWORDS: PLZT, Bimorph, Photovoltaic Effect, Photostrictive Effect, Photo-induced Mechanical Resonance

The photovoltaic effect is observed in certain ferroelectrics, wherein a constant electromotive force is induced with application of near-ultraviolet radiation [1),2),3)]. This effect was explained by Fridkin et al. in 1974 [4)], by Glass et al.[2)] and by Brody et al.[5)], and probably originated from an excitation of electrons from asymmetric impurity potentials. The main features of the bulk photovoltaic effect are summarized as follows:

1) This effect appears in poled single crystals or ceramics with noncentric- symmetry and is entirely different in nature from the P-N junction effect observed in semiconductors.
2) Constant photo-currents and -voltages are generated in the spontaneous polarization direction under uniform illumination in the ferroelectric phase only, disappearing in the paraelectric phase.
3) The magnitude of the induced voltage is proportional to the crystal length in the polarization direction and is much greater than the band gap energy of the crystal.

So far, most of the studies have been made on single crystals to clarify the origin of the effect. However, our research group has been focusing on polycrystalline samples such as $PbTiO_3$-based [6),7)] and Pb(Zr, Ti)O_3-based ceramics [8),9)] from a practical application point of view. High photovoltage (≈ 1 kV/cm) generator with relatively quick response (≈ 10 sec) have been developed in the (Pb, La)(Zr, Ti)O_3 (PLZT) system. Moreover, by superimposing the photovoltaic effect with the inherent piezoelectricity of these compounds, practical photostrictive materials have been realized [8),9)]. A bimorph-type photostrictive element can exhibit large tip deflections under UV light illumination. This actuator is applicable to remote control devices such as photo-driven relays [9)] and micro walking robots [10)].

In this paper, the photovoltaic effect in PLZT(3/52/48) based ceramics has been investigated as a function of B-site donor dopants. Then, using the PLZT bimorph, a photoacoustic device was trially fabricated and the fundamental mechanical resonance was observed under intermittent illumination.

SAMPLE PREPARATION

PLZT (x/y/z) samples were prepared in accordance with the following composition formula:

$$Pb_{1-y}La_y(Zr_{1-x}Ti_x)_{1-\frac{y}{4}}O_3.$$

Since the photostriction figure of merit is defined as the product of the photovoltaic voltage and piezoelectric coefficient ($x_{ph} = d_{33} \times E_{ph}$), PLZT(3/52/48) was selected due to its optimum photostrictive response within the PLZT system [8]. According to our preliminary study on impurity doping [9], WO_3 doped PLZT ceramics were prepared.

Ceramic powders were prepared by a conventional mixed oxide technique. $PbCO_3$, La_2O_3, ZrO_2, TiO_2 and WO_3 were weighed in the appropriate proportions and mixed in a ball mill for 2 days using ethanol and zirconia grinding media. 0.5 wt% excess $PbCO_3$ was added to compensate for weight loss during calcination and sintering. The slurry was dried, then calcined in a closed alumina crucible at 950 °C for 10 hours. The calcined powder was ball-milled again for 48 hours. The samples were sintered in sealed alumina crucibles at 1270 °C/2hrs. A PbO rich atmosphere was maintained with lead zirconate powder to minimize lead loss during sintering. Sintered samples were cut, polished and electroded with silver paste . Finally, each sample was poled at 15 kV/cm in silicone oil at 120 °C .

The poled PLZT ceramics were used to make bimorph actuators. The elements were $20 \times 4 \times 0.15$ mm^3: the 4×0.15 mm^2 surface was electroded with silver paste and silver wires were attached. The bimorph actuator consisted of two bonded oppositely-poled ceramic plates (refer to figure 1).

DOPING CONCENTRATION DEPENDENCE

The photovoltaic effect was measured in PLZT 3/52/48 bimorph samples doped with various concentrations of WO_3. Figure 2 shows the photovoltaic current, photovoltaic voltage, photo-induced tip displacement and stored energy (P=(1/2) Imax×Vmax) in PLZT doped with WO_3. It was found that higher photovoltaic current, photovoltage,

photostriction and potential power can be obtained in WO_3 doped samples. The photovoltaic voltage reaches 1 kV/cm, and the current is on the order of nA. The maximum tip displacement is about 120 μm for 0.4 atm% WO_3 doped samples. Notice that the strain magnitude increases as the photovoltaic voltage increases; and with increasing photo-current, there is an increase in the overall response. The photo-induced tip displacement was 30 μm in one second and saturated at 120 μm under a light intensity of 4 mW/cm^2 (λ = 370 nm).

MECHANICAL RESONANCE FREQUENCY MEASUREMENTS

The mechanical resonance frequency of the above-mentioned bimorph sample can be estimated according to the equation:

$$f_r = 0.158 \times \frac{t}{l^2}\sqrt{\frac{1}{\rho s_{11}^E}}, \qquad (1)$$

where t and l are the thickness and length of the bimorph sample, respectively, ρ is the density and s_{11}^E is the elastic compliance of the ceramic. The calculated resonance frequency of the PLZT based bimorph, using ρ = 7.9 g/cm^3 and $s_{11}^E = 16 \times 10^{-12}$ m^2/N, was about 3 kHz: too high for photo-induced resonance measurements. Therefore, a thin cover glass was attached to the bimorph sample to reduce the resonance frequency, as shown in figure 1. To determine the electromechanical resonance behavior, an ac. voltage was applied to the bimorph. The tip displacement was monitored as a function of frequency using the experimental setup shown in figure 3. Figure 4 shows the mechanical resonance characteristics obtained from this experiment. The resonance frequency was ~ 79 Hz with a mechanical quality factor Q of ~ 30. The maximum displacement of this thin-plate attached sample was about 14 μm at 80 V_{p-p}.

PHOTO-ACOUSTIC MEASUREMENT

PHOTO-ACOUSTIC MEASUREMENT

Radiation from a high-pressure mercury lamp (Ushio Electric USH-500D) was passed through a UV bandpass filter (Oriel Co., No.59811), an IR blocking filter (Oriel Co., No.59060), an optical focusing lens and an optical chopper to provide intermittent sample irradiation (see figure 5). A wavelength peak of 370 nm, where the maximum photovoltaic effect of PLZT is obtained, was used. A dual beam method was used to irradiate the two sides of the bimorph alternately [9]. Two beams, A and B, were chopped so as to cause a 180 degree phase difference as illustrated in figure 6. Notice the maximum intensity of 1 mW/cm^2. The slow recovery because of the low dark conductivity was overcome using this dual beam method. The mechanical resonance was then determined by changing the chopper frequency.

The tip displacement of the thin-plate-attached sample as a function of chopper frequency is presented in figure 7. Photo-induced mechanical resonance was successfully observed. The resonance frequency was about 75 Hz with the mechanical quality factor Q of about 30; in good agreement with the previous electromechanical data. The maximum tip displacement of this photostrictive sample was about 5 μm of resonance.

CONCLUSION

Photo-mechanical resonance of a PLZT ceramic bimorph actuator has been successfully induced using chopped UV irradiation. A thin cover glass was attached to decrease the resonance frequency to easily observe photo-induced resonance. The resonance frequency was 75 Hz with a mechanical quality factor Q of about 30 under dual beam operation. The maximum tip displacement of this sample was about 5 μm, smaller than the level required for audible sound. However, the achievement of photo-induced mechanical resonance in the audible frequency range suggests the promise of photostrictive PLZT bimorph-type devices as photo-acoustic components, or "photophones", for the next optical communication age.

ACKNOWLEDGEMENT

This work is supported by Army Research Office (ARO), No. DAALO3-92-G-0244. The authors would also thank Dr. Russell Brodeur for his critical review.

REFERENCES

[1] V. M. Fridkin, "Photoferroelectrics", Ed. by M. Cardona, P. Fulde, H. -J. Queisser, Solid State Sciences, New York, (1979), pp. 85.

[2] A. M. Glass, D. von der Linde, D. H. Austin and T. J. Negran, *J. Elec. Mat.* 4 [5], 915-943 (1975).

[3] V. M. Fridkin and B. N. Povov, *Sov. Phys. Usp.*, 21(12), 981-991 (1978).

[4] V. M. Fridkin, A. A. Grekov, P. V. Ionov, A. I. Rodin, E. A. Savchenko and K. A. Mikhailina, *Ferroelectrics*, 8 433-435 (1974).

[5] P. S. Brody and F. Growne, *J. Elec. Mat.* 4, [5], 955-971 (1975).

[6] K. Uchino, Y. Miyazawa and S. Nomura, *Jpn. J. Appl. Phys.*, 21, [12], 1671-1674 (1982).

[7] K. Uchino, Y. Miyazawa and S. Nomura, *Jpn. J. Appl. Phys.* Suppl. 22-2, 102-105 (1983).

[8] T. Sada, M. Inoue and K. Uchino, *J. Ceram. Soc. Jpn.*, 5, 545 (1987).

[9] M. Tanimura and K. Uchino, *Sensors and Materials*, 1, 47-56 (1988).

[10] K. Uchino, *J. Rob. Mech.*, 1(2), 124-127 (1989).

Figure Captions

Fig. 1 Configuration of a thin-plate attached photoacoustic bimorph.

Fig. 2 Photovoltaic current, voltage, power and tip displacement as a function of dopant concentration in WO_3 doped PLZT.

Fig. 3 Experimental setup for mechanical resonance measurements.

Fig. 4 Mechanical resonance behavior of WO_3 doped PLZT.

Fig. 5 Experimental setup for photo-induced mechanical resonance measurements.

Fig. 6 Wave forms for two beams of illuminating the bimorph sample.

Fig. 7 Photo-induced mechanical resonance behavior of WO_3 doped PLZT.

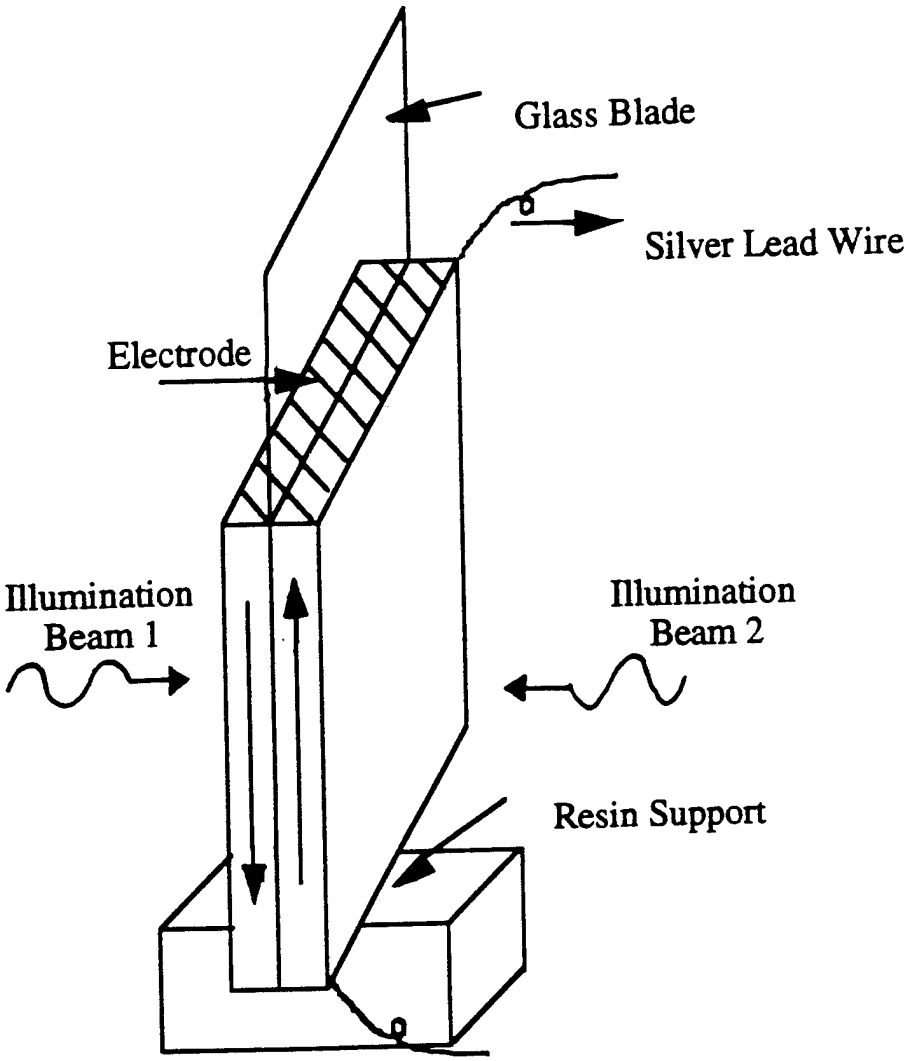

Figure 1: Configuration of a thin-plate attached photoacoustic bimorph.

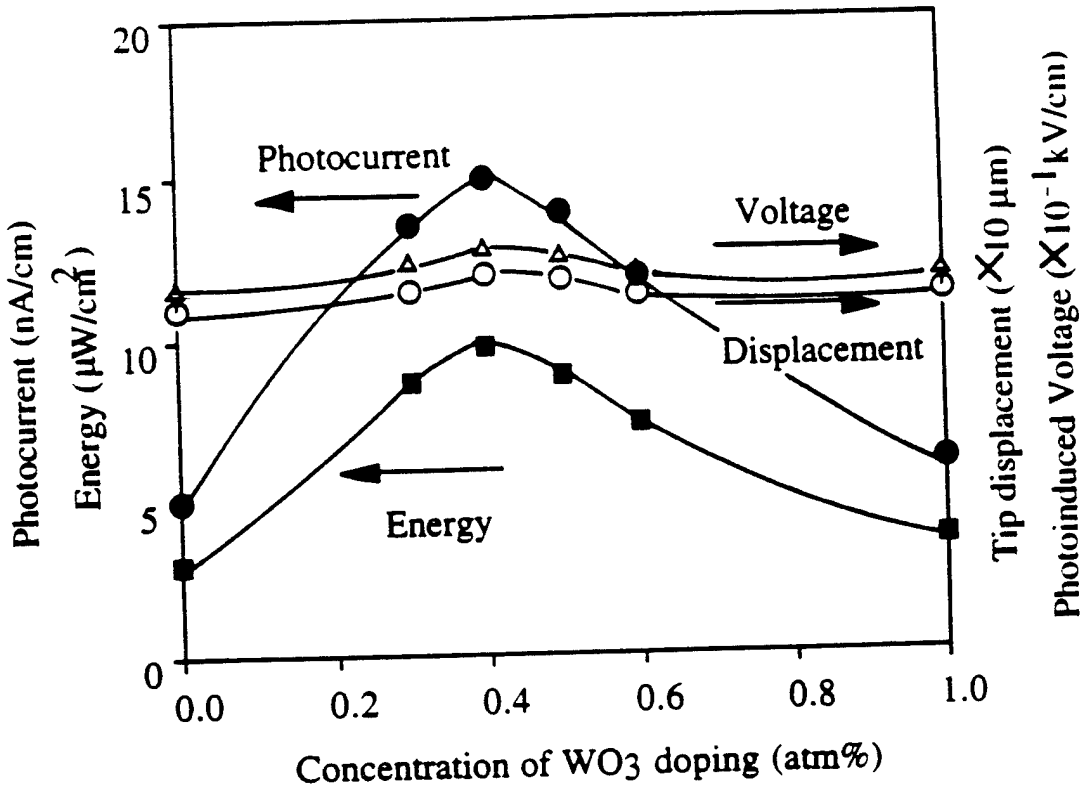

Figure 2: Photovoltaic current, voltage, power and tip displacement as a function of dopant concentration in WO_3 doped PLZT.

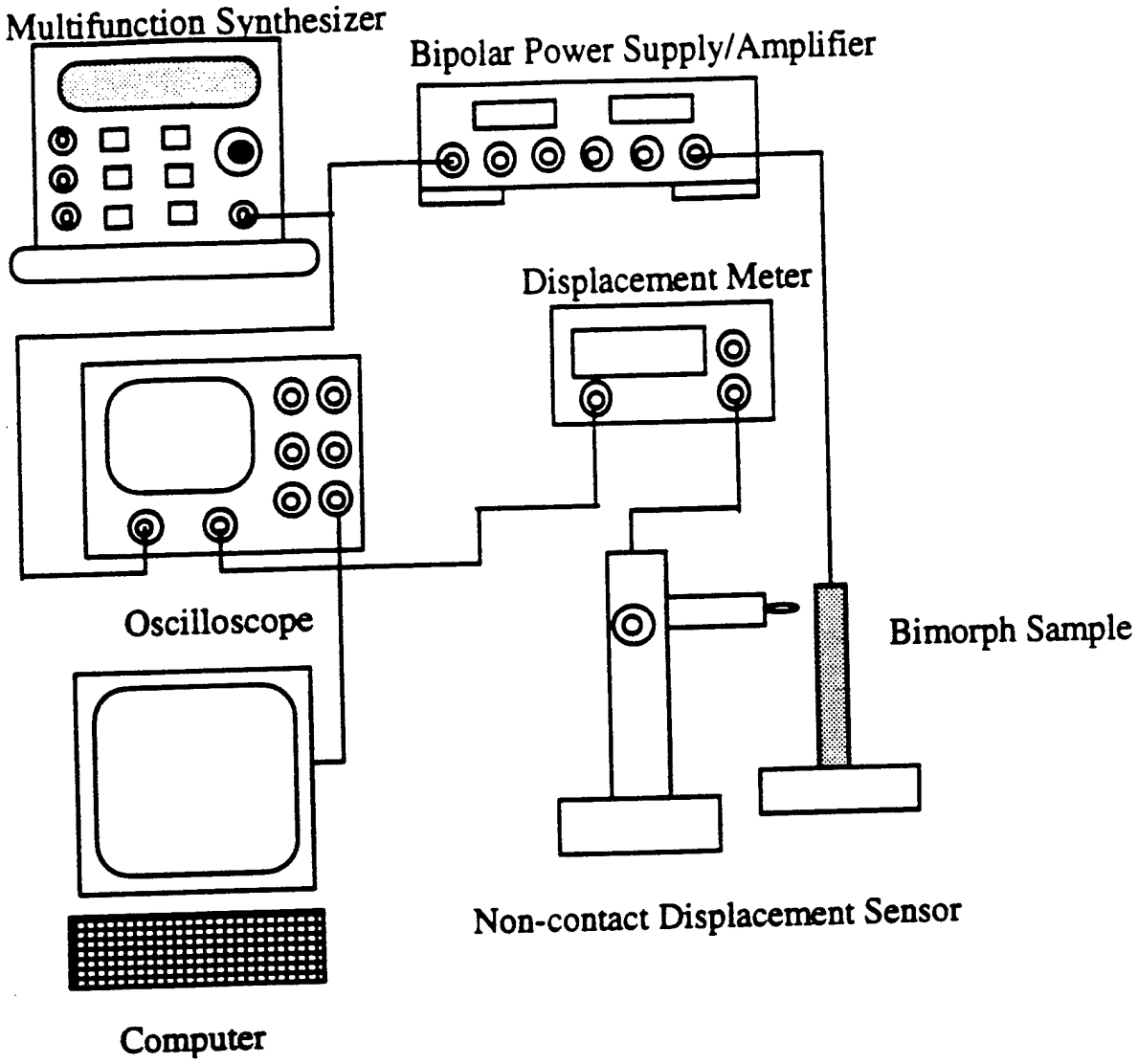

Figure 3 : Experimental setup for mechanical resonance measurements.

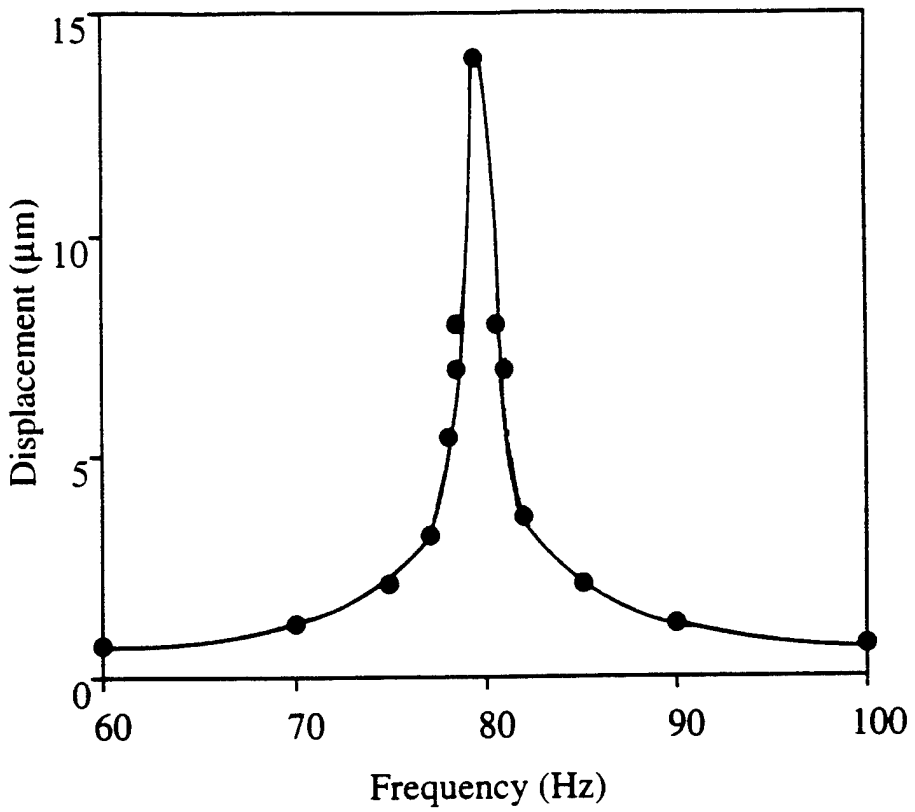

Figure 4: Mechanical resonance behavior of WO_3 doped PLZT.

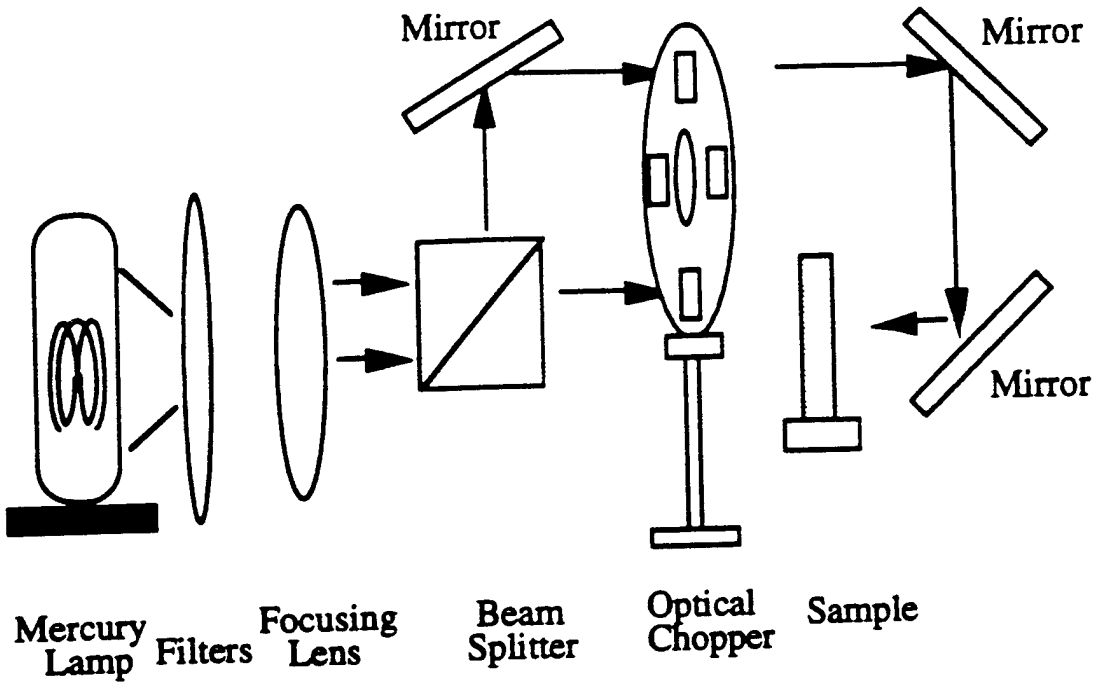

Figure 5: Experimental setup for photo-induced mechanical resonance measurements.

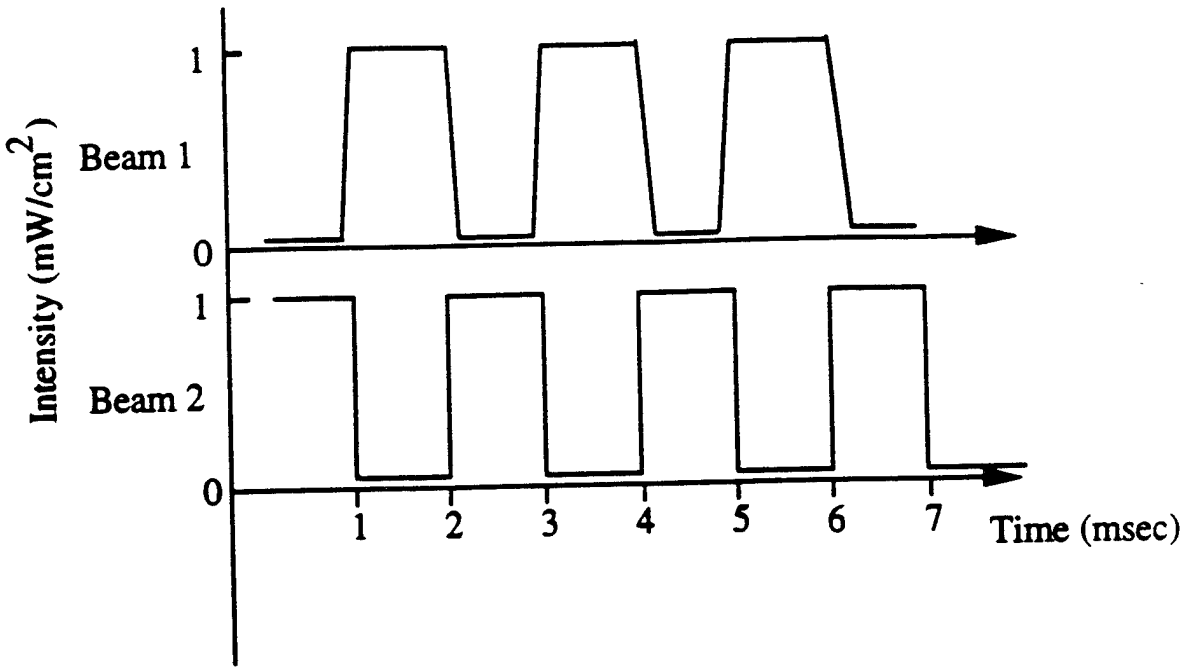

Figure 6: Wave forms for two beams of illuminating the bimorph sample.

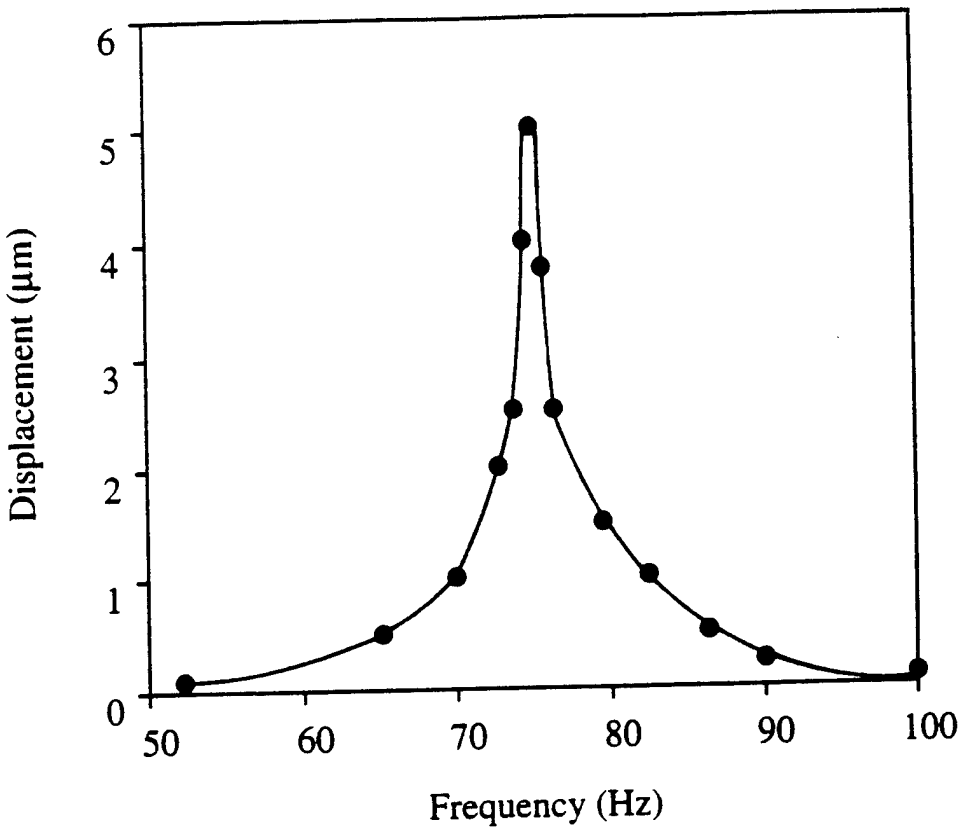

Figure 7: Photo-induced mechanical resonance behavior of WO_3 doped PLZT.

9. Chu, S. Y. and K. Uchino, "Photostrictive Effect in PLZT-Based Ceramics and Its Applications," Ferroelectrics (in press).

Ferroelectrics (Submitted)

PHOTOSTRICTIVE EFFECT IN PLZT-BASED CERAMICS AND ITS APPLICATIONS

Sheng-Yuan Chu, and Kenji Uchino

International Center for Actuators and Transducers,

Materials Research Laboratory

The Pennsylvania State University

University Park, PA 16802

ABSTRACT

Photostriction in ferroelectrics arises from a superimposed phenomenon of the photovoltaic and inverse piezoelectric effects. This paper reviews the recent developments in materials and their device applications: ion doping effect is described in (Pb, La)(Zr, Ti)O_3 based ceramics firstly to improve the response speed, then the drive/control methods (polarized light method and dual beam method) are presented, finally photo-driven relays, micro walking machines and photoacoustic devices are introduced. The devices based on a bimorph structure were designed to start moving by the irradiation without any external electric circuit.

INTRODUCTION

Photostrictive effect is a phenomenon in which strain is induced in the sample when it is illuminated and is expected as a superposition phenomenon of bulk photovoltaic effect and inverse piezoeletric effect. The photovoltaic effect is observed in certain ferroelectrics, wherein a constant electromotive force is induced with application of near-ultraviolet radiation [1]-[3]. This effect was explained by Fridkin et al. [4], Glass et al. [2] and Brody et al. [5], and is probably originated from an excitation of electrons from asymmetric impurity potentials, but the origin has not been clarified yet.. The main features of the bulk photovoltaic effect are summarized as follows:

1) This effect appears in poled uniform single crystals or ceramics with noncentro- 2
symmetry and is entirely different in nature from the P-N junction effect observed in semiconductors.
2) Constant photo-current and -voltage are generated in the spontaneous polarization direction under uniform illumination in the ferroelectric phase and disappears in the paraelectric phase.
3) The magnitude of the induced voltage is proportional to the crystal length in the polarization direction and is much greater than the band gap energy of the crystal.

So far, most of the studies have been made on single crystals to clarify the origin of the effect. However, our research group has been focusing on polycrystalline samples such as $PbTiO_3$- based [6, 7] and $Pb(Zr, Ti)O_3$-based ceramics [8, 9] from a practical application point of view. We have developed a high photovoltage ($\approx$ 1 kV/cm) generator with relatively quick response ($\approx$ 1 sec) in the (Pb, La)(Zr, Ti)O_3 (PLZT) system.

In this paper, the recent developments in photostrictive materials and their device applications will be reviewed. Ion doping effect on the photostriction in bulk PLZT(3/52/48) ceramics is described first, then the angular dependence of the photovoltaic voltage and current on the polarized light direction and a dual beam driving method are introduced. Finally, photostrictive devices such as photo-driven relays [10], micro walking robots [11] and photoacoustic devices are introduced. Bimorph-type photostrictive elements can exhibit more-than-one-hundred μm tip deflection under violet light illumination.

DOPING EFFECT ON THE PHOTOVOLTAIC PROPERTIES

PLZT (x/y/z) samples were prepared in accordance with the following composition formula:

$$Pb_{1-y}La_y(Zr_{1-x}Ti_x)_{1-\frac{y}{4}}O_3.$$

Since the photostriction figure of merit is evaluated by the product of the photovoltaic

voltage and the piezoelectric coefficient ($x_{ph} = d_{33} \times E_{ph}$), PLZT(3/52/48) was selected due to its optimum photostrictive response within the PLZT system [9].

A slight donor doping was found to reduce the grain size and to shift the Curie temperature to the higher temperature [12]. Figures 1(a), 1(b) and 1(c) show the scanning electron microscope (SEM) photographs of the thermally etched PLZT, PLZT-WO_3 and PLZT-Ta_2O_5, respectively. Pure PLZT has the largest grain size; however, it is difficult to determine grain size differences between WO_3 doped and Ta_2O_5 doped samples with different concentration. Figure 2(a) shows the change in the dielectric constant at room temperature and at 10 kHz with dopant concentration for WO_3 (0 - 1.0 at%), and figure 2(b) shows the dielectric constant maximum temperature, which almost coincides with the Curie temperature (T_C), as a function of WO_3 doping. The dielectric constant shows the minimum at 0.4 at% WO_3 doping, where the T_C provides the maximum. Figures 3(a) and 3(b) show the changes in the room-temperature dielectric constant (10 kHz) and the Curie temperature with Ta_2O_5 doping, respectively. In the case of Ta_2O_5 doping, the maximum Curie temperature and the minimum dielectric constant are obtained at 1.0 at% Ta_2O_5.

Consequently, impurity doping on PLZT affects the photovoltaic response significantly. Figures 4 and 5 show the photovoltaic current, photovoltaic voltage and maximum output power (P=(1/4) Imax×Vmax) in PLZT doped with WO_3 and with Ta_2O_5, respectively. Photovoltaic current and voltage show a peak at 0.4 at% for the WO_3 samples, while photovoltaic current and photovoltage show a peak at 1.5 at% and 1 at% for the Ta_2O_5 samples, respectively. It was found that the higher photovoltaic current can be obtained in WO_3 doped samples, while the higher photovoltage can be obtained in Ta_2O_5 doped samples [13]. The higher voltage generates the larger magnitude of the photostriction, while the higher current provides the quicker overall response.

(1) Polarized Light Illumination Drive

A polarizer was put between the focusing lens and the sample to monitor the angular dependence of the photovoltaic effect under linearly polarized light, as shown in figure 6 [14]. The angle θ was measured with respect to the origin of the remnant polarization direction. Figure 7 shows the experimental dependence of the photovoltaic current J and the corresponding voltage V on the light polarization direction. Both the photovoltage and photocurrent provide the maximum values at θ =0, 180 degree, and the minimum at θ = 90 degree. It was observed that the photocurrent and photovoltage deviations with respect to the change of light polarization direction are 2% and 14%, respectively, for the WO_3 doped samples, regardless of the absolute values of current and voltage. This angular dependence of the photovoltaic current is consistent with the symmetry of the poled ceramic. The difference between the peak-peak deviations in the current (2%) and voltage (14%) suggests relatively large dependence of photoconductivity on light polarization orientation.

(2) Dual Beam Control

Turning off the photostrictive device optically is a particular difficulty, because the very low conductivity under off illumination prohibits the device from discharging (see figure 8(a)) [9]. The method proposed here is the use of dual beams for quick control. Two samples of the same size are electrically connected together with antiparallel arrangement of the remnant polarization, so that the induced voltages may cancel each other when illuminated simultaneously (figure 8(b)). To drive this twin device, the main element (1) is irradiated first, then followed by the irradiation on the sub-element (2) immediately after turning off the main one. As shown in figure 8(c), this alternating illumination provides remarkable quick response in the turn-off process.

APPLICATIONS

(1)Photo Driven Relay

A photo-driven relay was made by a snap-action switch, which can be functioned by a 50 μm displacement, and a driver using a photostrictor.(see figure 9)[10]. The driving part is a bimorph which consists of two ceramic plates (5 mm×20 mm×0.16 mm in size) joined so that their polarization directions are opposing. A dummy plate is positioned adjacent to the bimorph to cancel the photovoltaic voltage generated on the bimorph. Utilizing the dual beam method, switching was controlled by alternately irradiating the bimorph and the dummy. The amount of displacement observed at the tip of this bimorph was 150 μm and the On/Off response of the photo-driven relay showed a typical delay time of 1 - 2 seconds.

(2) Micro-Walking Machine

A photo-driven micro walking machine has also been developed using the photostrictive bimorphs [11]. It has two ceramic legs (5 mm×20 mm×0.35 mm) fixed to a plastic board (figure 10). When the two legs were irradiated with purple light alternately with a 14-sec period, the device moved like an inchworm. The photostrictive bimorph as a whole was caused to bend by 150 μm as if it averts the radiation of light. The inchworm built on a trial basis exhibited rather slow walking speed (several μm/min) in comparison with the expected speed (several mm/min), since slip occurred between the contacting surface of its leg and the floor, as shown in figure 11.

(3) Photo-Acoustic Device

PLZT(3/52/48) doped with WO_3 samples were used for this study. The sample size for this measurement was $20 \times 4 \times 0.15$ mm^3: the 4×0.15 mm^2 surface was electroded with silver paste and silver wires were attached. A bimorph design consisting of two oppositely-poled ceramic plates was then used to trially fabricate a photoacoustic device. The displacement has been tested to reach 50 μm in several seconds and saturate at 120 μm

under a light intensity of 4 mW/cm^2 [13].

Thin cover glass was then attached to the bimorph sample to reduce the resonance frequency and the configuration of the sample is shown in figure 12. By changing the frequency of the applied voltage, the mechanical resonance frequency of the bimorph samples was initially determined. The mechanical resonance frequency was about 80 Hz and mechanical quality factor Q was calculated as 30.

Finally, by using chopped intermittent irradiation, the sample was illuminated alternately on the both sides and voltage was generated across the sample gradually. Radiation from a high-pressure mercury lamp (Ushio Electric USH-500D) was passed through a UV bandpass filter (Oriel Co., No.59811), an IR blocking filter (Oriel Co., No.59060), and an optical focusing lens. A wavelength peak around 370 nm, where the maximum photovoltaic effect of PLZT is obtained, was applied to the sample. The dual beam method was used in this experiment and the two beams had 180 degree phase difference. The experimental setup is shown in figure 13. The mechanical resonance was determined by changing the frequency of the chopper. Figure 14 plots the tip deflection of this thin-plate attached sample as a function of frequency. The mechanical resonance frequency was about 75 Hz, in good agreement with the value electrically excited, and the mechanical quality factor Q was also calculated about 30. The maximum displacement of this thin-plate attached sample was about 5 μm, which seems to be smaller than the level required for audible sound. However, the achievement of photo-induced mechanical resonance in the audible frequency range suggests the promise of photostrictive PLZT bimorph-type devices as photo-acoustic components, or "photophones", for the next optical communication age.

CONCLUSION

Donor doping into the perovskite B sites was found to reduce the grain size and increase the Curie temperature, improving photovoltaic response. The maximum

photocurrent is obtained for 0.4 at% WO_3 doping and the maximum photovoltage is 7
obtained for 1 at% Ta_2O_5 doping.

The angular dependence of the photovoltaic current and the corresponding voltage on the light polarization orientation with respect to the spontaneous polarization has been successfully observed in ceramic samples of PLZT. This angular dependence of the photovoltaic current is consistent with the symmetry of the poled ceramic. The difference between the peak-peak deviations in the current (2%) and voltage (14%) suggests relatively large dependence of photoconductivity on light polarization orientation.

The dual beam method was used to overcome the slow recovery due to low conductivity under no illumination.

The photostrictive actuators can be driven by the irradiation of light alone, so that they will be suitable for use in actuators, to which lead wires can hardly be connected because of their ultra-small size or of their employed conditions such as ultra-high vacuum. New actuators of this type have considerable effects upon the future micro-mechatronics.

ACKNOWLEDGMENTS

This work was supported by Army Research Office (ARO), No. DAALO3-92-G-0244. The authors would also thank Mr. Zhou Ye for his experimental help.

[1] V. M. Fridkin, Photoferroelectrics, solid state sciences, **9**. (1979).

[2] A. M. Glass, D. von der Linde, D. H. Austin and T. J. Negran, *J. Elec. Mat.* **4**, [5], 915-943 (1975).

[3] V. M. Fridkin and B. N. Povov, *Sov. Phys. Usp.* **21**[12], 981-991 (1978).

[4] V. M. Fridkin, A. A. Grekov, P. V. Ionov, A. I. Rodin, E. A. Savchenko and K. A. Mikhailina, *Ferroelectrics*, **8**, 433-435 (1974).

[5] P. S. Brody and F. Growne, *J. Elec. Mat.* **4**, [5], 955-971 (1975).

[6] K. Uchino, Y. Miyazawa and S. Nomura, *Jpn. J. Appl. Phys.* **21**, [12], 1671-1674 (1982).

[7] K. Uchino, Y. Miyazawa and S. Nomura, *Jpn. J. Appl. Phys. Suppl.* **22-2**, 102-105 (1983).

[8] K. Uchino and M. Aizawa, *Jpn. J. Appl. Phys. Suppl.* **24-3**, 139-141 (1985).

[9] K. Uchino and M. Aizawa and S. Nomura, *Ferroelectrics*, **64**, 199-208 (1985).

[10] M. Tanimura and K. Uchino, *Sensors and Materials*, **1**, 47-56 (1988).

[11] K. Uchino, *J. Rob. Mech.* **1**(2), 124-127 (1989).

[12] T. Yamamoto and K. Okazaki, 7th Int'l. Symp. Appl. Ferroelectrics, Book of Abstracts, VII.1. (1990).

[13] Sheng-Yuan Chu, Zhou Ye, and K. Uchino, *J. Adv. Performance Mater.*, submitted.

[14] Sheng-Yuan Chu, Zhou Ye, and K. Uchino, *J. Smart Mater. and Structures.*, to be published, 1994.

Figure Captions

Fig. 1 SEM photomicrographs of thermally-etched samples of (a) PLZT, (b) PLZT-WO_3 and (c)PLZT- Ta_2O_5.

Fig. 2 Room-temperature dielectric constant (a) and Curie temperature (b) vs. WO_3 doping level.

Fig. 3 Room-temperature dielectric constant (a) and Curie temperature (b) vs. Ta_2O_5 doping level.

Fig. 4 Photovoltaic current, voltage and potential power as a function of dopant concentration in WO_3 doped PLZT.

Fig. 5 Photovoltaic current, voltage and potential power as a function of dopant concentration in Ta_2O_5 doped PLZT.

Fig. 6 Experimental set up for light-polarization-dependence measurements.

Fig. 7 Dependence of the normalized photovoltaic current and photovoltage on the direction of the light polarization plane and the light for various WO_3 doped PLZT samples. (a) 0.4%, (b) 0.5%, (c) 0.6%, and (d) 1%. Solid lines are the theoretically fitted curves.

Fig. 8 Dual beam method for controlling the photostrictive device in quick response.

Fig. 9 Structure of the photo-driven relay.

Fig. 10 Structure of the photo-driven micro-walking machine.

Fig. 11 Position change of the photo-driven micro walking machine with time.

Fig. 12 The configuration of thin-plate attached bimorph sample.

Fig. 13 Experimental setup of chopped intermittent irradiation for mechanical resonance frequency measurements.

Fig. 14 Mechanical resonance frequency for WO_3 doped PLZT by using a chopped intermittent irradiation.

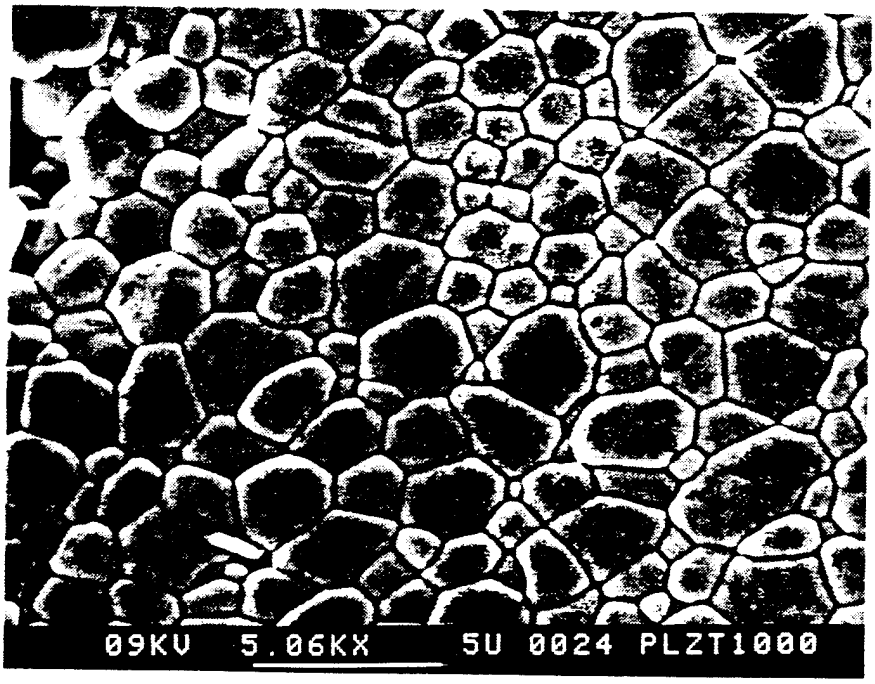

Figure 1(a)

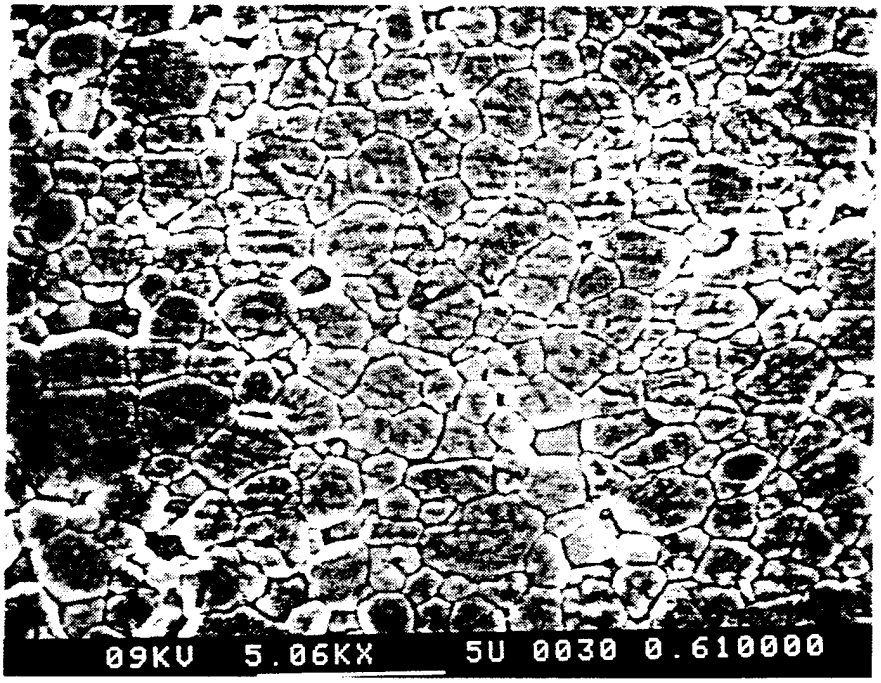

Figure 1(b)

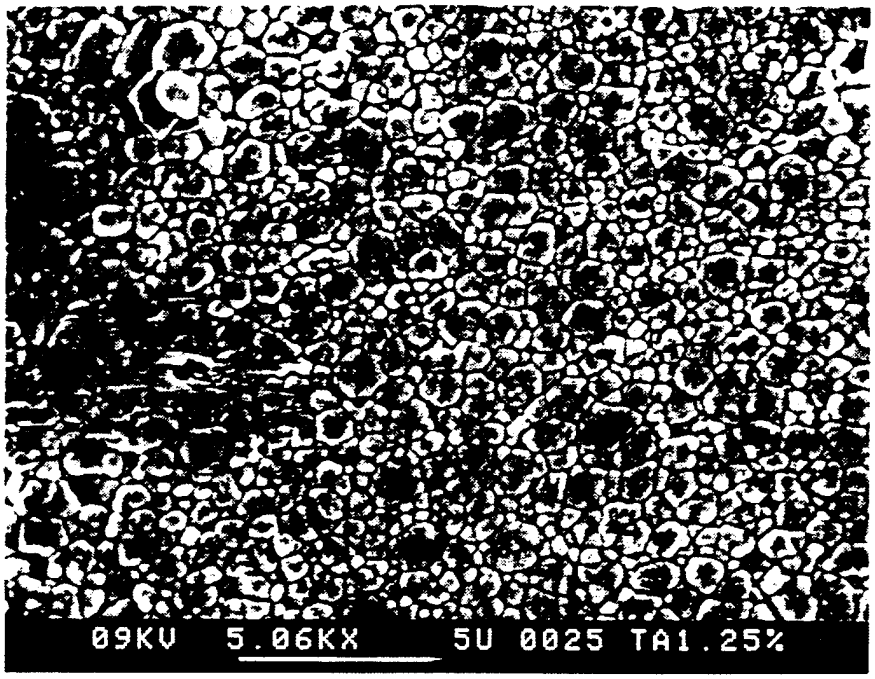

Figure 1(c)

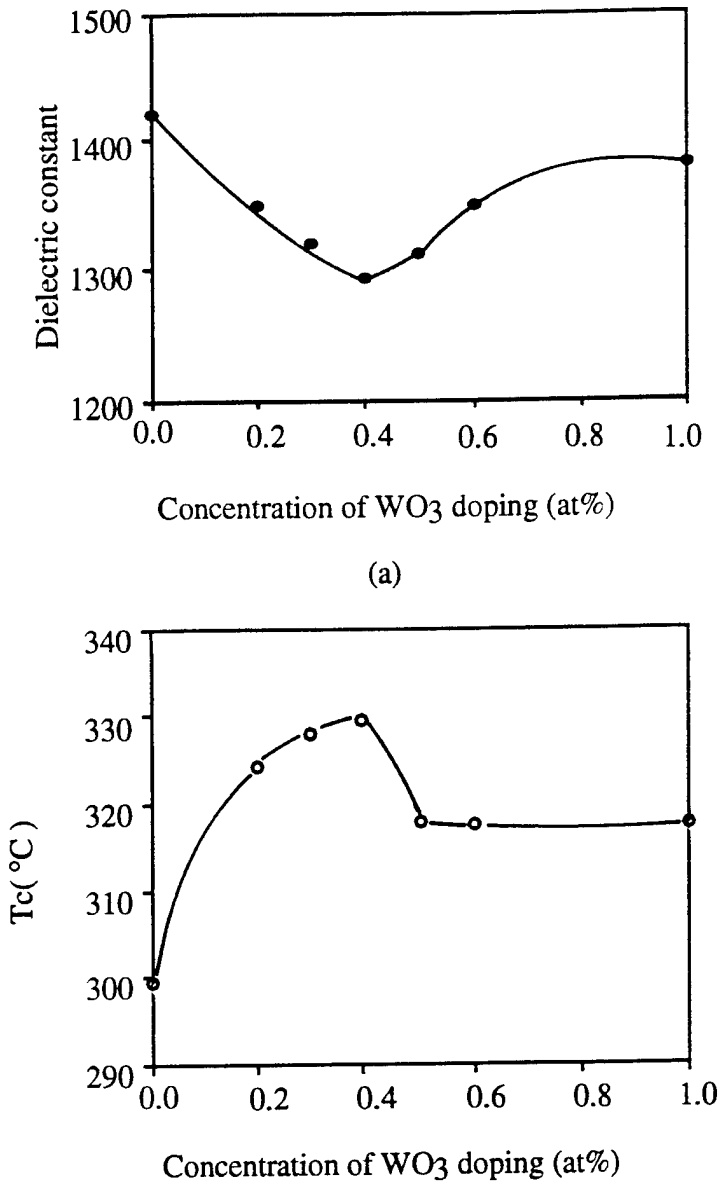

Figure 2: (a) Room-temperature dielectric constant (10 kHz data), and (b) peak temperature vs. WO_3 doping.

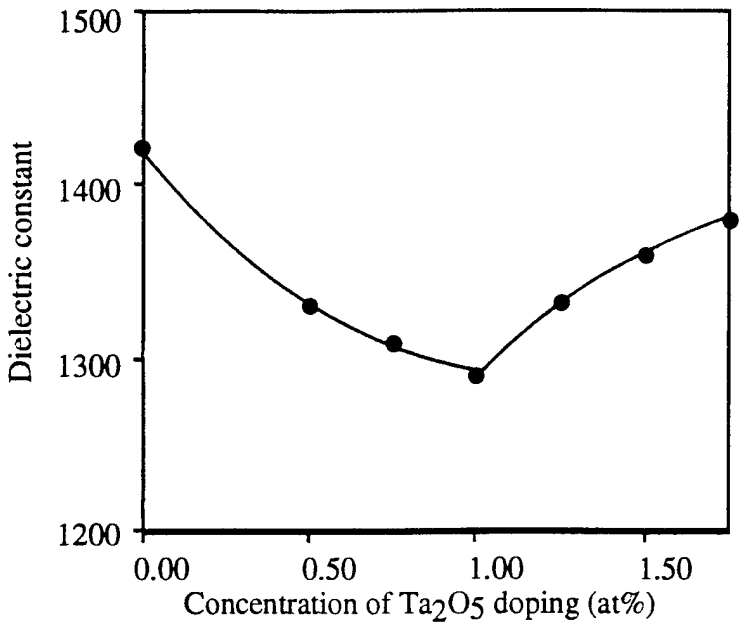

(a)

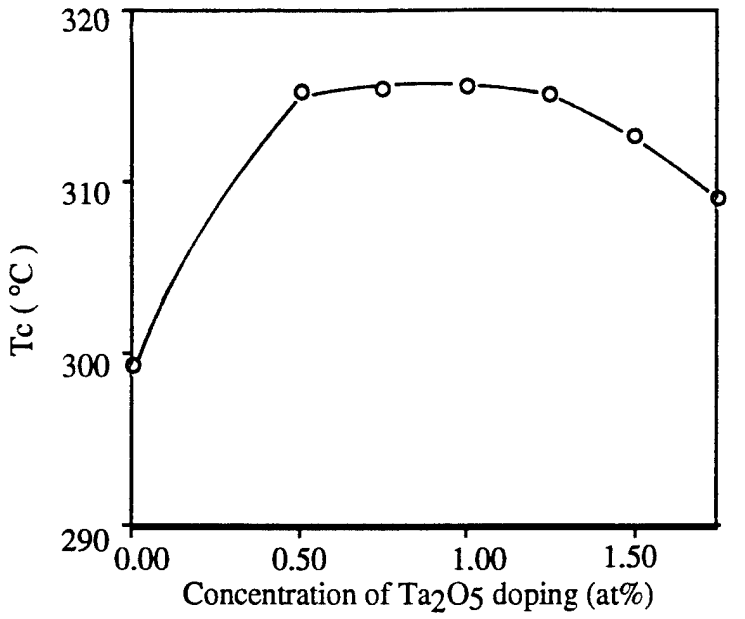

(b)

Figure 3: (a) Room-temperature dielectric constant (10 kHz data), and(b) peak temperature vs. Ta_2O_5 doping.

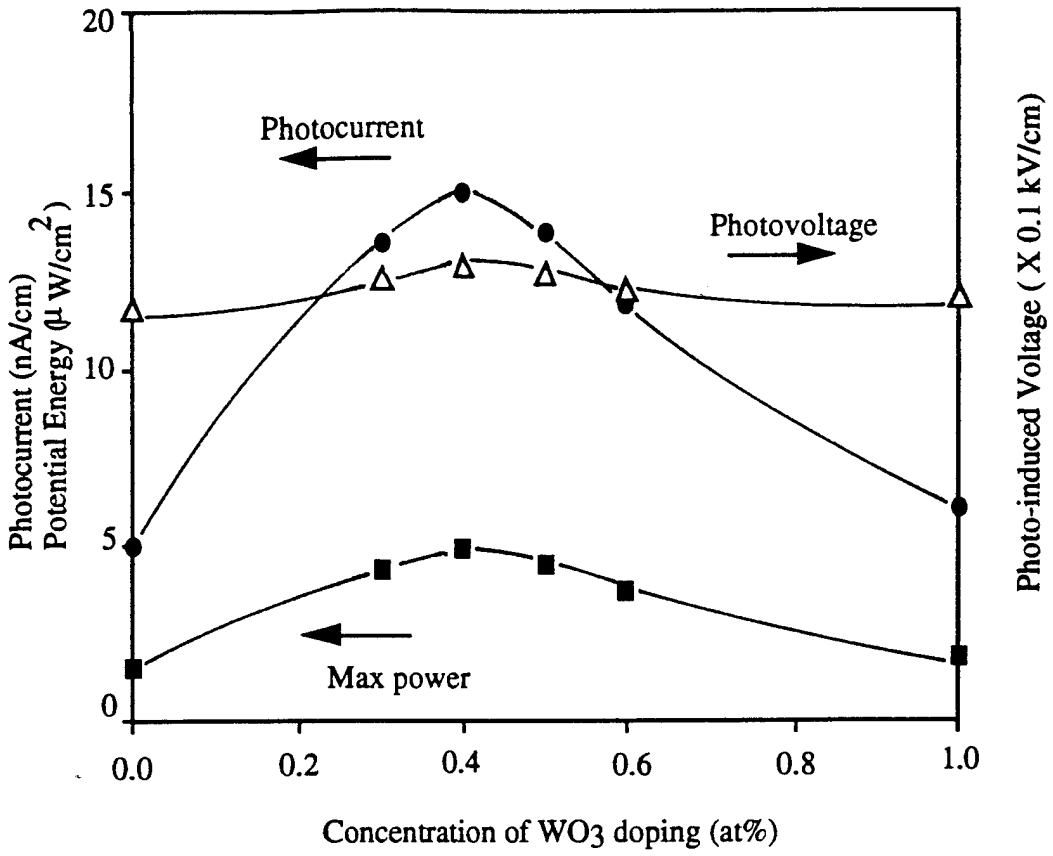

Figure 4: Photovoltaic current, voltage and potential power as a function of dopant concentration in WO_3 doped PLZT.

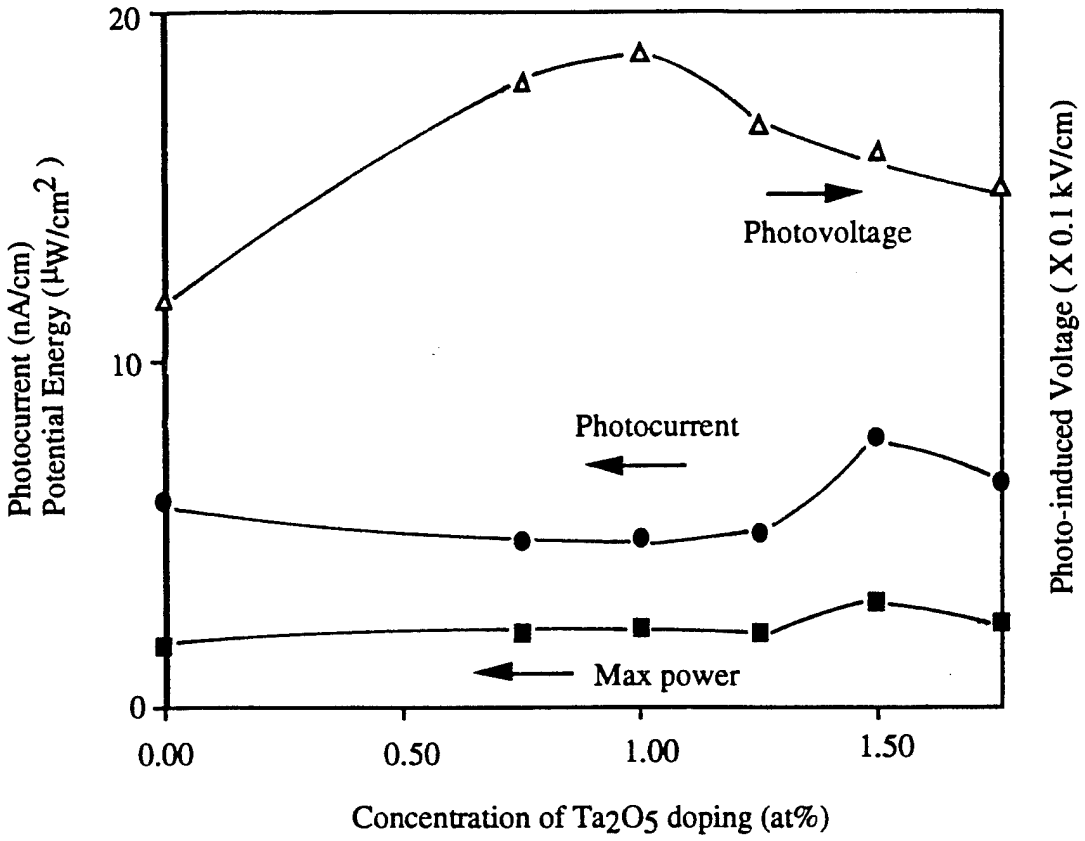

Figure 5: Photovoltaic current, voltage and potential power as a function of dopant concentration in Ta_2O_5 doped PLZT.

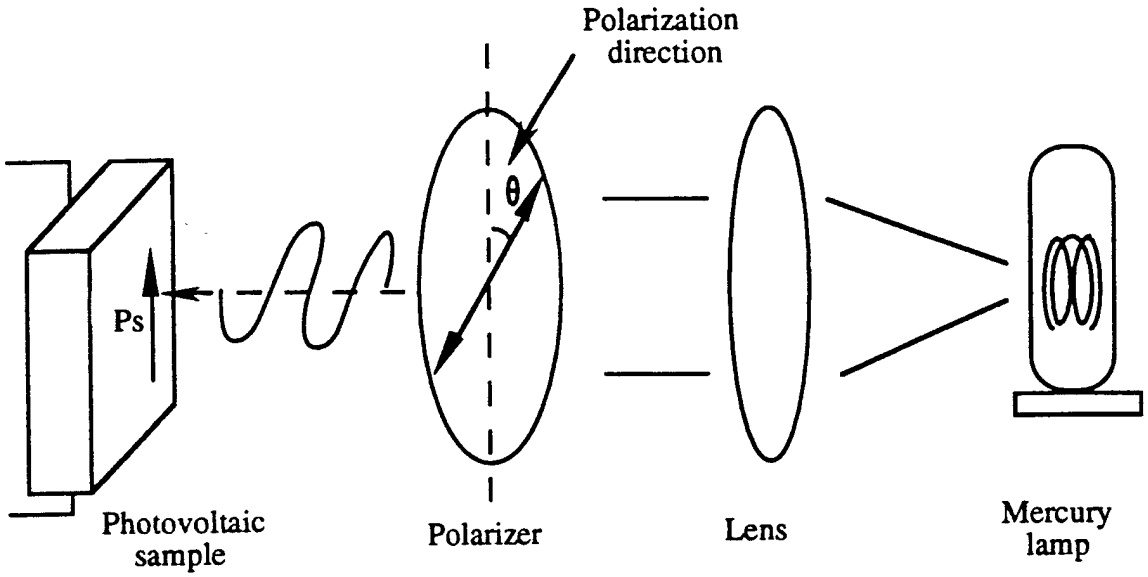

Figure 6: Experimental setup for light-polarization-dependence measurements.

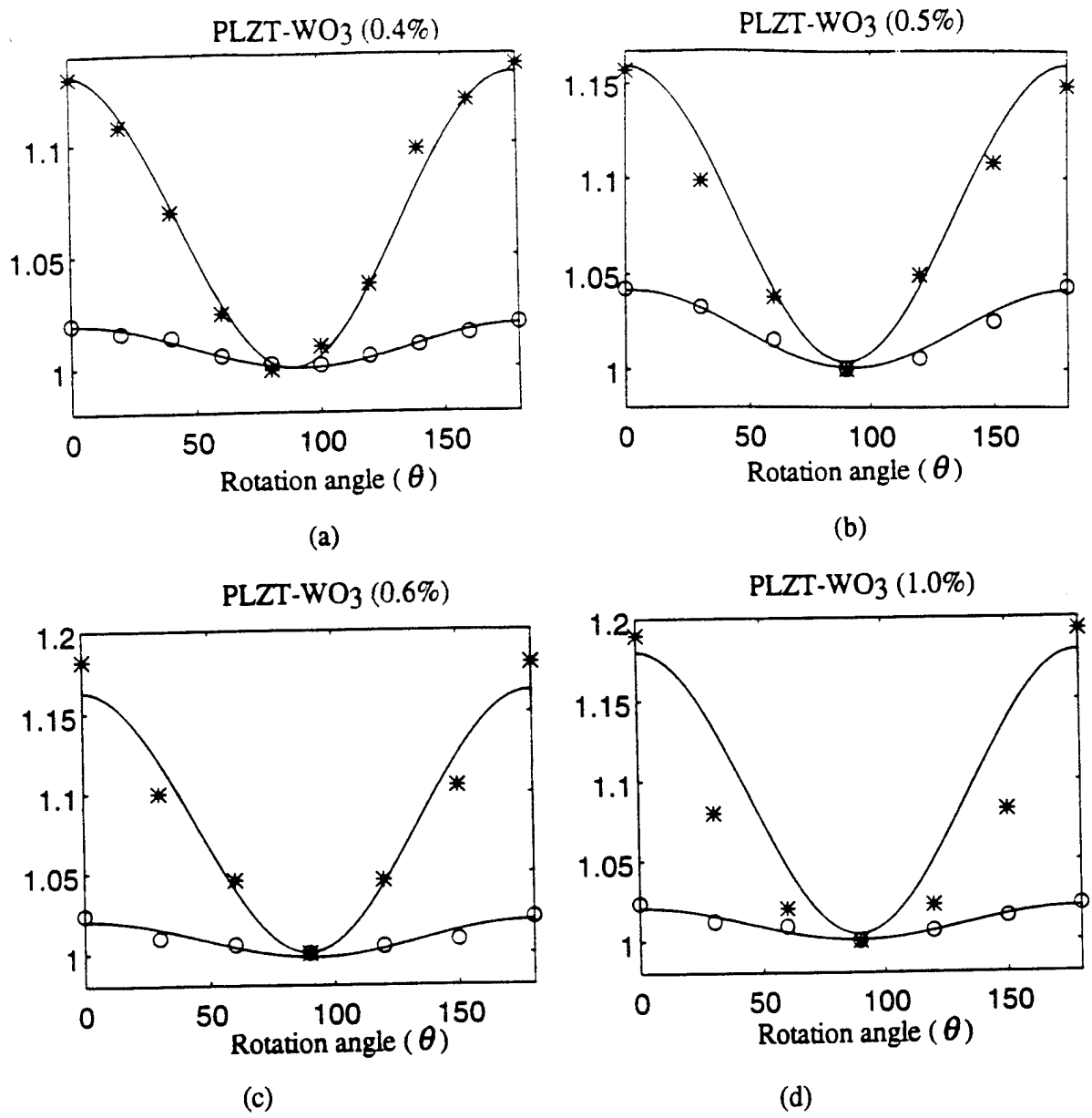

Figure 7: The experimental dependence of the normalized photovoltaic current and photovoltage on the direction of the light polarization plane with respect to the spontaneous polarization direction for WO_3 doped PLZT samples with (a) 0.4%, (b) 0.5%, (c) 0.6%, and (d) 1%. (o: photocurrent, *: photovoltage) Light power = 0.152 ± 0.001 mW.

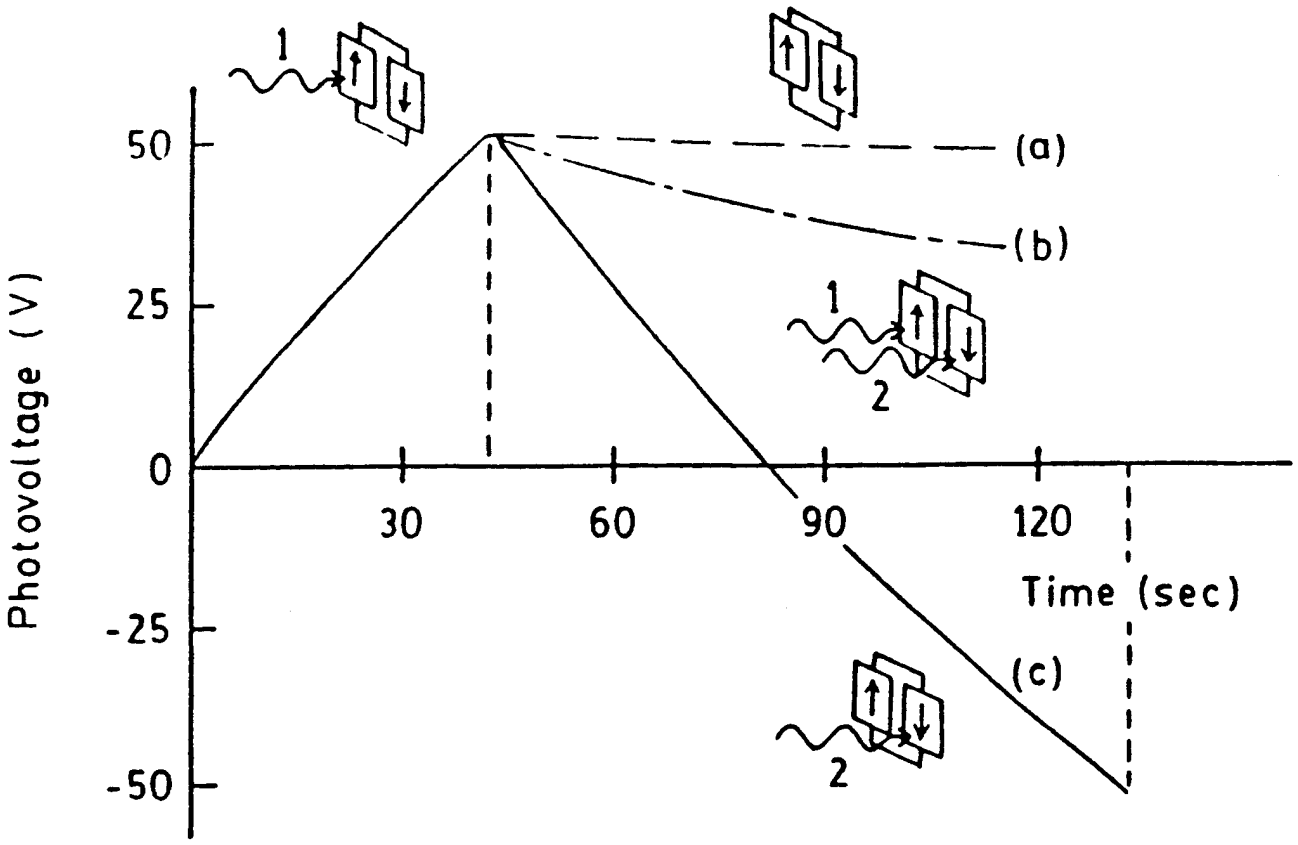

Fig. 8 Dual beam method for controlling the photostrictive device in quick response.

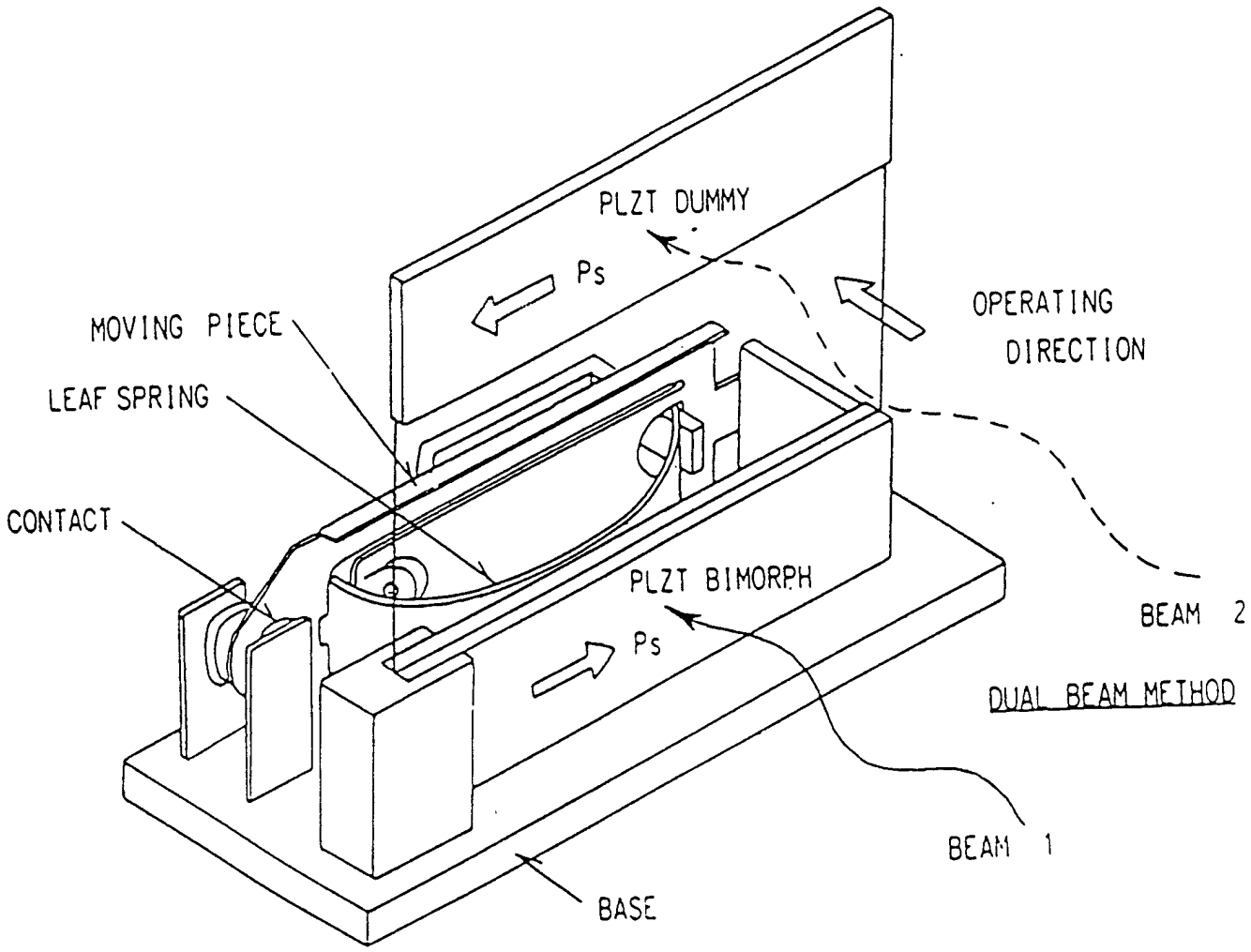

Figure 9: Structure of the photo-driven relay.

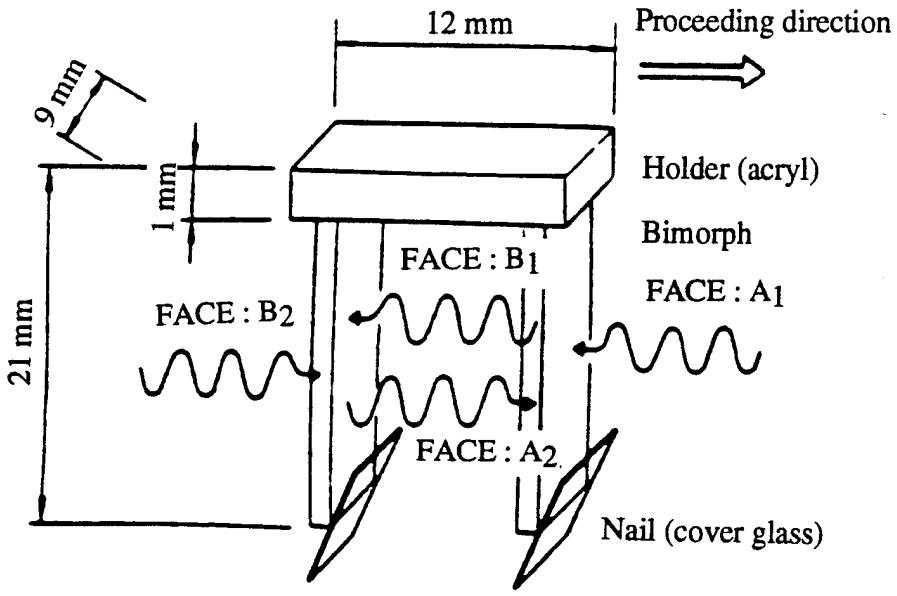

Figure 10: Structure of the photo-driven micro walking machine.

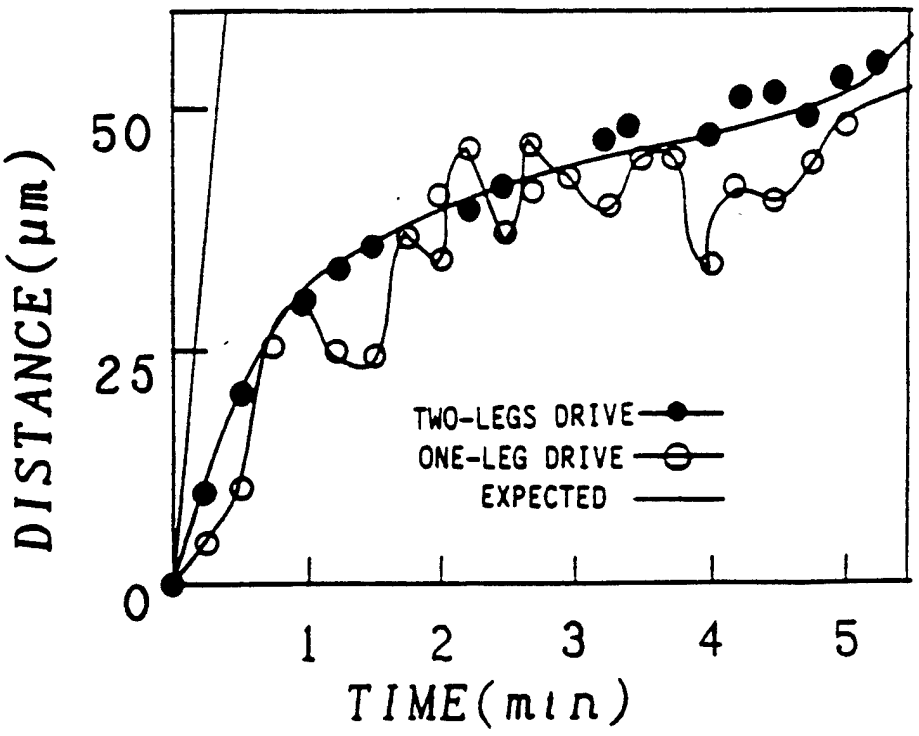

Figure 11: Position change of the photo-driven micro walking machine with time.

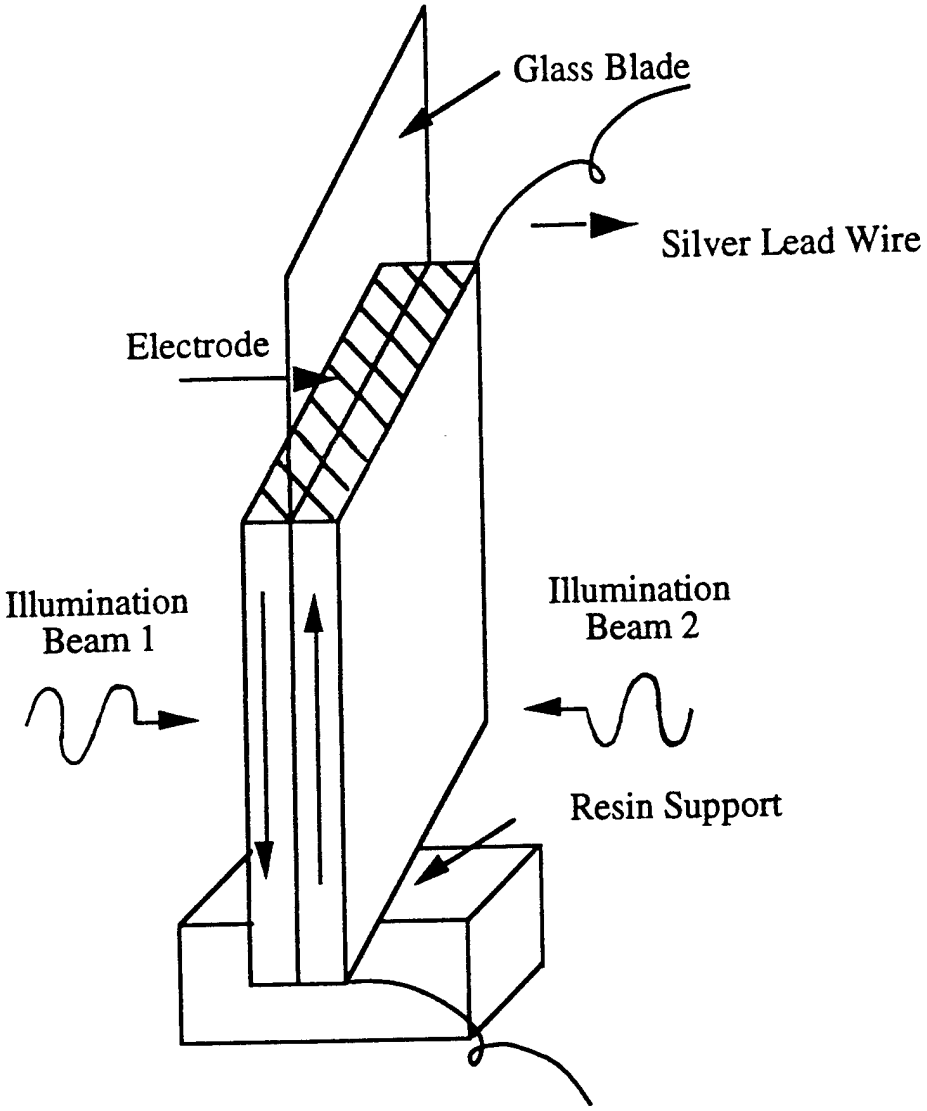

Figure 12: Configuration of a thin-plate attached photoacoustic bimorph.

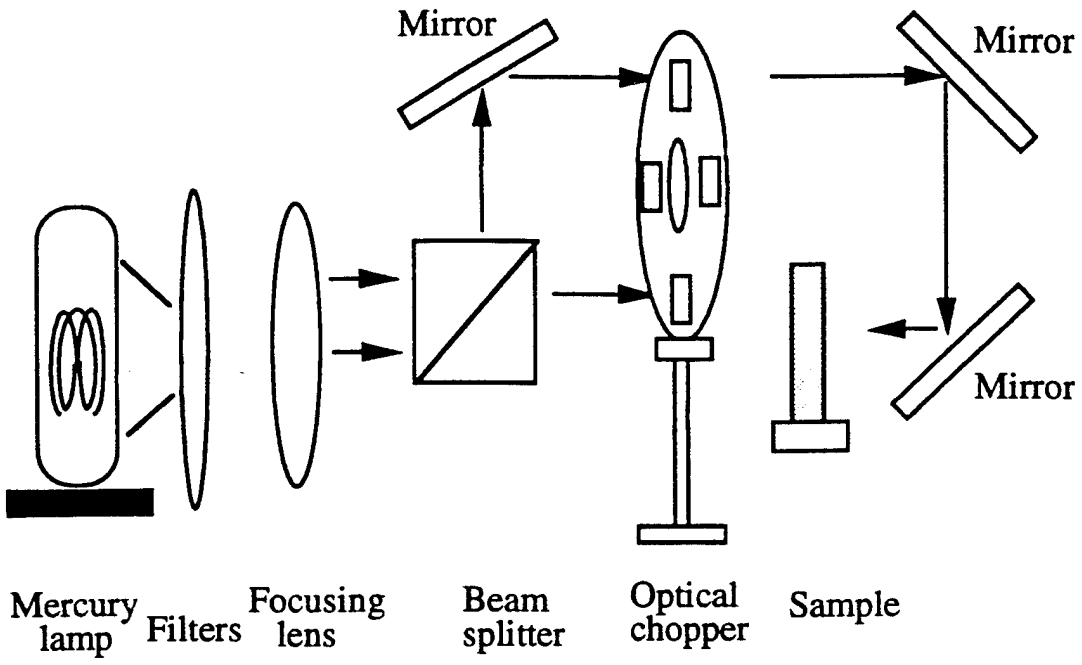

Figure 13: Experimental setup for photo-induced mechanical resonance measurements.

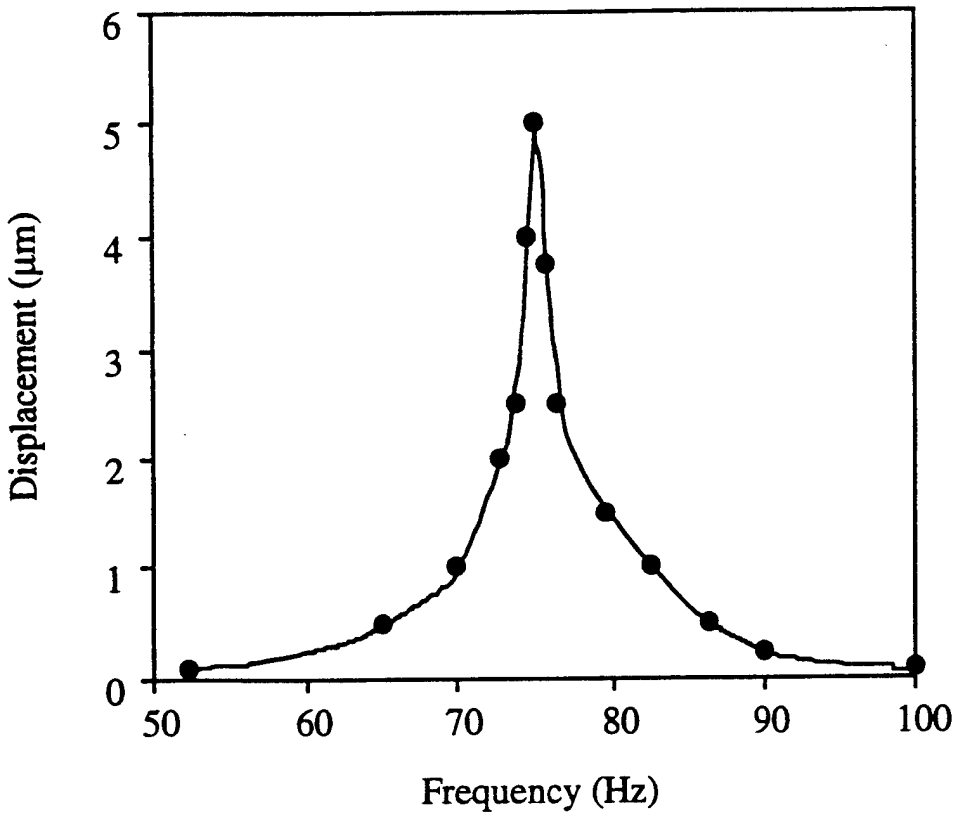

Figure 14: Photo-induced mechanical resonance behavior of WO_3 doped PLZT.

10. Uchino, K., "Review: Photostriction and Its Applications," J. Innovations in Mater. Res. (in press).

REVIEW: PHOTOSTRICTION AND ITS APPLICATIONS

Kenji Uchino
International Center for Actuators and Transducers
Materials Research Laboratory, The Pennsylvania State University
University Park, PA 16802

ABSTRACT

Photostriction in ferroelectrics arises from a superposition of photovoltaic and inverse piezoelectric effects. $(Pb,La)(Zr,Ti)O_3$ ceramics doped with WO_3 exhibit large photostriction under irradiation of near-ultraviolet light, and are applicable to remote control actuators and photoacoustic devices. Using a bimorph configuration, a photo-driven relay and a micro walking device have been developed, which are designed to start moving as a result from the irradiation, having neither electric lead wires nor electric circuits. The mechanical resonance of the bimorph was also induced by an intermittent illumination of purple-color light; this verified the feasibility of the photostriction to "photophone" applications.

Keywords: *Photostriction, Photovoltaic effect, Piezoelectricity, Bimorph, Photoacoustic, Photophone, Mechanical resonance*

INTRODUCTION

Photostrictive effect is a phenomenon in which strain is induced in the sample when it is illuminated. This effect is focused especially in the fields of micromechanism and optical communication.

With decreasing the size of miniature robots/actuators, the weight of the electric lead wire connecting the power supply becomes significant, and remote control will definitely be required for sub-millimeter devices. A photo-driven actuator is a very promising candidate for micro-robots. On the other hand, the key components in the optical communication are a solid state laser as a light source, an optical fiber as a transfer line, and a display/ a telephone as a visual/audible interface with the human. The former two components have been developed fairly successfully, and the photo-acoustic device (i. e. an optical telephone or a "photophone") will be eagerly anticipated in the next century.

Photostrictive devices which are actuated when they receive the energy of light will be particularly suitable for use in the above-mentioned fields. In principle, the photostrictive effect arises from a superposition of a photovoltaic effect, where a large voltage is generated in a ferroelectric through the irradiation of light,[1)] and a piezoelectric effect, where the material expands or contracts under the voltage applied. Ii is noteworthy that this photostriction is neither the thermal dilatation nor the pyroelectrically-produced strain associated with a temperature rise due to the light illumination. Also the photovoltaic effect mentioned here generates a greater-than-band-gap voltage (several kV/cm), and is quite different from that based on the p-n junction of semiconductors (i. e. solar battery).

This paper describes the details of the fundamental photostrictive effect in (Pb,La)(Zr,Ti)O_3 ceramics first, then introduces its applications to a photo-driven relay, a micro walking machine and a photophone, which are designed to function as a result of irradiation, having neither lead wires nor electric circuits.

PHOTOSTRICTIVE PROPERTIES

PRINCIPLE

The main features of the "bulk" photovoltaic effect are summarized as follows:

1) This effect is observed in a uniform crystal or ceramic having noncentric symmetry, and is entirely different in nature from the p-n junction effect observed in semiconductors.
2) A steady photovoltage/current is generated under uniform illumination.
3) The magnitude of the induced voltage is greater than the band gap energy of the crystal.

Although the origin of this photovoltaic effect has not been clarified yet, the key point to understand it is the necessity of both *impurity doping* and *crystal asymmetry*. Figure 1 illustrates one of the proposed models, the electron energy band model proposed for (Pb,La)(Zr,Ti)O_3.[2,3] The energy band is basically generated by the hybridized orbit of p-orbit of oxygen and d-orbit of Ti/Zr. The donor impurity levels induced in accordance with La doping (or other dopants) are present slightly above the valence band. The transition from these levels with an asymmetric potential due to the crystallographic anisotropy may provide the "preferred" momentum to the electron. Electromotive force is generated when electrons excited by light move in a certain direction of the ferroelectric crystal, which may arise along the spontaneous polarization direction.

The asymmetric crystal exhibiting a photovoltaic response is also piezoelectric in principle, and therefore, a photostriction effect is expected as a coupling of the bulk photovoltaic voltage (E^{ph}) with the piezoelectric strain constant (d).

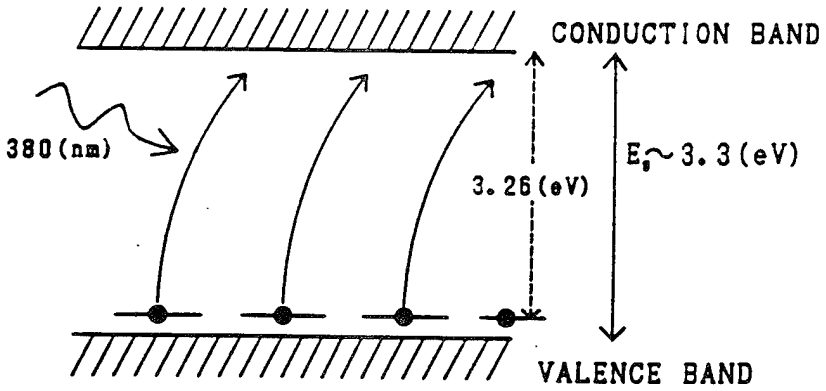

Figure 1 Energy band gap model of excited electron transition from impurity level in PLZT.

INSTRUMENTAION

The radiation from a high-pressure mercury lamp was passed through infrared-cut optical filters. The light with the wavelength peak around 370 nm, where the maximum photovoltaic effect of PLZT is obtained, was then applied to the sample. A xenon lamp was also used to measure the wavelength dependence of the photovoltaic effect. The light source was monochromated by a monochromator to 6 nm HWHM.

The photovoltaic voltage under illumination generally reaches several kV/cm, and the current is on the order of nA. The induced current was recorded as a function of the applied voltage over a range -100 V to +100 V, by means of a high-input impedance electrometer. The photovoltaic voltage and the current were determined from the intercepts of the horizontal and the vertical axes, respectively. The data are shown in Fig. 2.[3] Photostriction was directly measured by a differential transformer or an eddy current displacement sensor.

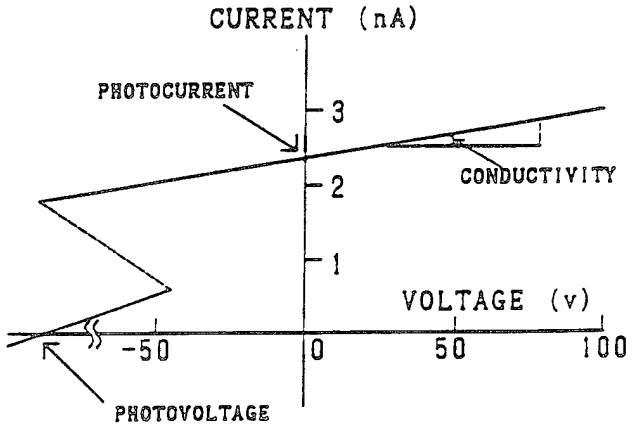

Figure 2 Photocurrent measured as a function of applied voltage under illumination.

MATERIALS RESEARCH

The figure of merit of the photostriction is evaluated by the product of the photovoltaic voltage (E^{ph}) and the piezoelectric coefficient (d). PZT based ceramics are currently focused because of their excellent piezoelectric properties, i. e. high d values. PLZT is one of such materials, which is also famous as a transparent (good sintered without pores) ceramic applicable to electrooptic devices.

PLZT (x/y/z) samples were prepared in accordance with the following composition formula:

$$Pb_{1-x}La_x(Zr_yTi_z)_{1-x/4}O_3.$$

Figures 3(a) and 3(b) illustrate the contour maps of the photovoltaic response and the piezoelectric strain constant d33 on the PLZT phase diagram.[4,5] The d33 shows the maximum around the morphotropic phase boundary (MPB) between the tetragonal and rhombohedral phases, and increases gradually with increasing the La concentration up to 9 mol %. On the contrary, the photovoltage exhibits the maximum also around the MPB, but in the tetragonal region with 3 mol % of La. The largest pruduct $d_{33}\cdot E^{ph}$ was obtained with the composition (3/52/48).

The interrelation of the photovoltaic current with the remanent polarization for the PLZT family is very intriguing (Fig. 4).[6] The average remanent polarization exhibiting the same magnitude of photocurrent differs by 1.7 times between the tetragonal and rhombohedral phases; this suggests the photo-induced electron excitation is related to the (0 0 1) axis-oriented orbit, i. e. the hybridized orbit of p-orbit of oxygen and d-orbit of Ti/Zr.

Impurity doping on PLZT also affects the photovoltaic response significantly.[3] Figure 5 shows the photovoltaic response for various dopants with the same concentration of 1 atomic % into the base PLZT (3/52/48) under an illumination intensity of 4 mW/cm^2 at 366 nm. The dashed line in Fig. 5 represents

the constant power curve corresponding to the non-doped PLZT (3/52/48). Regarding the photostriction effect, it is known that as the photovoltaic voltage increases, the strain value increases, and with increasing photocurrent, there is an increase in the overall response. The photovoltaic response is enhanced by donor doping onto the B-site (Nb^{5+}, Ti^{5+}, W^{6+}). On the other hand, impurity ions substituting at the A-site and/or acceptor ions substituting at the B-site, whose ionic valences are small (1 to 4), have no significant effect on the response. Figure 6 shows the photovoltaic response plotted as a function of at.% of WO_3 doping concentration.[7] Note that the maximum power is obtained at 0.4 at.% of the dopant.

Even when the composition is fixed, the photostriction still depends on the sintering condition or the grain size.[5] Figure 7 shows the dependence of the photostrictive characteristics on the grain size. The smaller grain sample is preferrable, if it is sintered to a high density.

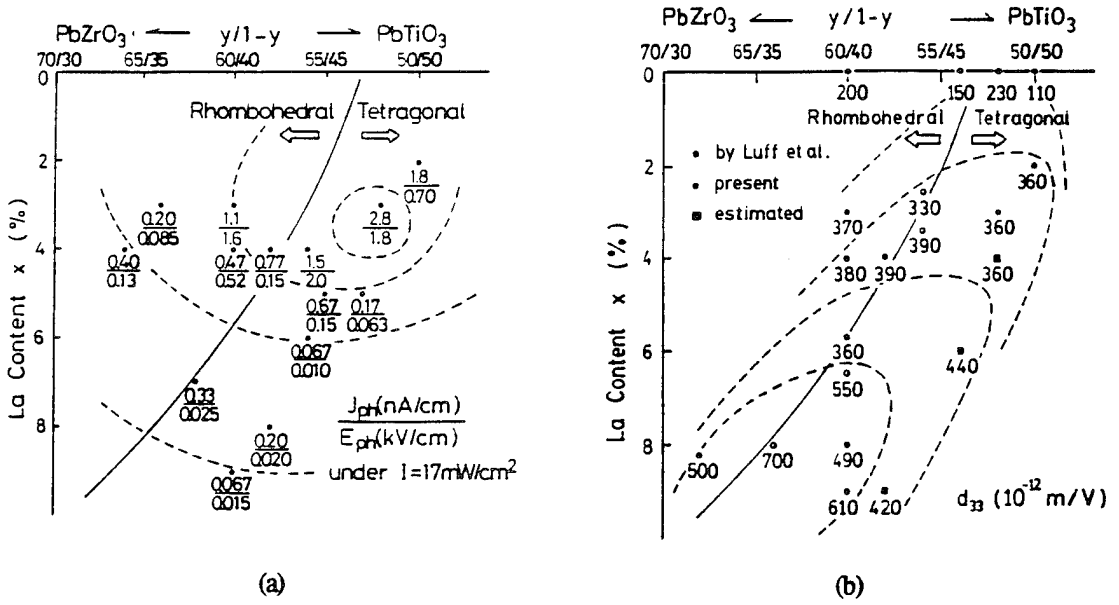

Figure 3 Photovoltaic response (a) and piezoelectric constant d33 (b) of PLZT plotted on the phase diagram near the morphotropic phase boundary between the tetragonal and rhombohedral phases.

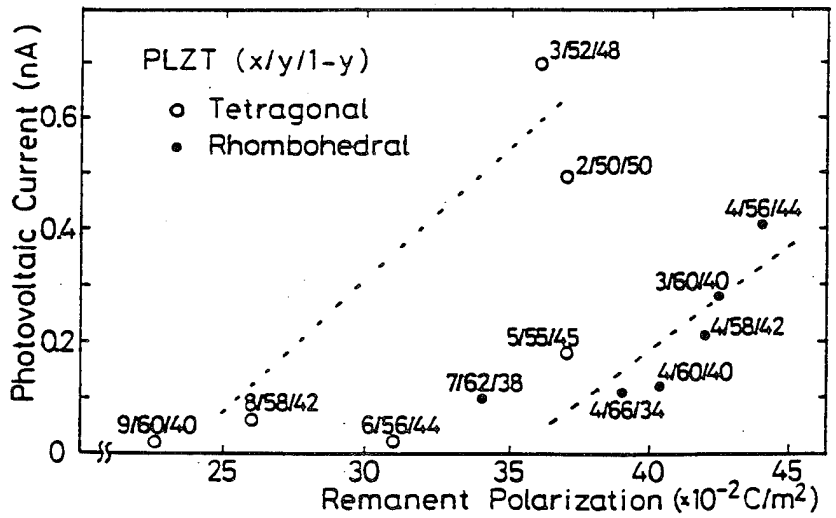

Figure 4 Interrelation of photovoltaic current with remanent polarization in PLZT family.

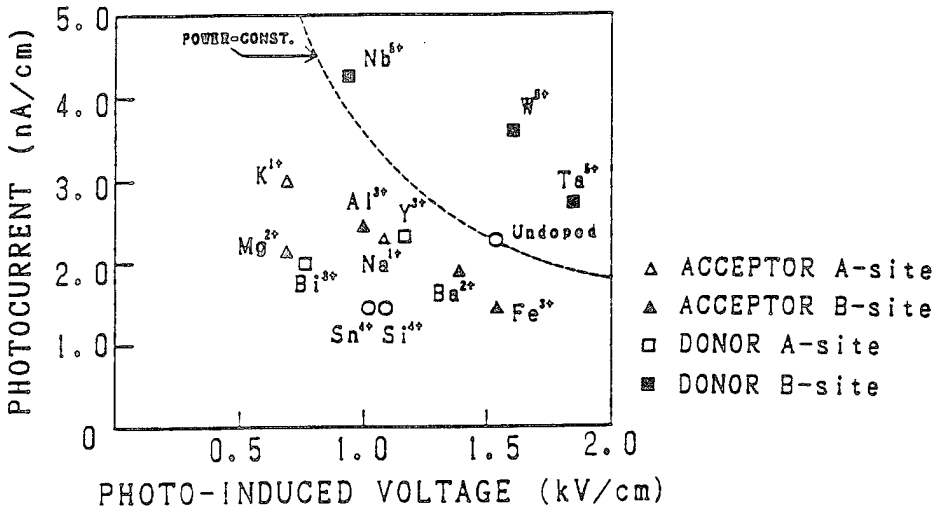

Figure 5 Photovoltaic response of PLZT for various impurity dopants (illumination intensity:4mW/cm^2).

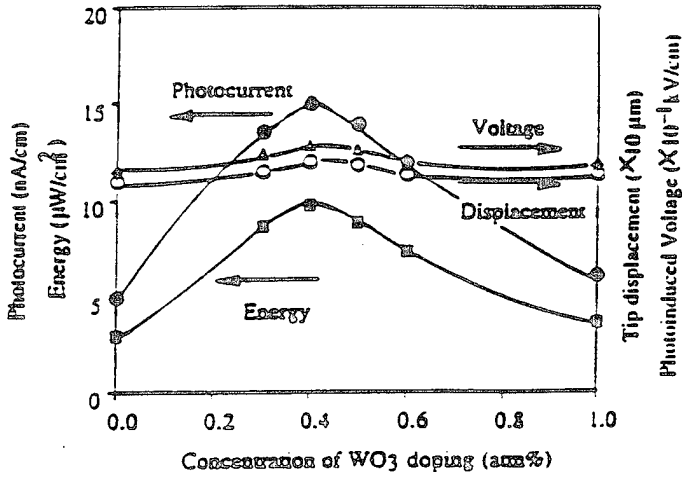

Figure 6 Photovoltaic current, voltage, power and tip displacement of a bimorph specimen as a function of dopant concentration in WO_3 doped PLZT (3/52/48).

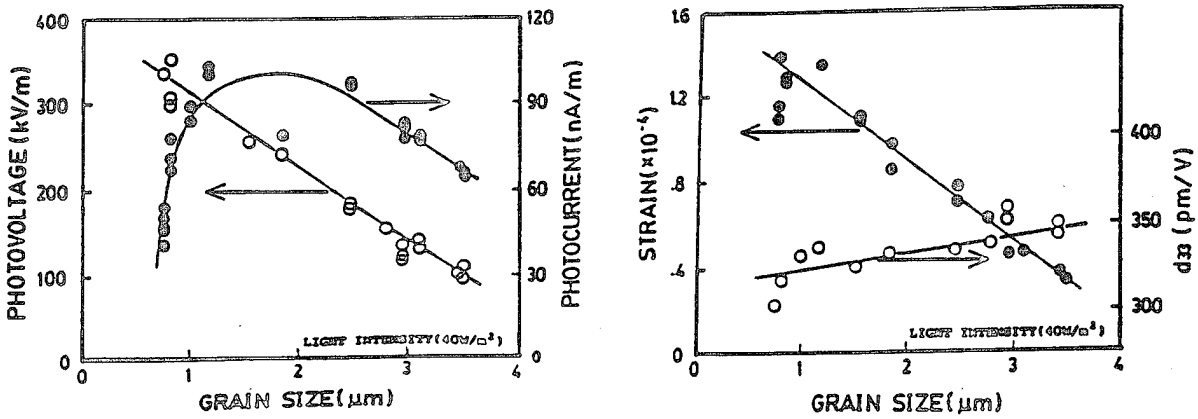

Figure 7 Grain size dependence of photostrictive characteristics in PLZT (3/52/48).

EFFECT OF LIGHT POLARIZATION DIRECTION

Effect of the light polarization direction on the photovoltaic phenomenon was investigated on the polycrystalline PLZT, using an experimental setup shown in Fig. 8(a).[8] This experiment is important when the photostriction is employed to "photophones", where the sample is illuminated with the polarized light traveling through an optical fiber. The rotation angle θ was taken from the vertical spontaneous polarization direction, as shown in Fig. 8(a). Even in a polycrystalline sample, both the photovoltaic voltage and current provided the maximum at θ = 0 and 180 deg and the minimum at θ = 90 deg (Fig. 8(b)); this also indicates that the contributing electron orbit may be the p-d hybridized orbit mentioned above.

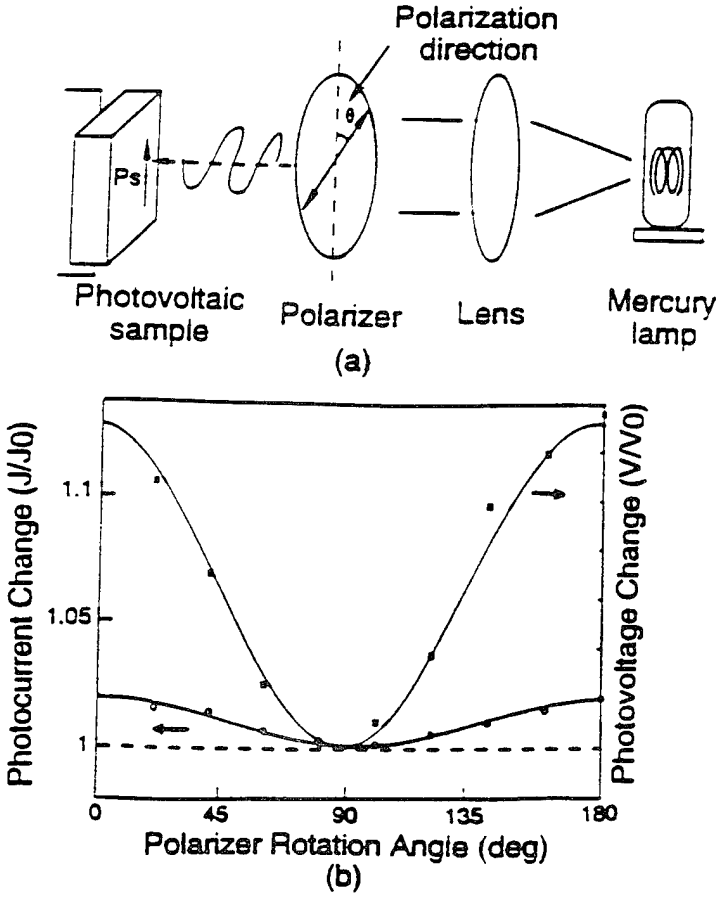

Figure 8 (a) Measuring system of the dependence of photovoltaic effect on light polarization direction, and (b) photovoltaic voltage and current as a function of the rotation angle.

DISPLACEMENT MAGNIFICATION MECHANISM

Since the maximum strain level of the photostriction is only 0.01 % (this corresponds to 1 μm displacement from a 10 mm sample), we need to consider a sophisticated magnification mechanism of the displacement. We employed a bimorph structure, which is anologous to a bimetal consisting of two metalic plates with different thermal expansion coefficients bonded together to generate a bending deformation according to a temperature change. Two PLZT plates were pasted back to back, but were placed in opposite polarization, then connected on the edges electrically, as shown in Fig. 9.[3] A purple light (366 nm) was shined to one side, which generated a photovoltaic voltage of 7 kV across the length. This caused the PLZT plate on that side to expand by nearly 0.01 % of its length, while the plate on the other (unlit) side contracted due to the piezoelectric effect through the photovoltage. Since the two plates were bonded together, the whole device bent away from the light. For this 20 mm long and 0.35 mm thick bi-plate, the displacement at the edge was 150 μm, and the response speed was a couple of seconds.

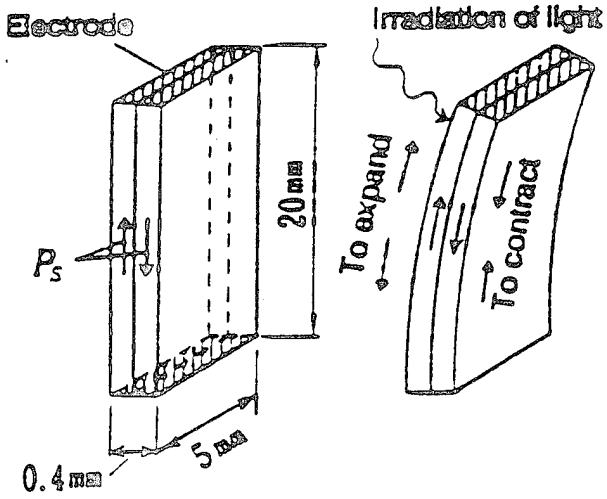

Figure 9 Structure of the photo-driven bimorph and its driving principle.

DEVICE APPLICATIONS

In this section we will introduce the applications of photostriction to a photo-driven relay, a micro walking machine and a photophone, which are designed to function as a result of irradiation, having neither lead wires nor electric circuits.

PHOTO-DRIVEN RELAY

A photo-driven relay was constructed using a PLZT photostrictive bimorph as a driver which consists of two ceramic plates bonded together with their polarization directions opposing each other (Fig. 10).[3] A dummy PLZT plate was positioned adjacent to the bimorph to cancel the photovoltaic voltage generated on the bimorph. Utilizing a dual beam method, switching was controlled by alternately irradiating the bimorph and the dummy. The time delay of the bimorph that ordinarily occurs in the off process due to a low dark conductivity could be avoided, making use of this dual beam method. Figure 11 shows the response of a photostrictive bimorph made from PLZT doped with 0.5 at% WO_3 under an illumination intensity of 10 mW/cm^2. The amount of displacement observed at a tip of the bimorph (20 mm long and 0.35 mm thick) was ±150 μm. A snap action switch was used for the relay. Switching by a displacement of several tens of micron was possible with this device. The on/off response of the photo-driven relay is shown in Fig. 12. The typical delay time was 1 - 2 seconds.

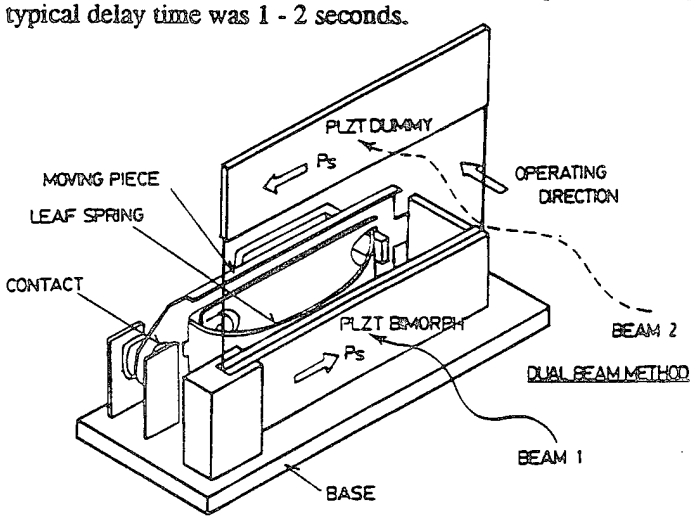

Figure 10 Structure of the photo-driven relay.

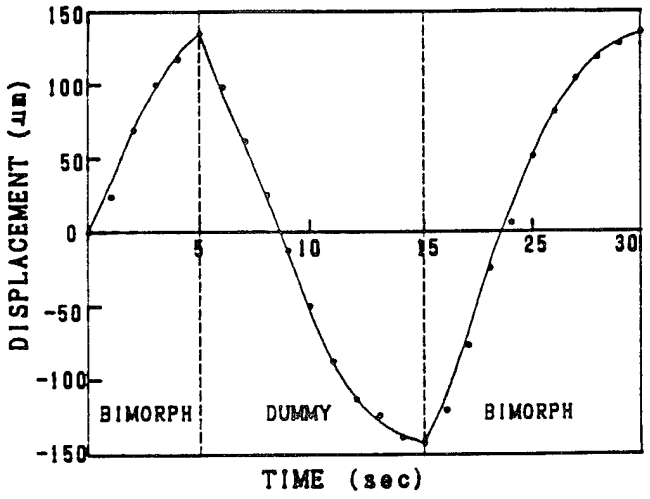

Figure 11 Tip deflection of the bimorph device made from WO_3 0.5 at.% doped PLZT under a dual beam control (illumination intensity: 10 mW/cm^2).

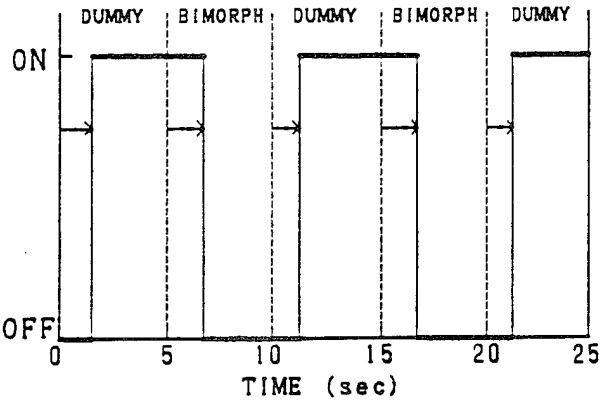

Figure 12 On/off response of the photo-driven relay.

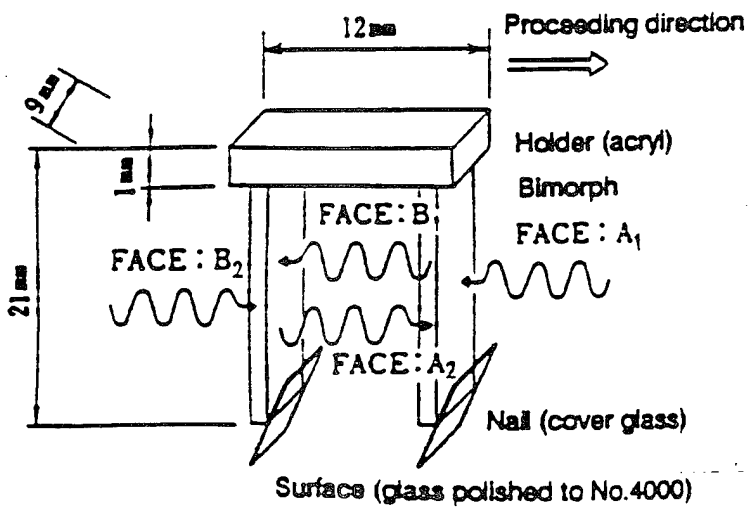

Figure 13 Structure of the photo-driven micro walking machine, and the irradiation directions.

MICRO WALKING DEVICE

A photo-driven micro walking machine has also been developed using the photostrictive bimorphs.[9] It was simple in structure, having only two ceramic legs (5mmx 20mmx 0.35mm) fixed to a plastic board (Fig. 13). When the two legs were irradiated with purple light alternately, the device moved like an inchworm. The photostrictive bimorph as a whole was caused to bend by ± 150 μm as if it averted the radiation of light. The inchworm built on a trial basis exhibited rather slow walking speed (several tens μm/min) as shown in Fig. 14, since slip occurred between the contacting surface of its leg and the floor. The walking speed can be increased to approximately 1 mm/min by providing some contrivances such as the use of a foothold having microgrooves fitted to the steps of the legs.

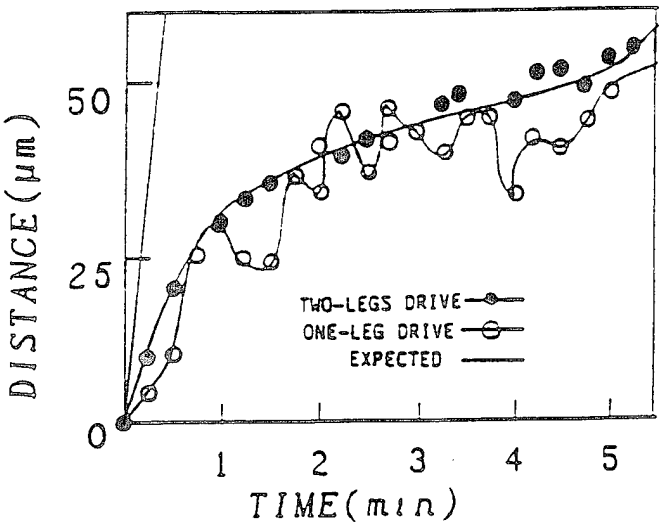

Figure 14 Position change of the photo-driven micro walking machine with time.

PHOTOPHONE

The technology to transmit voice data (i. e. a phone call) at the speed of light through lasers and fiber optics has been advancing rapidly. However, the end of the line -- interface speaker -- limits the technology, since optical phone signals must be converted from light energy to mechanical sound via electrical energy at present. The photostriction may provide new photoacoustic devices.

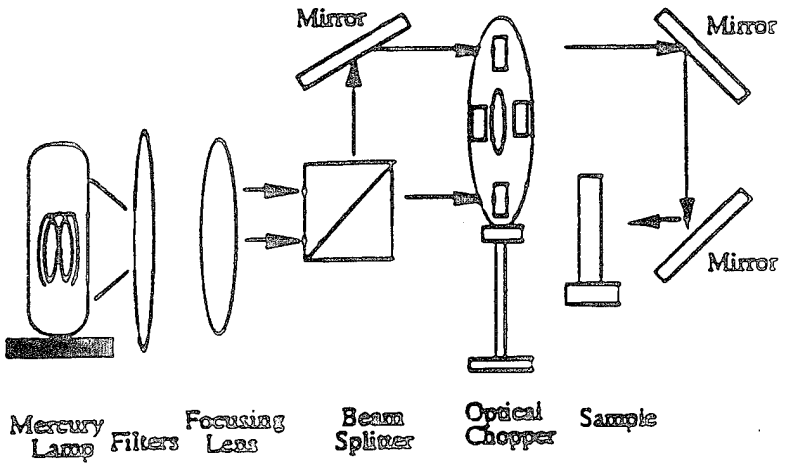

Figure 15 Experimental setup for the photo-induced mechanical resonance measurement.

Photo-mechanical resonance of a PLZT ceramic bimorph has been successfully induced using chopped near-ultraviolet irradiation, having neither electric lead wires nor electric circuits.[10] A thin cover glass was attached on the photostrictive bimorph structure to decrease the resonance frequency so as to easily observe the photo-induced resonance. Figure 15 shows the experimental setup with an optical chopper. A dual beam method was used to irradiate the two sides of the bimorph alternately; intermittently with a 180 deg phase difference. The mechanical resonance was then determined by changing the chopper frequency.

The tip displacement of the thin-plate-attached sample as a function of chopper frequency is presented in Fig. 16. Photo-induced mechanical resonance was successfully observed. The resonance frequency was about 75 Hz with the mechanical quality factor Q of about 30. The maximum tip displacement of this photostrictive sample was about 5 μm at the resonance point, smaller than the level required for audible sound. However, the achievement of photo-induced mechanical resonance in the audible frequency range suggests the promise of photostrictive PLZT bimorph-type devices as photo-acoustic components, or "photophones", for the next optical communication age.

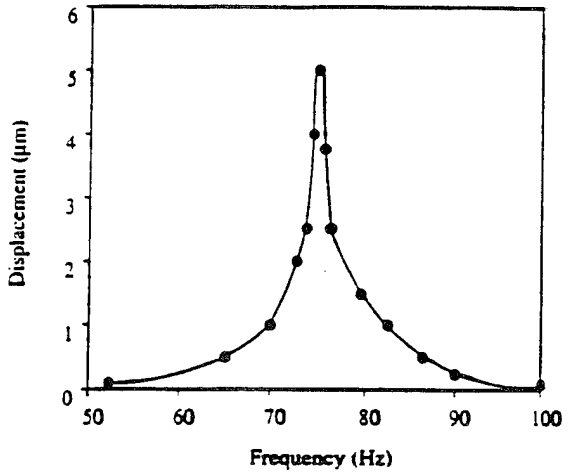

Figure 16 Photo-induced mechanical resonance behavior of the PLZT bimorph.

CONCLUSION

Photostrictive actuators can be driven only by the irradiation of light, so that they will be suitable for use in actuators, to which lead wires can hardly be connected because of their ultra-small size or of their employed conditions such as ultra-high vacuum or outer space. The photostrictive bimorphs will also be applicable to "photophones." The new principle actuators have considerable effects upon the future micro-mechatronics.

This work was partly supported by US Army Research Office through Contract No. DAAL 03-92-G-0244.

REFERENCES

1. V. M. Fridkin, *Photoferroelectrics*, Ed. by M. Cardona, P. Fulde, H. -J. , Queisser, Solid State Sciences 9, Springer-Verlag, New York (1979).
2. A. M. Glass, D. von der Linde, D. H. Austin and T. J. Negran, *J. Elec. Mater.*, 4 [5], 915 (1975).
3. M. Tanimura and K. Uchino, *Sensors and Materials*, 1, 47 (1988).
4. K. Uchino, M. Aizawa and Late S. Nomura, *Ferroelectrics*, 64,199 (1985).
5. T. Sada, M. Inoue and K. Uchino, *J. Ceram. Soc. Jpn.*, 5, 545 (1987).
6. K. Uchino and M. Aizawa, *Jpn. J. Appl. Phys.*, 24, Suppl. 24-3, 139 (1985).
7. S. Y. Chu, Z. Ye and K. Uchino, *J. Adv. Performance Mater.* [in press].
8. S. Y. Chu, Z. Ye and K. Uchino, *Smart Mater. Struct.*, 3, 114 (1994).
9. K. Uchino, *J. Rob. Mech.*, 1, 124 (1989).
10. S. Y. Chu and K. Uchino, *Proc. 9th Int'l Symp. Appl. Ferroelectrics*, State College (1994)[in press].

REVIEW PAPERS ON SMART MATERIALS

11. Uchino, K., "Ceramic Actuators: Principles and Applications," Mater. Res. Soc. Bull. 18, 42 - 48 (1993).

Ceramic Actuators: Principles and Applications

Kenji Uchino

Introduction

Piezoelectric and electrostrictive actuators, capable of moving something electromechanically, are forming a new field between electronic and structural ceramics.[1-3] Application fields are classified into three categories: positioners, motors, and vibration suppressors. The manufacturing precision of optical instruments such as lasers and cameras, and the positioning accuracy for fabricating semiconductor chips, which must be adjusted using solid-state actuators, is of the order of 0.1 μm. Regarding conventional electromagnetic motors, tiny motors smaller than 1 cm^3 are often required in office or factory automation equipment and are rather difficult to produce with sufficient energy efficiency. Ultrasonic motors whose efficiency is insensitive to size are superior in the mini-motor area. Vibration suppression in space structures and military vehicles using piezoelectric actuators is also a promising technology.

New solid-state displacement transducers controlled by temperature (shape memory alloy) or magnetic field (amorphous magnetostrictive alloy) have been proposed, but are generally inferior to the piezoelectric/electrostrictive actuators because of technological trends aimed at reduced driving power and miniaturization.

This article reviews recent developments of piezoelectric and related ceramic actuators for smart/intelligent systems.

Ceramic Actuator Materials

What happens on an atomic scale when a ceramic expands or contracts in response to an applied electric field? There are three types of strain (defined by the ratio $\Delta L/L$: the amount of deformation with respect to the original length) that may be induced by an electric field, depending on the crystal structure: piezoelectric, electrostrictive, and phase-change-related strains.

Figures 1a and b show ionic models for noncentrosymmetric (piezoelectric) and centrosymmetric (electrostrictive) crystals, respectively.[6] When an electric field is applied to the crystal, the cations are displaced in the direction of the field and the anions in the opposite direction. The ionic shift differences in noncentrosymmetric ceramic can be visualized as soft and hard springs, producing piezostriction. The induced strain is proportional to the applied field (i.e. $x = dE$). For the centrosymmetric structure in Figure 1b, anharmonicity of the springs is essential, resulting in a second-order electrostrictive effect. Here the induced strain is proportional to the square of the field ($x=ME^2$).

Actual strains in ceramics are induced in more complicated ways. The crystal pictured in Figure 1a possesses a spontaneous polarization. When a large reverse electric field is applied in the opposite direction of the spontaneous polarization, a transition phase is formed which is another stable crystal state in which the relative positions of the ions are reversed by 180°. This transition, referred to as polarization reversal, causes a jump and hysteresis of the strain during an electric-field cycle, superimposed on the pure piezostriction. Non-180° polarization reorientation, though not shown in the one-dimensional model in Figure 1a, also causes significant contribution to the strain hysteresis.

Modified lead zirconate titanate [PZT, $Pb(Zr,Ti)O_3$]-based ceramics are currently the leading materials for piezoelectric applications. The PLZT [$(Pb,La)(Zr,Ti)O_3$] 7/62/38 compound is one such composition.[7] The strain curve is shown in Figure 2a left. When the applied field is small, the induced strain is nearly proportional to the field. As the field becomes larger (i.e., greater than about 100 V/mm), however, the strain curve deviates from this linear trend and significant hysteresis is exhibited due to polarization reorientation. This sometimes limits the usage of this material in actuator applications that require nonhysteretic response.

An interesting new family of actuators has been fabricated from a barium stannate titanate [$Ba(Sn,Ti)O_3$] solid solution.[8] The useful property of $Ba(Sn_{0.15}Ti_{0.85})O_3$ is its unusual strain curve, in which the domain reorientation occurs only at low fields, and there is then a long linear range at higher fields (Figure 2a right); i.e., the coercive field is unusually small.

On the other hand, electrostriction in

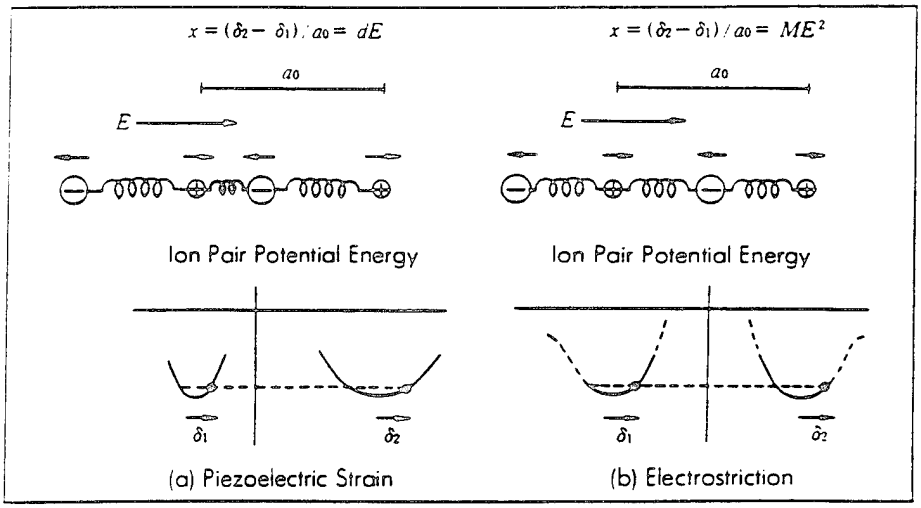

Figure 1. Diagrammatic explanation of the origins of piezoelectric strain (a) and electrostriction (b).

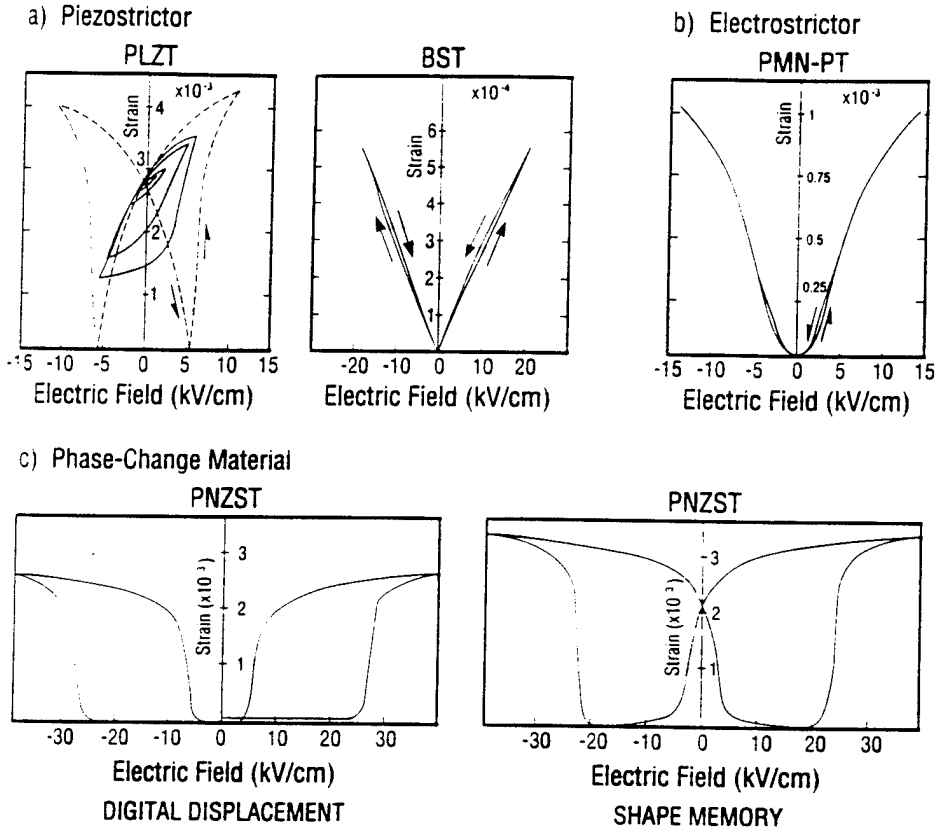

Figure 2. Electric field-induced strains in ceramics: (a) Piezoelectric for (Pb,La)(Zr,Ti)O_3 and Ba(Sn,Ti)O_3. (b) Electrostrictor, Pb($Mg_{1/3}Nb_{2/3}$,Ti)O_3. (c) Phase-change material Pb(Zr,Sn,Ti)O_3.

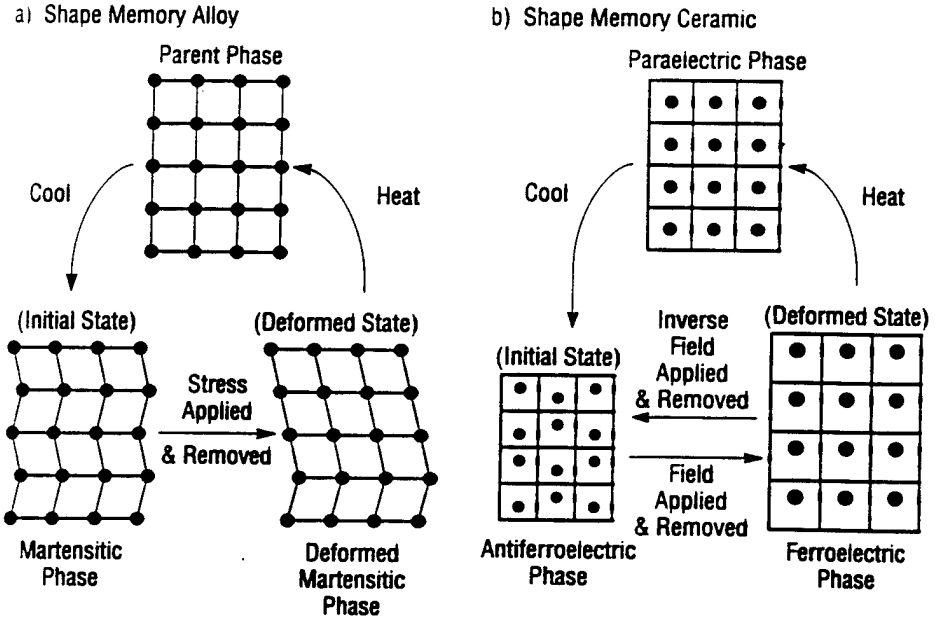

Figure 3. Shape-memory effects in an alloy (a) and an antiferroelectric ceramic (b).

PMN[Pb($Mg_{1/3}Nb_{2/3}$)O_3]-based ceramics, though a second-order phenomenon of electromechanical coupling, is extraordinarily large (more than 0.1%).[9] An attractive feature of these materials is the near absence of hysteresis (Figure 2b).

Concerning the phase-change-related strains, polarization induction by switching from a macroscopically nonpolar into a polar state, as in switching from an antiferroelectric to a ferroelectric state, has been proposed.[10] Figure 3 illustrates the phase transition mechanism under an applied electric field, in comparison with the phase change in a shape memory alloy.[11] Notice that the strain control is made thermally in shape memory alloys, leading to much slower response and higher drive power than in the antiferroelectrics.

Figure 2c shows the field-induced strain curves taken for the lead zirconate stannate-based system [$Pb_{0.99}Nb_{0.02}((Zr_xSn_{1-x})_{1-y}Ti_y)_{0.98}O_3$]. The longitudinally induced strain reaches up to 0.4%, which is much larger than that expected in normal piezostrictors/electrostrictors. A rectangular-shape hysteresis in Figure 2c left, referred to as a "digital displacement transducer" because of the two on/off strain states, is interesting. Moreover, this field-induced transition exhibits a shape memory effect in appropriate compositions (Figure 2c right). Once the ferroelectric phase has been induced, the material will "memorize" its ferroelectric state even under zero-field conditions, although it can be erased with the application of a small reverse bias field.[12] This shape memory ceramic is used in energy-saving actuators.

The fundamental features of ceramic actuators may be summarized as follows:

- Displacements of up to several tens of microns that can be controlled with a precision of ±0.01 μm.
- Response speeds on the order of 10 μsec.
- Generative forces as large as 400 kgf/cm².
- Driving power an order of magnitude smaller than electromagnetic motors.

As the requirements for ceramic actuators become more specific, inadequacies due to the preparation history of the ceramic arise in reproducibility of properties. High reproducibility is achieved only by precise control of the grain/particle size, which is not possible utilizing the conventional mixed-oxide method of preparation. Recent advances in preparation technology of ultrafine ceramic powders has been useful in producing reliable and durable ceramic actuators. The effect of grain size on the electrostrictive response and the mechanical fracture toughness in lead lanthanum zirconate titanate (PLZT 9/65/35) is shown in Figures 4a and 4b.[13] A significant reduction in hysteresis and in

the strain magnitude is observed for grain sizes less than 1.7 μm, as is a remarkable increase in the fracture toughness, suggesting the existence of an optimum grain size around 1 μm.

Actuator Designs

Two of the most popular actuator designs are multilayers and bimorphs (see Figure 5). The multilayer, in which roughly 100 thin piezoelectric/electrostrictive ceramic sheets are stacked together, has advantages in low driving voltage (100 V), quick response (10 μsec), high generative force (100 kgf) and high electromechanical coupling. But the displacement in the range of 10 μm is not sufficient for some applications. This contrasts with the bimorph, consisting of multiple piezoelectric and elastic plates bonded together to generate a large bending displacement of several hundred μm, but the response (1 msec) and the generative force (100 gf) are low.

A composite actuator structure called the "moonie" has been developed to provide characteristics intermediate between the multilayer and bimorph actuators;[14] this transducer exhibits an order of magnitude larger displacement than the multilayer, and much larger generative force with quicker response than the bimorph. The device consists of a thin multilayer piezoelectric element and two metal plates with narrow moon-shaped cavities bonded together as shown in Figure 5. The moonie with a size of 5 × 5 × 2.5 mm can generate a 20-μm displacement under 60 V, eight times as large as the generative displacement of the multilayer with the same size.[15] This new compact actuator has been applied to make a miniaturized laser beam scanner.

a)

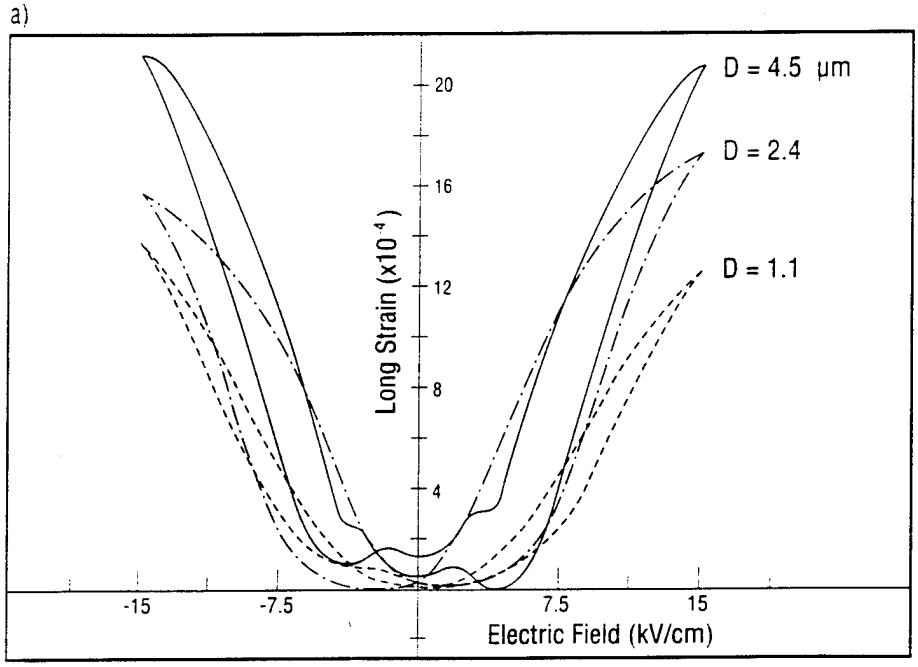

b)

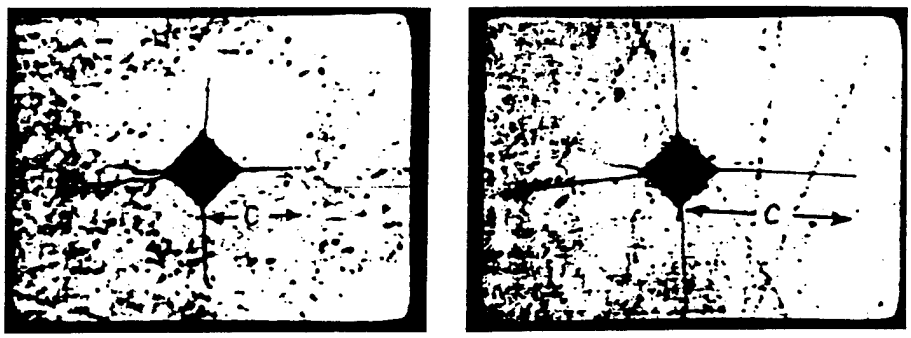

D = 1.1 (μm)
C = 208 ± 22 (μm)

D = 2.4 (μm)
C = 275 ± 30 (μm)

Figure 4. Grain-size dependence of field-induced strain (a) and Vicker's indentation test (b), observed in PLZT 9/65/35.

Applications of Piezoelectric/ Electrostrictive Actuators

Piezoelectric/electrostrictive actuators may be classified into two categories, based on the type of driving voltage applied to the device and the nature of the strain induced by the voltage (Figure 6): (1) rigid displacement devices for which the strain is induced unidirectionally along an applied dc field, and (2) resonating displacement devices for which the alternating strain is excited by an ac field at the mechanical resonance frequency (ultrasonic motors). The first can be further divided into two types: servo displacement transducers (positioners) controlled by a feedback system through a position-detection signal, and pulse-drive motors operated in a simple on/off switching mode. An actuator referred to as a flight actuator has been proposed that strikes a steel ball by means of a pulse-drive unit made from a multilayer piezo-device similar to that found in a pinball machine.[16]

The material requirements for these classes of devices are somewhat different, and certain compounds will be better suited to particular applications. The ultrasonic motor, for instance, requires a conventional hard-type piezoelectric with a high mechanical quality factor Q. The servo-displacement transducer suffers most from strain hysteresis and, therefore, a PMN electrostrictor is used for this purpose. The pulse-drive motor requires a low permittivity material aiming at quick response rather than a small hysteresis so that soft-PZT piezoelectrics are preferred to the high-permittivity PMN for this application.

Three typical application examples will now be considered.

Deformable Mirror

In the field of optical information processing, deformable mirrors have been proposed to control the phase of the incident light wave. The deformable mirror can be made convex or concave on the surface as necessary. This type of mirror, which is applicable to an accessory device

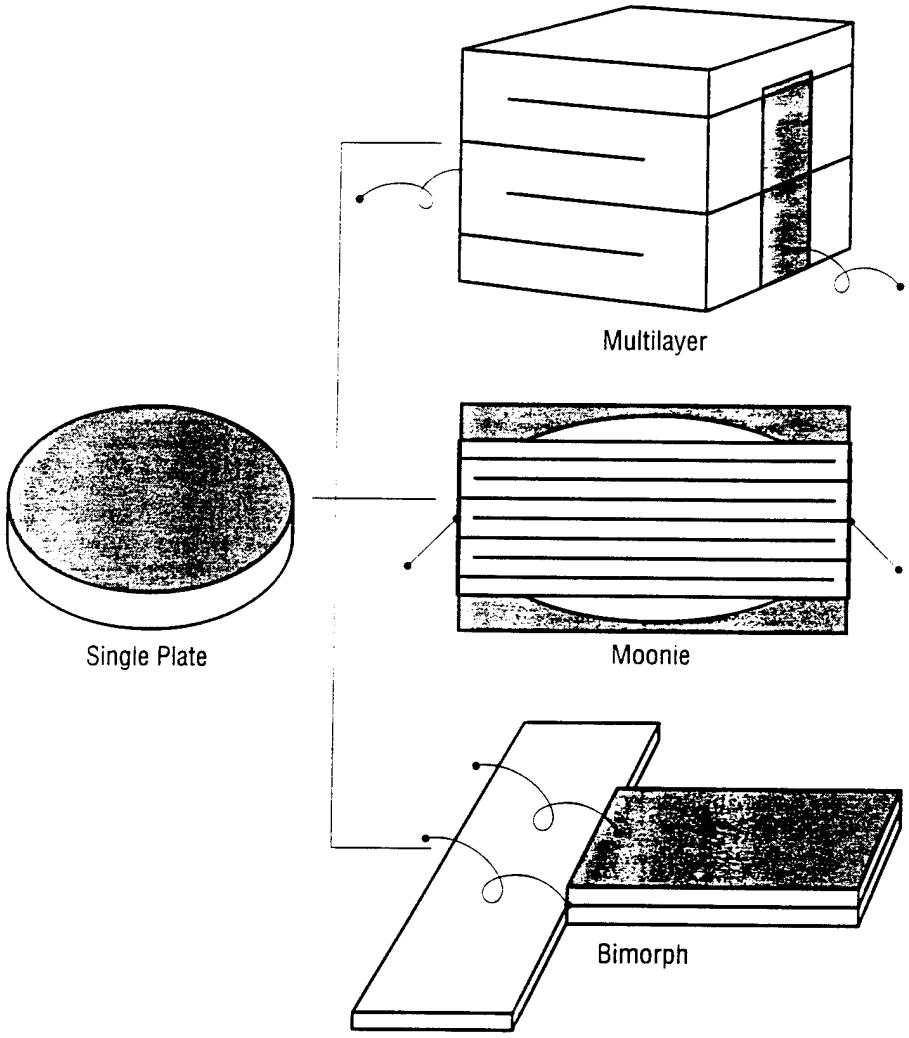

Figure 5. Typical designs for ceramic actuators: multilayer, moonie, and bimorph.

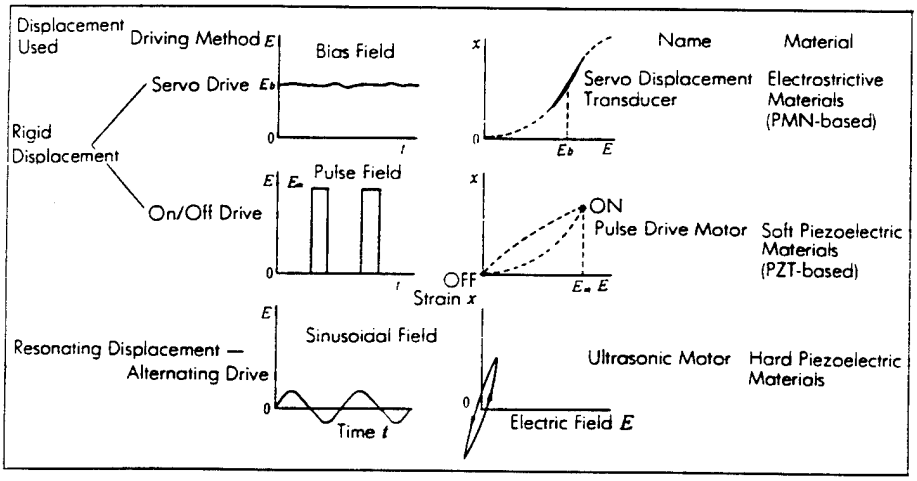

Figure 6. Classification of piezoelectric/electrostrictive actuators.

on observatory telescopes, effectively corrects for image distortions resulting from fluctuating airflow.

An example of a deformable mirror is the two-dimensional multimorph type illustrated in Figure 7.[17,18] When three layers of thin electrostrictive ceramic (PMN) plates are bonded to the elastic plate of a glass mirror, the mirror surface is deformed in various ways corresponding to the strain induced in the PMN layers. The nature of the deformation is determined by the electrode configurations and the distribution of the applied electric field. Trial devices have been designed by finite element methods such that the first layer, with a uniform electrode pattern, produces a spherical deformation (i.e., refocusing), while the second layer, with a 6-divided electrode pattern, corrects for coma aberration.

Aberration correction using such a simple three-layered device makes the image clear to the human eye. One may relate this situation to an eye examination at the optometrist. First you are asked "Which lens fits you best?" to adjust the focus degree. Then, "Do you have an uneven orientation distribution?" to correct the astigmatism. Usually, an optometrist does not further optically correct your lenses. Correction up to the second order is sufficient for the human eye.

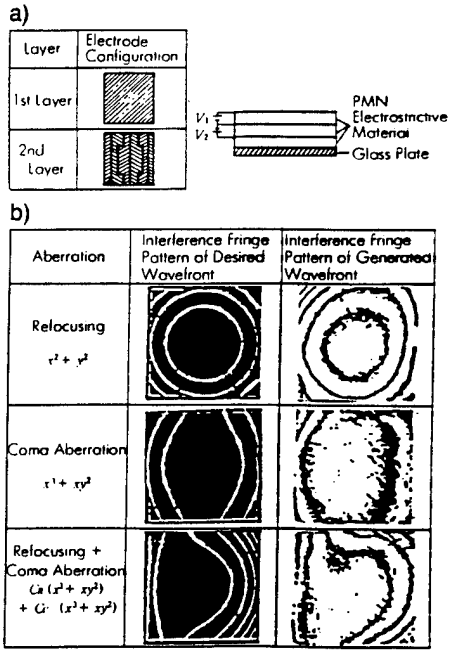

Figure 7. Structure of a multimorph deformable mirror (a) and actual control of light wavefront (b).

Impact Dot-Matrix Printer

Among the various types of printing devices, dot matrix printers are routinely employed at present. Each character formed by such a printer is composed of a 24 × 24-dot matrix. A printing ribbon is subsequently impacted by a multiwire array. A sketch of the printer head appears in Figure 8a.[19]

The printing element is composed of a multilayer piezoelectric device, in which 100 thin ceramic sheets 100 μm in thickness are stacked, together with a sophisticated magnification mechanism (Figure 8b). The advantages of using a multilayer actuator for this particular application include a low driving voltage, large displacement, and a high electromechanical coupling. The magnification unit is based on a monolithic hinged lever with a magnification of 30, resulting in an amplified displacement of 0.5 mm and an energy transfer efficiency greater than 50%.

The merits of the piezoelectric impact printer compared with the conventional electromagnetic types are: (1) higher printing speed by an order of magnitude, (2) lower energy consumption by an order of magnitude, and (3) reduced printing noise, which can be obtained with a sound shield because the actuators do not generate much heat.

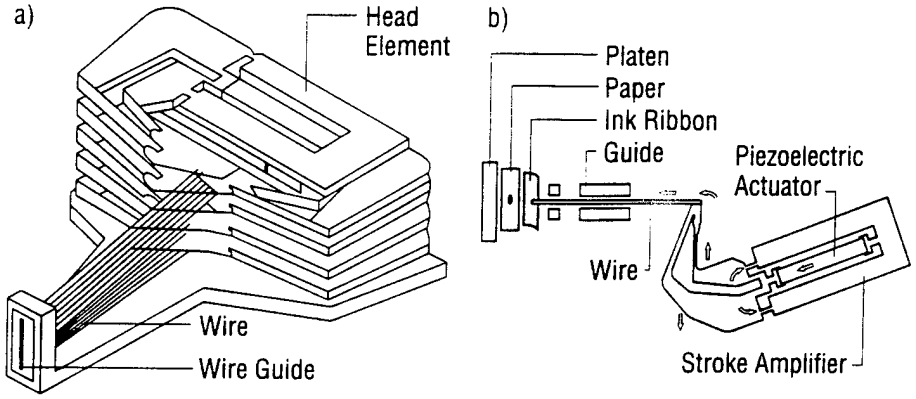

Figure 8. Structure of a printer head (a) and a differential-type piezoelectric printer-head element (b).

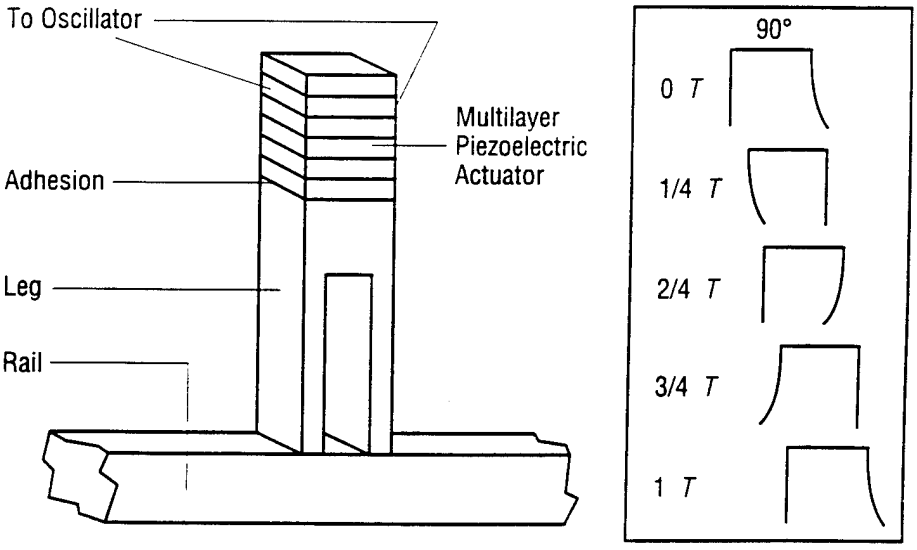

Figure 9. Ultrasonic linear motor of a vibratory coupler type.

Ultrasonic Motor

Efforts have been made to develop high-power ultrasonic vibrators as replacements for conventional electromagnetic motors. Two categories are being investigated for ultrasonic motors: a standing-wave type and a propagating-wave type.

The standing-wave type is sometimes referred to as a vibratory-coupler type or a "woodpecker" type, where a vibratory piece is connected to a piezoelectric driver and the tip portion generates flat-elliptical movement. Attached to a rotor or a slider, the vibratory piece provides intermittent rotational torque or thrust. The standing-wave type has, in general, high efficiency, but lack of control in both clockwise and counterclockwise directions is a problem.

An ultrasonic linear motor equipped with a multilayer piezoelectric actuator and fork-shaped metallic legs has been developed as shown in Figure 9.[20] Since there is a slight difference in the mechanical resonance frequency between the two legs, the phase difference between the bending vibrations of both legs can be controlled by changing the drive frequency. The walking slider moves in a way similar to a horse using its fore and hind legs when trotting. A trial motor 20 × 20 × 5 mm^3 in dimension exhibited a maximum speed of 20 cm/s and a maximum thrust of 0.2 kgf with a maximum efficiency of 20%, when driven at 98 kHz of 6 V (actual power ~0.7 W). This motor has been employed in a precision X-Y stage.

By comparison, the propagating-wave type (a surface-wave or "surfing" type) combines two standing waves with a 90° phase difference both in time and in space, and is controllable in both rotational directions.

By means of the traveling elastic wave induced by the thin piezoelectric ring, a ring-type slider in contact with the "rippled" surface of the elastic body bonded onto the piezoelectric is driven in both directions by exchanging the sine and cosine voltage inputs. Another advantage is its thin design, which makes it suitable for installation in VCR or movie cameras as an automatic focusing device.[21]

Future Developments of Ceramic Actuators

It is evident that the application field of ceramic actuators is remarkably wide. There still remain, however, problems in durability and reliability that need to be addressed before these devices can become general-purpose commercialized products. Investigations are primarily focused on the areas of material preparation, device design, and systemization of the actuator.[22] In particular, current topics include the preparation of homogeneous fine-grained ceramics by means of wet chemical

methods,[13] moonie actuators,[14] pulse-drive techniques based on analysis of transient vibrations and vibration suppression,[23] and prediction of breakdown within a ceramic actuator by means of acoustic emission measurements.[24]

Piezoceramic:carbon:polymer composites and photostrictive actuators have been under recent development for mechanical vibration suppression and remote control/drive of the actuator. These devices are described in the closing sections.

Piezoelectric Damper

The passive damper application is a smart usage of piezoelectrics, where mechanical noise vibration is radically suppressed by the converted electric energy dissipation through Joule heat when a suitable resistance, equal to an impedance of the piezoelectric element $1/\omega C$, is connected to the piezo-element.[25] Piezoceramic:carbon black:polymer composites are promising designs for practical applications (see Figure 10). The minimum damping time constant (i.e., quickest damping) is obtained at 6 vol % of carbon black, where a drastic electric conductivity change is observed (percolation threshold).[26] The vibration suppression effect is greatly enhanced by using a higher electromechanical coupling material.

Photostrictive Actuator

A photostrictive actuator is a fine example of an intelligent material incorporating illumination sensing and self production of drive/control voltage together with final actuation. In certain ferroelectrics, a constant electromotive force is generated with exposure of light, and a photostrictive strain results from the coupling of this bulk photovoltaic effect to inverse piezoelectricity.

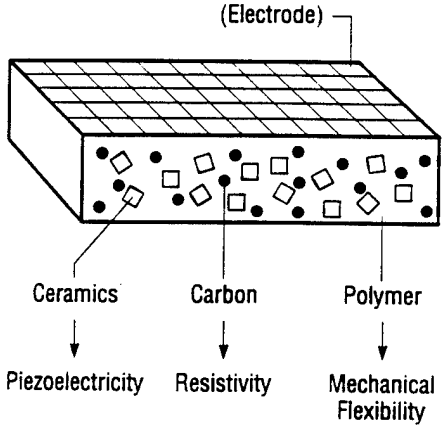

Figure 10. Passive damper using a piezoceramic/polymer composite.

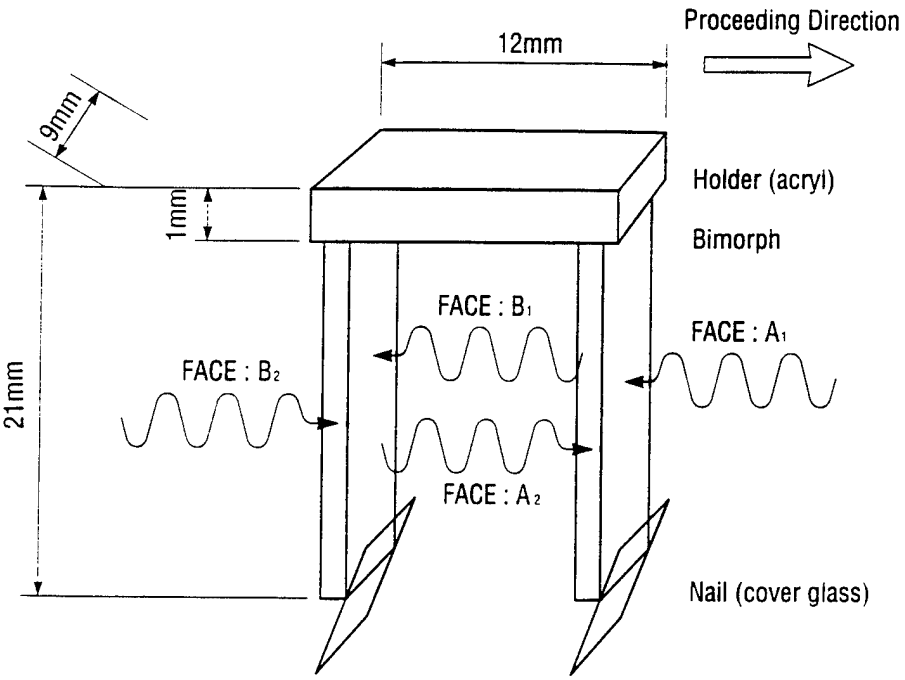

Figure 11. Structure of a photo-driven walking device and the illumination directions.

A bimorph unit has been made from PLZT (3/52/48) ceramic doped with slight additions of niobium and tungsten.[27] The remnant polarization of one PLZT layer is parallel to the plate and in the direction opposite to that of the other plate. When a violet light is irradiated to one side of the PLZT bimorph, a photovoltaic voltage of 0.7 kV/mm is generated, causing a bending motion. The displacement observed at the tip of a 20 mm bimorph 0.4 mm in thickness is 150 μm, with a response time of 1 sec.

A photo-driven micro walking device, designed to begin moving by light illumination, has been developed.[28] As shown in Figure 11, it is simple in structure, having neither lead wires nor electric circuitry, with two bimorph legs fixed to a plastic board. When the legs are irradiated alternately with light, the device moves like an inchworm with a speed of 100 μm/min.

Summary

In summary, piezoelectric/electrostrictive actuators and ultrasonic motors are expected to increase in market share to more than $10 billion in 1998, and a bright future is anticipated in many application fields.

References

1. K. Uchino, *Piezoelectric/Electrostrictive Actuators* (Morikita Publishing, Tokyo, 1986).
2. K. Uchino, *Problem Solving-Piezoelectric Actuators* (Morikita Publishing, Tokyo, 1991).
3. K. Uchino, *Bull. Am. Ceram. Soc.* **65** (4) (1986) p. 647.
4. K. Uchino, *FC Report for Overseas Readers* (1988) p. 23.
5. K. Uchino, *Proc. Intl. Symp. Appl. Ferroelectrics '90* (1991) p. 153.
6. K. Uchino and S. Nomura, *Jpn. J. Appl. Phys.* **52** (7) (1983) p. 575.
7. K. Furuta and K. Uchino, *Adv. Ceram. Mater.* **1** (1986) p. 61.
8. J. von Cieminski and H. Beige, *J. Phys. D* **24** (1991) p. 1182.
9. L.E. Cross, S.J. Jang, R.E. Newnham, S. Nomura, and K. Uchino, *Ferroelectrics* **23** (3) (1980) p. 187.
10. K. Uchino and S. Nomura, *Ferroelectrics* **50** (1) (1983) p. 191.
11. K. Uchino, *Proc. Intl. Meg. Adv. Mater.* **9** (1989) p. 489.
12. A. Furuta, K.Y. Oh, and K. Uchino, *Sensors and Mater.* **3** (4) (1992) p. 205.
13. K. Uchino and T. Takasu, *Inspec.* **10** (1986) p. 29.
14. Y. Sugawara, K. Onitsuka, S. Yoshikawa, Q.C. Xu, R.E. Newnham, and K. Uchino, *J. Am. Ceram. Soc.* **75** (4) (1992) p. 996.
15. H. Goto, K. Imanaka, and K. Uchino, *Ultrasonic Technol.* (5) (1992) p. 48.
16. T. Ota, T. Uchikawa, and T. Mizutani, *Jpn. J. Appl. Phys.* **24** (Suppl. 24-3) (1985) p. 193.
17. K. Uchino, Y. Tsuchiya, S. Nomura, T. Sato, H. Ishikawa, and O. Ikeda, *Appl. Optics* **20** (17) (1981) p. 3077.
18. T. Sato, H. Ishikawa, O. Ikeda, S. Nomura,

and K. Uchino, *Appl. Optics* **21** (1982) p. 3669.
19. T. Yano, I. Fukui, E. Sato, O. Inui, and Y. Miyazaki, *Electr. & Commun. Soc. Proc.* (Spring 1984) p. 1–156.
20. K. Uchino, *J. Rob. Mech.* **1** (1989) p. 124.
21. *Ultrasonic Motors/Actuators*, edited by Y. Akiyama (Triceps, Tokyo, 1986).
22. *Annual Report of Solid State Actuator Soc.*, edited by K. Uchino (Jpn. Tech. Transfer Assoc., Tokyo, 1991); *Smart Materials and Structures*, edited by R.O. Claus et al. (IOP, Philadelphia, 1992).
23. S. Sugiyama and K. Uchino, *Proc. Intl. Symp. Appl. Ferroelectrics '86* (IEEE, 1986) p. 637.
24. T. Hirose and K. Uchino, *Ferroelectrics* **87** (1988) p. 295.
25. K. Uchino and T. Ishii, *J. Jpn. Ceram. Soc.* **96** (8) (1988) p. 863.
26. Y. Suzuki, K. Uchino, H. Gouda, M. Sumita, R.E. Newnham, and A.R. Ramachandran, *J. Jpn. Ceram. Soc.* **99** (11) (1991) p. 1135.
27. M. Tanimura and K. Uchino, *Sensors and Mater.* **1** (1988) p. 47.
28. K. Uchino, *O plus E* (New Technology, Tokyo, May, 1989) p. 58. □

12. Uchino, K., "New Piezoelectric Devices for Smart Actuator/Sonsor Systems," Proc. 4th Int'l Conf. Electronic Ceramics & Appl., p.179-191 (1994).

NEW PIEZOELECTRIC DEVICES FOR SMART ACTUATOR/SENSOR SYSTEMS

Kenji Uchino
International Center for Actuators and Transducers
Materials Research Laboratory, The Pennsylvania State University
University Park, PA 16802, USA

Abstract. In these several years, piezoelectric and electrostrictive materials have bocome key components in smart actuator/sensor systems such as precision positioners, miniature ultrasonic motors and adaptive mechanical dampers. This paper reviews recent applications of piezoelectric and related ceramics to actuators and sensors, including the improvement of actuator materials, design of the devices, drive/control techniques and integration of actuators and sensors.

1 Introduction

Evolutionary steps of the materials include trivial, smart, intelligent and finally wise materials. The conductor and elastic, which generate current and strain output, respectively, for the input, voltage or stress (well-known phenomena!), are called trivial materials. On the contrary, the pyroelectric and piezoelectric, which generate the electric field for the input of heat or stress (unexpected phenomena!), are called smart materials. These off-diagonal couplings have a corresponding converse effect such as electrocaloric and inverse-piezoelectric effects, and both "sensing" and "actuating" functions can be realized in the same materials. An example is found in the electronic shock absorber of automobile suspension (Fig.1) by Toyota Motors[1]. The sensor to detect the road roughness and the actuator to change the valve position to change the shock absorbing rate are both multilayered piezoelectric devices. Intelligent materials must possess a "drive/control" function which is adaptive to the environmental condition change, in addition to the actuator and sensor functions. Photostrictor is a good example. Finally, if the material would obtain morality such as "this motion may cause a trouble to the human," and would stop the actuation by itself, it would be called a wise material.

Among the smart solid-state actuators, capable of moving something mechanically, controlled by temperature (shape memory alloy), magnetic field (magnetostrictive alloy) and electric field (piezoelectric/electrostrictive ceramic), the former two are generally inferior to the piezoelectric actuators because of technological trends aimed at reduced driving power and miniaturization.

This article reviews recent applications of piezoelectric and related ceramics to smart actuator/sensor systems, including the improvement of actuator materials, design of the devices, drive/control techniques and integration of actuators and sensors.

Piezoelectric actuators are forming a new field between electronic and structural ceramics [2-4]. Application fields are classified into three categories: positioners, motors and

vibration suppressors. The manufacturing precision of optical instruments such as lasers and cameras, and the positioning accuracy for fabricating semiconductor chips, which must be adjusted using solid-state actuators, is of the order of 0.1 μm. Regarding conventional electromagnetic motors, tiny motors smaller than 1 cm^3 are often required in office or factory automation equipment and are rather difficult to produce with sufficient energy efficiency. Ultrasonic motors whose efficiency is insensitive to size are superior in the mini-motor area. Vibration suppression in space structures and military vehicles using piezoelectric actuators is also a promising technology.

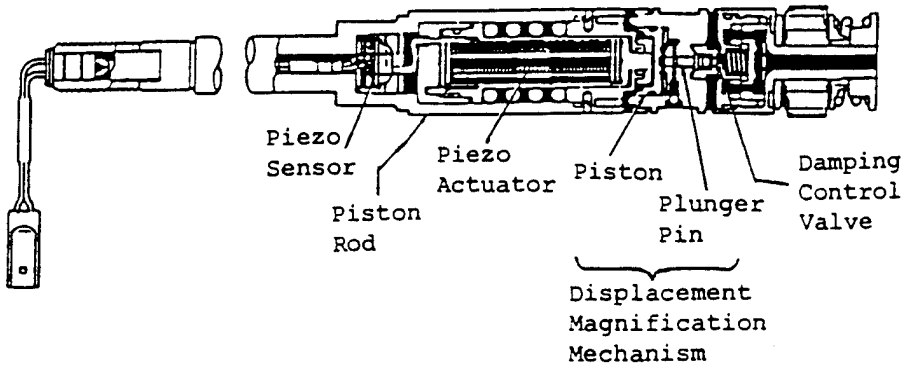

Fig.1 Smart electronic shock absorber of automobile suspension with a piezoelectric sensor/actuator system.

2 Ceramic Actuator Materials

2.1 PRACTICAL ACTUATOR MATERIALS

Actuator materials are classified into three categories; piezoelectric, electrostrictive and phase-change materials. Modified lead zirconate titanate [PZT, $Pb(Zr,Ti)O_3$] ceramics are currently the leading materials for piezoelectric applications. The PLZT [$(Pb,La)(Zr,Ti)O_3$] 7/62/38 compound is one such composition [5]. The strain curve is shown in Fig.2(a) left. When the applied field is small, the induced strain is nearly proportional to the field ($x = dE$). As the field becomes larger (i.e., greater than about 100 V/mm), however, the strain curve deviates from this linear trend and significant hysteresis is exhibited due to polarization reorientation. This sometimes limits the usage of this material in actuator applications that require nonhysteretic response.

An interesting new family of actuators has been fabricated from a barium stannate titanate solid solution [$Ba(Sn,Ti)O_3$] [6]. The useful property of $Ba(Sn_{0.15}Ti_{0.85})O_3$ is its unusual strain curve, in which the domain reorientation occurs only at low fields, and there is then a long linear range at higher fields (Fig.2(a) right); i.e., the coercive field is unusually small.

On the other hand, electrostriction in PMN [$Pb(Mg_{1/3}Nb_{2/3})O_3$] based ceramics, though a second-order phenomenon of electromechanical coupling ($x = ME^2$), is extraordinarily large (more than 0.1 %) [7]. An attractive feature of these materials is the near absence of hysteresis (Fig.2(b)). The superiority of PMN to PZT was demonstrated in a Scanning Tunneling Microscope (STM) [8]. The PMN actuator could provide extremely small distortion of the image even when the probe was scanned in the opposite direction.

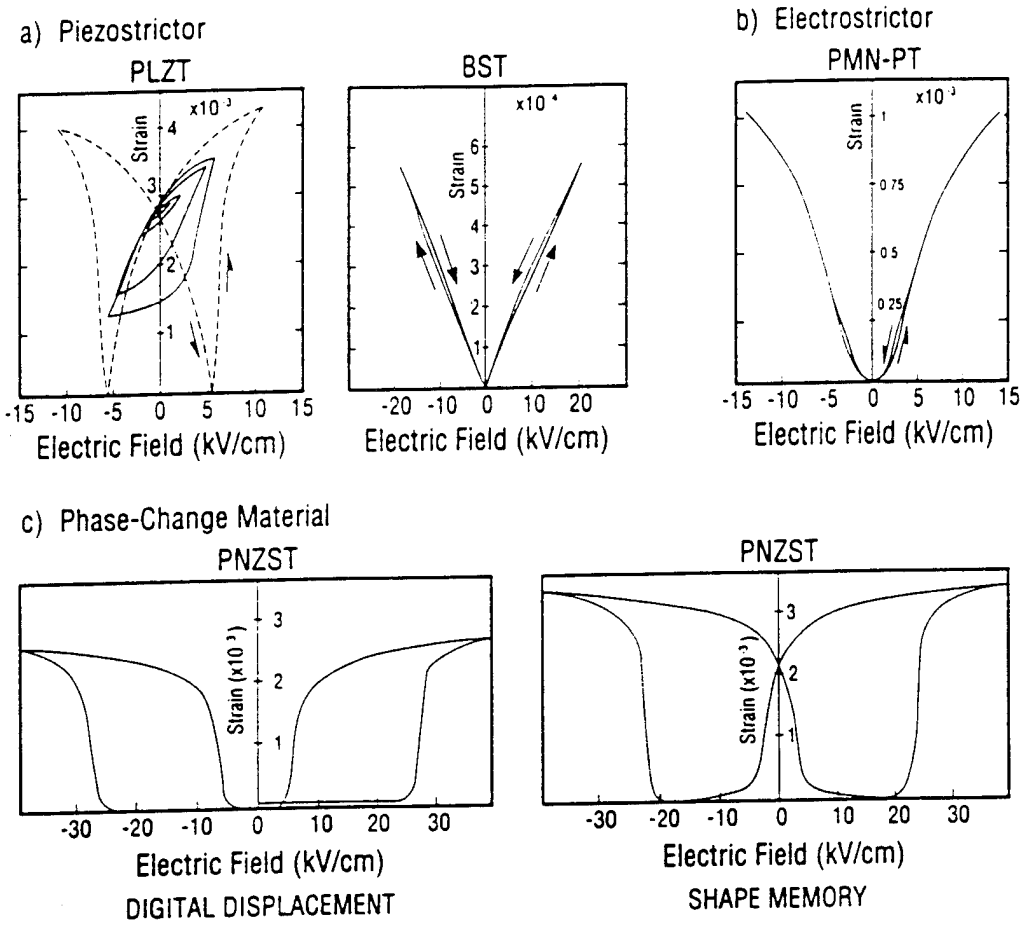

Fig.2 Electric field-induced strains in ceramics; (a) Piezoelectric (Pb,La)(Zr,Ti)O_3 and Ba(Sn,Ti)O_3.(b) Electrostrictive Pb($Mg_{1/3}Nb_{2/3}$,Ti)O_3.(c) Phase-change material Pb(Zr,Sn,Ti)O_3.

Concerning the phase-change-related strains, polarization induction by switching from an antiferro-electric to a ferroelectric state, has been proposed [9]. Figure 2(c) shows the field-induced strain curves taken for the lead zirconate stannate based system[$Pb_{0.99}Nb_{0.02}((Zr_xSn_{1-x})_{1-y}Ti_y)_{0.98}O_3$]. The longitudinally induced strain reaches up to 0.4%, which is much larger than that expected in normal piezostrictors or electrostrictors. A rectangular-shape hysteresis in Fig.2(c) left, referred to as a "digital displacement transducer" because of the two on/off strain states, is interesting. Moreover, this field-induced transition exhibits a shape memory effect in appropriate compositions (Fig.2(c) right). Once the ferroelectric phase has been induced, the material will "memorize" its ferroelectric state even under zero-field conditions, although it can be erased with the application of a small reverse bias field [10]. This shape memory ceramic is used in energy saving actuators. A latching relay in Fig.3 is composed of a shape memory ceramic unimorph and a mechanical snap action switch, which is driven by a pulse voltage of 4ms. Compared with the conventional electromagnetic relays, the new relay is much simple and compact in structure with almost the same response time.

2.2 NOVEL ACTUATOR MATERIALS

A monomorph device has been developed to replace the conventional bimorphs, with simpler structure and manufacturing process. The principle is a superposed effect of piezoelectricity and semiconductivity (Fig.4) [11]. The contact between a semiconductor and a metal (Schottky barrier) causes non-uniform distribution of the electric field, even in a compositionally uniform ceramic. Suppose that the ceramic possesses also piezoelectricity, only one side of a ceramic plate tends to contract, leading to a bending deformation in total. A monomorph plate with 30mm in length and 0.5 mm in thickness can generate 200μm tip displacement, in equal magnitude of that of the conventional bimorphs [12]. The "rainbow" actuator by Aura Ceramics [13] is a modification of the above-mentioned semiconductive piezoelectric monomorphs, where half of the piezoelectric plate is reduced so as to make a thick semiconductive electrode to cause a bend.

A photostrictive actuator is a fine example of an intelligent material, incorporating "illumination sensing" and self production of "drive/control voltage" together with final "actuation." In certain ferroelectrics, a constant electromotive force is generated with exposure of light, and a photostrictive strain results from the coupling of this bulk photovoltaic effect to inverse piezoelectricity. A bimorph unit has been made from PLZT 3/52/48 ceramic doped with slight addition of tungsten [14]. The remnant polarization of one PLZT layer is parallel to the plate and in the direction opposite to that of the other plate. When a violet light is irradiated to one side of the PLZT bimorph, a photovoltage of 1 kV/mm is generated,causing a bending motion. The tip displacement of a 20mm bimorph 0.4mm in thickness was 150μm, with a response time of 1 sec.

A photo-driven micro walking device, designed to begin moving by light illumination, has been developed [15]. As shown in Fig.5, it is simple in structure, having neither lead wires nor electric circuitry, with two bimorph legs fixed to a plastic board. When the legs are irradiated alternately with light, the device moves like an inchworm with a speed of 100μm/min.

3 Actuator Designs

Two of the most popular actuator designs are multilayers and bimorphs (see Fig.6). The multilayer, in which roughly 100 thin piezoelectric/electrostrictive ceramic sheets are stacked together, has advantages in low driving voltage (100V), quick response (10μsec), high generative force (100kgf) and high electromechanical coupling. But the displacement in the range of 10μm is not sufficient for some applications. This contrasts with the bimorph, consisting of multiple piezoelectric and elastic plates bonded together to generate a large bending displacement of several hundred μm, but the response (1msec) and the generative force (100gf) are low.

A composite actuator structure called the "moonie" has been developed to provide characteristics intermediate between the multilayer and bimorph actuators; this transducer exhibits an order of magnitude larger displacement than the multilayer, and much larger generative force with quicker response than the bimorph [16]. The device consists of a thin multilayer piezoelectric element and two metal plates with narrow moon-shaped cavities bonded together as shown in Fig.6. The moonie with a size of 5 x 5 x 2.5 mm can generate a 20μm displacement under 60V, eitht times as large as the generative

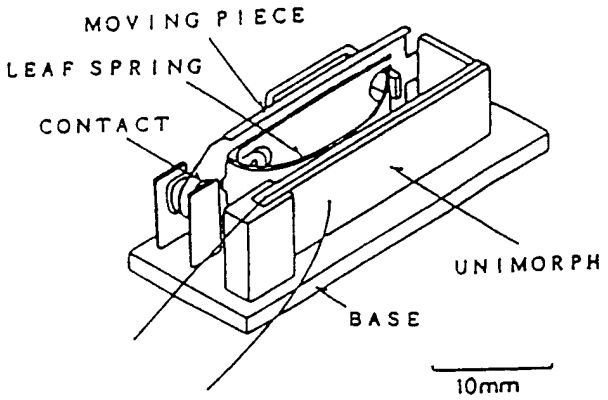

Fig.3 Latching relay using a shape memory ceramic unimorph.

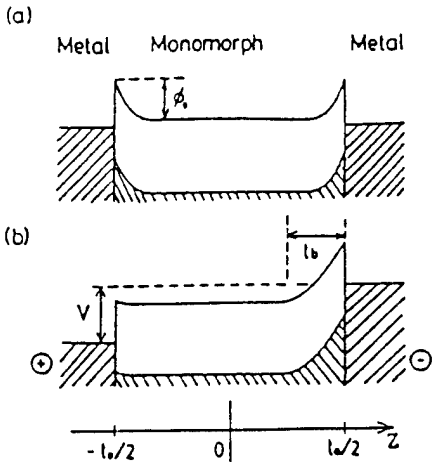

Fig.4 Electron energy band (Schottky barrier) model in monomorph devices (n-type semiconductor).

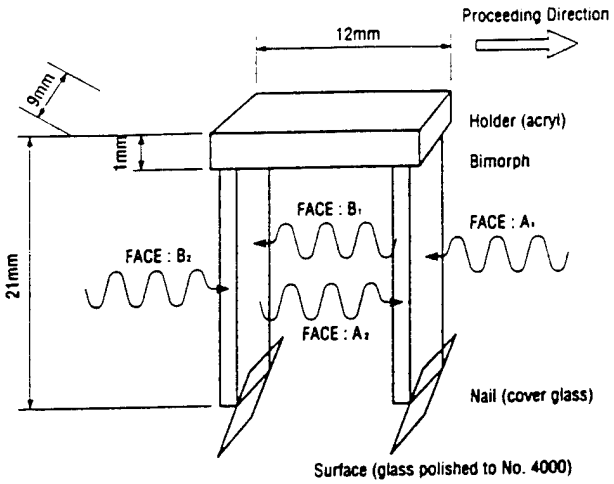

Fig.5 Structure of a photo-driven walking device and the illumination directions.

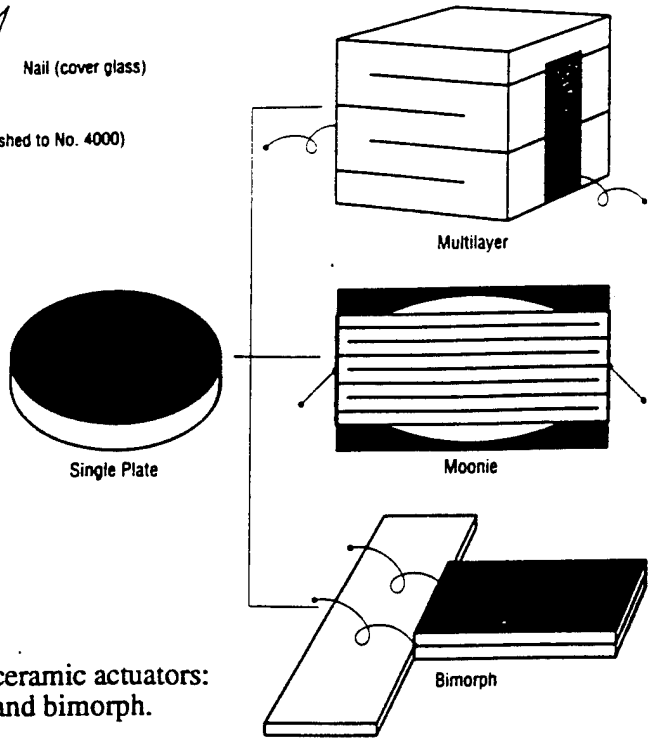

Fig.6 Typical designs for ceramic actuators: multilayer, moonie and bimorph.

displacement of the multilayer with the same size [17]. This new compact actuator has been applied to make a miniaturized laser bean scanner.

4 Drive/Control Techniques

Piezoelectric/electrostrictive actuators may be classified into two categories, based on the type of driving voltage applied to the device and the nature of the strain induced by the voltage (Fig.7): (1) rigid displacement devices for which the strain is induced unidirectionally along an applied dc field, and (2) resonating displacement devices for which the alternating strain is excited by an ac field at the mechanical resonance frequency (ultrasonic motors). The first can be further divided into two types: servo displacement transducers (positioners) controlled by a feedback system through a position-detection signal, and pulse-drive motors operated in a simple on/off switching mode, exemplified by dot-matrix printers.

The materials requirements for these classes of devices are somewhat different, and certain compounds will be better suited to particular applications. The ultrasonic motor, for instance, requires a very hard type piezoelectric with a high mechanical quality factor Q, leading to the suppression of heat generation. Driving the motor at the antiresonant frequency, rather than at the resonant state, is also an intriguing technique to reduce the load on the piezo-ceramic and the power supply [18]. The servo-displacement transducer suffers most from strain hysteresis and, therefore, a PMN electrostrictor is used for this purpose. The pulse-drive motor requires a low permittivity material aiming at quick response with a certain power supply rather than a small hysteresis so that soft PZT piezoelectrics are preferred to the high-permittivity PMN for this application.

Pulse drive techniques of the ceramic actuator is very important for improving the response of the device [19]. Figure 8 shows transient vibrations of a bimorph excited after a pseudo-step voltage is applied. The rise time is varied around the resonance period. It is concluded that the overshoot and ringing of the tip displacement is completely suppressed when the rise time is precisely adjusted to the resonance period of the piezo-device. A flight actuator was developed using a pulse-drive piezoelectric element and a steel ball. A 2mm steel ball can be hit up to 20mm by a 5μm displacement induced in a multilayer actuator with quick response [19]. A dot-matrix printer head has been trially manufactured using a flight actuator as shown in Fig.9 [20]. By changing the drive voltage pulse width, the movement of the armature was easily controlled to realize no vibrational ringing or double hitting.

5 Device Applications

5.1 PRECISION POSITIONERS

Deformable mirrors and "hubble" telescopes have been proposed using multilayer PMN electrostrictive actuators to control the phase of the incident light wave in the field of optical information processing [21,22]. The PMN actuators also have been installed in precision cutting machines [23]. Fig.10 shows a micro-displacement transducer composed of a PMN multilayer actuator, a magneto-resistive strain sensor and an adaptive control circuitry, which was installed at the bottom of the cutting tool. The feedback control has suppressed the position deviation of the cutting edge when pushing stress was produced during cutting process. Figures 11(a) and 11(b) show the edge position change under

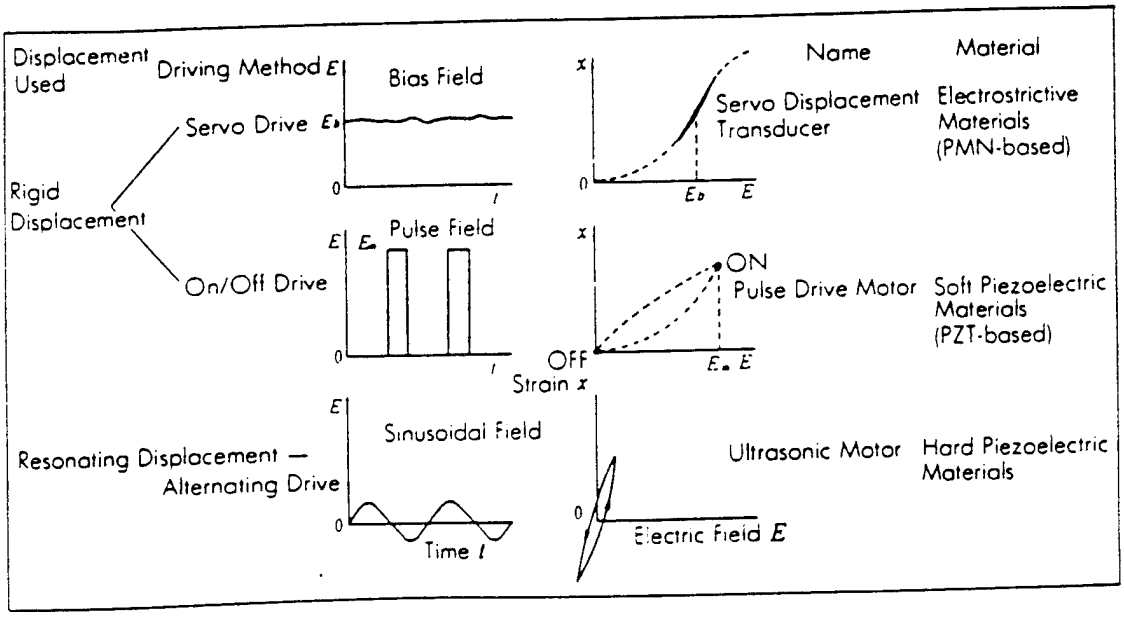

Fig.7 Classification of piezoelectric/electrostrictive actuators.

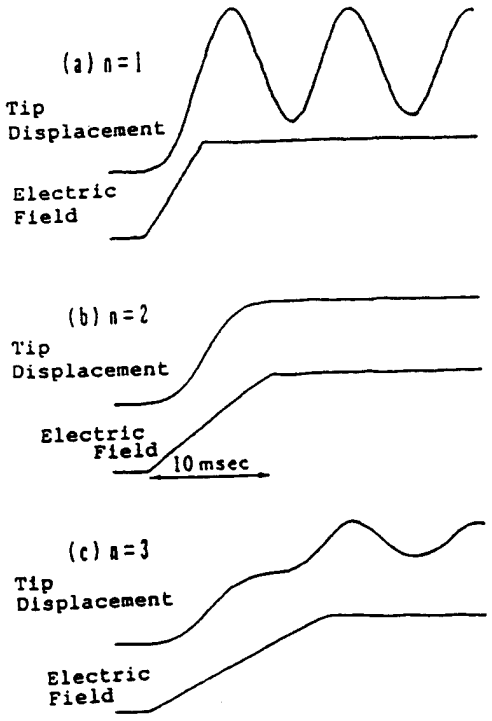

Fig.8 Transient vibration of a bimorph excited after a pseudo-step voltage applied. (2n=resonance period)

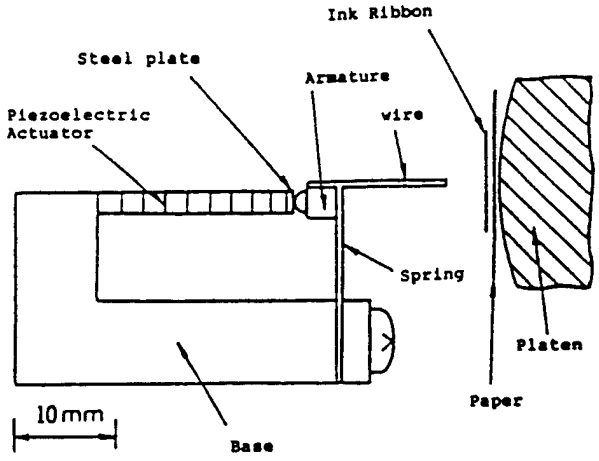

Fig.9 Dot-matrix printer head using a flight actuator mechanism.

external stresses without and with the feedback system, respectively. The cutting accuracy in less than 0.01μ was available.

5.2 VIBRATION SUPPRESSORS

Noise vibrations in automobiles and space structures can be suppressed significantly with using smart ceramic actuators [24]. The above-mentioned automobile suspension [1] is a good example (Fig.1). The roughness of the road is detected as a vibration acceleration with a 5-layered piezosensor, and the signal is fed-back to a 88-layered piezoactuator through a power amplifier, in order to change the shock-absorption control valve. This feedback system can provide the controllability and the comfortability of a car simultaneously.

Passive damper application is another smart usage of piezoelectrics, where mechanical noise vibration is radically suppressed by the converted electric energy dissipation through Joule heat when a suitable resistance, equal to an impedance of the piezoelectric element $1/\omega C$, is connected to the piezo-element [25]. Piezoceramic:carbon black:polymer composites are promising useful designs for practical application. Figure 12 shows the damping time constant change with volume percentage of the carbon black. The minimum time constant (i.e. quickest damping) is obtained at 6 % of carbon black, where a drastic electric conductivity change is observed (percolation threshold) [26].

Piezoelectric gyro-sensors are now widely used to detect the noise motion of a handy video camera.
Figure 13 shows a Tokin's cylinder type gyroscope [27]. Among the 6 electrode strips, two of them are used to excite total vibration and the other two pairs of electrode are used to detect the Corioli's force or the rotational acceleration cause by the hand motion. By using the gyro signal, the image vibration can be compensated electrically on a monitor display.

5.3 SMALL MOTORS

A dot matrix printer is an example of pulse drive motors. Each character formed by such a printer is composed of a 24 x 24 dot matrix. A printing ribbon is subsequently impacted by a multiwire array. A sketch of the printer head appears in Fig.14(a) [28]. The printing element is composed of a multilayer piezoelectric device, in which 100 thin ceramic sheets 100μm in thickness are stacked, together with a sophisticated magnification mechanism (Fig.14(b)). The magnification unit is based on a monolithic hinged lever with a magnification of 30, resulting in an amplified displacement of 0.5 mm and an energy transfer efficiency greater than 50%. The merits of the piezoelectric impact printer compared with the conventional electromagnetic types are: (1) higher printing speed by an order of magnitude, (2) lower energy consumption by an order of magnitude, and (3) reduced printing noise, which can be obtained with a sound shield because the actuators do not generate much heat.

Efforts have been made to develop high-power ultrasonic vibrators as replacements for conventional electromagnetic motors. The ultrasonic motor is characterized by "low speed and high torque," which is contrasted with "high speed and low torque" of the electromagnetic motors. Two categories are being investigated for ultrasonic motors: a standing-wave type and a propagating-wave type.

The standing-wave type is sometimes referred to as a vibratory-coupler type or a "woodpecker" type, where a vibratory piece is connected to a piezoelectric driver and the

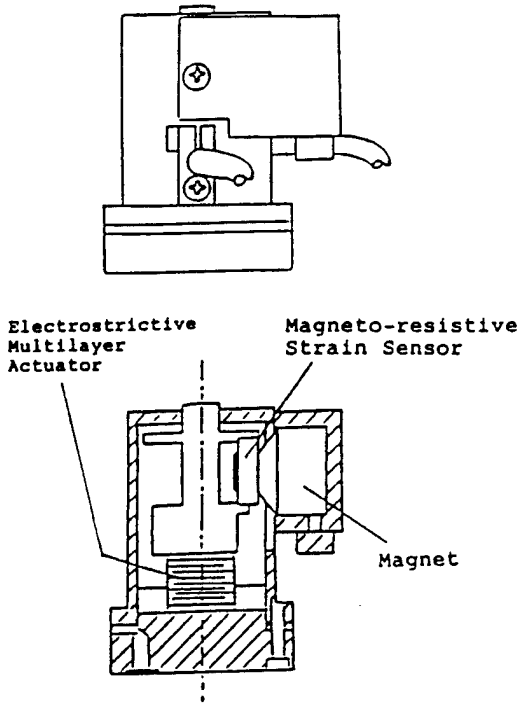

Fig.10 Micro displacement actuator with a magneto-resistive strain sensor.

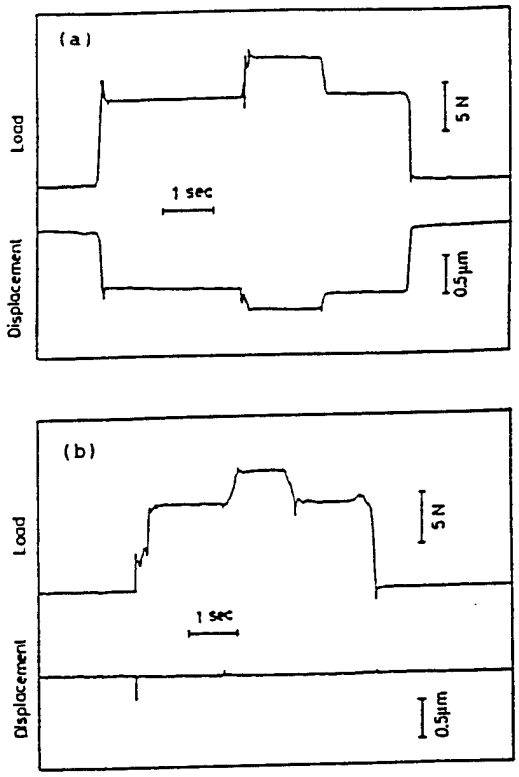

Fig.11 Edge position change under external stresses without (a) and with (b) the feedback system.

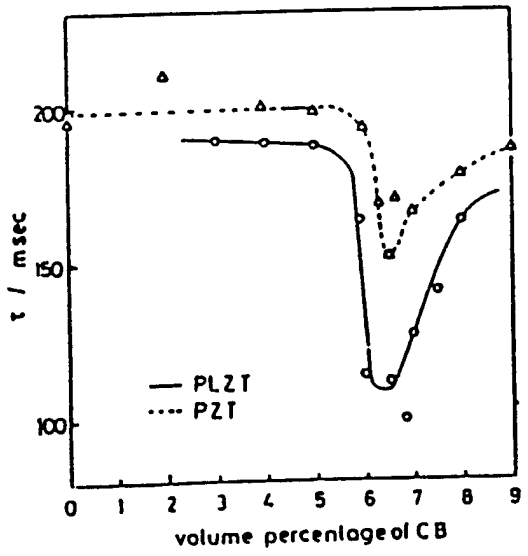

Fig.12 Damping time constant change with volume percentage of carbon black in piezoelectric composite dampers.

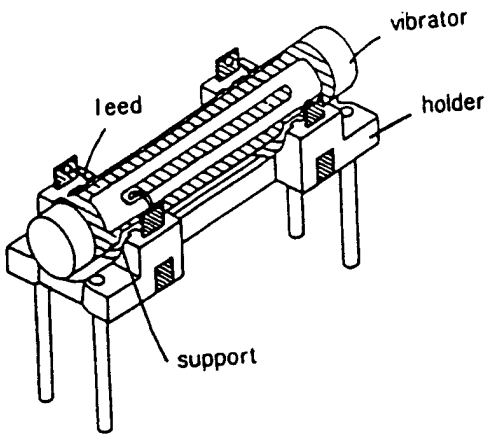

Fig.13 Piezo-ceramic cylinder vibratory gyroscope.

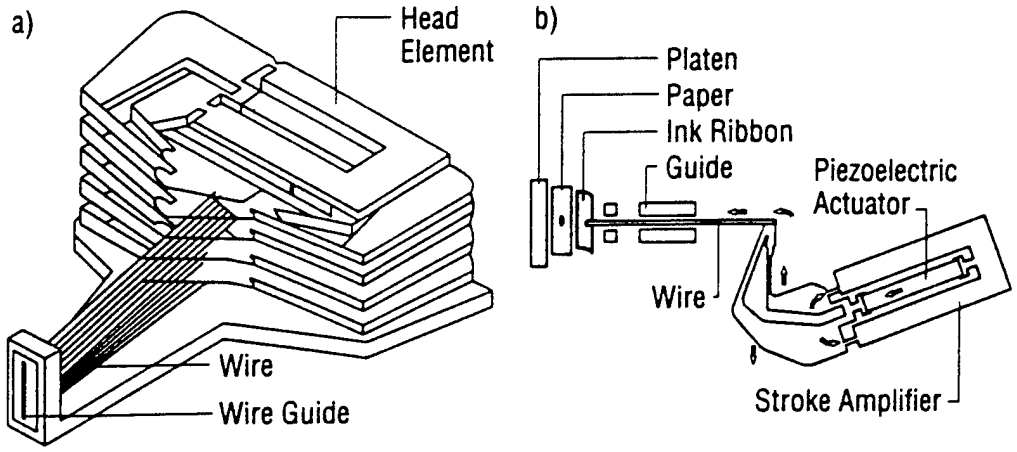

Fig.14 Structure of a printer head (a), and a differential-type piezoelectric printer-head element (b).

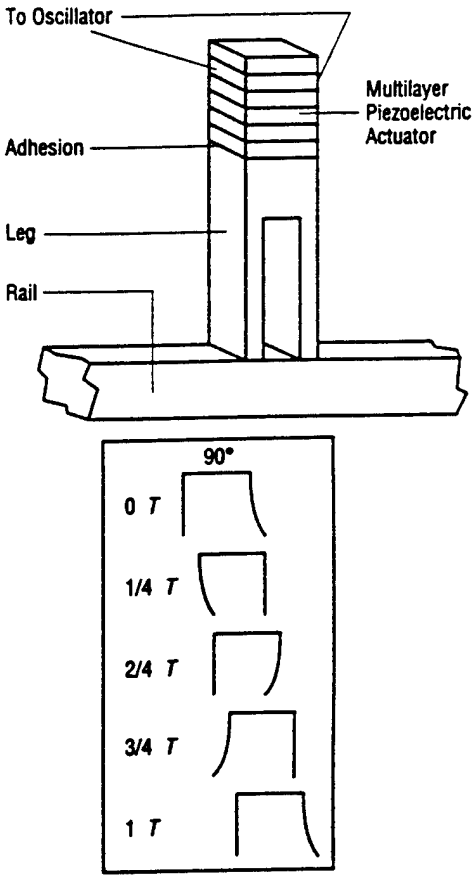

Fig.15 Ultrasonic linear motor of a vibratory coupler type.

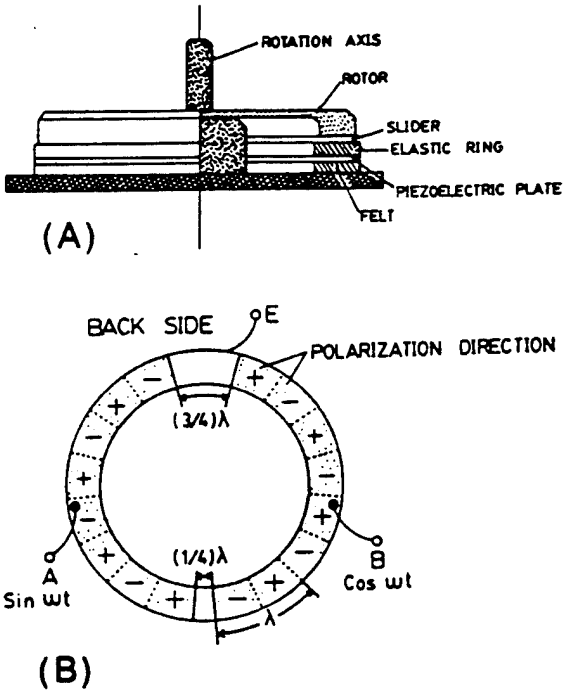

Fig.16 Design of the surface wave type motor (a), and its electrode configuration (b).

tip portion generates flat-elliptical movement. Attached to a rotor or a slider, the vibratory piece provides intermittent rotational torque or thrust. The standing-wave type has , in general, high efficiency, but lack of control in both clockwise and counterclockwise directions is a problem.

An ultrasonic linear motor equipped with a multilayer piezoelectric actuator and fork-shaped metallic legs has been developed as shown in Fig.15 [29]. Since there is a slight difference in the mechanical resonance frequency between the two legs, the phase difference between the bending vibrations of both legs can be controlled by changing the drive frequency. The walking slider moves in a way similar to a horse using its fore and hind legs when trotting. A trial motor 20 x 20 x 5 mm^3 in dimension exhibited a maximum speed of 20 cm/s and a maximum thrust of 0.2 kgf with a maximum efficiency of 20%, when driven at 98kHz of 6V (actual power = 0.7 W). This motor has been employed in a precision X-Y stage.

By comparison, the propagating-wave type (a surface-wave or "surfing" type) combines two standing waves with a 90 degree phase difference both in time and in space, and is controllable in both rotational directions (Fig.16) [30]. By means of the traveling elastic wave induced by the thin piezoelectric ring, a ring-type slider in contact with the "rippled" surface of the elastic body bonded onto the piezoelectric is driven in both directions by exchanging the sine and cosine voltage inputs. Another advantage is its thin design, which makes it suitable for installation in cameras as an automatic focusing device. 80 % of the exchange lenses in Canon's "EOS" camera series have already been replaced by the ultrasonic motor mechanism.

6 Future of Ceramic Actuators

18 years have passed since the intensive development of piezoelectric actuators began and, presently, the focus has been shifted to practical device applications. Piezoelectric shutters (Minolta Camera) and automatic focusing mechanisms in cemeras (Canon), dot-matrix printers (NEC) and part-feeders (Sanki) are now commercialized and mass-produced by tens of thousands of pieces per month. During the commercialization, new designs and drive-control techniques of the ceramic actuators have been mainly developed in the past few years. A number of patent disclosures have been found particularly in NEC, TOTO Corporation, Matsushita Electric, Brother Industry, Toyota Motors, Tokin, Hitachi Metal, Toshiba etc.

Several years ago Mr. T. Sekimoto, President of NEC, expressed his desire to the piezoelectric actuators in his New Year's speech that the market-share of piezoelectric actuators and their employed devices would reach up to $10 billion ($10^{10}$) in the future. If we estimate the annual sales in 2000, ceramic actuator units, camera-related devices and ultrasonic motors will be expected to reach $500 million, $300 million and $150 million, respectively. Regarding the final actuator-related products, $10 billion will not be very different from the realistic amount.

It is evident that the application field of ceramic actuators is remarkably wide. There still remain, however, problems in durability and reliability that need to be overcome before these devices can become general-purpose commercialized products. The final goal is, of course, to develop much tougher actuator ceramics mechanically and electrically. However, the reliability can be improved significantly if the destruction symptom of the actuator is monitored.

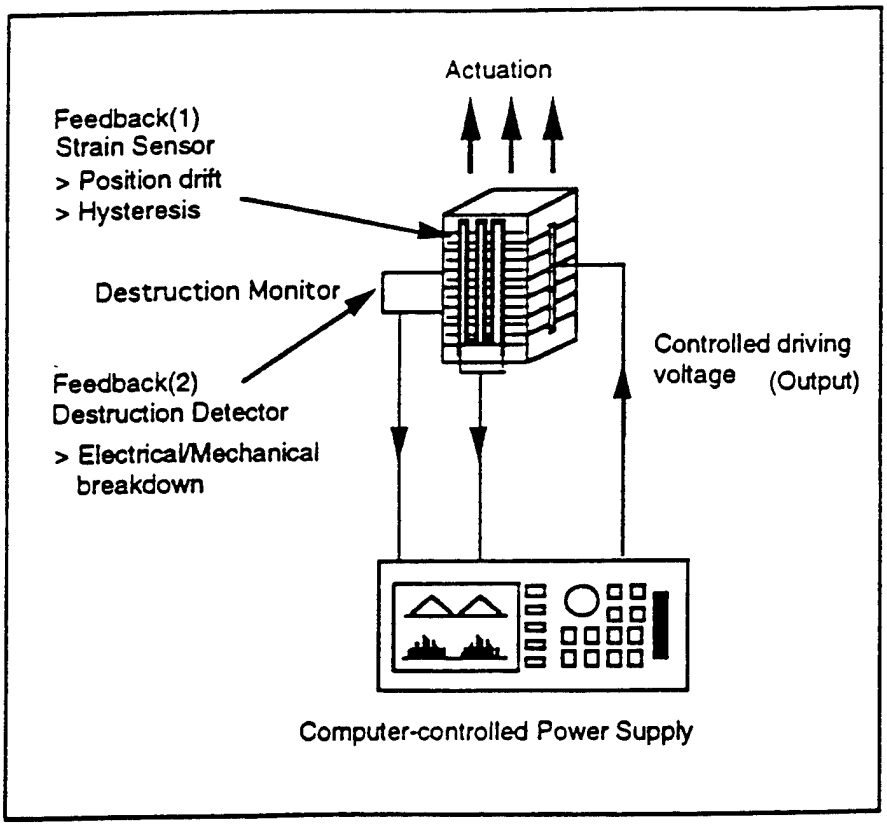

Fig.17 Intelligent actuator system with a breakdown-detection mechanism.

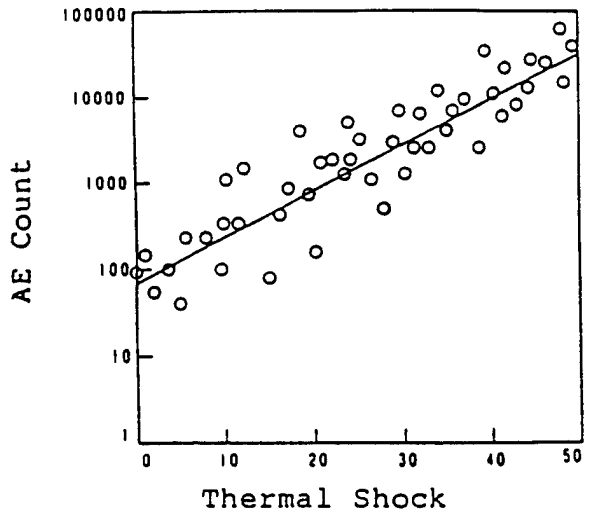

Fig.18 Acoustic emission measured during a normal drive of a multilayer piezoactuator. Each measurement was done after successive thermal-shock treatment.

Safety, which is the number one priority of a famous airline company, will be also important in actuator systems. We have proposed an intelligent actuator system composed of two feedback mechanisms: position feedback which can compensate the position drift and the hysteresis, and breakdown detection feedback which can stop the actuator system safely without causing any serious damages onto the work, e.g. in a lathe machine (Fig.17) [31]. Acoustic emission measurement of a piezo-actuator under a cyclic electric field is a good predictor for the life time [32]. Acoustic emission (AE) was detected largely when a crack propagate in the ceramic actuator at the maximum speed. During a normal drive of a 100-layer piezoelectric actuator, the number of AE was counted and a drastic increase by three orders of magnitude was detected just before the complete destruction (Fig.18). Note that part of the piezo-device can be utilized as an AE sensor.

Future research and development should focus on superior systems ecologically (i.e. fit for human!) as well as technologically. Safety systems, which can monitor the fatigue or the destruction symptom of materials/devices, and stop the equipment safely without causing serious problems, will be desired; which seem to be already "wise" materials/systems.

7 References

[1] Y.Yokoya, Electronic Ceramics, **22**, No.111, 55 (1991)
[2] K.Uchino, Piezoelectric/Electrostrictive Actuators, Morikita Publishing, Tokyo 1986
[3] K.Uchino, Bull.Am.Ceram.Soc., **65**(4), 647 (1986)
[4] K.Uchino, MRS Bull., **18**(4), 42 (1993)
[5] K.Furuta and K.Uchino, Adv.Ceram.Mater., **1**, 61 (1986)
[6] J.von Cieminski and H.Beige, J.Phys.D, **24**, 1182 (1991)
[7] L.E.Cross, S.J.Jang, R.E.Newnham, S.Nomura and K.Uchino, Ferroelectrics, **23**(3), 187(1980)
[8] K.Uchino, Ceramic Data Book'88 (Chap.:Ceramic Actuators), Inst. Industrial Manufacturing Tech., Tokyo 1988
[9] K.Uchino and S.Nomura, Ferroelectrics, **50**(1), 191 (1983)
[10] A.Furuta, K.Y.Oh and K.Uchino, Sensors and Mater., **3**(4), 205 (1992)
[11] K.Uchino, M.Yoshizaki, K.Kasai, H.Yamamura, N.Sakai and H.Asakura, Jpn.J.Appl.Phys., **26**(7), 1046 (1987)
[12] K.Uchino, M.Yoshizaki and A.Nagao, Ferroelectrics, **95**, 161 (1989)
[13] Aura Ceramics, Inc., Catalogue "Rainbow"
[14] M.Tanimura and K.Uchino, Sensors and Mater., **1**, 47 (1988)
[15] K.Uchino, J.Rob.Mech., **1**(2), 124 (1989)
[16] Y.Sugawara, K.Onitsuka, S.Yoshikawa, Q.C.Xu, R.E.Newnham and K.Uchino, J.Am.Ceram.Soc., **75**(4), 996 (1992)
[17] H.Goto, K.Imanaka and K.Uchino, Ultrasonic Techno, **5**, 48 (1992)
[18] N.Kanbe, M.Aoyagi, S.Hirose and Y.Tomikawa, J.Acoust.Soc.Jpn.(E), **14**(4), 235 (1993)
[19] S.Sugiyama and K.Uchino, Proc.Int'l.Symp.Appl.Ferroelectrics'86, IEEE, p.637 (1986)
[20] T.Ota, T.Uchikawa and T.Mizutani, Jpn.J.Appl.Phys., **24**, Suppl.24-3, 193 (1985)
[21] J.W.Hardy, Proc.IEEE, **66**, 651 (1978)
[22] T.Sato,H.Ishikawa,O.Ikeda, K.Uchino and S.Nomura, J.Opt.Soc.Amer., **71**(12), 1645 (1981)
[23] K.Uchino, Ultrasonic Techno **5**(8), 19 (1993)
[24] R.O.Claus et al.(Editor), Smart Materials and Structures, IOP, Philadelphia 1992
[25] K.Uchino and T.Ishii, J.Jpn.Ceram.Soc., **96**(8), 863 (1988)
[26] Y.Suzuki, K.Uchino,H.Gouda,M.Sumita,R.E.Newnham and A.R.Ramachandran, J.Jpn.Ceram.Soc., **99**(11), 1135 (1991)
[27] Tokin Corporation, Catalogue "Ceramic Gyro"
[28] T.Yano, I.Fukui, E.Sato, O.Inui and Y.Miyazaki, Proc. Electr. & Commun.Soc., p.1-156 (Spring,1984)
[29] M.Tohda, S.Ichikawa, K.Uchino and K.Kato, Ferroelectrics, **93**, 287 (1989)
[30] Y.Akiyama (Editor), Ultrasonic Motors/Actuators, Triceps, Tokyo 1986

13. Uchino, K., "Worldwide Research and Development of Ceramic Actuators," New Ceramics (TCI, Tokyo) Vol.7(11), 5-13 (1994).

●特集

内外のセラミックアクチュエータの研究開発動向

Worldwide Research and Development of Ceramic Actuators

内野　研二　Pennsylvania State University　Director, International Center for Actuators & Transducers
Professor, Electnical Engineering
Kenji Uchino

問合せ／ウチノ　ケンジ　134 Materials Research Lab. The Penn State University, University Park, PA 16802　Tel. 814(863)8035

1　序論

セラミックアクチュエータの開発が本格化して，早18年が経過し，その焦点は実用的なデバイス応用へと移行している．圧電シャッタ（ミノルタカメラ）やカメラ自動焦点機構（キャノン），ドットマトリクスプリンタ（NEC），パーツフィーダ（産機）などは商品化され，月に数万台のペースで量産されている．1986年以降は，商品化の進む中で，アクチュエータのデザインとドライブ／コントロール技術の開発に精力がそそがれている．ここ数年の公開特許件数の多い企業としては，NEC，TOTO，松下電器，ブラザー，トヨタ自動車，トーキン，日立金属，東芝等がある[1]．

圧電アクチュエータ／超音波モータの開発の主導権は，日本においては企業にあり，用途は精密位置決めと小型モータが中心である．政府のスポンサ開発領域となるには実用的過ぎるのか，大きなプロジェクトは見あたらない．シリコンのマイクロマシーニングによるマイクロモータの開発を主眼に置いた「マイクロメカニズム」プロジェクトの一部に名前を見る程度である．

一方，米国における研究の多くは，政府機関，特に軍によるスポンサでささえられており，開発焦点はアクティブ制振機構にある．ヨーロッパでは，フィリップスとジーメンスが積層型セラミック素子の供給に本格的に乗り出し，小型モータ，ポジショナを中心に試作が行われている．

本稿では，最近のアクチュエータ材料，デバイスのデザイン，ドライブ／コントロール技術，センサの集積化といった面から，セラミックアクチュエータの開発動向を解説する．

2　セラミックアクチュエータ材料

現在のアクチュエータ材料は，圧電体，電歪材料，相転移材料の3種に分類される[2]．ジルコン酸チタン酸鉛 [PZT.Pb(Zr.Ti)O_3] 系セラミックスは，圧電性応用での主流である．PLZT[(Pb.La)(Zr.Ti)O_3]7/62/38はその1つで，**図1**(a) 左に歪み曲線を示す[3]．印加電界の小さなうちは，誘起歪みは電界にほぼ比例するが ($x = dE$)，電界が大きくなると（100V/mm以上），線形からはずれ，かつ履歴を示すようになる．分極の回転に由来するこの履歴現象は，圧電体においては本質的で，精密位置決め等の応用での妨げとなっている．

すず酸チタン酸バリウム [Ba(Sn.Ti)O_3] 系の新しいアクチュエータ材料も興味深い[4]．**図1**(a) 右に$Ba(Sn_{0.15}Ti_{0.85})O_3$の歪み曲線を示す．分極回転の抗電界が非常に小さいために，履歴が小さくかつ広い線形領域の歪みが実現できる．この材料は，鉛成分フリーと

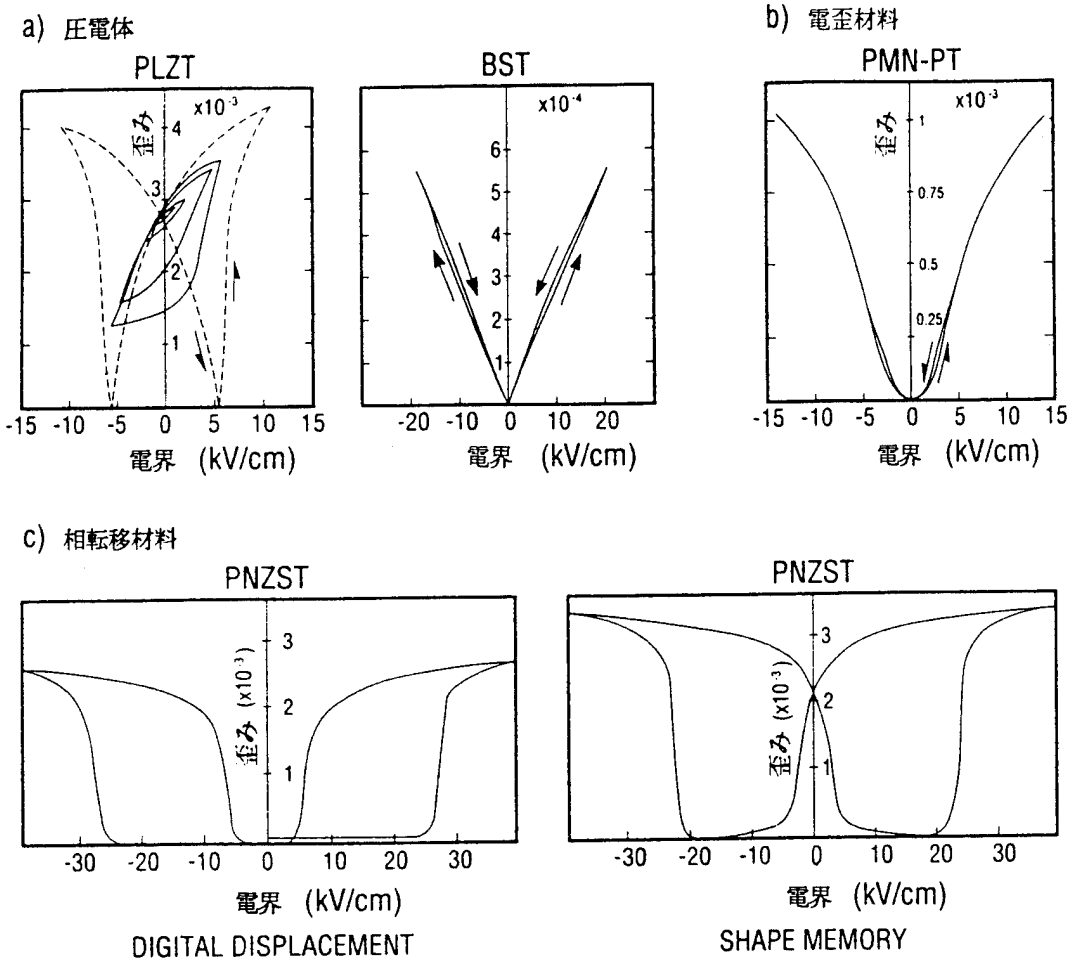

図 1 セラミックスにおける電界誘起歪み曲線．(a) 圧電体 (Pb.La)(Zr.Ti)O_3 と Ba(Sn.Ti)O_3　(b) 電歪材料 $Pb(Mg_{1/3}Nb_{2/3})O_3$　(c) 相転移材料

いったエコロジカルな面からも注目される．

一方，PMN[$Pb(Mg_{1/3}Nb_{2/3})O_3$] 系セラミックスの電歪は，2 次の電気機械相互作用 ($x = ME^2$) であるにもかかわらず非常に大きい (0.1%以上) [5]．加えて，履歴がほとんど観測されない点に魅力がある (**図 1**(b))．電歪材料の圧電体に対する優位性は，スペースシャトルに搭載されたハブル天体望遠鏡で実証された[6]．PMN 系積層素子によって光路長補正された，地球上の鮮明な映像を，読者の皆さんもテレビで御覧になったことであろう (**図 9** 参照)．

相転移材料としては，反強誘電相－強誘電相転移を利用する PNZST[$Pb_{0.99}Nb_{0.02}((Zr_xSn_{1-x})_{1-y}Ti_y)_{0.98}O_3$] が提案されている[7]．電界誘起相転移に伴う歪みの変化は，縦効果で 0.4%に達し，通常の圧電／電歪による歪み量の 4 倍に及ぶ．**図 1**(c) 左の矩形履歴は，オン／オフ 2 つの歪み状態の存在を意味し，ディジタル変位素子と呼ばれる．加えて，相転移材料には形状記憶効果を示す組成もある (**図 1**(c) 右)．電界によって強誘電相がいったん誘起されると，電界を零にしてもそのオン状態は維持 (記憶) される．オフ (反強誘電相) 状態に戻すには，小さな逆バイアス電界を印加する．

新方式キープリレーは，**図 2** に示すように，形状記憶セラミックユニモルフと機械的スナップアクションスイッチとから成っている[8]．わずか 4 ミリ秒ほどのパルス電圧 (250V) の印加によって，ユニモルフ (20mm 長) は 150 ミクロンの先端変位を生じ，スイッチをオンにする．従来の電磁式のものと比較して，構造の簡単化，小型化が応答性をそこなわずに行えた．

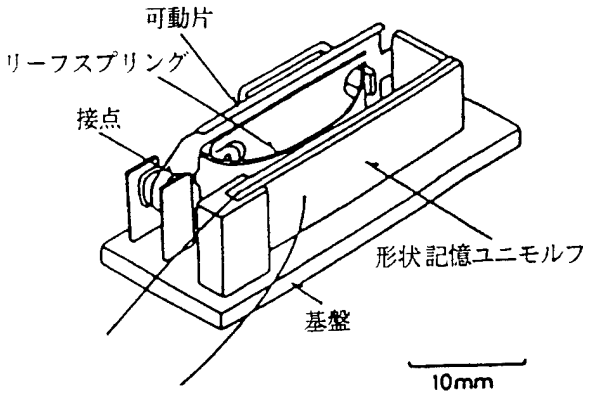

図 2 形状記憶セラミックユニモルフを用いたキープリレー

次世代のアクチュエータとして注目されているのが，光歪材料である．照射光量を「センシング」して，自分で駆動電圧を発生し，機械的に「アクチュエート」するという，まさにインテリジェント材料である．ある種の強誘電体には，紫色光の照射によって 1kV/mm に達する電界を生じる光起電力効果がある．光歪効果は，この光起電力効果と，強誘電体が合わせ持つ逆圧電効果の重畳作用としておこる．1979 年の発見以来，歪み量と応答性は年々向上し，現在は，最大歪み 0.05%，応答性 1 秒程度である．

光歪素子の基本構造として，バイモルフ型が用いられている[9]．WO_3 を添加した PLZT 3/52/48 薄板を 2 枚貼りあわせる．電界分極方向が板に平行で，電極が板両端（板面でない！）であることに注意されたい．このことが照射面積をかせぎ，静電容量を下げ，応答性を上げている．紫色光 $1mW/cm^2$ の照射が 1kV/mm の電界を発生し，20mm 長，0.4mm 厚のバイモルフ先端が 1 秒で 150μm の変位を示した．

図 3 には，光駆動型微小歩行デバイスの構造を示す[10]．2 本の光歪バイモルフ及びプラスチック板で固定されただけで，電気的リード線や電源は全くない．足の両側を交互に照射すると，インチワームのように 100μm/min のゆっくりした速度で歩行する．ごく最近，光照射によって機械的共振が励起されて，話題になっている．やはり光歪バイモルフの両側を交互に照射して，75Hz あたりで小さな音響を発した[11]．次世代光通信における電話器に代わる「光話器」の誕生である．

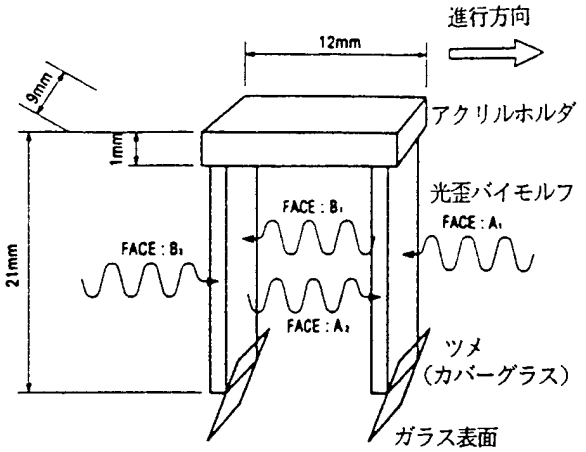

図 3 光駆動型微小歩行デバイスの構造．

3 アクチュエータのデザイン

セラミックアクチュエータのデザインとして汎用的なのが，積層型とバイモルフ型である（図 4）．積層型は，100 枚程度のセラミック薄板を重ねた構造をしており，長所として，低駆動電圧（100V），高応答性（10μs），高発生力（100kgf），高電気機械変換率がある．しかし，10μm の歪み量は多くの応用分野で不充分である．一方，バイモルフは，多層の圧電セラミック板と弾性板を貼り合わせた構造をしており，数 100μm に及ぶ屈曲変位を生じることができる．ただし，応答性（1ms）と発生力（100gf）の低さに難がある．

複合アクチュエータ「ムーニー」は，積層型とバイモルフ型の難点をちょうど補償するように考案された．ムーニーは，同サイズの積層型の 10 倍の変位量を出力し，発生力，応答性はバイモルフをはるかに上回る．図 4 に構造を示すが，薄い積層素子に三ケ月状空隙をもうけた 2 枚の金属板が貼り合わされている[12]．圧電体の横縮み歪みが，金属板のドームを持ち上げるように変形して，変位を拡大する．5×5×2.5mm のムーニーは 60V の印加で 20μm の変位を示し，同サイズの積層素子の 8 倍である点に注目されたい．

このムーニー素子は，超小型レーザビームスキャナとして利用されている[12]．最近，変種として，金属板の成型手段としてプレスを用いた「シンバル型」も提案され[13]，今後の展開が期待される．

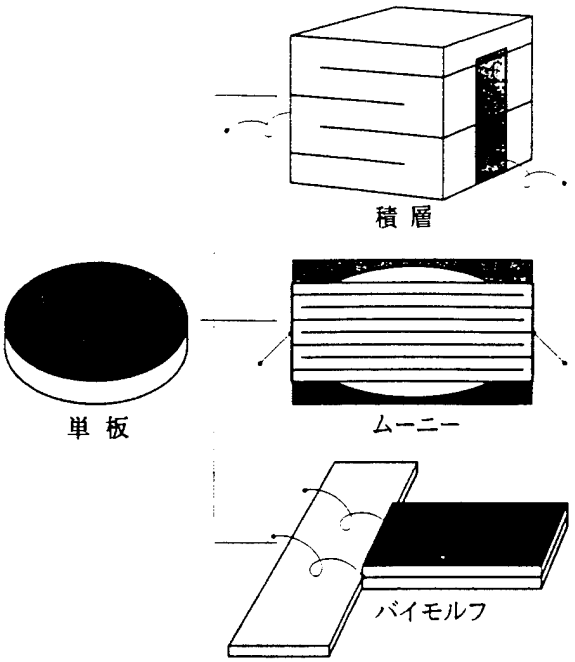

図 4 セラミックアクチュエータのデザイン：積層型，ムーニー，バイモルフ

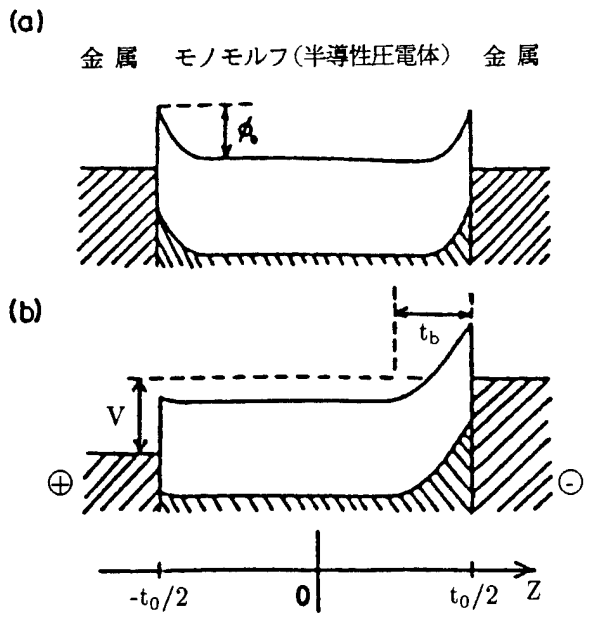

図 5 モノモルフ素子（n 型半導性圧電体）における電子エネルギーバンドモデル（ショットキ障壁）

一枚板で屈曲変位を起こす「モノモルフ」は，その構造の簡単さ，製造の手軽さから，バイモルフを置き換えるものとして注目されている．原理は，半導体の障壁効果と圧電性の重畳で起こる[14]．図 5 にエネルギーバンド構造を示すが，半導性圧電体と金属電極の接触部（ショットキ障壁）には，組成的には一様なセラミックスにおいてでも，不均一な電界分布が発生する．この特定の電極部に偏った電界分布が圧電効果と重畳して，セラミック板の屈曲変位を引き起こす．半導性 PZT セラミック板（30mm 長，0.5mm 厚）に銀電極をつけたとき，先端変位は 200μm に達し，バイモルフにひけをとらない[15]．

最近，G.Haertling らによって開発の進められている「レインボウ」アクチュエータは，上記モノモルフの変種で，圧電体板の半分を還元して半導体化したものである[16]．半導体化した部分が，厚手の電極として働き，屈曲変形を引き起こす．また，空孔率の高いモノモルフによって，雰囲気を感知するアクチュエータも試作されている[17]．

4 駆動／制御方式

圧電／電歪アクチュエータは，駆動電圧と誘起歪みのタイプによって 2 種に分類される（図 6）．(1) リジッド変位素子：dc 的電圧により一方向的な変位を生ずる．(2) 共振変位素子：ac 的電圧により共振点で増幅された交番変位を生ずる（これを超音波モータという）．前者はさらに 2 種に分かれる．サーボ変位素子（ポジショナ）：位置センサによりフィードバック制御される．パルス駆動モータ：ドット式プリンタに代表されるオン／オフ駆動を行う．

以上の分類用途に応じて，アクチュエータ材料が使い分けられる点に注意されたい．超音波モータには，機械的性能指数 Q の高いハード圧電体が，熱発生を避ける点から使用される．同じ圧電体においても，共振点よりも反共振点で駆動した方が，圧電セラミックスおよび電源への負荷が軽くなることがわかってきた[18]．サーボ変位素子では，歪みの履歴の小さい電歪材料が好まれ，パルス駆動では，高速応答性が実現できるように，誘電率の小さなソフト圧電体が使われる．

セラミックアクチュエータのパルス駆動法は，素子

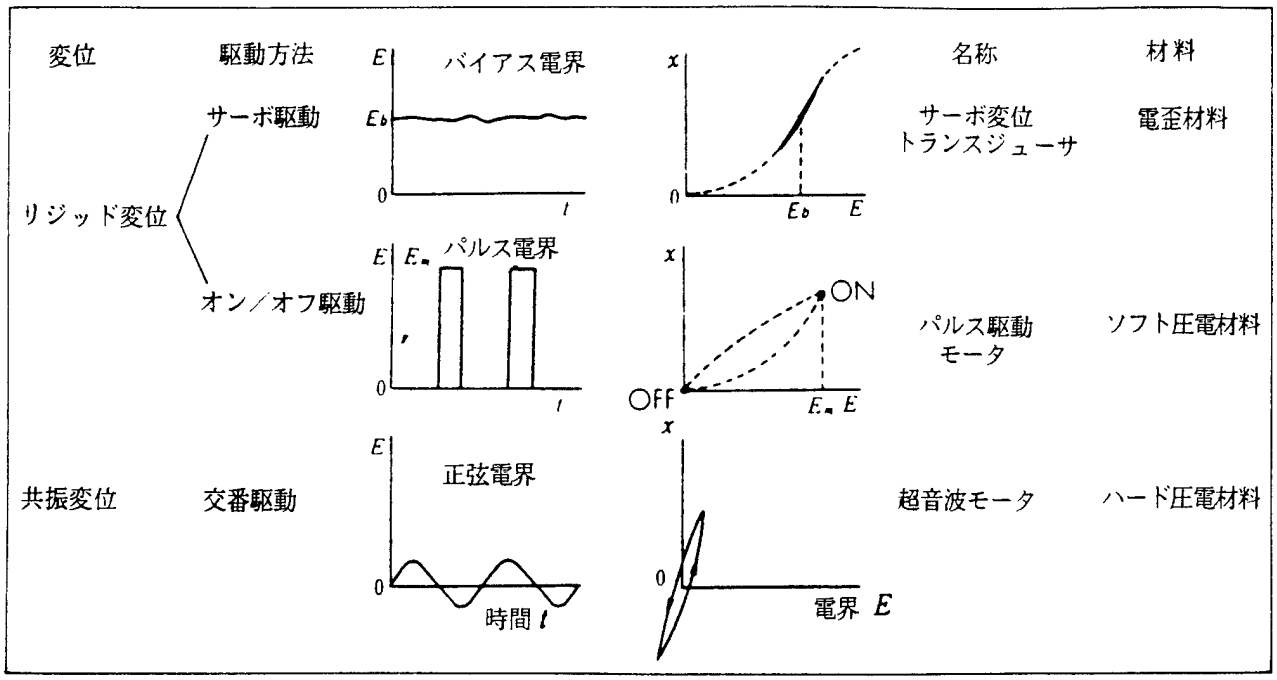

図 6 圧電／電歪アクチュエータの分類

の応答性向上に不可欠である[19]．図 7 には，擬ステップ電圧を加えた後のバイモルフアクチュエータの過渡振動を示す．電圧の立ち上がりが適当でないと，アクチュエータはオーバーシュートとリンギングを示し，位置制御はできない．立ち上がり時間を系の共振周期に合わせてやると，オーバーシュートとリンギングは完全に抑制できる．

図 8 に示したフライト方式のプリンタヘッドにおいても[20]，印加電圧パルス幅の制御によって，アーマチャのリンギングを止めたり，むしろ 2 度打ちをさせたりできる．

5 デバイスへの応用

5.1 精密位置決め機構

スペースシャトル搭載用の可変形鏡や「ハブル」天体望遠鏡には，積層型 PMN 電歪アクチュエータが採用され，入射光波面の位相制御を行なっている[21,6]．図 9 には，「ハブル」の構造を示す．PMN 系電歪アクチュエータは，精密旋盤にも組み込まれ，0.01μm の切削精度をもたらしている[22]．

5.2 制振機構

圧電アクチュエータは，自動車や宇宙構造物の雑音振動を除去するのにも有用である．図 10 には，トヨタ自動車の適応的ショックアブソーバの構造を示す[23]．道路の凹凸を 5 層の圧電センサが振動加速度として検知する．その信号が，フィードバック回路を通して 88 層の圧電アクチュエータに帰還される．アクチュエータの作動によって，ショックアブソーバの制御バルブ位置が変えられ，振動減衰率が変化する．車の操縦性と乗りごこちの両方が改善される．

圧電材料を利用したパッシブダンパも興味深い．振動を除去したい物体の上に貼りつけられた圧電体には，交番的な電界が発生する．その圧電体に適当な抵抗を結合しておくと，電気的エネルギーはジュール熱として散逸してしまうので，振動は急速に減衰することになる．実用ダンパ材としては，圧電セラミックス：カーボン：高分子複合体が検討されている[24]．

5.3 小型モータ

パルス駆動モータの典型例にドットマトリクスプリンタがある[25]．プリンタ要素は，積層圧電アクチュエー

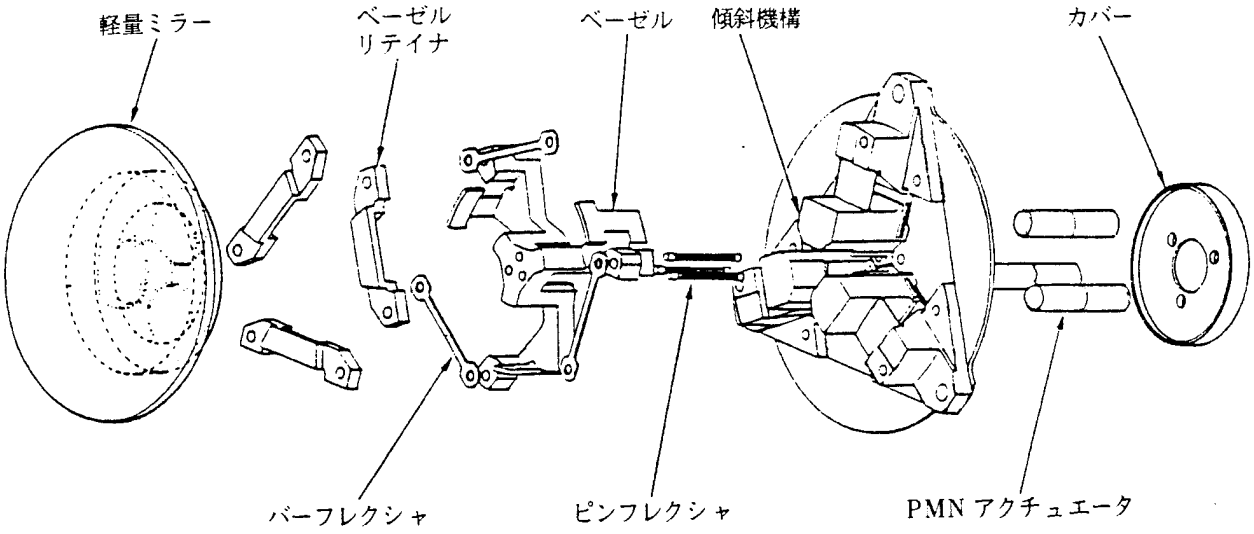

図 9 PMN 系電歪アクチュエータを利用したハブル天体望遠鏡

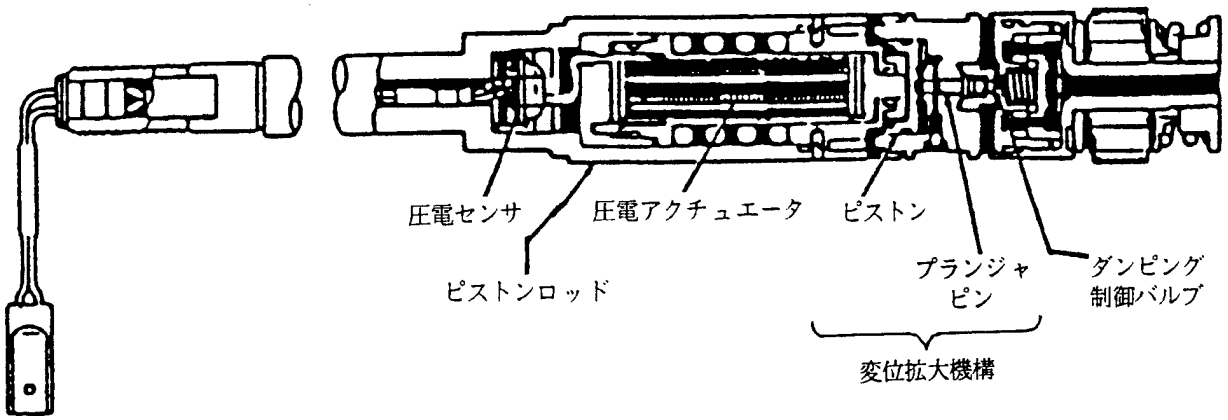

図 10 圧電センサとアクチュエータを搭載した自動車用適応的ショックアブソーバ

タを切り欠き変位拡大機構に組み込んだ構成をしている．同様の切り欠き機構を用いて，フィリップスはインチワームを試作している（**図 11**）[26]．$33\times30\times6mm^3$のサイズの素子が，速度 0.01μm/s から 16mm/s，引張り力 1N 程度を実現している．

強力超音波振動を利用して，電磁モータに代わるアクチュエータを開発する試みは，1970 年代後半からスタートしている．超音波モータの特徴は，「低速高トルク」で，電磁式モータの「高速低トルク」と対比される．

超音波モータは大きく定常波型と進行波型の 2 種類に分けられる．定常波型は，「キツツキ」型とも呼ばれ，圧電体に結合された振動片先端が楕円軌道を描き，その上に圧着されたロータあるいはスライダが間断的に駆動される．一般に高効率が実現できるが，駆動方向が変えられない．**図 12** にπ字型リニアモータの構造を示す[27]．2 本の足のサイズを若干変えることで，駆動周波数変化により両方向移動を可能にしている．

一方進行波型は，「サーフィン」型ともいわれ，時間的空間的位相差 90°の 2 つの定常波の組み合わせで，進行波を実現している．効率は低いが，駆動方向変化が容易である特徴をもつ．**図 13** には新生工業のリング状ユニモルフモータの構成を示す[28]．このタイプには，薄型という特徴があり，キャノンがカメラの自動焦点補正機構に採用した．EOS シリーズの交換レンズの 80%が既に超音波モータを載せている．超音波駆動であるから当たり前であるが，駆動の際の静粛性が超音波モータの人気

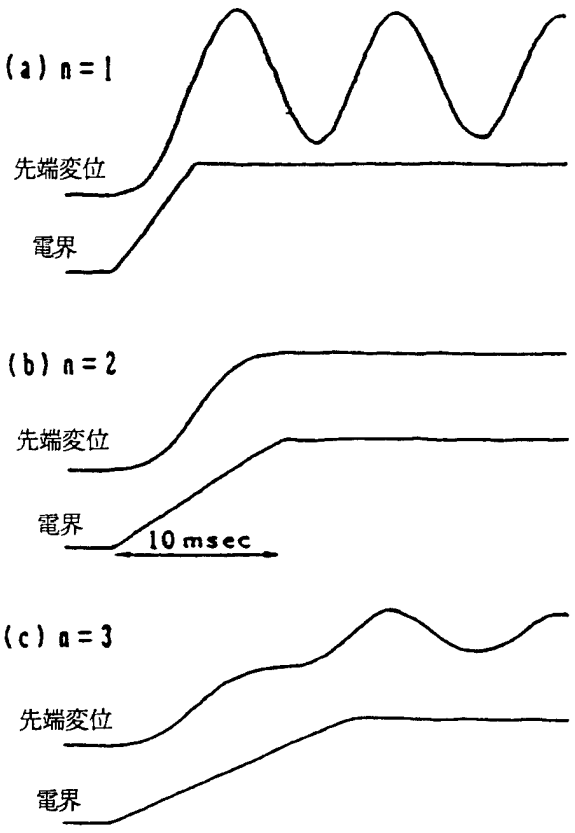

図 7 擬ステップ電圧印加時のバイモルフアクチュエータの過渡振動（n は半分共振周期を単位とした時間）

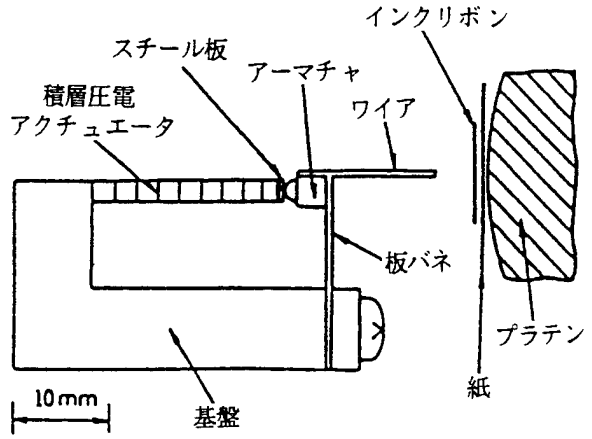

図 8 フライトアクチュエータ機構を利用したドットマトリクスプリンタヘッド

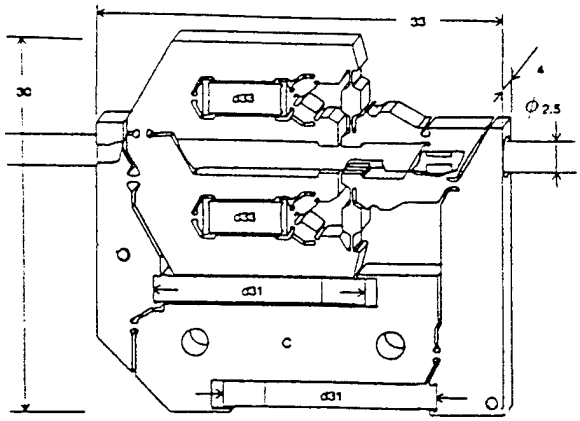

図 11 積層圧電アクチュエータと切り欠き機構を組み合わせたインチワーム

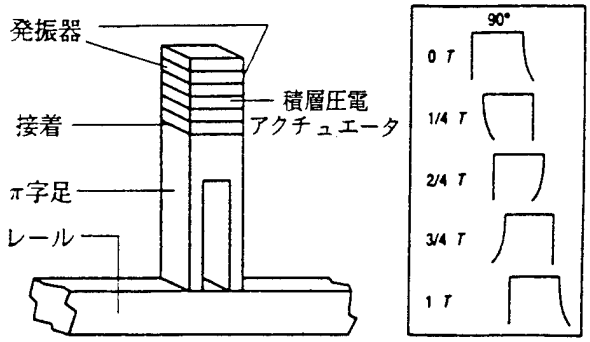

図 12 π字型振動子と積層圧電素子を組み合わせた超音波リニアモータ

に一役買っている.

6 結論

数年前，NEC の前社長関本氏は，年始のスピーチで圧電アクチュエータの市場は近い将来 1 兆円に達するであろうと述べている．2000 年における年間売上げ予測をしてみると，セラミックアクチュエータ類，カメラ関連部品，超音波モータはそれぞれ 500 億円，300 億円，150 億円が見込まれており，最終製品としての付加価値を 10 倍と見れば，1 兆円もまんざら唐突な数字ではない[1]．

セラミックアクチュエータの応用分野は広く，将来性は明るい．ただし，セラミック自身のもつ突然の破壊が問題で，ユーザに対する信頼性をそこねている．セラミックスの破壊じん性を上げることが最終的な目標ではあるが，アクチュエータの破壊予知システムの開発も信

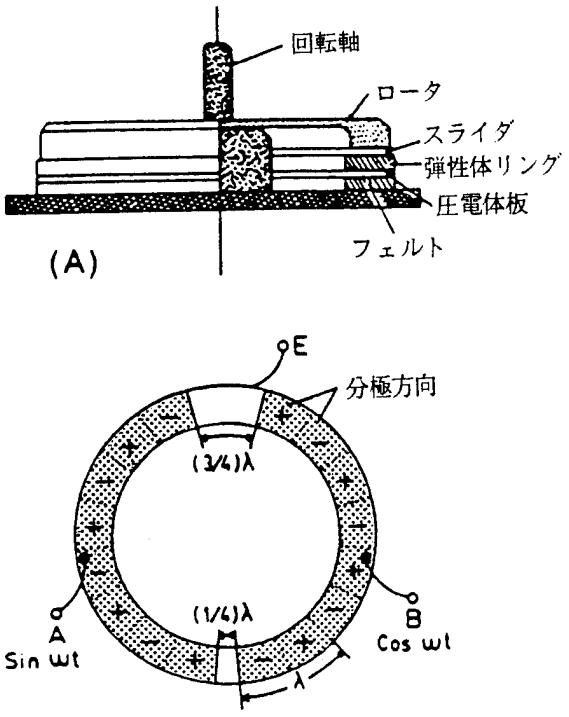

図 13 表面波型超音波モータの構成 (A) と圧電体の分極および電極状態 (B)

頼性向上には役に立つ．図 14 にはセイフティフィードバックを含むインテリジェントアクチュエータシステムを示した[29]．圧電アクチュエータ自身の一部で，アコースティックエミッションを検知し，破壊を予知できる．

材料の進化過程として，トリビアル，スマート，インテリジェント，ワイズマテリアルの 4 階層が考えられる[22]．電圧の入力に対して電流を出力する導電体，応力に対して歪みを出力する弾性体などは，よく知られた効果を利用しており，トリビアル材料といわれる．それに対して，熱に対して電界を発生する焦電材料や，応力によって電界を出力する圧電体には意外性があり，スマート材料と呼ばれる．入力－出力マトリックスの非対角位置にあるこうした相互作用には，対称位置に逆効果（電気熱量効果と逆圧電効果）が存在し，原理的に「センサ」と「アクチュエータ」の両機能を，一物質で兼ね備えることができる．一例を，トヨタの自動車用電子制御ショックアブソーバに見ることができる[23]．インテリジェント材料は，センサとアクチュエータの機能に加えて，駆動／制御のような「知能」まで有するものをいう．光歪材

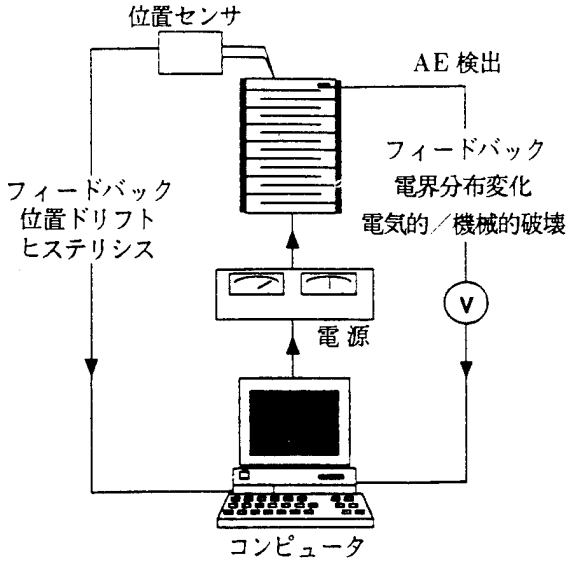

図 14 破壊予知機構を取り入れたインテリジェントアクチュエータシステム

料の例を見ることができる．インテリジェント材料にモラリティが伴うと，究極的なワイズ材料となる．「この動きは人間に危害を与えそうだ」，あるいは「環境破壊につながる」などと判断されると，自動的に停止されるような機能である．

将来の研究開発は，セラミックアクチュエータも含めて，技術的に優れたものを追うだけでなく，エコロジカルに優れたもの（人間にフィットする！）を追う必要があると思われる．その意味では，アクチュエータの破壊予知，セイフティシステムは，「ワイズ」素子／システムと呼ぶにふさわしいかも知れない．

[参考文献]

1) K.Uchino. Proc. ISAF'94. IEEE (in press)
2) K.Uchino. *MRS Bull.*, **18** (4). 42 (1993)
3) K.Furuta and K.Uchino. *Adv. Ceram. Mater.*, **1**. 61 (1986)
4) J.von Cieminski and H.Beige. *J.Phys. D.* **24**. 1182 (1991)
5) L.E. Cross. S.J. Jang, R.E. Newnham. S. Nomura and K. Uchino. *Ferroelectrics*. **23** (3). 178 (1980)
6) B.K.Wada. JPL D-10659 (1993)
7) K.Uchino nad S.Nomura. *Ferroelectrics*. **50** (1). 191 (1983)
8) A.Furuta. K.Y.Oh and K.Uchino. *Sensors and Mater.*, **3** (4). 205 (1992)

9) M.Tanimura and K.Uchino, *Sensors and Mater.*, **1**, 47 (1988)

10) K.Uchino, *J. Rob. Mech.*, **1** (2), 124 (1989)

11) S.Y.Chu, Z.Ye and K.Uchino, *J. Ceram. Soc. Japan* (submitted)

12) H. Goto, K. Imanaka and K. Uchino, *Ultrasonic Techno.* **5**, 48 (1992)

13) A. Dogan, K. Uchino and R.E. Newnham, Proc. Electroceram. IV, p.1061 (1994)

14) K. Uchino M. Yoshizaki, K. Kasai, H. Yamamura, N. Sakai and H. Asakura, *Jpn. J. Appl. Phys.*, **26** (7), 1046 (1987)

15) K. Uchino, M. Yoshizaki and A. Nagao, *Ferroelectrics*, **95**, 161 (1989)

16) Aura Ceramics, Inc., Catalogue "Rainbow"

17) H.Asakura, H.Yamamura and K.Uchino, *Ferroelectrics*, **93**, 205 (1989)

18) N.Kanbe, M.Aoyagi, S.Hirose and Y.Tomikawa, *J. Acoust. Soc. Jpn* (E), **14** (4), 235 (1993)

19) S.Sugiyama and K.Uchino, Proc. Int'l. Symp. Appl. Ferroelectrics '86, IEEE p.637 (1986)

20) T.Ota, T.Uchikawa and T.Mizutani, *Jpn. J. Appl. Phys.*, **24**, Suppl. 24-3, 193 (1985)

21) T. Sato, H. Ishikawa, O. Ikeda, K. Uchino and S. Nomura, *J. Opt. Soc. Amer.*, **71** (12), 1645 (1981)

22) K.Uchino, *Ultrasonic Techno.* **5** (8), 19 (1993)

23) Y.Yokoya, *Electronic Ceramics*, **22**, No.111, 55 (1991)

24) Y. Suzuki, K. Uchino, H. Gouda, M. Sumita, R.E. Newnham and A.R. Ramachandran, *J. Ceram. Soc. Japan*, **99** (11), 1135 (1991)

25) T.Yano, I.Fukui, E.Sato, O.Inui and Y.Miyazaki, Proc. Electr. & Commun. Soc., p.1-156 (Spring, 1984)

26) Philips CFT Tech., Walking Piezo Motors

27) M.Tohda, S.Ichikawa, K.Uchino and K.Kato, *Ferroelectrics*, **93**, 287 (1989)

28) Y. Akiyama (Editor), Ultrasonic Motors /Actuators, Triceps, Tokyo 1986

29) H.Aburatani, S.Harada, K.Uchino, A.Furuta and Y.Fuda, *Jpn. J. Appl. Phys.* **33**, 3091 (1994)

14. Uchino, K., "Advances in Ceramic Actuator Materials," Mater. Let., Vol.22, 1-4 (1995).

ELSEVIER

January 1995

MATERIALS LETTERS

Materials Letters 22 (1995) 1–4

Materials Update
Advances in ceramic actuator materials

Kenji Uchino

International Center for Actuators and Transducers, Materials Research Laboratory, The Pennsylvania State University, University Park, PA 16802, USA

Piezoelectric and electrostrictive actuators, capable of moving something electromechanically, are forming a new field between electronic and structural ceramics. The application fields are classified into three categories: positioners, motors and vibration suppressors. The manufacturing precision of optical instruments such as lasers and cameras, and the positioning accuracy for fabricating semiconductor chips are of the order of 0.1 μm, which must be adjusted using solid-state actuators. Regarding conventional electromagnetic motors, tiny motors smaller than 1 cm^3, are often required in equipment for office use or for factory automation and are rather difficult to produce with sufficient energy efficiency. Ultrasonic motors whose efficiency is insensitive to size are superior in the minimotor area. Vibration suppression in space structures and vehicles using piezoelectric actuators is also a promising technology. New solid-state displacement transducers controlled by temperature (shape memory alloy) or magnetic field (magnetostrictive alloy) have been proposed, but are generally inferior to the piezoelectric/electrostrictive actuators because of technological trends aimed at reduced driving power and at miniaturization.

Ceramic actuator materials are classified into three categories; piezoelectric, electrostrictive and phase-change materials. Modified lead zirconate titanate [PZT, $Pb(Zr, Ti)O_3$] ceramics are currently the leading materials for piezoelectric applications. The compound PLZT [$(Pb,La)(Zr,Ti)O_3$] 7/62/38 is one such composition. The strain curve is shown on the left in Fig. 1a. When the applied field is small, the induced strain is nearly proportional to the field ($x=dE$). As the field becomes larger, however, the strain curve deviates from this linear trend and significant hysteresis is exhibited due to polarization reorientation. This sometimes limits the usage of this material in actuator applications that require non-hysteretic response. An interesting new family of actuators has been fabricated from barium stannate titanate [$Ba(Sn,Ti)O_3$] solid solution. The useful property of $Ba(Sn_{0.15}Ti_{0.85})O_3$ is a very unusual strain curve, in which the domain reorientation occurs only at low fields and there is then a long linear range at higher fields (Fig. 1a, right-hand side).

On the other hand, electrostriction in PMN [$Pb(Mg_{1/3}Nb_{2/3})O_3$] based ceramics, though a second-order phenomenon of electromechanical coupling ($x=ME^2$), is extraordinarily large (more than 0.1%). An attractive feature of these materials is the near absence of hysteresis (Fig. 1b). The superiority of PMN to PZT was demonstrated in a scanning tunneling microscope (STM). The PMN actuator could provide extremely small distortion of the image even when the probe was scanned in the opposite direction.

With regard to the phase-change related strains, polarization induction by switching from an antiferroelectric to a ferroelectric state, has been proposed. Fig. 1c shows the field-induced strain curves taken for the lead zirconate stannate based system [$Pb_{0.99}Nb_{0.02}((Zr_xSn_{1-x})_{1-y}Ti_y)_{0.98}O_3$]. The longitudinally induced strain reaches up to 0.4%, which is much larger than that expected in normal piezostrictors or electrostrictors. A rectangular-shaped hyster-

SSDI 0167-577x(94)00231-2

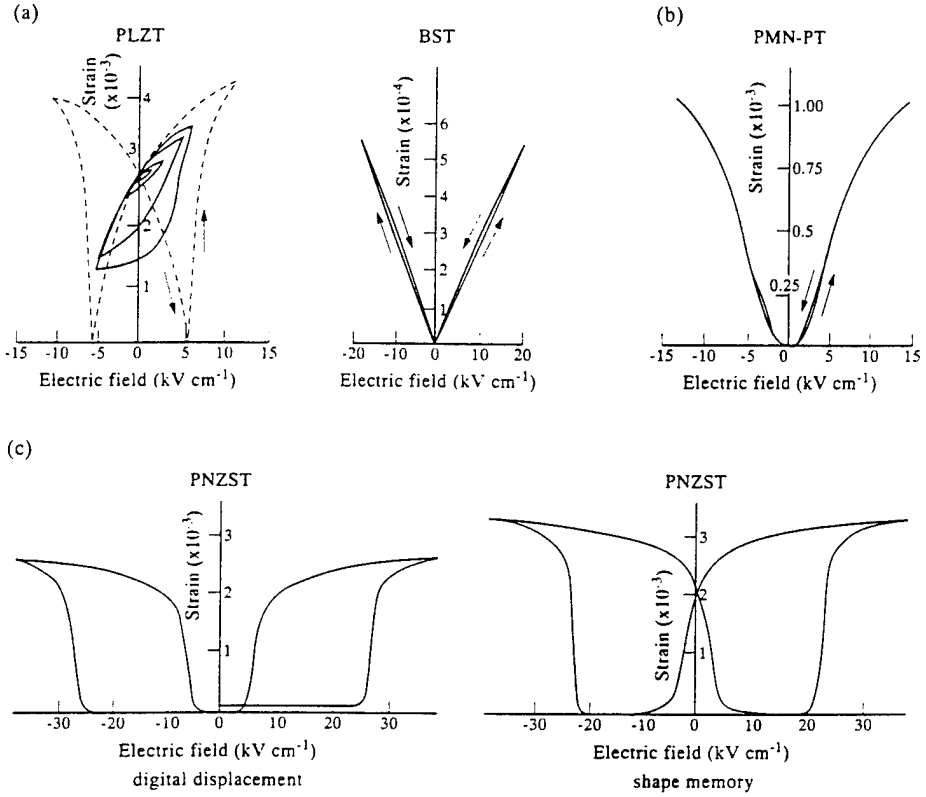

Fig. 1. Electric field-induced strains in ceramics: (a) piezoelectric $(Pb,La)(Zr,Ti)O_3$ and $Ba(Sn,Ti)O_3$; (b) electrostrictor $Pb(Mg_{1/3}Nb_{2/3},Ti)O_3$; (c) phase-change material $Pb(Zr,Sn,Ti)O_3$.

esis in Fig. 1c, left-hand side, is referred to as a "digital displacement transducer" because of the two on/off strain states. Moreover, this field-induced transition exhibitByashape memory effect in appropriate compositions (Fig. 1c, right-hand side). Once the ferroelectric phase has been induced, the material will "memorize" its ferroelectric state even under zero-field conditions, although it can be erased with the application of a small reverse bias field. This shape memory ceramic is used in energy saving actuators such as latching relays. Compared with the conventional electromagnetic relays, the new relay is much simpler and more compact in structure with almost the same response time.

Two of the most popular actuator designs are multilayers and bimorphs (Fig. 2). The multilayer, in which roughly 100 thin piezoelectric/electrostrictive ceramic sheets are stacked together, has the advantages of: low driving voltage (50 V), quick response (10 μs), high generative force (1 kN) and high electromechanical coupling. But the displacement in the

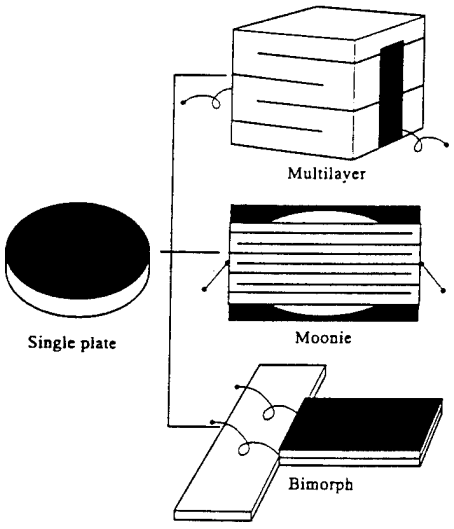

Fig. 2. Typical designs for ceramic actuators: multilayer, moonie and bimorph.

range of 10 μm is not sufficient for some applications. This contrasts with the bimorph consisting of multiple piezoelectric and elastic plates bonded together to generate a large bending displacement of several hundred microns, but the response (1 ms) and the generative force (1 N) are low.

A composite actuator structure called the "moonie" has been developed to provide characteristics intermediate between the multilayer and bimorph actuators; this transducer exhibits a displacement an order of magnitude larger than the multilayer, and a much larger generative force with a quicker response than the bimorph. The device consists of a thin multilayer piezoelectric element and two metal plates with narrow moon-shaped cavities bonded together as shown in Fig. 2. A moonie with a size of $5 \times 5 \times 2.5$ mm can generate a 20 μm displacement under 60 V, which is eight times as large as the generative displacement of the multilayer having the same size. This new compact actuator has been applied to make a miniaturized laser beam scanner.

A monomorph device has been developed to replace to conventional bimorphs, with simpler structure and manufacturing process. The principle is a superimposed effect of piezoelectricity with semiconductivity. The contact between a semiconductor and a metal electrode (Schottky barrier) causes nonuniform distribution of the electric field, even in a compositionally uniform ceramic. Suppose that the ceramic possesses also piezoelectricity, only one side of a ceramic plate tends to contract, leading to a bending deformation in total.

A monomorph plate with 20 mm in length and 0.4 mm in thickness can generate 200 μm tip displacement, in equal magnitude of that of the conventional bimorphs. The "rainbow" actuator is a modification of the abovementioned semiconductive piezoelectric monomorphs, where half of the piezoelectric plate is reduced so as to make a thick semiconductive electrode to cause a bend.

Piezoelectric/electrostrictive actuators may be classified into two categories based on the type of driving voltage applied to the device and the nature of the strain induced by the voltage: (a) rigid displacement devices for which the strain is induced unidirectionally along an applied dc field; and (b) resonating displacement devices for which the alternating strain is excited by an ac field at the mechanical resonance frequency (ultrasonic motors). The first can be further divided into two types: servo displacement transducers (positioners) controlled by a feedback system through a position-detection signal, and pulse-drive motors operated in a simple on/off switching mode, exemplified by dot-matrix printers. An actuator, referred to as a flight actuator, has been proposed which strikes a steel ball by means of a pulse-drive unit made from a multilayer piezodevice similar to that found in a pinball machine.

The materials requirements for these classes of devices are somewhat different, and certain compounds will be better suited to particular applications. The ultrasonic motor requires a very hard type piezoelectric with a high mechanical quality factor Q, leading to the suppression of heat generation. The servo-displacement transducer suffers the most from strain hysteresis and, therefore, a PMN electrostrictor is used for this purpose. The pulse-drive motor requires a low permittivity material aiming at a quick response rather than a small hysteresis so that soft PZT piezoelectrics are preferred to the high-permittivity PMN for this application.

Eighteen years have passed since the intensive development of piezoelectric actuators began, and piezoelectric shutters and automatic focusing mechanisms in cameras, dot-matrix printers and part-feeders have been commercialized and mass-produced by tens of thousands of pieces per month. Taking account of the annual sales estimation in 2000 for ceramic actuator units ($500 million), camera-related devices ($300 million) and ultrasonic motors ($150 million), the market-share of piezoelectric actuators would reach up to $1 billion in the future.

It is evident that the application field of ceramic actuators is remarkably wide. There still remain, however, problems in durability and reliability that need to be overcome before these devices can become general-purpose commercialized products. The final goal is, of course, to develop much tougher actuator ceramics mechanically and electrically. However, the reliability can be improved significantly if the destruction symptom of the actuator is monitored. An intelligent actuator system composed of two feedback mechanisms has been proposed: position feedback which can compensate the position drift and the hysteresis, and breakdown detection feedback which can stop the actuator system safely without

causing any serious damage to the equipment. Acoustic emission measurement of a piezo-actuator under a cyclic electric field, which exhibits a maximum when the crack propagates extensively, is a good predictor for the lifetime.

Finally, a future promising actuator material is introduced: photostrictive actuators developed recently exhibit an intelligent function incorporating sensing of illumination, and self-production of drive/control voltage together with final actuation. In certain ferroelectrics, a constant electromotive force is generated with exposure to light, and a photostrictive strain results from the coupling of this bulk photovoltaic effect with inverse piezoelectricity. A bimorph unit has been made from PLZT 3/52/48 ceramic doped with slight addition of tungsten. The remnant polarization of one PLZT layer is parallel to the plate and in the direction opposite to that of the other plate. When violet light is radiated onto one side of the PLZT bimorph, a photovoltage of 1 kV/mm is generated, causing a bending motion. The tip displacement of a 20 mm bimorph was 150 μm with a response time of 1s. A photo-driven micro walking device, a relay and a photoacoustic device ("photophone") have been designed to begin moving by light illumination without any electrical circuitry.

Further reading

[1] K. Uchino, Piezoelectric/electrostrictive actuators (Morikita Publishing, Tokyo, 1986).
[2] K. Uchino, Bull. Am. Ceram. Soc. 65 (1986) 647.
[3] K. Uchino, J. Rob. Mech., 1 (1989) 124.
[4] K. Uchino, Mater. Res. Soc. Bull. 18 (1993) 42.

15. **Uchino, K., "Novel Ceramic Actuator Materials," Proc. US/Japan Workshop on Smart Mater. and Structures (in press).**

NOVEL CERAMIC ACTUATOR MATERIALS

Kenji Uchino

International Center for Actuators and Transducers
Materials Research Laboratory, The Pennsylvania State University
University Park, PA 16802-4801

Abstract

Novel functions of materials are sometimes realized by superimposing two different effects. Newly discovered materials, shape memory ceramics, monomorphs and photostrictors, are using sophisticatedly coupled effects of piezoelectricity with another different phenomenon. The shape memory function arises from a phase transition, while the monomorph and the photostriction are associated with a semiconductor contact effect and a bulk photovoltaic effect, respectively. These "very smart" multifunctional actuator materials will be utilized for future promising devices. This paper reviews principles and fundamental and applicational developments of these three materials.

INTRODUCTION

Recent developments in micro-electromechanical systems (MEMS), particularly in solid state actuators, have been remarkable.[1,2] Application fields are classified into three categories: positioners, motors and vibration suppressors. The manufacturing precision of optical instruments such as lasers and cameras, and the positioning accuracy for fabricating semiconductor chips, which must be adjusted using solid-state actuators, is of the order of 0.1 μm. Regarding conventional electromagnetic motors, tiny motors smaller than 1 cm^3 are often required in office or factory automation equipment and are rather difficult to produce with sufficient energy efficiency. Ultrasonic motors whose efficiency is insensitive to size are superior in the mini-motor area. Vibration suppression in space structures and military vehicles using piezoelectric actuators is also a promising technology.

Among the smart solid-state actuators, capable of moving something mechanically, controlled by temperature (shape memory alloy), magnetic field (magnetostrictive alloy) and electric field (piezoelectric/electrostrictive ceramic), the former two are generally inferior to the piezoelectric actuators because of technological trends aimed at reduced driving power and miniaturization.

This paper concerns newly discovered ceramic actuator materials using sophisticatedly coupled effects of piezoelectricity with another different phenomenon: shape memory

ceramics, monomorphs and photostrictors. Novel functions of materials are sometimes realized by superimposing two different effects. The shape memory function arises from a phase transition, while the monomorph and the photostriction are associated with a semiconductor contact effect and bulk photovoltaic effect, respectively. These "very smart" multifunctional actuator materials will be utilized for future promising devices. This paper reviews principles and fundamental and applicational developments of these three materials.

SHAPE MEMORY CERAMICS

Concerning the phase-change-related strains, polarization induction by switching from a macroscopically nonpolar into a polar state, as in switching from an antiferroelectric to a ferroelectric state, has been proposed. Different from a shape memory alloy, the strain control is made electrically in the antiferroelectric ceramic, leading to much faster response and lower drive power than in the alloy. After the first report by Berlincourt et al.,[3] lead zirconate based ceramics were investigated intensively on the field induced strain characteristics by the authors, and a shape memory effect was discovered.[4-6]

Figure 1 shows the field-induced strain curves taken for the lead zirconate stannate-based system $[Pb_{0.99}Nb_{0.02}((Zr_xSn_{1-x})_{1-y}Ti_y)_{0.98}O_3]$. The longitudinally induced strain reaches up to 0.4%, which is much larger than that expected in normal piezoelectrics or electrostrictors. A rectangular-shape hysteresis in Fig.1 left, referred to as a "digital displacement transducer" bacause of the two on/off strain states, is interesting. Moreover, this field-induced transition exhibits a shape memory effect in appropriate compositions (Fig.1 right). Once the ferroelectric phase has been induced, the material will "memorize" its ferroelectric state even under a zero-field condition, although it can be erased with the application of a small reverse bias field. The shape memory effect was also verified in the domain observation with an optical CCD microscope (Fig.2).[7] While no domain was observed at the initial state, clear domains appeared with an electric field due to the phase transition and remained even when the electric field was removed. Recent researches by other groups were focused on sample fabrication processes and composition search for obstaining larger induced strains.[8,9]

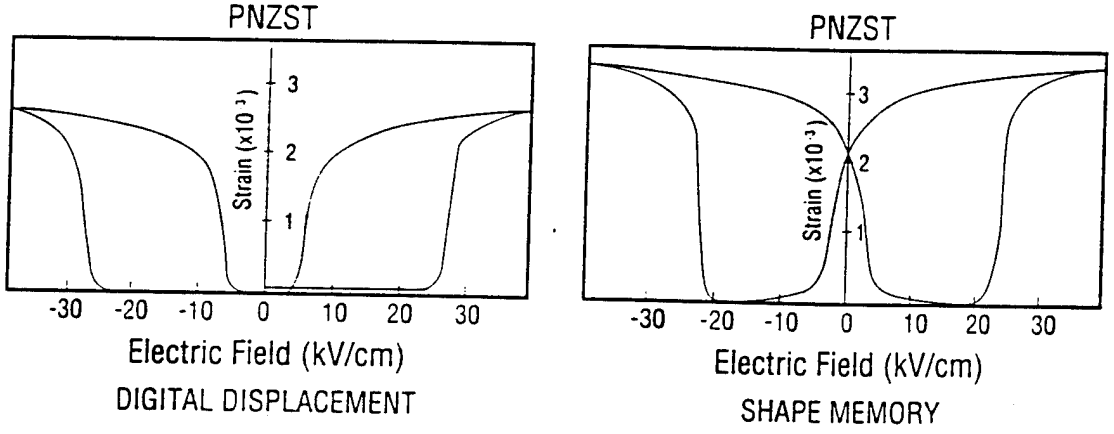

Figure 1 Electric field-induced strains in phase-change materials $Pb(Zr,Sn,Ti)O_3$.

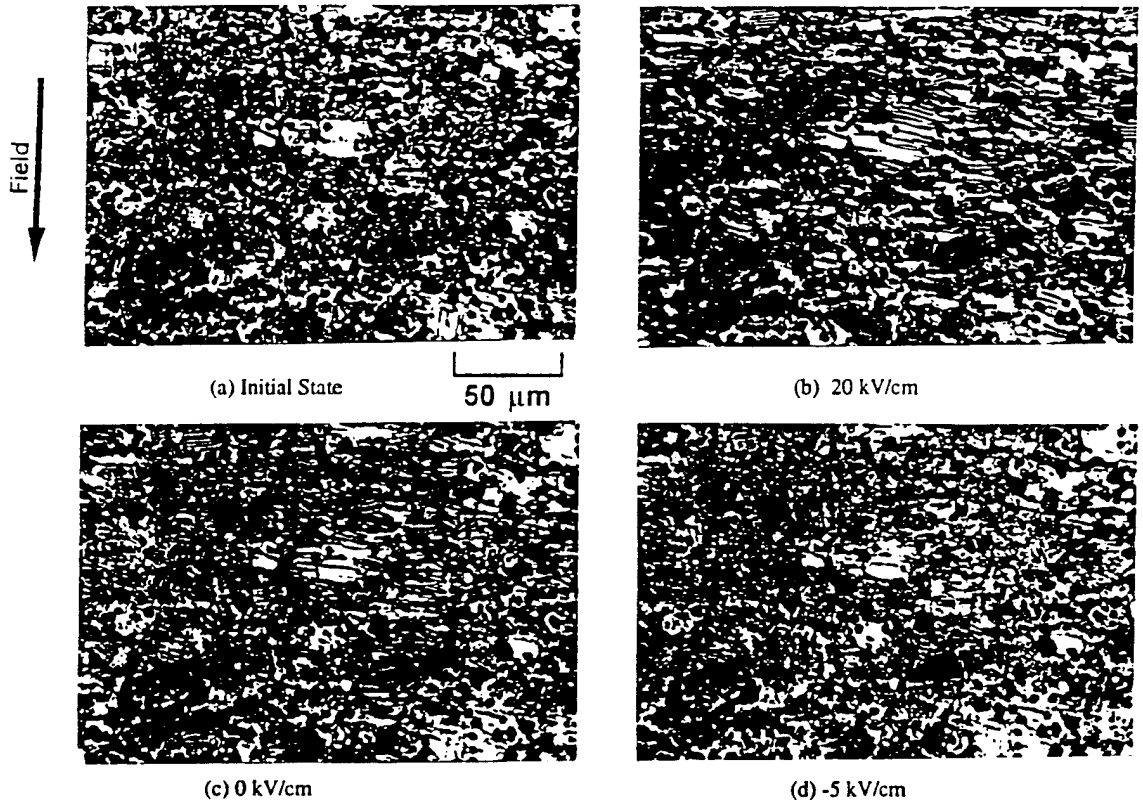

Figure 2 Variation of the domain structure in a shape memory material $Pb(Zr,Sn,Ti)O_3$ with an electric field.

This shape memory ceramic was used in energy saving actuators. A latching relay in Fig.3 was composed of a shape memory ceramic unimorph and a mechanical snap action switch, which was driven by a pulse voltage of 4ms.[10] Compared with the conventional electromagnetic relays, the new relay was much simple and compact in structure with almost the same response time.

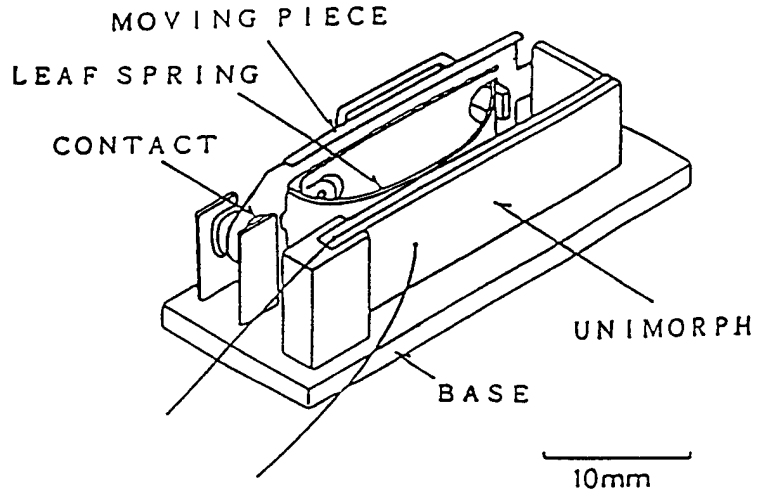

Figure 3 Latching relay using a shape memory ceramic unimorph.

MONOMORPH ACTUATORS

A conventional bimorph-type actuator consists of two piezoelectric plates bonded together and electroded so that their piezoelectric expansion/contraction directions are opposing one another. This actuator will execute a large bending motion of several 100μm with the application of an electric field. The most serious problem associated with this type of actuator concerns the bonding of the ceramic plates and the elastic shim. Poor adhesion between these individual elements results in the rapid deterioration of the device after repeated use and displacement drift (creep). The monomorph actuator made from only one ceramic plate, which can achieve the bending displacement, will be a promising design in its simple construction. While avoiding the bonding problems of the bimorph structure, it also allows for significant cost reduction and production efficiency in manufacturing.

The operating principle is based on the coupling of a semiconductor contact phenomenon with the piezoelectric/electrostrictive effect.[11] When metal electrodes are applied to both surfaces of a semiconductor plate and a voltage is applied as shown in Fig.4(a), electric field is concentrated on one side (Schottky barrier), thereby generating a non-uniform field within the plate. By making the piezoelectric slightly semiconductive in this manner, contraction along the surface occurs through the piezoelectric effect only on the side at which the electric field is concentrated. The non-uniform field distribution generated in the ceramic causes an overall bending of the entire plate. Figure 4(b) is a modified structure, where a very thin insulative layer improves the breakdown voltage.[12]

Research is underway focused on barium titanate-based and lead zirconate titanate-based piezoelectric ceramics to which additives have been doped to produce semiconductive properties. The PZT ceramics were made semiconductive by preparing solid solutions with a semiconductive perovskite compound $(K_{1/2}Bi_{1/2})ZrO_3$. When 300V was applied to a ceramic plate with 20 mm in length and 0.4 mm in thickness, fixed at one end, the tip deflection as much as 200 μm could be obtained, equal in magnitude to that of bimorphs (Fig.5).[13]

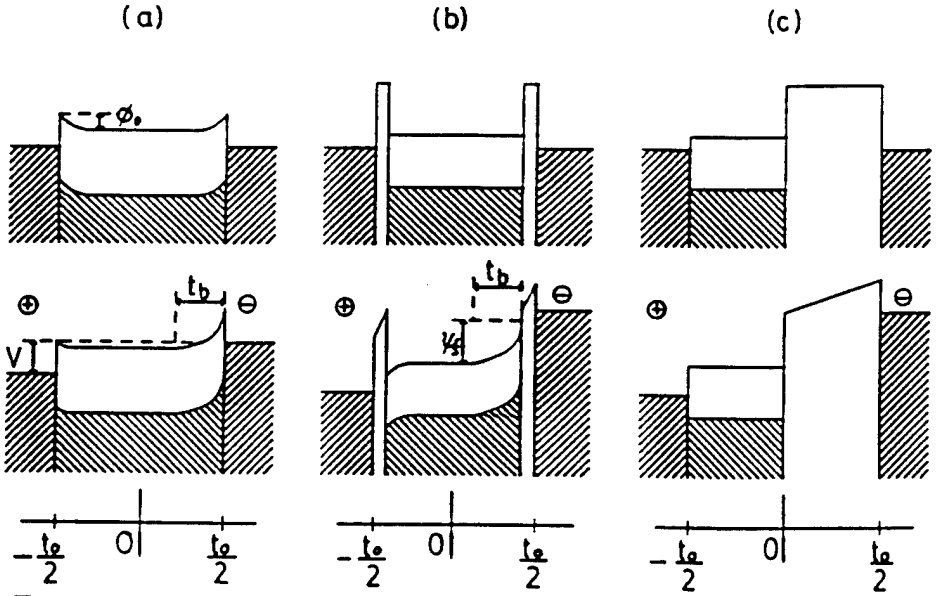

Figure 4 Energy band models for the monomorph actuator: (a) Schottky type, (b) Metal-Insulator-Semiconductor structure with very thin insulative layers, (c) MIS structure with a very thick insulative layer.

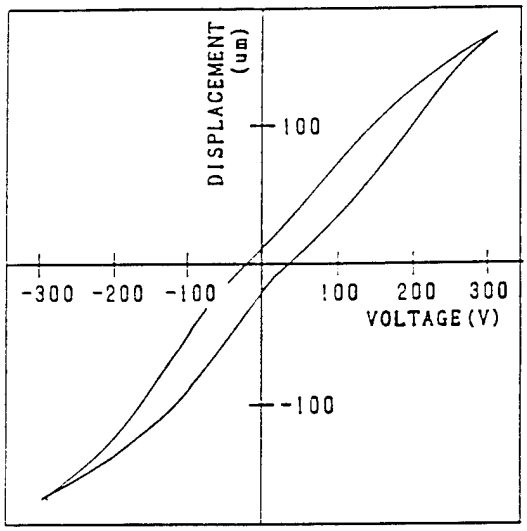

Figure 5 Drive voltage versus tip displacement of a monomorph plate. The sample was made of $0.7Pb(Zr_{0.9}Ti_{0.1})O_3$-$0.3(K_{1/2}Bi_{1/2})ZrO_3$ (20mm x 10mm x 0.4mm in size).

The "rainbow" actuator by Aura Ceramics[14] is a modification of the above-mentioned semiconductive piezoelectric monomorphs, where half of the piezoelectric plate is reduced so as to make a thick semiconductive electrode to cause a bend. Figure 4(c) shows the electron energy band structure of the "rainbow".[12]

The monomorph was applied to a simple speaker. Figure 6 shows the sound pressure level versus frequency relation.[15] Though its acoustic characteristics were not satisfactory in comparison with the conventional piezoelectric unimorph types, the monomorph speaker has advantages in mass-production and cost.

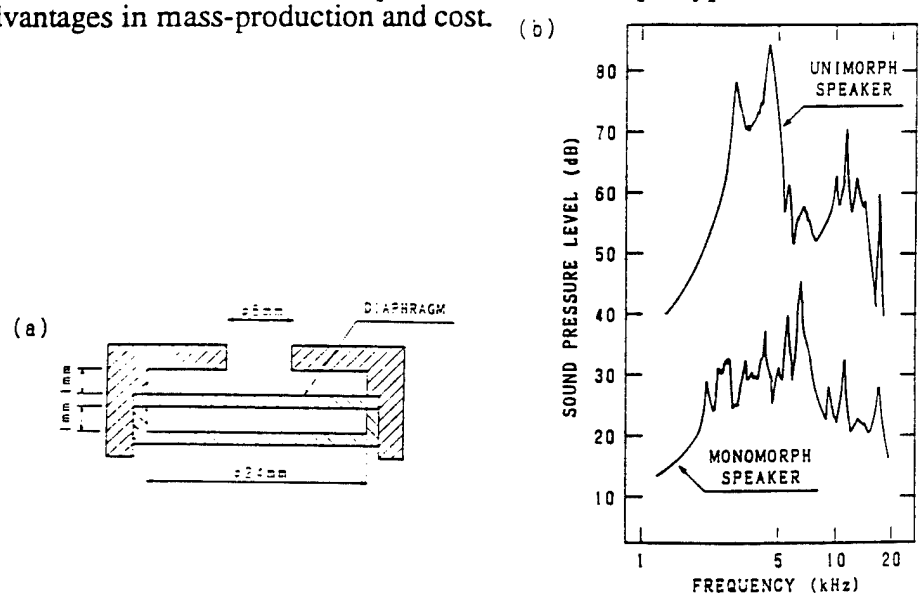

Figure 6 Frequency dependence of the sound pressure level measured at 10 cm in front of the monomorph or unimorph speaker.

PHOTOSTRICTIVE ACTUATORS

The photostrictive effect is a phenomenon in which strain is induced in the sample when it is illuminated. This effect is focused especially in the field of micromechanism. On decreasing the size of miniaturized robots/actuators, the weight of the electric lead wire connecting the power supply becomes significant, and remote control will be definitely required for sub-millimeter devices. A photo-driven actuator is a very promising candidate for micro-robots.[16)]

In certain ferroelectrics, a constant electromotive force is generated with exposure of light, and a photostrictive strain results from the coupling of this bulk photovoltaic effect to inverse piezoelectricity. A bimorph unit has been made from PLZT 3/52/48 ceramic doped with slight addition of niobium or tungsten.[17,18)] The remnant polarization of one PLZT layer is parallel to the plate and in the direction opposite to that of the other plate. Figure 7 shows the structure of a photo-driven bimorph in contrast to a voltage-driven one. Notice large illumination area, small capacitance and d33 usage, leading to large bending with quick response. When a violet light is irradiated to one side of the PLZT bimorph, a photovoltaic voltage of 1 kV/mm is generated, causing a bending motion. Figure 8 shows the displacement response observed at the tip of a 20 mm bimorph 0.4 mm in thickness. 150 μm was obtained within a couple of seconds.

A photo-driven micro walking device, designed to begin moving by light illumination, has been developed.[19)] As shown in Fig.9, it is simple in structure, having neither lead wires nor electric circuitry, with two bimorph legs fixed to a plastic board. When the legs are irradiated alternately with light, the device moves like an inchworm with a speed of 100 μm/min.

Very recently photo-mechanical resonance of a PLZT ceramic bimorph has been successfully induced using chopped near-ultraviolet irradiation, having neither electric lead wires nor electric circuits.[20)] A dual beam method was used to irradiate the two sides of the bimorph alternately. The tip displacement of the sample is plotted as a function of chopper frequency in Fig.10. The resonance frequency was about 75 Hz with the mechanical quality factor Q of about 30. The achievement of photo-induced mechanical resonance suggests the promise of photostrictors as vibration actuators such as "ultrasonic motors."

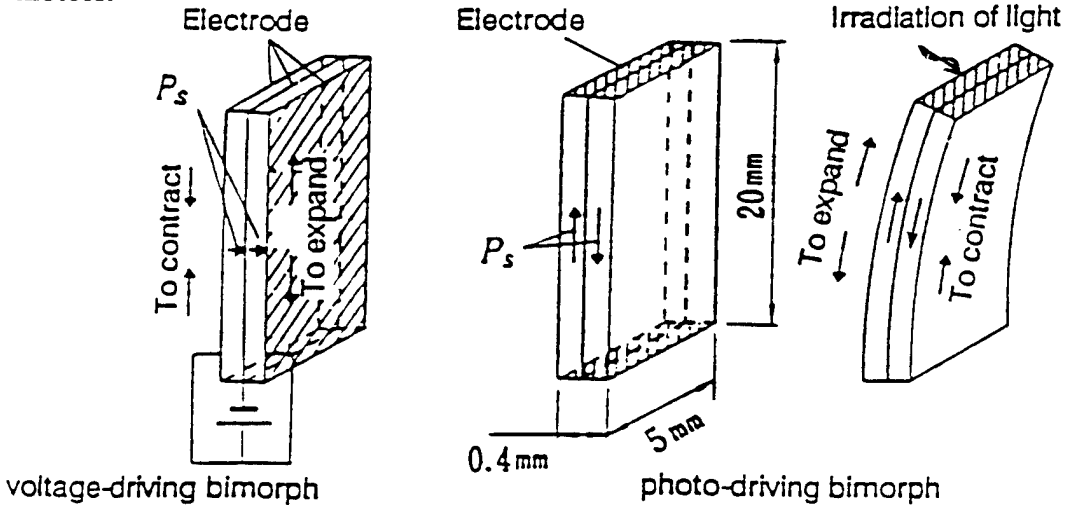

Figure 7 Structures of voltage- and photo-driven bimorphs and their driving principles.

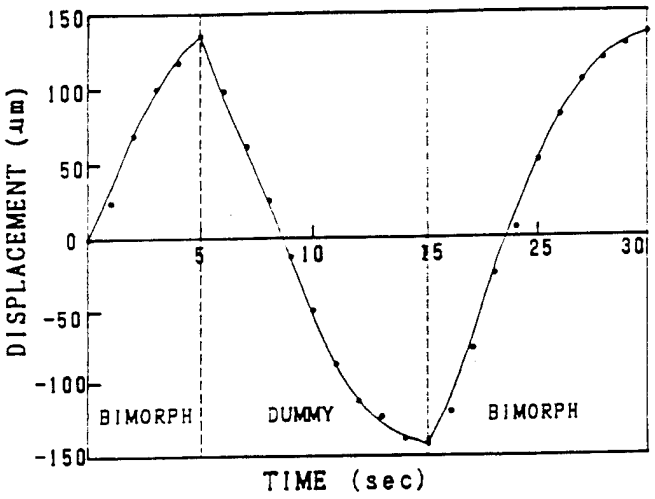

Figure 8 Tip deflection of the bimorph device made of WO_3 0.5 at.% doped PLZT under a dual beam control (illumination intensity: 10 mW/cm^2).

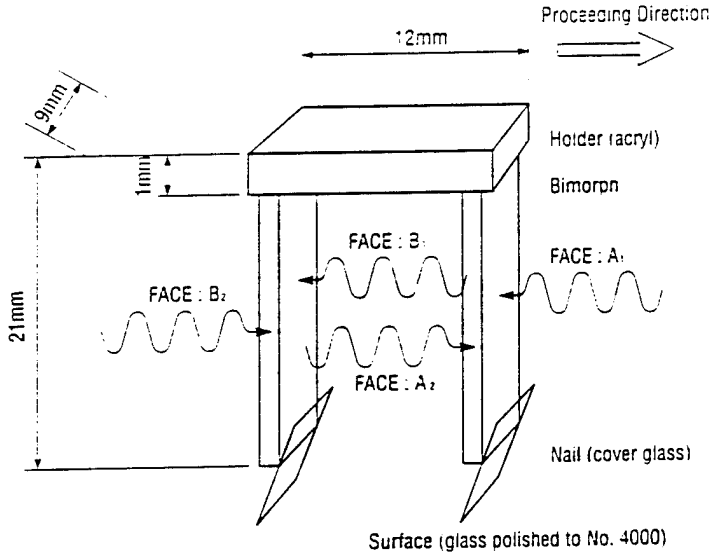

Figure 9 Structure of the photo-driven micro walking machine.

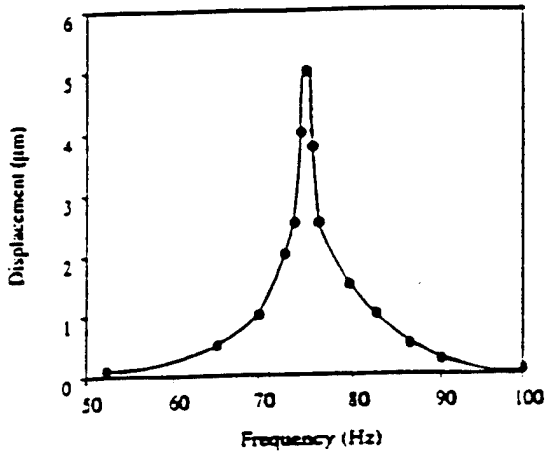

Figure 10 Photo-induced mechanical resonance behavior of the PLZT bimorph.

Acknowledgement

This work was partly supported by US Army Research Office and Office of Naval Research through Contracts No. DAAL 03-92-G-0244 and No. N00014-91-J-4145.

REFERENCES

1) K.Uchino, "Ceramic Actuators: Principles and Applications," Mater. Res. Soc. Bull. **18** (1993) 42-48.
2) K.Uchino, "New Piezoelectric Devices for Smart Actuator/Sensor Systems," Proc. Electroceramics IV, Aachen, Sept. 5-7 (1994) 179-191.
3) D.Berlincourt, H.H.A.Krueger and B.Jaffe, J. Phys. & Chem. Solids **25** (1964) 659.
4) K.Uchino and S.Nomura, "Electrostriction in PZT-Family Antiferroelectrics," Ferroelectrics **50** (1983) 191.
5) K.Uchino, "Shape Memory Effect Associated with the Forced Phase Transition in Antiferroelectrics," Proc. MRS Int'l. Mtg. on Adv. Mater. **9** (1989) 489.
6) K.Y.Oh, A.Furuta and K.Uchino, "Shape Memory Unimorph Actuators Using Lead Zirconate-Based Antiferroelectrics," J. Ceram. Soc. Jpn. **98** (1990) 905.
7) K.Y.Oh, K.Uchino and L.E.Cross, "Optical Study of Domains in Antiferroelectric Ceramics," J. Adv. Performance Mater. [in press].
8) W.Y.Pan, Q.Zhang, A.Bhalla and L.E.Cross, J. Amer. Ceram. Soc. **72** (1989) 571.
9) Z.Xu, D.Viehland and D.A.Payne, J. Appl. Phys. **74** (1993) 3406.
10) A.Furuta, K.Y.Oh and K.Uchino, "Shape Memory Ceramics and Their Application to Latching Relays," Sensors and Mater. **3** (1992) 205.
11) K.Uchino, M.Yoshizaki, K.Kasai, H.Yamamura, N.Sakai and H.Asakura, Jpn. J. Appl. Phys. **26** (1987) 1046.
12) K.Uchino, M.Yoshizaki and A.Nagao, Jpn. J. Appl. Phys. **26**, Suppl.26-2 (1987) 201.
13) K.Uchino, M.Yoshizaki and A.Nagao, "Monomorph Characteristics in $Pb(Zr,Ti)O_3$ Based Ceramics," Ferroelectrics **95** (1989) 161-164.
14) Aura Ceramics, Inc., USA, Catalogue "Rainbow".
15) K.Uchino and S.Suzuki, "Speakers Utilizing Semiconductive Piezoelectric Monomorph Devices," J. Ceram. Soc. Jpn. **100** (1992) 1221-1224.
16) S.Y.Chu and K.Uchino, "Photostrictive Effect in PLZT-Based Ceramics and Its Applications," Ferroelectrics [in press].
17) K.Uchino, M.Aizawa and S.Nomura, Ferroelectrics **64** (1985) 199-208.
18) M.Tanimura and K.Uchino, Sensors and Mater. **1** (1988) 47-56.
19) K.Uchino, "Micro Walking Machines Using Piezoelectric Actuators," J. Rob. Mech. **1** (1989) 124-127.
20) S.Y.Chu, Z.Ye and K.Uchino, J. Adv. Performance Mater. **1** (1994) 129-143.